

# Towards Automatic and Reliable Localized Model Order Reduction

Localized Training, a Posteriori Error Estimation,  
and Online Enrichment

arXiv:1908.02074v1 [math.NA] 6 Aug 2019

Andreas Buhr  
- 2019 -



# Towards Automatic and Reliable Localized Model Order Reduction

Inauguraldissertation zur Erlangung des Doktorgrades der  
Naturwissenschaften im Fachbereich Mathematik und Informatik der  
Mathematisch-Naturwissenschaftlichen Fakultät der Westfälischen  
Wilhelms-Universität Münster.

Andreas Buhr

geboren in München

Münster

–2019–

---

**Dekan:** Prof. Dr. Xiaoyi Jiang  
**Erstgutachter:** Prof. Dr. Mario Ohlberger  
**Zweitgutachter:** Prof. Dr. Christian Engwer  
**Externer Gutachter:** Prof. Dr. Robert Scheichl, Heidelberg

**Tag der mündlichen Prüfung: 11. Juli 2019**  
**Tag der Promotion: 11. Juli 2019**



## English Abstract

Finite element based simulation of phenomena governed by partial differential equations is a standard tool in many engineering workflows today. However, the simulation of complex geometries is computationally expensive. Many engineering workflows require multiple simulations with small, non parametric changes in between. The use of localized model order reduction for subsequent simulations of geometries with localized changes is very promising. It produces lots of computational tasks with little dependencies and thus parallelizes well. Furthermore, the possibility to reuse intermediary results in the subsequent simulations can lead to large computational savings. In this thesis, we investigate different aspects of localized model order reduction and propose various improvements. A simulation methodology named ArbiLoMod, comprising a localized training, a localized a posteriori error estimator and an enrichment procedure is proposed. A new localized a posteriori error estimator with computable constants is presented and analyzed. A new training algorithm which is based on a transfer operator is derived. It can be shown to converge nearly as fast as the singular value decay of this operator. The transfer operator's spectrum is observed to decay fast in electromagnetic simulations in printed circuit boards. New online enrichment algorithms are proposed. All results are supported by numerical experiments, for which the source code for reproduction is provided.

---

## German Abstract

Finite Elemente basierte Simulationen von Phänomenen, die durch partielle Differentialgleichungen beschrieben werden können, sind heutzutage fester Bestandteil von vielen Arbeitsabläufen im Ingenieurwesen. Allerdings sind Simulationen von komplexen Geometrien sehr rechenintensiv. In vielen Arbeitsabläufen sind wiederholte Simulationen mit lokalisierten, nichtparametrischen Änderungen dazwischen notwendig. Lokalisierte Modellordnungsreduktion verspricht ein großes Verbesserungspotential für Sequenzen von Simulationen mit geringfügigen Änderungen zwischen den Simulationen. Bei der Anwendung von lokalisierter Modellordnungsreduktion entsteht eine große Anzahl von Berechnungsabschnitten mit nur wenigen Datenabhängigkeiten, was Parallelisierung einfach macht. Weiterhin existiert die Möglichkeit, Zwischenergebnisse in den folgenden Simulationen wiederzuverwenden, was zu Einsparungen von Rechenzeit führen kann. In dieser Dissertationsschrift untersuchen wir verschiedene Aspekte von lokalisierter Modellordnungsreduktion und schlagen einige Verbesserungen vor. Eine Simulationsmethodik, genannt ArbiLoMod, die ein lokalisiertes Training, eine a posteriori Fehlerabschätzung sowie ein online enrichment enthält, wird vorgeschlagen. Ein neuer lokalisierter a posteriori Fehlerschätzer mit berechenbaren Konstanten wird gezeigt und analysiert. Ein neuer Trainingsalgorithmus wird präsentiert, der auf einem Transferoperator basiert und beweisbar nahezu so gut konvergiert wie der Singulärwertabfall dieses Operators. In elektromagnetischen Simulationen von Leiterplatten wird ein schneller Abfall des Spektrums des Transferoperators beobachtet. Neue Algorithmen zum online enrichment werden vorgeschlagen. Alle Ergebnisse werden mit numerischen Experimenten bestätigt, deren Quellcode zwecks Reproduktion zur Verfügung gestellt wird.

---

## Acknowledgments

---

I would like to thank my supervisors, Mario Ohlberger and Christian Engwer, and Stefan Reitzinger from CST AG for the opportunity to pursue this research project. The idea to have interactive simulations of physical phenomena in complex geometries has fascinated me for a long time. Having had the opportunity to concentrate on research heading in this direction for an extended period of time is a privilege which I appreciate greatly. I would like to thank Mario Ohlberger, Christian Engwer, Stephan Rave, and Kathrin Smetana for productive collaborations on the central research questions, which lead to significant progress toward this goal. Finally I would like to thank all colleagues from my work groups for a stimulating and enjoyable working environment and Julia Brunken, Annika Bürger, Dennis Eickhorn, René Fritze, Tim Keil, and Tobias Leibner for proofreading parts of this thesis.

This thesis was supported by CST AG:

CST Computer Simulation Technology AG (as of August 2017: GmbH)  
Bad Nauheimer Straße 19  
64289 Darmstadt  
Germany



<b>Contents</b>		<b>vii</b>
<b>1. Introduction</b>		<b>1</b>
1.1. Target Application . . . . .		1
1.2. Changing Computing Landscape . . . . .		2
1.3. Research Questions . . . . .		2
1.4. Existing Research . . . . .		4
1.4.1. Localization of Reduced Basis Methods . . . . .		4
1.4.2. Generalization of Numerical Multiscale Methods . . . . .		6
1.4.3. Domain Decomposition Methods . . . . .		6
1.4.4. Other Related Developments . . . . .		7
1.5. Collaborations and Previous Publications . . . . .		8
1.6. Overview over this Document . . . . .		9
<b>2. Preliminaries</b>		<b>11</b>
2.1. Variational Problem . . . . .		11
2.2. Reduced Problem . . . . .		12
2.2.1. Properties of Reduced Variational Problem in Coercive Case . . . . .		12
2.2.2. Properties of Reduced Variational Problem in inf-sup Stable Case . . . . .		13
2.3. Parameterized Problem . . . . .		13
2.4. Localized Model Order Reduction . . . . .		13
2.4.1. Localizing Space Decomposition . . . . .		14
2.4.2. Localized Model Order Reduction . . . . .		14
2.4.3. Examples for Localizing Space Decomposition . . . . .		14
2.5. Heat Conduction . . . . .		15
2.5.1. Full Heat Conduction Equation . . . . .		15
2.5.2. Stationary Heat Conduction . . . . .		16
2.5.3. Weak Formulation of Heat Conduction . . . . .		16
2.6. Maxwell's Equations . . . . .		17
2.6.1. Full Maxwell's Equations in Original Form . . . . .		17
2.6.2. Time Harmonic Maxwell's Equation . . . . .		18
2.6.3. Reduction to one Unknown Field . . . . .		18
2.6.4. Weak Formulation of Time Harmonic Maxwell's Equation . . . . .		18
2.6.5. Finite Element Approximation in $H(\text{curl}, \Omega)$ . . . . .		20

2.6.6.	2D Version of Maxwell's Equations . . . . .	21
2.7.	Examples Used for Numerical Experiments . . . . .	22
2.7.1.	Thermal Block Example . . . . .	23
2.7.2.	Example for Stationary Heat Equation With Channels . . . . .	24
2.7.3.	Example for 2D Maxwell Equation . . . . .	26
2.7.4.	Olimex A64 Example . . . . .	28
<b>3.</b>	<b>ArbiLoMod</b>	<b>31</b>
3.1.	Method Design . . . . .	31
3.1.1.	Design Decision: Handling Channels . . . . .	32
3.1.2.	Design Decision: Interface Spaces . . . . .	32
3.1.3.	Design Decision: Using a-harmonic Extensions . . . . .	33
3.2.	Space Decomposition . . . . .	34
3.3.	Local Basis Generation . . . . .	37
3.3.1.	Basis Construction for Reduced Vertex Spaces . . . . .	37
3.3.2.	Local Training for Basis Construction of Reduced Face Spaces . . . . .	38
3.3.3.	Basis Construction for Reduced Cell Spaces Using Local Greedy . . . . .	39
3.4.	Enrichment Procedure . . . . .	41
3.5.	Runtime and Communication . . . . .	42
3.6.	Numerical Experiments . . . . .	44
3.6.1.	Numerical Example 1: Thermal Channels . . . . .	44
3.6.2.	Numerical Example 2: 2D Maxwell's . . . . .	48
3.7.	Ideas For Future Extension of ArbiLoMod . . . . .	53
<b>4.</b>	<b>Dual Norm Localization – A Posteriori Error Estimation</b>	<b>55</b>
4.1.	Requirements on Localized a Posteriori Error Estimator . . . . .	55
4.2.	Abstract Estimates for Dual Norm Localization . . . . .	56
4.3.	Choosing Spaces and Bounding Constants . . . . .	60
4.4.	Relative Error Estimators . . . . .	65
4.5.	Improved Offline/Online Splitting . . . . .	65
4.6.	Future Research on Localized a Posteriori Error Estimation . . . . .	69
<b>5.</b>	<b>Improved Local Training</b>	<b>71</b>
5.1.	Abstract Training Configuration . . . . .	71
5.2.	Randomized Range Finder Algorithm . . . . .	75
5.2.1.	Randomized Numerical Linear Algebra . . . . .	75
5.2.2.	Setting . . . . .	75
5.2.3.	Optimal Spaces . . . . .	76
5.2.4.	Generation of Random Vectors . . . . .	76
5.2.5.	A Probabilistic a Posteriori Norm Estimator . . . . .	78
5.2.6.	Randomized Range Finder Algorithm . . . . .	80
5.2.7.	A probabilistic a priori error bound . . . . .	81
5.3.	Numerical Experiments for Isolated Range Finder . . . . .	83
5.4.	Olimex A64 Example . . . . .	90
5.5.	Future Research on Randomized Range Finder . . . . .	93
5.6.	Future Research for Transferoperator Based Training . . . . .	94
<b>6.</b>	<b>Online Enrichment</b>	<b>95</b>
6.1.	Introduction . . . . .	95
6.2.	Enrichment Algorithms . . . . .	95
6.3.	A Priori Convergence Estimates . . . . .	97
6.4.	Application to Partition of Unity Decomposition . . . . .	99

6.5. Numerical Example . . . . .	100
6.6. Discussion . . . . .	104
6.7. Future Research in the Context of Localized Online Enrichment . . . . .	105
<b>7. Conclusion</b>	<b>107</b>
<b>A. Reproduction of Results</b>	<b>109</b>
A.1. Reproduction of Figure 2.1 . . . . .	109
A.2. Reproduction of Figure 2.3 . . . . .	110
A.3. Reproduction of Figure 2.5 . . . . .	110
A.4. Reproduction of Figure 2.7 . . . . .	110
A.5. Reproduction of Figure 3.5 . . . . .	110
A.6. Reproduction of Figure 3.8 . . . . .	110
A.7. Reproduction of Table 3.1, Figure 3.9, and Figure 3.10 . . . . .	110
A.8. Reproduction of Figure 3.11 . . . . .	110
A.9. Reproduction of Table 3.2 . . . . .	110
A.10.Reproduction of Table 3.3 . . . . .	111
A.11.Reproduction of Figure 3.12 . . . . .	111
A.12.Reproduction of Figure 3.13 . . . . .	111
A.13.Reproduction of Figure 3.14 . . . . .	111
A.14.Reproduction of Figure 3.16 . . . . .	111
A.15.Reproduction of Figure 3.17 . . . . .	111
A.16.Reproduction of Figure 3.18 . . . . .	111
A.17.Reproduction of Figure 3.20 . . . . .	111
A.18.Reproduction of Figure 4.1 . . . . .	112
A.19.Reproduction of Figure 5.2 . . . . .	112
A.20.Reproduction of Figure 5.3 . . . . .	112
A.21.Reproduction of Table 5.1 . . . . .	112
A.22.Reproduction of Figure 5.4 . . . . .	112
A.23.Reproduction of Figure 5.5 . . . . .	112
A.24.Reproduction of Figure 5.6 . . . . .	112
A.25.Reproduction of Figure 5.7 . . . . .	112
A.26.Reproduction of Figure 5.8 . . . . .	113
A.27.Reproduction of Figures 5.11 and 5.12 . . . . .	113
A.28.Reproduction of Figure 6.1 . . . . .	113
A.29.Reproduction of Figures 6.3 to 6.6 . . . . .	113
A.30.Reproduction of Figure C.1, Figure C.2, and Figure C.3 . . . . .	114
A.31.Reproduction of Table D.1 . . . . .	114
<b>B. A Posteriori Error Estimation for Relative Errors</b>	<b>115</b>
B.1. Introduction . . . . .	115
B.2. Two relative error estimators . . . . .	115
B.2.1. Setting . . . . .	115
B.3. Definition of Relative a Posteriori Error Estimators . . . . .	115
B.4. Rigorosity and Effectivity of Relative a Posteriori Error Estimators . . . . .	116
B.5. Comparison of Relative A Posteriori Error Estimators . . . . .	117
B.5.1. Comparison of Range of Validity . . . . .	117
B.5.2. Comparison of Sharpness . . . . .	118
B.5.3. Comparison of Efficiency . . . . .	118
B.6. Conclusion on Relative A Posteriori Error Estimators . . . . .	118

<b>C. Numerically Stable Gram-Schmidt Algorithm</b>	<b>119</b>
C.1. Introduction . . . . .	119
C.2. Algorithms . . . . .	119
C.3. Numerical Comparison . . . . .	120
C.4. Summary . . . . .	122
<b>D. High Performance Nédélec Assembly</b>	<b>123</b>
D.1. Problem Setting . . . . .	123
D.2. Source Code . . . . .	124
D.3. Quality Control . . . . .	124
D.4. Performance Measurement . . . . .	124
<b>E. Handling of Complex Numbers in pyMOR</b>	<b>127</b>
<b>Bibliography</b>	<b>137</b>



---

## List of Theorems

---

2.1.1.	Definition (Variational problem) . . . . .	11
2.1.2.	Remark (Antilinear inner product) . . . . .	12
2.2.1.	Definition (Reduced variational problem) . . . . .	12
2.2.2.	Theorem (Best approximation for coercive problems (Céa's Lemma)) . . . . .	12
2.2.3.	Theorem (Best approximation for inf-sup stable problems) . . . . .	13
2.4.1.	Definition (Localizing Space Decomposition) . . . . .	14
3.2.1.	Definition (Basic subspaces) . . . . .	35
3.2.2.	Remark (Basic space decomposition) . . . . .	35
3.2.3.	Definition (Extended subspaces) . . . . .	36
3.2.4.	Remark (Extended subspaces) . . . . .	36
3.2.5.	Definition (Local projection operators) . . . . .	37
4.2.1.	Lemma (Efficiency of dual element localization) . . . . .	56
4.2.2.	Proposition (Localization of dual norm with local stability constants) . . . . .	57
4.2.3.	Proposition (Localization of dual norm with global stability constant) . . . . .	58
4.2.4.	Corollary (Localization of a posteriori error estimator) . . . . .	59
4.3.1.	Definition (Overlapping space decomposition) . . . . .	60
4.3.2.	Proposition (Estimate of localization constant) . . . . .	60
4.3.3.	Proposition ( $H$ independent localization constant estimate) . . . . .	62
4.3.4.	Proposition (Localized efficiency estimate) . . . . .	64
4.3.5.	Remark (Improved efficiency estimates) . . . . .	64
4.4.1.	Proposition (Relative error estimators) . . . . .	65
5.1.1.	Definition (Localized training configuration) . . . . .	71
5.1.2.	Lemma (Norm of sum of localized functions) . . . . .	73
5.1.3.	Proposition (Training a priori estimate) . . . . .	73
5.2.1.	Lemma (Distribution of inner product) . . . . .	77
5.2.2.	Definition (Probabilistic a posteriori norm estimator) . . . . .	78
5.2.3.	Proposition (Norm estimator failure probability) . . . . .	78
5.2.4.	Proposition (Norm estimator effectivity) . . . . .	79
5.2.5.	Lemma (Projection error of operators and their matrices) . . . . .	81
5.2.6.	Theorem (A priori convergence of randomized range finder for matrices) . . . . .	82
5.2.7.	Lemma (Singular values of operators and their matrices) . . . . .	82
5.2.8.	Proposition (A priori convergence of randomized range finder) . . . . .	83

---

5.2.9.	Remark (Improved constants for a priori convergence estimate) . . . . .	83
6.3.1.	Theorem (Exponential convergence of residual based online enrichment) . . .	97
6.3.2.	Corollary (Exponential convergence from iteration 0) . . . . .	98
6.3.3.	Theorem (Optimality of globally coupled online enrichment (Algorithm 6.2)) .	99
6.3.4.	Corollary (Exponential convergence of globally coupled online enrichment) . .	99
6.4.1.	Proposition (Upper bound of $c_{\text{pu},\tilde{\nu}}$ ) . . . . .	100
B.3.1.	Definition (Classic relative a posteriori error estimator) . . . . .	116
B.3.2.	Definition (New relative a posteriori error estimator) . . . . .	116
B.3.3.	Remark (Dividing by reduced error norm) . . . . .	116
B.4.1.	Proposition (Classic relative a posteriori error estimator) . . . . .	116
B.4.2.	Proposition (New relative a posteriori error estimator) . . . . .	117
B.5.1.	Proposition (Sharpness of relative a posteriori error estimators) . . . . .	118
B.5.2.	Proposition (Efficiency constant of relative a posteriori error estimators) . . .	118

---

## List of Figures

---

1.1. DDR memory channel on a printed circuit board subject to local modification. . . . .	1
2.1. Visualization of Nédélec ansatz functions (edge elements) for one triangle. . . . .	20
2.2. Geometry of <i>Thermal Block Example</i> . . . . .	23
2.3. High-dimensional solution of <i>Thermal Block Example</i> . . . . .	24
2.4. First structure in sequence of simulated structures in <i>Thermal Channels Example</i> . . . . .	24
2.5. Sequence of structures simulated in <i>Thermal Channels Example</i> along with solutions. . . . .	25
2.6. Geometries simulated in <i>2D Maxwell Example</i> . . . . .	27
2.7. Example solutions for <i>2D Maxwell Example</i> . . . . .	27
2.8. Front and perspective view of <i>Olimex A64 Example</i> . . . . .	28
2.9. Back and detail view of <i>Olimex A64 Example</i> . . . . .	29
2.10. Mesh detail of <i>Olimex A64 Example</i> . . . . .	29
2.11. Stackup of <i>Olimex A64 Example</i> . . . . .	29
3.1. Main components of localized model order reduction . . . . .	32
3.2. Overview of ArbiLoMod. . . . .	33
3.3. Visualization of basic spaces $V_i^{\text{basic}}$ and their extension spaces for $Q^1$ ansatz functions. . . . .	35
3.4. Visualization of some example elements of the local subspaces $V_i^{\text{wb}}$ . . . . .	36
3.5. Extend operator is executed in two steps for spaces $V_i^{\text{wb}}, i \in \Upsilon_2$ . . . . .	36
3.6. Visualization of basic spaces $V_i^{\text{basic}}$ , training space, and coupling space. . . . .	38
3.7. Data dependencies in ArbiLoMod . . . . .	43
3.8. Maximum relative $H^1$ -error on training set $\Xi$ for <i>Thermal Channels Example</i> . . . . .	44
3.9. Relative error with training during iteration for <i>Thermal Channels Example</i> . . . . .	45
3.10. Relative error without training during iteration for <i>Thermal Channels Example</i> . . . . .	46
3.11. Error estimators $\Delta_{\text{rel}}(\tilde{u}_\mu)$ , $\Delta_{\text{loc,rel}}^g(\tilde{u}_\mu)$ during iteration for <i>Thermal Channels Example</i> . . . . .	46
3.12. Distribution of local basis sizes after initial training for <i>Thermal Channels Example</i> . . . . .	48
3.13. inf-sup and continuity constant of bilinear form for <i>2D Maxwell Example</i> . . . . .	49
3.14. Upper bound for Kolmogorov n-width for <i>2D Maxwell Example</i> . . . . .	49
3.15. Domain decomposition used for <i>2D Maxwell Example</i> . . . . .	49
3.16. Maximum error when solving <i>2D Maxwell Example</i> with a localized basis. . . . .	50
3.17. inf-sup constant of <i>2D Maxwell Example</i> vs. basis size. . . . .	50
3.18. Maximum error over all frequencies for both geometries of <i>2D Maxwell Example</i> . . . . .	51
3.19. Impact of geometry change in <i>2D Maxwell Example</i> . . . . .	52
3.20. Basis size distribution in <i>2D Maxwell Example</i> . . . . .	52

---

4.1. Maximum relative reduction errors and estimated errors in <i>Thermal Block Example</i> .	68
5.1. Geometry of <i>Rangefinder Example 1</i> . . . . .	84
5.2. Comparison of optimal with randomized basis functions for <i>Rangefinder Example 1</i> .	85
5.3. Projection error over basis size for <i>Rangefinder Example 1</i> . . . . .	85
5.4. Projection error over target projection error for <i>Rangefinder Example 1</i> . . . . .	87
5.5. $h$ dependency in <i>Rangefinder Example 1</i> . . . . .	88
5.6. Singular value decay for <i>Rangefinder Example 2</i> . . . . .	88
5.7. Projection error over basis size $n$ for <i>Rangefinder Example 2</i> . . . . .	89
5.8. Projection error over target projection error for <i>Rangefinder Example 2</i> . . . . .	89
5.9. Domain decomposition used for <i>Olimex A64 Example</i> . . . . .	90
5.10. Example solution in oversampling domain in <i>Olimex A64 Example</i> . . . . .	91
5.11. Singular value decay of $T_{816}$ for <i>Olimex A64 Example</i> . . . . .	92
5.12. Runtimes for randomized range finder on <i>Olimex A64 Example</i> . . . . .	92
6.1. Coefficient field $\sigma$ and right hand side $f$ of <i>Thermal Channels Variant</i> . . . . .	101
6.2. Overlapping domain decomposition $\omega_i$ for <i>Thermal Channels Variant</i> . . . . .	101
6.3. Error decay during online enrichment for <i>Thermal Channels Variant</i> (zoom) . . . .	102
6.4. Decay of relative energy error during iteration in <i>Thermal Channels Variant</i> . . . .	102
6.5. Convergence of online enrichment in <i>Thermal Channels Variant</i> . . . . .	103
6.6. Sharpness of inequalities in Algorithm 6.1 . . . . .	103
C.1. Orthogonality Error of Gram-Schmidt algorithms. . . . .	121
C.2. Reproduction Error of Gram-Schmidt algorithms. . . . .	121
C.3. Median of Iterations in Adaptive Re-Iterated Gram-Schmidt. . . . .	121

---

## List of Tables

---

3.1. Number of iterations of online enrichment for <i>Thermal Channels Example</i> . . . . .	45
3.2. Runtimes for selected parts of ArbiLoMod for <i>Thermal Channels Example</i> . . . . .	47
3.3. Influence of domain size $H$ in ArbiLoMod for <i>Thermal Channels Example</i> . . . . .	47
4.1. Run-time complexities of traditional and new algorithm for error estimator. . . . .	69
5.1. CPU times for <i>Rangefinder Example 1</i> . . . . .	87
D.1. Number of instructions for one local integral evaluation . . . . .	124



---

## List of Algorithms

---

3.1. Projections of wirebasket decomposition $\mathcal{P}_{V_i^{\text{wb}}}$ . . . . .	37
3.2. SnapshotGreedy . . . . .	40
3.3. Training to construct reduced face spaces. . . . .	40
3.4. LocalGreedy to construct local cell spaces. . . . .	42
3.5. Online Enrichment in ArbiLoMod. . . . .	43
5.1. Adaptive Randomized Range Approximation. . . . .	80
6.1. Residual Based Online Enrichment. . . . .	96
6.2. Globally Coupled Online Enrichment. . . . .	96
C.1. Erhard Schmidt's variant of Gram-Schmidt algorithm. . . . .	120
C.2. Jørgen Pedersen Gram's variant of Gram-Schmidt algorithm. . . . .	120
C.3. Gram-Schmidt with re-iteration. . . . .	122
C.4. Gram-Schmidt with adaptive re-iteration. . . . .	122





### 1.1. Target Application

Nowadays, finite element based simulation of phenomena which are governed by partial differential equations, such as heat conduction, elasticity, fluid flow, or electromagnetics is an essential part of many engineering workflows. Commercial tools are available from different vendors. However, many tools have a simple simulation pipeline which goes from geometry to meshing, to matrix assembly, to the solution of a matrix equation, to postprocessing and finally visualization of results. Often, all intermediary results are discarded and the complete pipeline is reprocessed on any non parametric change of the model under consideration, even if the change is localized.

The research presented in this thesis was motivated by the desire to improve on this. Often, engineers improve a structure manually in an iterative approach, where in each iteration they change the structure slightly and resimulate. A particular example is the design of printed circuit boards (PCBs). The design of PCBs has all of the above mentioned properties: PCBs are nowadays very complex, there is no scale separation, improvements are often obtained by local changes of the electronic components and conductive tracks, and when solved in frequency domain, it is a parameterized problem with the frequency as a parameter. The idea to use localized model reduction for PCBs was already published by the authors in [Buhr(2009)]. A possible change is depicted in Figure 1.1. The same applies to integrated circuit (IC) packages, which are in structure similar to PCBs. When the changes are localized, one can take advantage of this. To this end, we designed a processing pipeline which keeps everything localized as long as possible. With a localized meshing procedure, the mesh has to be regenerated only in an environment of the change. With a localized matrix assembly, matrices have to be reassembled only in an environment of the change. When only a small part of the geometry is changed, this bears the potential for large speedups.

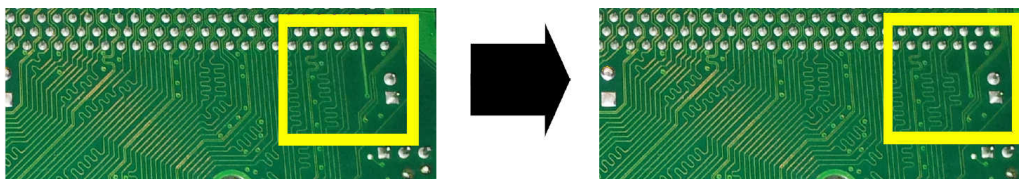


Figure 1.1.: DDR memory channel on a printed circuit board subject to local modification of conductive tracks (own photo, manipulated with GIMP).

The next step of the pipeline is the solution of a matrix equation, which cannot easily be localized, since everything is coupled. Localizing this part is the central goal of this thesis. To this end, we designed a simulation methodology named method designed for Arbitrary Local Modifications (ArbiLoMod). It localizes this step by first creating localized, reduced models and then coupling these local models to solve the global problem. This way, only the reduced models in an environment of the change have to be regenerated. The following solution of the global problem is fast, as it is based on the reduced models. While this localized pipeline was designed to improve simulation times after localized changes, it has in addition the advantage that the computational workload it creates parallelizes well. It fits to the current development of computers to become more and more parallel. While only a few localized meshes, matrices and reduced models are created upon a localized change to the model, thousands of tasks have to be processed in the initial run. These tasks have little data dependencies and are thus well suited for cloud environments.

### *Vision*

Today, the use of finite element based simulation tools needs skilled engineers and is a time consuming task where simulations often take hours, days or even weeks. We believe that in the future, by advances in computing technology and the development of more efficient algorithms, simulation tools will provide results almost instantaneously. The goal is that results are 'just there' and the engineer using the simulation software can forget about the fact that there is a sophisticated simulation happening.

## 1.2. Changing Computing Landscape

The finite element method was developed in the second half of the previous century. As the clock frequencies of PCs as well as the amount of available RAM have risen, the analysis of increasingly bigger models became feasible. For a long time, sequential performance of CPUs was rising according to Moore's law. The speed doubled approximately every 18 month until around the year 2005, when high end CPUs reached over 3 GHz. Since then, at the time of writing for 14 years, CPUs became more parallel by broader SIMD units and an increasing number of cores per socket, but the clock rates stayed around 3 GHz. Applications need to be adapted to these parallel architectures to exploit the available computing power. There are efforts to use this kind of parallelism in today's FEM codes, see for example the EXA-DUNE project [Bastian et al.(2014)] within the "German Priority Programme 1648 – Software for Exascale Computing" by the Deutsche Forschungsgemeinschaft (DFG).

But now we witness the rise of cloud computing, where everyone has potential access to thousands of computers, albeit accessed through a rather slow network connection. To successfully exploit the potential of cloud computing for finite element analysis in an interactive setting, new algorithms with greatly reduced communication demands are required. For example, if a user wants to start 1000 compute tasks within a second and has a 20 MB/s internet connection, each task can be given only 20kB of input data. If the task runs on a recent multicore machine, it can have  $\mathcal{O}(10^{11})$  floating point operations available in one second. This discrepancy of  $\mathcal{O}(10^{11})$  floating point operations to  $\mathcal{O}(10^5)$  bytes of input data is the challenge in using highly parallel cloud computing for interactive Finite Element Analysis (FEA) applications. The algorithms we develop in this thesis are targeted at this setting.

## 1.3. Research Questions

As already mentioned, localized model order reduction has the potential to vastly decrease simulation times in a finite element based simulation software for sequences of geometries with localized changes, as it is common in many engineering workflows. It has attracted a lot of attention from

different research communities recently. The main questions in research on localized model order reduction are the following.

1. ***How to decompose the global problem?***

Each localized model order reduction method has to decompose the global problem in local parts and to couple the local parts. The question how to do this decomposition is central, as it impacts all other questions. While in general, a decomposition into local problems of very different kind is possible, we concentrate on the decomposition of a global solution space into localized subspaces in this thesis, as this gives a consistent mathematical framework.

2. ***How to generate local reduced models?***

Having decomposed the global problem into local coupled parts, the second question is how to generate reduced approximations of these. This is usually the question getting the most attention. The models are often constructed to fulfill some form of local convergence criterion or error bound. In order to obtain the projected benefits, especially the reuse of reduced models after a localized geometry change, it is necessary to use only local information in the construction of local reduced models. This step is often called “training”.

3. ***How does the local error propagate to the global problem?***

Having constructed reduced approximations of all parts of a localizing decomposition, one can compute an approximate solution of the global problem using these. Quantifying a priori how the errors of the local reduced models influence the error of the global approximate solution is another topic in research on localized model order reduction.

4. ***How to estimate the global error a posteriori?***

Having computed a global approximate solution, one wants to quantify its error. This is the topic of a posteriori error estimation. It is especially important in situations where an a priori estimate is not available. But even when an a priori estimate is available, an a posteriori estimate might give a much sharper bound. Most existing a posteriori error estimators for reduced models involve global computations and are thus unsuitable for the localized setting.

5. ***How can the local reduced models be improved, once we solved the global reduced problem?***

Having solved the global reduced problem, the a posteriori error estimator might indicate an insufficient quality of the obtained approximation. In order to improve, one wants to improve the local, reduced problems. This is the question of “online enrichment”.

Besides these five research questions, there are additional implementation related questions which come into focus when the knowledge is transferred to the application domain and the method is implemented in an engineering context, among those:

6. ***How to mesh the geometry localized?***

When using Finite Element Method (FEM) based methods, as we do throughout this thesis, a mesh is required. In order to realize the advantages of localized model order reduction, also the meshing has to be localized. Meshing is a very complex task in practice. The additional constraints of localization may lead to additional difficulties.

7. ***How to implement the method parallelized?***

The intended method should react quickly to geometry changes and should be heavily parallelized. The resulting workload requires many computing resources, but only in short bursts. To be cost effective, the computational resources must be shared with other users. Implementing a suitable runtime system is a challenging task.

## 1.4. Existing Research

Our motivating application is the handling of localized, unforeseen changes in the model under consideration. Despite its importance, this question gained surprisingly little attention from the research community. Similar to our motivation is localized model order reduction for crack propagation, where the location of the crack is not known in advance [Kerfriden et al.(2013)]. While only few researchers share our motivation of arbitrary localized changes, the field of localized model order reduction has gained a large amount of attention recently. Localized model order reduction is a research topic in between of three traditional research fields. It can be seen as an extension to the Reduced Basis (RB) method, using basis functions with localized support only instead of basis functions with global support, as it is common in RB methods. It can also be seen as a generalization of numerical multiscale methods, relaxing the requirement of scale separation and using an adaptive number of basis functions for each coarse grid element. As a third option, it can be seen as a part of domain decomposition research, as the construction of a coarse space good enough so that the coarse space solution is of sufficient quality. In the following, we review related developments in these three fields.

### 1.4.1. Localization of Reduced Basis Methods

The RB method [Noor and Peters(1980), Fink and Rheinboldt(1983), Patera and Rozza(2007)] is by now an established model order reduction method for parameterized problems in real-time or many-query contexts. Introductory texts were published recently [Benner et al.(2017), Hesthaven et al.(2016), Quarteroni et al.(2016)]. Multiple approaches combining the RB method with some form of localization were published.

In 2002, Maday and Rønquist published the Reduced Basis Element (RBE) method, introduced in [Maday and Rønquist(2002)] and applied to the thermal fin problem and the Stokes problem [Maday and Rønquist(2004), Løvgrén et al.(2006)], combining the reduced basis approach with a domain decomposition, coupling local basis vectors by polynomial Lagrange multipliers on domain boundaries in a mortar type. Later, the RBE was applied to the two dimensional Maxwell's problem in [Chen et al.(2011)], using Discontinuous Galerkin (DG) coupling instead of mortar type coupling. This was named Seamless Reduced Basis Element Method (SRBE). This approach is unsuitable for our setting. While using polynomials at the boundaries might work in most cases, it could fail for complex interfaces or if singularities in the solution are close to the interfaces. In addition, to construct the reduced spaces, in [Chen et al.(2011)] it is proposed to build up a global RB space first and then decompose these function into local parts. This is incompatible with our goal of only local computations and reuse after changes.

The Reduced Basis Hybrid Method (RBHM) which is built upon the RBE was introduced in [Iapichino et al.(2012)]. It combines the local RB approximations with a global coarse Finite Element (FE) space, but still using polynomial Lagrange multipliers at domain boundaries.

The Reduced Basis - Domain Decomposition - Finite Element Method (RDF), whose preliminary version was introduced in [Iapichino(2012)] and which was introduced in [Iapichino et al.(2016)] uses parameterized interface spaces of Lagrange- or Fourier functions for basis generation and it includes FE basis functions along interfaces in the global reduced space. It thereby has more accurate solutions, but this again is unsuitable for our setting, as we aim at relatively large interfaces, where model reduction at the interfaces is crucial and including all FE basis functions at the interface would be prohibitively expensive.

The Discontinuous Galerkin Reduced Basis Element (DGRBE) was introduced in [Antonietti et al.(2016)] and applied to the Stokes problem in [Pacciarini et al.(2016)]. It extends on the RDF, but it removes the FE functions at the interfaces and instead, like the SRBE, couples local bases on subdomains using a DG coupling. Local basis functions are computed by prescribing parameterized Neumann data on the subdomain boundaries. For the Neumann data, either using all FE functions at the interface or using Legendre functions is proposed. Both is unsuitable for

our setting. Using all FE functions leads to too many possible boundary conditions. Legendre functions might not approximate the true interface data in complex geometries or if singularities are close to the domain boundaries.

Also combining RB with domain decomposition but different in motivation is the Reduced Basis for Heterogeneous Domain Decomposition (RBHDD) [Maier and Haasdonk(2014), Martini et al.(2014), Martini et al.(2017)], aiming at the coupling of different physical formulations on the domains.

Similar to ours in motivation is the Static Condensation Reduced Basis Element Method (SCRBE) method [Phuong Huynh et al.(2013)], which also aims at systems composed of components, where the geometry of the components can be mapped to reference geometries. While the connection between the components is simply achieved by polynomial Lagrange multipliers in the RBE, significant research has been conducted on choosing the right coupling spaces in the context of the SCRBE. Choosing the right space at the interfaces is called “Port Reduction” and was included in the name, leading to the Port Reduced Static Condensation Reduced Basis Element Method (PR-SCRBE) method [Eftang and Patera(2013), Eftang and Patera(2014)] which employs a so-called “pairwise training”. A variation of this idea is used in our method. Recently, also an algorithm to obtain optimal interface spaces for the PR-SCRBE was proposed [Smetana and Patera(2016)] and a framework for a posteriori error estimation was introduced [Smetana(2015)]. While the PR-SCRBE performs excellent in using the potentials of cloud environments, its goals are different from ours. While being able to handle various changes to the simulated system, it does not aim at arbitrary modifications. And it does not try to hide the localization from the user, but rather exposes it to let the user decide how the domain decomposition should be done. One further drawback is that the SCRBE is only specified for non intersecting domain interfaces and thus not applicable to a domain decomposition of 3D space but only to systems which naturally decompose into components like bridges or cranes.

Very close to our motivation is the Localized Reduced Basis Multiscale Method (LRBMS). It is a localized model order reduction method building upon a non overlapping domain decomposition and a DG coupling at the domain boundaries. Reduced spaces are constructed for each domain. The LRBMS was developed in the groups of Mario Ohlberger at the University of Münster and Bernard Haasdonk at the University of Stuttgart during the last decade. The first publication mentioning localized spaces and the DG coupling appeared in 2011 [Kaulmann et al.(2011)], the first publication mentioning the LRBMS appeared 2012 [Albrecht et al.(2012)]. This method interpolates between a standard DG method when the domain decomposition is chosen to be equal to the fine mesh and a classic RB method when the domain decomposition consists of only one element containing the full domain. It has been proposed to generate local basis functions by solving the global, unreduced problem and restricting the global solution to the local domains. This strategy is uncommon in the realm of localized model order reduction and thus a specialty of the LRBMS. Improvement of the local reduced spaces by online enrichment was introduced in [Albrecht and Ohlberger(2013)], solving local problems on localized oversampling domains in an *solve*  $\rightarrow$  *estimate*  $\rightarrow$  *mark*  $\rightarrow$  *refine* loop. Rigorous a posteriori error estimators have been developed in [Ohlberger and Schindler(2014)] and [Ohlberger and Schindler(2015)], estimating not only the reduction error with respect to a reference solution, but also the full error with respect to the analytic solution. Recently, the LRBMS was adapted to parabolic problems in [Ohlberger and Rave(2017)]. In [Ohlberger and Schindler(2017)] and [Ohlberger et al.(2018)], usage of the LRBMS in the context of PDE constrained optimization was investigated, performing online enrichment of the localized reduced approximation spaces inside of an optimizer loop. Unlike other localized model order reduction methods, no local training procedures have been investigated so far in the context of the LRBMS. The implementation of the LRBMS led to a comprehensive software library extending the Distributed and Unified Numerics Environment (DUNE) [Bastian et al.(2008a), Bastian et al.(2008b)] framework, namely the `dune-xt` modules [Milk et al.(2017)]

and `dune-gdt`<sup>1</sup>. The main difference between the LRBMS and the ArbiLoMod is that ArbiLoMod is based on a conforming discretization, allowing for reuse of existing conforming FE software libraries to build an ArbiLoMod implementation on top. Furthermore, during the development of ArbiLoMod, there was a focus on localized training procedures (presented in Section 3.3.2 and Chapter 5). While these training procedures could also be applied in the context of LRBMS, no research has been conducted in this area to date.

#### 1.4.2. Generalization of Numerical Multiscale Methods

Numerical multiscale methods are designed for applications in which the problem has a fine structure which is too fine to be discretized directly, as for example in ground water flow simulations. In most cases, these methods require a scale separation. For problems with scale separation, there are established methods to reduce the model such as Multiscale Finite Element Method (MsFEM), Variational Multiscale Method (VMM), Heterogeneous Multiscale Method (HMM), or Local Orthogonal Decomposition Method (LOD).

VMM was introduced in [Hughes(1995),Hughes et al.(1998)]. An adaptive variant was introduced in [Larson and Målqvist(2005),Larson and Målqvist(2007)] which was later extended in [Larson and Målqvist(2009a),Larson and Målqvist(2009b)]. HMM was introduced in [Weinan and Engquist(2003),E and Engquist(2003),E and Engquist(2005)]. An a posteriori error estimator was derived in [Ohlberger(2005)]. Fully discrete a priori estimates are presented in [Abdulle(2005)]. LOD was introduced in [Målqvist and Peterseim(2014),Henning et al.(2014a)]. Efficient implementation was recently analyzed in [Engwer et al.(2019)].

All the established methods which employ a coarse grid and use a fixed number of coarse basis functions per coarse grid cell are unsuitable for our setting, as the existence of many channels through a coarse grid cell might require a larger number of ansatz functions in some cells.

Closest to our approach are the developments in the Generalized Multiscale Finite Element Method (GMsFEM), which originated in developments in the MsFEM. MsFEM was introduced in [Hou and Wu(1997)]. An introductory book to the MsFEM was published in [Efendiev and Hou(2009)]. Very similar in spirit is the Residual Free Bubbles Method (RFB) [Sangalli(2003)] where it is proposed to enrich a standard FE space by intra-element bubble functions removing the inside residual, essentially constructing a space very similar to the MsFEM space. An adaptive MsFEM was published in [Henning et al.(2014b)]. In [Efendiev et al.(2011)], the MsFEM space is enriched with eigenfunctions multiplied with a partition of unity, thus an adaptive number of basis functions per coarse cell is used. A postprocessing step is used to differentiate between local basis functions for inclusions, which can be eliminated, and local basis functions for channels. This development led to the GMsFEM, introduced in [Efendiev et al.(2013)]. Plenty of interesting ideas were published in the context of the GMsFEM. GMsFEM uses the idea of the MsFEM and constructs reduced spaces which are spanned by ansatz functions on local patches, using only local information. It allows for non-fixed number of ansatz functions on each local patch. GMsFEM uses local eigenproblems and a partition of unity for basis generation. Adaptive enrichment for the GMsFEM is presented by Chung et al. in [Chung et al.(2018a),Chung et al.(2014)] and online-adaptive enrichment in [Chung et al.(2015)]. Very recently, the Edge Spectral Multiscale Finite Element Method (ESMsFEM) has been proposed in [Fu et al.(2018)], using dominant eigenvectors of the local Dirichlet-to-Neumann (DtN) operator multiplied with a partition of unity as basis functions.

#### 1.4.3. Domain Decomposition Methods

The generation of localized approximation spaces is closely related to the problem of constructing coarse spaces in domain decomposition methods. Especially the adaptive construction of multiscale

---

<sup>1</sup><https://github.com/dune-community/dune-gdt>

coarse spaces for problems with heterogeneous coefficients with high contrast is interesting in this regard. Similar local problems and similar constants are used. However, most research on coarse spaces in domain decomposition methods targets at estimates for the condition of the preconditioned operator matrix while generation of local bases in localized model order reduction targets at the approximation properties of local spaces.

MsFEM coarse spaces are used in [Aarnes and Hou(2002)] for a non overlapping domain decomposition method. In [Graham et al.(2007), Graham and Scheichl(2007)], coarse spaces are constructed where robustness of the Domain Decomposition (DD) iteration in case of large coefficient variations inside of domains can be shown. These approaches still have a fixed number of coarse space functions per domain. In [Galvis and Efendiev(2010)], a large gap in the spectrum of local eigenvalue problems is used to steer the adaptive number of coarse grid basis functions per domain. In [Nataf et al.(2010),Dolean et al.(2012)], coarse spaces are constructed adaptively using an eigenvalue problem based on the DtN operator in each subdomain. Robustness with regard to large coefficient variations which are not confined in a domain (i.e. channels) is shown in [Spillane et al.(2014)], where coarse spaces are constructed from an eigenvalue problem including the partition of unity in the overlap region. Also in the context of finite element tearing and interconnecting - dual primal (FETI-DP), there were similar developments. [Mandel and Sousedik(2007),Pechstein and Scheichl(2008),Klawonn et al.(2016)]. Recently, “optimal” coarse spaces have been proposed leading to convergence in one iteration, see for instance [Gander and Loneland(2017)]. An interesting connection between multiscale methods and domain decomposition methods has been established in [Kornhuber et al.(2018),Kornhuber et al.(2017),Kornhuber and Yserentant(2016)]. Coarse spaces from Approximate Component Mode Synthesis (ACMS) are proposed for two-level overlapping Schwarz in [Heinlein et al.(2018)].

#### 1.4.4. Other Related Developments

CMS Component Mode Synthesis (CMS) component mode synthesis (CMS) introduced in [Hurty(1965),Bampton and Craig(1968)]: uses an approximation based on the eigenmodes of local constrained eigenvalue problems (approximation in the interior of the domain)

To realize a fast simulation response also for large component-based structures it is vital to reduce the number of Degree of Freedom (DoF)s on the ports, too. Within the CMS approach this is realized by utilizing an eigenmode expansion [Bourquin(1992),Hetmaniuk and Lehoucq(2010), Jakobsson et al.(2011),Hetmaniuk and Klawonn(2014)].

## 1.5. Collaborations and Previous Publications

The research presented in this thesis was conducted in collaboration with different partners. Most of the results presented in this dissertation have been published by the authors and collaborators in peer reviewed journals or conference proceedings. In the following, all collaborations and previous publications are given.

1. The numerically stable formulation of the standard a posteriori error estimator for the reduced basis method which is presented in Section 4.5 was developed together with Christian Engwer, Mario Ohlberger, and Stephan Rave. The results have been published in the article  
A. BUHR, C. ENGWER, M. OHLBERGER, S. RAVE. *A Numerically Stable a Posteriori Error Estimator for Reduced Basis Approximations of Elliptic Equations*. In X. O. E. ONATE, A. HUERTA, eds., *Proceedings of the 11th World Congress on Computational Mechanics*. CIMNE, Barcelona, 2014 pp. 4094–4102. doi: n/a [Buhr et al.(2014)].
2. The simulation method ArbiLoMod in Chapter 3, was devised together with Christian Engwer, Mario Ohlberger and Stephan Rave. The first publication presenting ArbiLoMod was the article  
A. BUHR, C. ENGWER, M. OHLBERGER, S. RAVE. *ArbiLoMod, a Simulation Technique Designed for Arbitrary Local Modifications*. *SIAM Journal on Scientific Computing*, 39 (2017a) (4), pp. A1435–A1465. doi: 10.1137/15M1054213 [Buhr et al.(2017a)].
3. ArbiLoMod was tested on the time harmonic Maxwell’s equations in collaboration with Christian Engwer, Mario Ohlberger and Stephan Rave, the results are given in Section 3.6.2 and were published in the article  
A. BUHR, C. ENGWER, M. OHLBERGER, S. RAVE. *ArbiLoMod: Local Solution Spaces by Random Training in Electrodynamics*, pp. 137–148. Springer International Publishing, Cham. ISBN 978-3-319-58786-8, 2017b. doi: 10.1007/978-3-319-58786-8\_9 [Buhr et al.(2017b)].
4. The randomized range finder algorithm presented in Section 5.2 was developed together with Kathrin Smetana. Results were published in the article  
A. BUHR, K. SMETANA. *Randomized Local Model Order Reduction*. *SIAM Journal on Scientific Computing*, 40 (2018) (4), pp. A2120–A2151. doi: 10.1137/17M1138480 [Buhr and Smetana(2018)].
5. The convergence analysis for the online enrichment given in Section 6.3 was done by the author alone. It was published in the article  
A. BUHR. *Exponential Convergence of Online Enrichment in Localized Reduced Basis Methods*. *IFAC-PapersOnLine*, 51 (2017) (2), pp. 302–306. doi: n/a. MATHMOD 2018 [Buhr(2017)].
6. The localized a posteriori error estimator presented in Section 4.1 and the randomized training procedure shown in Section 5.2 were published along with a common framework for localized model order reduction in the book chapter  
A. BUHR, L. IAPICHINO, M. OHLBERGER, S. RAVE, F. SCHINDLER, K. SMETANA. *Handbook on Model Order Reduction*, chap. Localized model reduction for parameterized problems. Walter De Gruyter GmbH, 2019+. Submitted for publication [Buhr et al.(2019)].



## 1.6. Overview over this Document

In the following Chapter 2 we will introduce the abstract, variational problem, detail how stationary heat conduction and the time harmonic Maxwell's equation lead to a problem in variational form and introduce the numerical examples used. In Chapter 3 we present the method ArbiLoMod and show how the parts integrate. Thereafter, three chapters diving deeper into selected topics follow. In Chapter 4 we detail variants of a localized a posteriori error estimator. In Chapter 5 we apply the theory of randomized numerical linear algebra to the problem of localized training, yielding a priori and a posteriori error bounds for randomized training algorithms. In Chapter 6 some first a priori results on convergence of online enrichment are shown and a new enrichment algorithm is introduced. Chapter 7 concludes this thesis.



In this chapter, we present the abstract, variational problem definition consisting of a bilinear or sesquilinear form and a linear or antilinear form on an abstract Hilbert space. We will build upon this formulation throughout this thesis. We introduce the Galerkin projected, reduced problem. Based on the coercivity or the inf-sup stability of the bilinear (sesquilinear) form we will review the most important results, namely uniqueness, stability and best approximation. We introduce the parameterized problem and its affine decomposition. Furthermore, we introduce an abstract notation for localized model order reduction. We detail how the problems of stationary heat conduction and time harmonic electromagnetism in two or three dimensions lead to a problem in this variational form. Finally, we introduce the four examples which are used for numerical experiments in this thesis.

### 2.1. Variational Problem

Let  $V$  be a Hilbert space over the field  $\mathbb{K}$  where  $\mathbb{K}$  is either  $\mathbb{R}$  or  $\mathbb{C}$ . Let further  $a$  be a bilinear or sesquilinear form, which is coercive or inf-sup stable and bounded. Let  $f$  be a linear or antilinear, bounded form on  $V$ . We then define the variational problem as follows.

**Definition 2.1.1** (Variational problem). *Find  $u$  in  $V$ , such that*

$$a(u, v) = f(v) \quad \forall v \in V. \quad (2.1)$$

We denote the stability constant by  $\gamma$ . It is defined as

$$\gamma := \sup_{\varphi_1 \in V \setminus \{0\}, \varphi_2 \in V \setminus \{0\}} \frac{|a(\varphi_1, \varphi_2)|}{\|\varphi_1\| \|\varphi_2\|}. \quad (2.2)$$

The coercivity constant  $\alpha$  and the inf-sup constant  $\beta$  are defined as

$$\alpha := \inf_{\varphi \in V \setminus \{0\}} \frac{|a(\varphi, \varphi)|}{\|\varphi\|^2} \quad (2.3)$$

$$\beta := \inf_{\varphi_1 \in V \setminus \{0\}} \sup_{\varphi_2 \in V \setminus \{0\}} \frac{|a(\varphi_1, \varphi_2)|}{\|\varphi_1\| \|\varphi_2\|}. \quad (2.4)$$

In the inf-sup stable case, we further assume that

$$\inf_{\varphi_2 \in V \setminus \{0\}} \sup_{\varphi_1 \in V \setminus \{0\}} \frac{|a(\varphi_1, \varphi_2)|}{\|\varphi_1\| \|\varphi_2\|} > 0. \quad (2.5)$$

In the coercive case ( $\alpha > 0$ ), the variational problem in Definition 2.1.1 has a unique solution due to the Lax-Milgram lemma [Lax and Milgram(1954), Theorem 2.1] and it holds

$$\|u\| \leq \frac{1}{\alpha} \|f\|_{V'}. \quad (2.6)$$

In the inf-sup stable case ( $\beta > 0$ ), the variational problem in Definition 2.1.1 has a unique solution [Nečas(1962), Théorème 3.1] and it holds

$$\|u\| \leq \frac{1}{\beta} \|f\|_{V'}. \quad (2.7)$$

**Remark 2.1.2** (Antilinear inner product). *We denote the inner product between two vectors  $a$  and  $b$  in  $V$  by  $(a, b)$ . In complex vector spaces, we define the inner product  $(a, b)$  to be linear in the second argument and antilinear in the first argument, i.e. for two vectors  $a$  and  $b$  and a scalar  $\lambda \in \mathbb{C}$  we have*

$$(\lambda a, b) = \bar{\lambda}(a, b) \quad \text{and} \quad (a, \lambda b) = \lambda(a, b). \quad (2.8)$$

*We use this definition because it is prevalent in numerical codes, cf. Appendix E.*

## 2.2. Reduced Problem

At the core of projection based model order reduction is the (Petrov-)Galerkin projection of the variational problem in Definition 2.1.1. We consider only Galerkin projection in this thesis. To define the projected variational problem, let  $\tilde{V}$  be a subspace of  $V$ . We define

**Definition 2.2.1** (Reduced variational problem). *Find  $\tilde{u}$  in  $\tilde{V}$ , such that*

$$a(\tilde{u}, v) = f(v) \quad \forall v \in \tilde{V}. \quad (2.9)$$

Accordingly, we define the reduced stability constant  $\tilde{\gamma}$ , the reduced coercivity constant  $\tilde{\alpha}$ , and the reduced inf-sup constant  $\tilde{\beta}$  by

$$\tilde{\gamma} := \sup_{\varphi_1 \in \tilde{V} \setminus \{0\}, \varphi_2 \in \tilde{V} \setminus \{0\}} \frac{|a(\varphi_1, \varphi_2)|}{\|\varphi_1\| \|\varphi_2\|} \quad (2.10)$$

$$\tilde{\alpha} := \inf_{\varphi \in \tilde{V} \setminus \{0\}} \frac{|a(\varphi, \varphi)|}{\|\varphi\|^2} \quad (2.11)$$

$$\tilde{\beta} := \inf_{\varphi_1 \in \tilde{V} \setminus \{0\}} \sup_{\varphi_2 \in \tilde{V} \setminus \{0\}} \frac{|a(\varphi_1, \varphi_2)|}{\|\varphi_1\| \|\varphi_2\|}. \quad (2.12)$$

### 2.2.1. Properties of Reduced Variational Problem in Coercive Case

From these definitions follows that  $\tilde{\gamma} \leq \gamma$  and  $\tilde{\alpha} \geq \alpha$  and thus in the coercive case it holds

$$\|\tilde{u}\| \leq \frac{1}{\tilde{\alpha}} \|f\|_{V'} \leq \frac{1}{\alpha} \|f\|_{V'}. \quad (2.13)$$

In the coercive case, the reduced variational problem inherits its stability from the full variational problem. Furthermore, it holds the following best approximation theorem.

**Theorem 2.2.2** (Best approximation for coercive problems (Céa's Lemma)). *Let  $a$  be coercive and symmetric. The error of the solution  $\tilde{u}$  of the reduced variational problem in Definition 2.2.1 with respect to the full variational problem in Definition 2.1.1 is bounded by the constant  $\sqrt{\frac{\gamma}{\alpha}}$  times the smallest error possible in  $\tilde{V}$ . It holds*

$$\|u - \tilde{u}\| \leq \sqrt{\frac{\gamma}{\alpha}} \inf_{\tilde{v} \in \tilde{V}} \|u - \tilde{v}\|. \quad (2.14)$$

*Proof.* [Céa(1964), Proposition 3.1] □

### 2.2.2. Properties of Reduced Variational Problem in inf-sup Stable Case

While the reduced problem inherits the coercivity constant from the full problem in the coercive case, the inf-sup stable case is more involved. The stability still holds, i.e.

$$\|\tilde{u}\| \leq \frac{1}{\tilde{\beta}} \|f\|_{V'} \quad (2.15)$$

and there is still a best approximation estimate:

**Theorem 2.2.3** (Best approximation for inf-sup stable problems). *Let  $a$  be inf-sup stable. The error of the solution  $\tilde{u}$  of the reduced variational problem in Definition 2.2.1 with respect to the full variational problem in Definition 2.1.1 is bounded by the constant  $\frac{\gamma}{\tilde{\beta}}$  times the smallest error possible in  $\tilde{V}$ . It holds*

$$\|u - \tilde{u}\| \leq \frac{\gamma}{\tilde{\beta}} \inf_{\tilde{v} \in \tilde{V}} \|u - \tilde{v}\|. \quad (2.16)$$

*Proof.* [Xu and Zikatanov(2003)] □

However, the reduced inf-sup constant  $\tilde{\beta}$  might be larger or smaller than the inf-sup constant in the full space  $\beta$ . This means that the reduced variational problem might not be inf-sup stable at all or have a very small inf-sup constant, even if the full problem has good constants.

## 2.3. Parameterized Problem

While the methods developed in this thesis work well for non parametric problems, they work especially well for parametric problems, inheriting the favorable properties of the reduced basis method, as already described in Section 1.4.1 above. For the parametric case, let  $\mathcal{D} \subset \mathbb{R}^P$  be the parameter space and  $\mu$  in  $\mathcal{D}$  be the parameter. The entities  $a$ ,  $f$ ,  $u$ ,  $\tilde{u}$ ,  $\alpha$ ,  $\tilde{\alpha}$ ,  $\beta$ ,  $\tilde{\beta}$ ,  $\gamma$ , and  $\tilde{\gamma}$  are replaced by parameter dependent counterparts  $a_\mu$ ,  $f_\mu$ ,  $u_\mu$ ,  $\tilde{u}_\mu$ ,  $\alpha_\mu$ ,  $\tilde{\alpha}_\mu$ ,  $\beta_\mu$ ,  $\tilde{\beta}_\mu$ ,  $\gamma_\mu$ , and  $\tilde{\gamma}_\mu$ . The spaces  $V$  and  $\tilde{V}$  are not parameter specific. Moreover, we assume that  $a_\mu$  and  $f_\mu$  exhibit an affine parameter dependence, i.e. there exist parameter independent bilinear forms  $a^q : V \times V \rightarrow \mathbb{K}$  ( $1 \leq q \leq Q_a$ ), continuous (anti-)linear functionals  $f^q \in V'$  ( $1 \leq q \leq Q_f$ ) and coefficient functionals  $\theta_a^q : \mathcal{D} \rightarrow \mathbb{K}$  and  $\theta_f^q : \mathcal{D} \rightarrow \mathbb{K}$  such that

$$a_\mu(\varphi_1, \varphi_2) = \sum_{q=1}^{Q_a} \theta_a^q(\mu) a^q(\varphi_1, \varphi_2) \quad \text{and} \quad f_\mu(\varphi) = \sum_{q=1}^{Q_f} \theta_f^q(\mu) f^q(\varphi). \quad (2.17)$$

We further assume that there is a lower bound for the coercivity constant  $\alpha_{\text{LB}} \in \mathbb{R}$  for which holds

$$0 < \alpha_{\text{LB}} \leq \alpha_\mu \quad \forall \mu \in \mathcal{D} \quad (2.18)$$

and an upper bound for the continuity constant  $\gamma_{\text{UB}} \in \mathbb{R}$  for which holds

$$\gamma_{\text{UB}} \geq \gamma_\mu \quad \forall \mu \in \mathcal{D}. \quad (2.19)$$

## 2.4. Localized Model Order Reduction

In this section, we introduce an abstract notation for localized model order reduction. First, we define an abstract localizing space decomposition and subsequently detail how we define the model order reduction based on this decomposition.

### 2.4.1. Localizing Space Decomposition

Localization of the reduced basis method is based on a space decomposition of a global space  $V$ . We define an abstract localizing space decomposition.

**Definition 2.4.1** (Localizing Space Decomposition). *A localizing space decomposition consists of*

1. an open, bounded and connected domain  $\Omega \subset \mathbb{R}^d$  with smooth boundary,
2. a Hilbert space  $V$  of functions on  $\Omega$  which is a continuous or discrete function space,
3.  $N_{V_i}$  subdomains  $\omega_i$  which form an overlapping or non overlapping domain decomposition of the global domain  $\Omega$ ,
4.  $N_{V_i}$  local spaces  $V_i$  which are subspaces of the global ansatz space  $V$  and satisfy

$$\sum_i V_i = V \quad (2.20)$$

and

$$\text{supp}(\varphi) \subseteq \omega_i \quad \forall \varphi \in V_i, \quad (2.21)$$

5.  $N_{V_i}$  linear mappings  $\mathcal{P}_{V_i} : V \rightarrow V_i$  for which it holds

$$\sum_i \mathcal{P}_{V_i}(\varphi) = \varphi \quad \forall \varphi \in V. \quad (2.22)$$

### 2.4.2. Localized Model Order Reduction

Based on the abstract space decomposition introduced above, we can define an abstract scheme for localized model order reduction. The core task in localized model order reduction is the construction of reduced subspaces  $\tilde{V}_i \subset V_i$  for all localized spaces. Each local reduced subspace  $\tilde{V}_i$  should approximate the local part of the solution  $\mathcal{P}_{V_i}(u_\mu)$ . The global reduced space is then defined as

$$\tilde{V} := \sum_i \tilde{V}_i \quad (2.23)$$

which is used as the reduced space in the Problem in Definition 2.2.1.

### 2.4.3. Examples for Localizing Space Decomposition

We present two examples for localizing space decompositions. The space decomposition used mostly throughout this thesis, the “wirebasket space decomposition”, is introduced in Section 3.2.

#### Restriction Decomposition

Let  $V^{\text{DG}}$  be a discrete DG space on a fine mesh on the domain  $\Omega$ . Let  $\omega_i^{\text{no1}}$ ,  $i \in \{1, \dots, N_{\text{no1}}\}$  be a non overlapping domain decomposition which is resolved by the fine mesh:

$$\bar{\Omega} = \bigcup_{i=1}^{N_{\text{no1}}} \overline{\omega_i^{\text{no1}}} \quad \omega_i^{\text{no1}} \cap \omega_j^{\text{no1}} = \emptyset \text{ for } i \neq j. \quad (2.24)$$

In this setting, we can define the local spaces as

$$V_i^{\text{res}} := \left\{ \varphi|_{\omega_i^{\text{no1}}} \mid \varphi \in V^{\text{DG}} \right\} \quad (2.25)$$

and define the linear mappings  $\mathcal{P}_{V_i^{\text{res}}}$  as the restriction of  $\varphi \in V^{\text{DG}}$  to  $\omega_i^{\text{noI}}$ :

$$\mathcal{P}_{V_i^{\text{res}}}(\varphi) := \varphi|_{\omega_i^{\text{noI}}}. \quad (2.26)$$

We call  $\left\{ \Omega, V^{\text{DG}}, \{\omega_i^{\text{noI}}\}_{i=1}^{N_{\text{noI}}}, \{V_i^{\text{res}}\}_{i=1}^{N_{\text{noI}}}, \{\mathcal{P}_{V_i^{\text{res}}}\}_{i=1}^{N_{\text{noI}}} \right\}$  the "restriction decomposition". This is the space decomposition used in the LRBMS [Ohlberger and Schindler(2015)]. It has the advantages that it is easy to understand, the mappings to the local subspaces are projections, and functions which are in two different local subspaces can not be linear dependent. Its main disadvantage is that the function space has to be a DG space. A restriction decomposition can not be implemented on top of existing FEM codes using conforming function spaces.

#### *Partition of Unity Decomposition*

Another option is to base the space decomposition on a continuous partition of unity on an overlapping domain decomposition  $\omega_i^{\text{ol}}$ . Let  $\omega_i^{\text{ol}}, i \in \{1, \dots, N_{\text{ol}}\}$  be an overlapping domain decomposition which is resolved by the fine mesh. Let further  $\varrho_i$  be a partition of unity functions for which it holds

$$\varrho_i \geq 0, \quad \sum_i \varrho_i \equiv 1, \quad \text{supp}(\varrho_i) \subseteq \omega_i^{\text{ol}}, \quad \|\nabla \varrho_i\|_{L^\infty} < C \quad (2.27)$$

and let  $V_h$  be a global finite element space. With a linear interpolation operator  $\mathcal{I} : V \rightarrow V_h$ , the local spaces are defined as

$$V_i^{\text{pou}} := \left\{ \mathcal{I}(\varrho_i \varphi) \mid \varphi \in V_h \right\} \quad (2.28)$$

and the linear mappings are defined as

$$\mathcal{P}_{V_i^{\text{pou}}}(\varphi) := \mathcal{I}(\varrho_i \varphi) \quad \forall \varphi \in V_h. \quad (2.29)$$

We call  $\left\{ \Omega, V_h, \{\omega_i^{\text{ol}}\}_{i=1}^{N_{\text{ol}}}, \{V_i^{\text{pou}}\}_{i=1}^{N_{\text{ol}}}, \{\mathcal{P}_{V_i^{\text{pou}}}\}_{i=1}^{N_{\text{ol}}} \right\}$  the "partition of unity decomposition". This space decomposition is quite popular. It or its continuous counterpart is used for example in the partition of unity finite element method [Melenk and Babuška(1996)] and in the Generalized Finite Element Method (GFEM) [Strouboulis et al.(2001)]. It is easy to understand and easy to implement. Its main disadvantage is the fact that functions in different local subspaces sharing support can be linear dependent. This can lead to singular system matrices. Note that the restriction decomposition can be seen as a partition of unity decomposition with a discontinuous partition of unity.

## **2.5. Heat Conduction**

In this section, we define the problem of stationary heat conduction and derive the corresponding bilinear and linear form of the underlying physical equations. While we aim at the time harmonic Maxwell's equation in this thesis, it is often beneficial to test numerical methods on the simpler case of the stationary heat equation first. The stationary heat equation leads to a coercive bilinear form and thus avoids stability problems in the model order reduction, which are discussed above in Section 2.2.2.

### *2.5.1. Full Heat Conduction Equation*

The full heat equation is a parabolic Partial Differential Equation (PDE) describing the diffusion of heat over time. The unknown is the temperature  $u(x, t)$ , a scalar field dependent on space and time. With the space dependent heat conductivity  $\sigma(x)$  and a space and time dependent heating term  $q(x, t)$ , the full heat equation reads

$$\frac{\partial}{\partial t} u(x, t) = \text{div}(\sigma(x) \nabla u(x, t)) + q(x, t). \quad (2.30)$$

The gradient of the temperature  $\nabla u(x, t)$  leads to a flux of thermal energy of  $\sigma(x)\nabla u(x, t)$ . The divergence of this flux of thermal energy results in a temperature change over time. This equation is assumed to hold pointwise. It does not define a solution  $u$  without specifying a domain, boundary, and initial conditions.

### 2.5.2. Stationary Heat Conduction

Systems governed by the full heat equation (Equation (2.30)) evolve towards a steady state if the heat term  $q(x, t)$  does not depend on time (and thus is stationary). This steady state is characterized by a vanishing time derivative. We can compute the steady state solution using the stationary heat equation, which we derive from the full heat equation (Equation (2.30)) by setting the time derivative to zero and replacing the space and time dependent fields by only space dependent fields  $u(x)$  and  $q(x)$ . We obtain

$$-\operatorname{div}\left(\sigma(x)\nabla u(x)\right) = q(x). \quad (2.31)$$

### 2.5.3. Weak Formulation of Heat Conduction

For the FE approximation, one considers the stationary heat equations in weak form. We consider the problem on a domain  $\Omega$  which we assume to be Lipschitz. We multiply by a sufficiently smooth test function  $v$  and integrate over the calculation domain  $\Omega$ . We obtain

$$-\int_{\Omega} \operatorname{div}\left(\sigma(x)\nabla u(x)\right)v(x) \, dx = \int_{\Omega} q(x)v(x) \, dx. \quad (2.32)$$

Using the identity

$$\operatorname{div}\left(\sigma(x)\nabla u(x)v(x)\right) = \operatorname{div}\left(\sigma(x)\nabla u(x)\right)v(x) + \sigma(x)\nabla u(x) \cdot \nabla v(x) \quad (2.33)$$

and Stokes' law

$$\int_{\Omega} \operatorname{div}\left(\sigma(x)\nabla u(x)v(x)\right) \, dx = \int_{\partial\Omega} \sigma(x)\left(\nabla u(x) \cdot n\right)v(x) \, dx \quad (2.34)$$

where  $n$  is the outer unit normal, we can rewrite Equation (2.32) as

$$\int_{\Omega} \sigma(x)\nabla u(x) \cdot \nabla v(x) \, dx - \int_{\partial\Omega} \sigma(x)\left(\nabla u(x) \cdot n\right)v(x) \, dx = \int_{\Omega} q(x)v(x) \, dx. \quad (2.35)$$

In this form, we only require  $H^1$  regularity and can formulate the problem in the variational form with the bilinear form and linear form

$$\begin{aligned} a(u, v) &:= \int_{\Omega} \sigma(x)\nabla u(x) \cdot \nabla v(x) \, dx - \int_{\partial\Omega} \sigma(x)\left(\nabla u(x) \cdot n\right)v(x) \, dx \\ f(v) &:= \int_{\Omega} q(x)v(x) \, dx. \end{aligned} \quad (2.36)$$

For a parameterized heat conductivity  $\sigma_{\mu}(x)$ , the bilinear form inherits the affine parameter dependence if the heat conductivity itself has an affine parameter dependence of the form

$$\sigma_{\mu}(x) = \sum_{q=1}^{Q_{\sigma}} \theta_{\sigma}^q(\mu)\sigma^q(x). \quad (2.37)$$

On the boundary  $\Gamma$  we impose either Dirichlet boundary conditions

$$u(x) = 0 \quad \text{on } \Gamma_D \quad (2.38)$$



or Neumann boundary conditions

$$\nabla u(x) \cdot n = 0 \quad \text{on } \Gamma_N \quad (2.39)$$

where  $\Gamma_D \cup \Gamma_N = \Gamma := \partial\Omega$  and we assume  $\Gamma_D$  has a measure greater zero, so Friedrich's inequality holds.

We consider the space

$$V := \left\{ \varphi \in H^1(\Omega) \mid \varphi|_{\Gamma_D} = 0 \right\} \quad (2.40)$$

where the restriction to the boundary is to be understood in the sense of traces.

The problem defined in Definition 2.1.1 with the bilinear and linear form defined in Equation (2.36) poses a well defined problem in the space  $V$  defined above if  $\sigma$  is bound from below and from above, i.e.

$$0 < \sigma_{\min} \leq \sigma(x) \leq \sigma_{\max} \quad \forall x \in \Omega. \quad (2.41)$$

In the usual  $H^1(\Omega)$  norm it holds  $\gamma \leq \sigma_{\max}$  and  $\alpha \geq \frac{\sigma_{\min}}{1+c_F^2}$  where  $c_F$  is the constant in the Friedrich's inequality  $\|u\|_{L^2(\Omega)} \leq c_F \|\nabla u\|_{L^2(\Omega)}$ . Because of the coercivity and continuity of  $a$ , we could also use the energy norm induced by  $\|\varphi\|_E^2 := (\varphi, \varphi)_E := a(\varphi, \varphi)$  where the coercivity and continuity constant are equal to one, but we stick to the  $H^1$  norm throughout this thesis.

For the FE discretization, we use linear finite elements.

## 2.6. Maxwell's Equations

### 2.6.1. Full Maxwell's Equations in Original Form

The Maxwell's equations were first published by James Clerk Maxwell in 1861 [Maxwell(1861)] and 1865 [Maxwell(1865)]. However, he did not have the vector notation which is common today. The form of the Maxwell's equations which is commonly in use today and stated below was published by Oliver Heaviside in 1892 [Heaviside(1892)]. In Maxwell's equations, the unknowns are the electric field  $\mathbf{E}$ , the electric flux  $\mathbf{D}$ , the magnetic field  $\mathbf{H}$ , and the magnetic flux  $\mathbf{B}$ . In addition, there is the charge density  $\varrho$  and the current density  $\mathbf{J}$ , which are sources or unknowns, depending on the problem setting.  $\mathbf{E}$ ,  $\mathbf{D}$ ,  $\mathbf{H}$ ,  $\mathbf{B}$ , and  $\mathbf{J}$  are space- and time-dependent vector fields while  $\varrho$  is a space- and time-dependent scalar field. The classic Maxwell's equations read

$$\nabla \cdot \mathbf{D} = \varrho \quad (2.42a)$$

$$\nabla \cdot \mathbf{B} = 0 \quad (2.42b)$$

$$\nabla \times \mathbf{E} = -\frac{\partial}{\partial t} \mathbf{B} \quad (2.42c)$$

$$\nabla \times \mathbf{H} = \frac{\partial}{\partial t} \mathbf{D} + \mathbf{J}. \quad (2.42d)$$

Together with the electric permittivity  $\varepsilon$  and the magnetic permeability  $\mu_0$  in the material laws

$$\mathbf{D} = \varepsilon \mathbf{E} \quad \mathbf{B} = \mu_0 \mathbf{H} \quad (2.43)$$

and suitable boundary conditions they define the problem. Equation (2.42a) is also known as Gauss's law, Equation (2.42b) is also known as Gauss's law for magnetism, Equation (2.42c) is also known as Faraday's law, and Equation (2.42d) is also known as Ampère's law with Maxwell's addition.

The material properties  $\varepsilon$  and  $\mu_0$  are in general time, space, and field dependent tensors, but we assume them to be only space dependent scalars throughout this thesis. We only consider examples where the magnetic permeability is equal to the magnetic permeability in vacuum  $\mu_0$ .

### 2.6.2. Time Harmonic Maxwell's Equation

Depending on the application, it might be advantageous to consider the time harmonic Maxwell's equations. The time harmonic Maxwell's equations can be derived in two ways (see also [Monk(2003), Zaglmayr(2006)]). One either assumes that all quantities are time harmonic and uses the ansatz

$$\mathbf{X}(x, t) = \Re \left( \widehat{\mathbf{X}}(x) e^{i\omega t} \right) \quad (2.44)$$

for  $\mathbf{X}$  in  $\{\mathbf{E}, \mathbf{D}, \mathbf{H}, \mathbf{B}, \varrho, \mathbf{J}\}$  where  $\widehat{\mathbf{E}}(x), \widehat{\mathbf{D}}(x), \widehat{\mathbf{H}}(x), \widehat{\mathbf{B}}(x)$ , and  $\widehat{\mathbf{J}}(x)$  are complex valued vector fields only dependent on space and  $\widehat{\varrho}(x)$  is a complex valued scalar field only dependent on space.

The second option to obtain the time harmonic Maxwell's equations is to use the Fourier transform of the fields involved and use

$$\widehat{\mathbf{X}}(x, \omega) = \int_{-\infty}^{\infty} \mathbf{X}(x, t) e^{-i\omega t} dt \quad \mathbf{X}(x, t) = \frac{1}{2\pi} \int_{-\infty}^{\infty} \widehat{\mathbf{X}}(x, \omega) e^{i\omega t} d\omega \quad (2.45)$$

for  $\mathbf{X}$  in  $\{\mathbf{E}, \mathbf{D}, \mathbf{H}, \mathbf{B}, \varrho, \mathbf{J}\}$ . Under the assumption that the materials are linear, one can obtain the time harmonic Maxwell's equations

$$\nabla \cdot \widehat{\mathbf{D}} = \widehat{\varrho} \quad (2.46a)$$

$$\nabla \cdot \widehat{\mathbf{B}} = 0 \quad (2.46b)$$

$$\nabla \times \widehat{\mathbf{E}} = -i\omega \widehat{\mathbf{B}} \quad (2.46c)$$

$$\nabla \times \widehat{\mathbf{H}} = i\omega \widehat{\mathbf{D}} + \widehat{\mathbf{J}} \quad (2.46d)$$

where  $\omega$  is the angular frequency. In the following, we do not differentiate between the time-dependent and time-harmonic quantities.

### 2.6.3. Reduction to one Unknown Field

Maxwell's equations can be reduced to one equation for the electric field by first dividing Faraday's law (Equation (2.42c)) by the magnetic permeability  $\mu_0$  and taking its curl, obtaining

$$\nabla \times \frac{1}{\mu_0} \nabla \times \mathbf{E} = -\nabla \times \frac{\partial}{\partial t} \mathbf{H}. \quad (2.47)$$

Exchanging the curl with the time derivative on the right hand side and plugging in Ampère's law (Equation (2.42d)) one obtains

$$\nabla \times \frac{1}{\mu_0} \nabla \times \mathbf{E} = -\frac{\partial^2}{\partial t^2} \varepsilon \mathbf{E} - \frac{\partial}{\partial t} \mathbf{J} \quad (2.48)$$

or in the time harmonic setting

$$\nabla \times \frac{1}{\mu_0} \nabla \times \mathbf{E} = \omega^2 \varepsilon \mathbf{E} - i\omega \mathbf{J}. \quad (2.49)$$

We will use this equation as starting point for our simulations.

### 2.6.4. Weak Formulation of Time Harmonic Maxwell's Equation

For the FE approximation, one considers Maxwell's equations in weak form. We consider the problem on a domain  $\Omega$  which we assume to be Lipschitz. For the time harmonic setting, one starts with Equation (2.49), multiplies it with a sufficiently smooth, vector valued test function and integrates over the domain  $\Omega$ . In the weak setting, we denote the solution for the electric field

by  $u$  and the test function by  $\bar{v}$  and omit the space dependency for notational brevity. One obtains

$$\int_{\Omega} \left( \nabla \times \frac{1}{\mu_0} \nabla \times u - \omega^2 \varepsilon u \right) \cdot \bar{v} \, dx = -i\omega \int_{\Omega} \mathbf{J} \cdot \bar{v} \, dx \quad \forall v \in V. \quad (2.50)$$

We use Stokes' theorem (see e.g. [Monk(2003), Eq. 3.27])

$$\int_{\Omega} (\nabla \times \mathbf{X}) \cdot \bar{v} \, dV = \int_{\Omega} \mathbf{X} \cdot (\nabla \times \bar{v}) \, dV + \int_{\partial\Omega} (n \times \mathbf{X}) \cdot \bar{v} \, dA \quad (2.51)$$

where  $n$  is the outer normal on the boundary. Applying this with  $\mathbf{X} = \frac{1}{\mu_0} \nabla \times u$  yields

$$\int_{\Omega} \frac{1}{\mu_0} (\nabla \times u) \cdot (\nabla \times \bar{v}) - \omega^2 \varepsilon u \cdot \bar{v} \, dx + \int_{\partial\Omega} \left( n \times \frac{1}{\mu_0} \nabla \times u \right) \cdot \bar{v} \, dx = -i\omega \int_{\Omega} \mathbf{J} \cdot \bar{v} \, dx \quad \forall v \in V. \quad (2.52)$$

The term

$$\int_{\partial\Omega} \left( n \times \frac{1}{\mu_0} \nabla \times u \right) \cdot \bar{v} \, dx \quad (2.53)$$

is a triple product, which is invariant under cyclic permutation. So it is equal to

$$\int_{\partial\Omega} \left( \frac{1}{\mu_0} \nabla \times u \right) \cdot (\bar{v} \times n) \, dx. \quad (2.54)$$

On the boundary  $\Gamma := \partial\Omega$  we impose either Dirichlet, Neumann, or conducting wall boundary conditions. We denote the parts of the boundary by  $\Gamma_D$ ,  $\Gamma_N$ , and  $\Gamma_R$  respectively and assume  $\Gamma_D \cup \Gamma_N \cup \Gamma_R = \Gamma$ . On the Dirichlet boundary we set the tangential part of the electric field to zero

$$u \times n = 0 \quad \text{on } \Gamma_D. \quad (2.55)$$

On the Neumann boundary we set the normal derivative to the electric field to zero

$$n \times \nabla \times u = 0 \quad \text{on } \Gamma_N. \quad (2.56)$$

On the conducting wall boundary, we impose the radiation condition (cf. [Monk(2003), Eq. (1.25c)]<sup>1</sup>)

$$\left( n \times \frac{1}{\mu_0} \nabla \times u \right) \cdot \bar{v} = i\omega\kappa u_T \quad (2.57)$$

where  $u_T = n \times (u \times n)$  is the tangential part of the solution at the boundary and  $\kappa$  is the specific electric conductivity at the boundary.

The problem can thus be formulated using a sesquilinear form and an antilinear form defined by

$$\begin{aligned} a(u, v; \omega) &:= \int_{\Omega} \frac{1}{\mu_0} (\nabla \times u) \cdot (\nabla \times \bar{v}) - \varepsilon \omega^2 (u \cdot \bar{v}) \, dx \\ &\quad + i\omega\kappa \int_{\Gamma_R} (u \times n) \cdot (\bar{v} \times n) \, dx, \\ f(v; \omega) &:= -i\omega \int_{\Omega} (\mathbf{J} \cdot \bar{v}) \, dx \end{aligned} \quad (2.58)$$

where  $\omega$  is again the angular frequency. Note that we have chosen the sesquilinear form to be antilinear in the test function, as this is the common choice in the literature (cf. Appendix E). We see  $\omega$  as a parameterization to this problem.

We consider the space

$$V := \left\{ \varphi \in H(\text{curl}, \Omega) \mid (\varphi \times n) \big|_{\Gamma_D} = 0 \right\} \quad (2.59)$$

<sup>1</sup>Note that we use a different sign convention than Peter Monk.

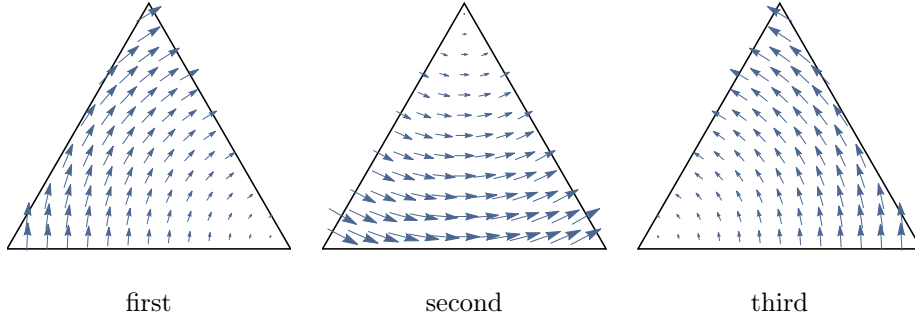


Figure 2.1.: Visualization of Nédélec ansatz functions (edge elements) for one triangle (reproduction: Appendix A.1).

where the restriction to the boundary is to be understood in the sense of traces. The space  $H(\text{curl}, \Omega)$  is defined as usual as

$$H(\text{curl}, \Omega) := \left\{ \varphi \in (L^2(\Omega))^d \mid \nabla \times \varphi \in (L^2(\Omega))^d \right\}. \quad (2.60)$$

We consider the problem defined in Definition 2.1.1 with the bilinear and linear form defined in Equation (2.58) in the space  $V$  defined above. We use the problem specific inner product

$$\begin{aligned} (\varphi_1, \varphi_2) &:= \int_{\Omega} \frac{1}{\mu_0} (\nabla \times \varphi_2) \cdot (\nabla \times \bar{\varphi}_1) + \varepsilon \omega_{\max}^2 (\varphi_2 \cdot \bar{\varphi}_1) \, dx \\ &\quad + \omega_{\max} \kappa \int_{\Gamma_R} (\varphi_2 \times n) \cdot (\bar{\varphi}_1 \times n) \, dx \end{aligned} \quad (2.61)$$

and the thereby induced norm where  $\omega_{\max}$  is the problem specific maximum angular frequency considered. We can thus estimate the continuity constant by one, but we cannot in general estimate the inf-sup constant from below. Obtaining a lower bound for the inf-sup constant is a challenging task which we omit in this thesis. Lower bounds can be obtained numerically for example by solving an eigenvalue problem or by the Successive Constraint Method (SCM) [Huynh et al.(2007), Chen et al.(2009)], but these approaches are unsuitable for our targeted application.

The bilinear form has an affine parameter dependence

$$a(u, v; \omega) = a_{cc}(u, v) - \omega^2 a_{ii}(u, v) + i\omega a_b(u, v) \quad (2.62)$$

with

$$a_{cc} := \int_{\Omega} \frac{1}{\mu_0} (\nabla \times u) \cdot (\nabla \times \bar{v}) \quad (2.63a)$$

and

$$a_{ii} := \int_{\Omega} \varepsilon (u \cdot \bar{v}) \, dx \quad (2.63b)$$

and

$$a_b := \int_{\Gamma_R} \kappa (u \times n) \cdot (\bar{v} \times n) \, dx. \quad (2.63c)$$

### 2.6.5. Finite Element Approximation in $H(\text{curl}, \Omega)$

For the finite element approximation of  $H(\text{curl}, \Omega)$  the most common approach is to use Nédélec's ansatz functions. Nédélec published two articles introducing his ansatz functions, one in 1980 [Nedelec(1980)] and the second in 1986 [Nedelec(1986)]. For the construction of higher order  $H(\text{curl}, \Omega)$  conforming elements, we refer to [Zaglmayr(2006)]. In this thesis, Nédélec elements of first kind of lowest order are used, as formulated in [Zaglmayr(2006), Lemma 4.12]. These elements are also called Whitney elements, as they appeared in [Whitney(1957)]. For a visualization of these ansatz functions, see Figure 2.1.

### 2.6.6. 2D Version of Maxwell's Equations

There are two common variants of deriving two dimensional equations from the three dimensional Maxwell's equations, which are shown in the following. We denote the three space dimensions by  $x$ ,  $y$ , and  $z$  and we will eliminate the  $z$ -direction. In both variants, one assumes that the derivatives with respect to the  $z$  dimension vanish for all quantities, i.e.

$$0 = \frac{\partial}{\partial z} \mathbf{E}_x = \frac{\partial}{\partial z} \mathbf{E}_y = \frac{\partial}{\partial z} \mathbf{E}_z = \frac{\partial}{\partial z} \mathbf{D}_x = \frac{\partial}{\partial z} \mathbf{D}_y = \frac{\partial}{\partial z} \mathbf{D}_z = \frac{\partial}{\partial z} \mathbf{H}_x = \dots \quad (2.64)$$

We present the two approaches in the following.

#### Normal Electric Approach

The first common approach is to assume that the electric field has only a component perpendicular to the  $xy$ -plane and the magnetic field has only components in the plane. One assumes

$$0 = \mathbf{E}_x = \mathbf{E}_y = \mathbf{H}_z = \rho = \mathbf{J}_x = \mathbf{J}_y. \quad (2.65)$$

This assumptions lead to a good approximation of electric fields between two Perfect Electric Conductor (PEC) plates separated by a very small gap. With these assumptions, Maxwell's equations reduce to

$$\nabla \cdot \mathbf{D} = \frac{\partial}{\partial x} \mathbf{D}_x + \frac{\partial}{\partial y} \mathbf{D}_y + \frac{\partial}{\partial z} \mathbf{D}_z = 0 \quad (2.66a)$$

$$\nabla \cdot \mathbf{B} = \frac{\partial}{\partial x} \mathbf{B}_x + \frac{\partial}{\partial y} \mathbf{B}_y + \frac{\partial}{\partial z} \mathbf{B}_z = \frac{\partial}{\partial x} \mathbf{B}_x + \frac{\partial}{\partial y} \mathbf{B}_y = 0 \quad (2.66b)$$

$$\nabla \times \mathbf{E} = \begin{pmatrix} \partial_y \mathbf{E}_z - \partial_z \mathbf{E}_y \\ \partial_z \mathbf{E}_x - \partial_x \mathbf{E}_z \\ \partial_x \mathbf{E}_y - \partial_y \mathbf{E}_x \end{pmatrix} = \begin{pmatrix} \partial_y \mathbf{E}_z \\ -\partial_x \mathbf{E}_z \\ 0 \end{pmatrix} = -\frac{\partial}{\partial t} \mathbf{B} \quad (2.66c)$$

$$\nabla \times \mathbf{H} = \begin{pmatrix} \partial_y \mathbf{H}_z - \partial_z \mathbf{H}_y \\ \partial_z \mathbf{H}_x - \partial_x \mathbf{H}_z \\ \partial_x \mathbf{H}_y - \partial_y \mathbf{H}_x \end{pmatrix} = \begin{pmatrix} 0 \\ 0 \\ \partial_x \mathbf{H}_y - \partial_y \mathbf{H}_x \end{pmatrix} = \frac{\partial}{\partial t} \mathbf{D} + \mathbf{J}. \quad (2.66d)$$

or in short

$$\frac{\partial}{\partial x} \mathbf{B}_x + \frac{\partial}{\partial y} \mathbf{B}_y = 0 \quad (2.67a)$$

$$\partial_x \mathbf{H}_y - \partial_y \mathbf{H}_x = \frac{\partial}{\partial t} \mathbf{D}_z + \mathbf{J}_z \quad (2.67b)$$

$$\begin{pmatrix} \partial_y \mathbf{E}_z \\ -\partial_x \mathbf{E}_z \end{pmatrix} = -\frac{\partial}{\partial t} \begin{pmatrix} \mathbf{B}_x \\ \mathbf{B}_y \end{pmatrix}. \quad (2.67c)$$

Applying the same procedure as in Section 2.6.3, we end up with the Helmholtz-like equation

$$\operatorname{div} \left( \frac{1}{\mu_0} \operatorname{grad} (\mathbf{E}_z) \right) + \omega^2 \varepsilon \mathbf{E}_z = i\omega \mathbf{J}_z \quad (2.68)$$

for the time harmonic case. This equation is scalar. In the development of numerical methods for Maxwell's equations, it is often a good first step to analyze this equation. It requires only little modifications of codes which were written for the heat equation but already exposes the challenges of inf-sup stable problems. In this thesis, this equation is used in Section 5.3.

*Normal Magnetic Approach*

The second common approach is to assume that the electric field has only components in the plane and that the magnetic field is perpendicular to the plane. One assumes

$$0 = \mathbf{E}_z = \mathbf{H}_x = \mathbf{H}_y = \mathbf{J}_z. \quad (2.69)$$

With these assumptions, Maxwell's equations reduce to

$$\nabla \cdot \mathbf{D} = \frac{\partial}{\partial x} \mathbf{D}_x + \frac{\partial}{\partial y} \mathbf{D}_y + \frac{\partial}{\partial z} \mathbf{D}_z = \frac{\partial}{\partial x} \mathbf{D}_x + \frac{\partial}{\partial y} \mathbf{D}_y = \varrho \quad (2.70a)$$

$$\nabla \cdot \mathbf{B} = \frac{\partial}{\partial x} \mathbf{B}_x + \frac{\partial}{\partial y} \mathbf{B}_y + \frac{\partial}{\partial z} \mathbf{B}_z = 0 = 0 \quad (2.70b)$$

$$\nabla \times \mathbf{E} = \begin{pmatrix} \partial_y \mathbf{E}_z - \partial_z \mathbf{E}_y \\ \partial_z \mathbf{E}_x - \partial_x \mathbf{E}_z \\ \partial_x \mathbf{E}_y - \partial_y \mathbf{E}_x \end{pmatrix} = \begin{pmatrix} 0 \\ 0 \\ \partial_x \mathbf{E}_y - \partial_y \mathbf{E}_x \end{pmatrix} = -\frac{\partial}{\partial t} \mathbf{B} \quad (2.70c)$$

$$\nabla \times \mathbf{H} = \begin{pmatrix} \partial_y \mathbf{H}_z - \partial_z \mathbf{H}_y \\ \partial_z \mathbf{H}_x - \partial_x \mathbf{H}_z \\ \partial_x \mathbf{H}_y - \partial_y \mathbf{H}_x \end{pmatrix} = \begin{pmatrix} \partial_y \mathbf{H}_z \\ -\partial_x \mathbf{H}_z \\ 0 \end{pmatrix} = \frac{\partial}{\partial t} \mathbf{D} + \mathbf{J}. \quad (2.70d)$$

or in short

$$\frac{\partial}{\partial x} \mathbf{D}_x + \frac{\partial}{\partial y} \mathbf{D}_y = \varrho \quad (2.71a)$$

$$\partial_x \mathbf{E}_y - \partial_y \mathbf{E}_x = -\frac{\partial}{\partial t} \mathbf{B}_z \quad (2.71b)$$

$$\begin{pmatrix} \partial_y \mathbf{H}_z \\ -\partial_x \mathbf{H}_z \end{pmatrix} = \frac{\partial}{\partial t} \begin{pmatrix} \mathbf{D}_x \\ \mathbf{D}_y \end{pmatrix} + \begin{pmatrix} \mathbf{J}_x \\ \mathbf{J}_y \end{pmatrix}. \quad (2.71c)$$

Applying the same procedure as in Section 2.6.3, one obtains

$$\begin{pmatrix} \partial_y \frac{1}{\mu_0} \partial_y \mathbf{E}_x - \partial_y \frac{1}{\mu_0} \partial_x \mathbf{E}_y \\ \partial_x \frac{1}{\mu_0} \partial_x \mathbf{E}_y - \partial_x \frac{1}{\mu_0} \partial_y \mathbf{E}_x \end{pmatrix} + \omega^2 \varepsilon \begin{pmatrix} \mathbf{E}_x \\ \mathbf{E}_y \end{pmatrix} = i\omega \begin{pmatrix} \mathbf{J}_x \\ \mathbf{J}_y \end{pmatrix}. \quad (2.72)$$

In the development of numerical methods for Maxwell's equations, it is often a good second step to analyze this equation. It is vector-valued, thus requiring vector-valued ansatz functions like Nédélec ansatz functions and the usual discretization has a low frequency instability. But the problems arising from discretizing this equation are still two dimensional and thus the number of unknowns stays rather small in comparison with a three dimensional problem. In this thesis, this equation is used in the example presented in Section 2.7.3 and analyzed in Section 3.6.2.

## 2.7. Examples Used for Numerical Experiments

In this section, we define the problems which are used as examples in the numerical experiments. We use four different examples: The *Thermal Block Example*, the *Thermal Channels Example*, the *2D Maxwell Example*, and the *Olimex A64 Example*. Their numerical treatment is increasingly challenging. *Thermal Channels Example* adds high contrast and thereby strong nonlocal effects, *2D Maxwell Example* is additionally vector-valued and inf-sup stable and *Olimex A64 Example* is the most challenging, having channels, inf-sup stability, vector-valued unknowns and a high DoF count. In Section 5.3 we will introduce two additional examples: The *Rangefinder Example 1* and *Rangefinder Example 2*. They are used only in that particular chapter and thus stated there.

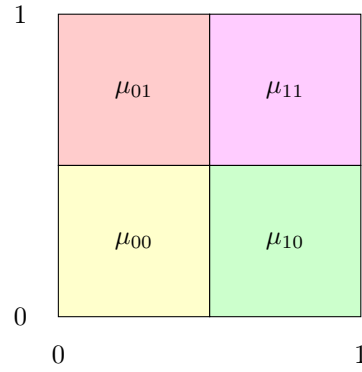


Figure 2.2.: Geometry of *Thermal Block Example*: Four blocks of constant, but parameterized, heat conductivity.

### 2.7.1. Thermal Block Example

The first numerical example we denote by *Thermal Block Example*. It is a simple parametric example which is often used in introductory texts on parameterized model order reduction (for example in [Patera and Rozza(2007)] or [Haasdonk(2017)]).

We solve the problem in Definition 2.1.1 with the bilinear form and the linear form defined as in Equation (2.36) and the space  $V$  defined in Equation (2.40). On the domain  $\Omega := (0, 1)^2$  we consider the stationary heat conduction (cf. Equation (2.31))

$$-\operatorname{div}(\sigma(x)\nabla u(x)) = 1 \quad (2.73)$$

with Dirichlet zero boundary conditions on  $\Gamma_D := \partial\Omega$ . The heat conductivity is defined as

$$\sigma_\mu := \sum_{i,j=0}^1 \mu_{ij} \cdot \chi_{[i/2,(i+1)/2] \times [j/2,(j+1)/2]} \quad (2.74)$$

(see Figure 2.2), denoting by  $\chi_A$  the characteristic function of the set  $A$ . This heat conductivity has an affine parameter decomposition as specified in Equation (2.37) and thus the corresponding bilinear form has an affine parameter decomposition. Denoting the local blocks by

$$\begin{aligned} \Omega_{00} &:= (0, 0.5) \times (0, 0.5) & \Omega_{10} &:= (0.5, 1) \times (0, 0.5) \\ \Omega_{01} &:= (0, 0.5) \times (0.5, 1) & \Omega_{11} &:= (0.5, 1) \times (0.5, 1) \end{aligned} \quad (2.75)$$

the affine decomposition of the bilinear form is

$$\begin{aligned} a_\mu(u, v) &= \mu_{00} \int_{\Omega_{00}} \nabla u \cdot \nabla v \, dx + \mu_{10} \int_{\Omega_{10}} \nabla u \cdot \nabla v \, dx \\ &+ \mu_{01} \int_{\Omega_{01}} \nabla u \cdot \nabla v \, dx + \mu_{11} \int_{\Omega_{11}} \nabla u \cdot \nabla v \, dx. \end{aligned} \quad (2.76)$$

The parameters  $\mu := \{\mu_{ij}\}_{i,j=0}^1$  were allowed to vary in the space  $\mathcal{D} = [0.1, 1.0]^4$ .

The problem is discretized using linear finite elements on a regular mesh with  $500 \times 500 \times 4$  triangular entities, an example solution is shown in Figure 2.3. Discretization is done using pyMOR – Model Order Reduction with Python (pyMOR). The *Thermal Block Example* is used in Section 4.5.

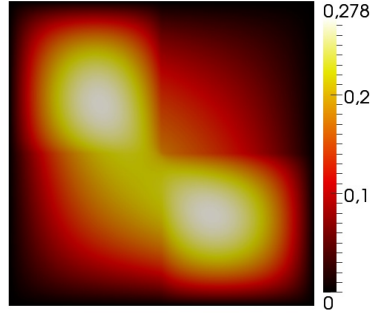


Figure 2.3.: High-dimensional solution of Equation (2.73) in *Thermal Block Example* for  $\mu = (0.1, 1.0, 0.4, 0.1)$ . (reproduction: Appendix A.2)

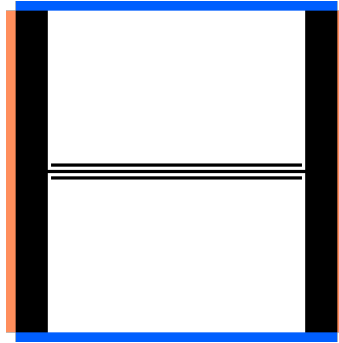


Figure 2.4.: First structure in sequence of simulated structures in *Thermal Channels Example*. Unit square with high and low conductivity regions. White: constant conductivity region ( $\sigma = 1$ ), black: parameterized high conductivity region ( $\sigma_\mu = 1 + \mu$ ). Homogeneous Neumann boundaries  $\Gamma_N$  at top and bottom marked blue, inhomogeneous Dirichlet boundaries  $\Gamma_D$  at left and right marked light red.

### 2.7.2. Example for Stationary Heat Equation With Channels

The second numerical example is an example of heat conduction, but with the additional features of having a very high contrast (up to  $10^5$ ) and conducting channels. We denote the second numerical example by *Thermal Channels Example*. We solve the problem in Definition 2.1.1 with the bilinear form and the linear form defined as in Equation (2.36) and the space  $V$  defined in Equation (2.40).

As we target on changing geometries with local changes, we define a sequence of five geometries. We consider heat conduction without heat sources in the domain on the unit square  $\Omega := (0, 1)^2$ . We approximate  $u_\mu$  solving

$$-\nabla \cdot (\sigma_\mu \nabla u_\mu) = 0. \quad (2.77)$$

We apply homogeneous Neumann boundaries at the top and the bottom

$$\Gamma_N := ((0, 1) \times 0) \cup ((0, 1) \times 1) \quad (2.78)$$

and inhomogeneous Dirichlet boundaries at the left and right:

$$u_\mu = 1 \text{ on } \Gamma_{D,1} := 0 \times (0, 1) \quad u_\mu = -1 \text{ on } \Gamma_{D,-1} := 1 \times (0, 1) \quad (2.79)$$

(see also Figure 2.4).



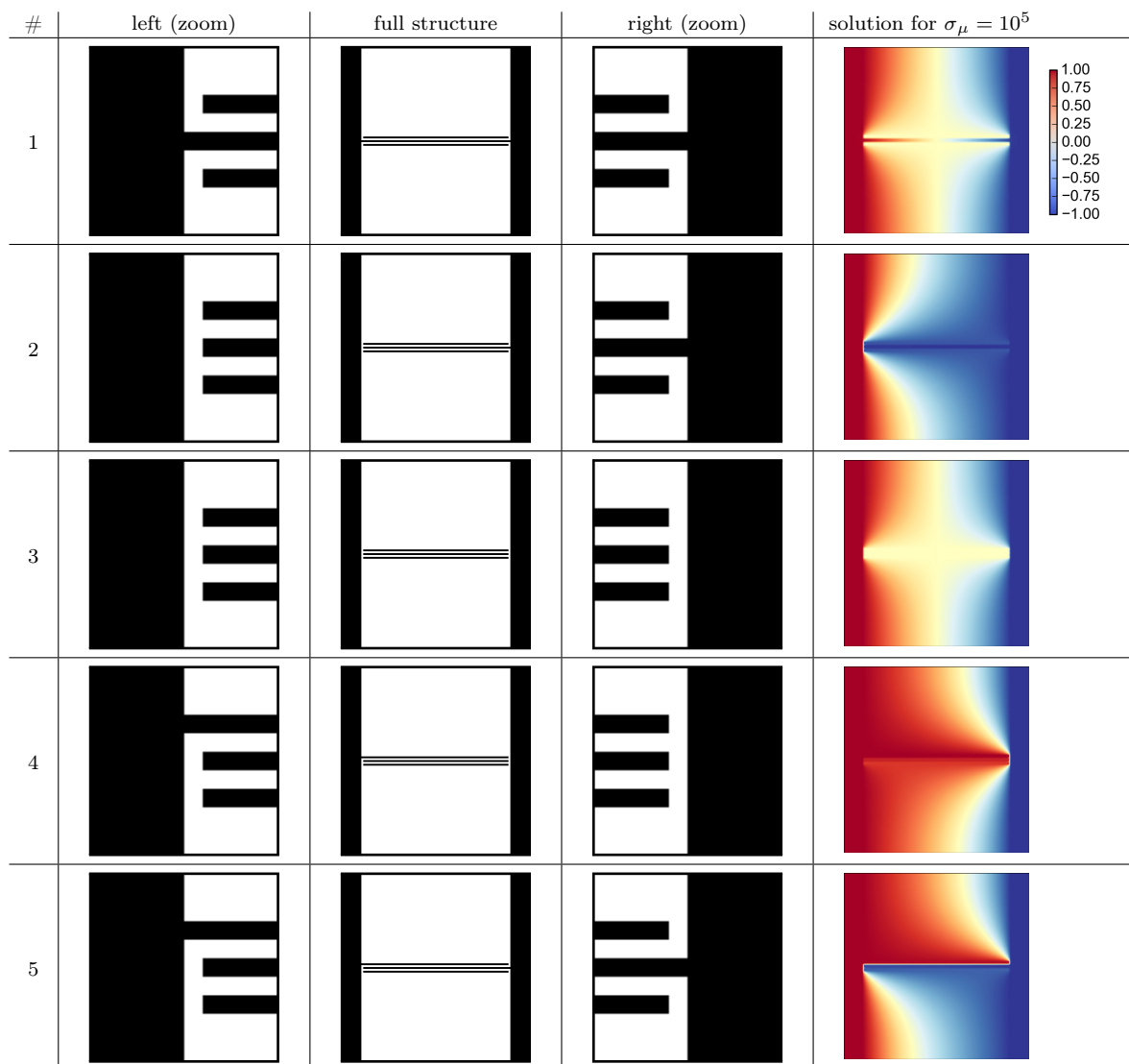


Figure 2.5.: Sequence of structures simulated in *Thermal Channels Example* along with solutions for one parameter value. Localized changes in the geometry cause global changes in the solution. (reproduction: Appendix A.3)

The unit square is partitioned into two regions: one region with constant heat conductivity  $\sigma_\mu = 1$  and one region with constant, but parameterized conductivity

$$\sigma_\mu = 1 + \mu \text{ where } \mu \in \mathcal{D} := [10^0, 10^5]. \quad (2.80)$$

We call this second region the “high conductivity region”  $\Omega_{h,i}$ . For reproduction or benchmarking, we give precise definitions in the following. In the first geometry, the high conductivity region is

$$\begin{aligned} \Omega_{h,1} := & [(0.0, 0.1) \times (0, 1)] \cup [(0.9, 1.0) \times (0, 1)] \cup \\ & [(0.11, 0.89) \times (0.475, 0.485)] \cup [(0.1, 0.9) \times (0.495, 0.505)] \cup \\ & [(0.11, 0.89) \times (0.515, 0.525)], \end{aligned} \quad (2.81)$$

see also Figure 2.4. The inhomogeneous Dirichlet boundary conditions are handled by a shift function  $u_s$  and we solve for  $u_0$  having homogeneous Dirichlet values where  $u = u_0 + u_s$ . The parameterization of the conductivity in the high conductivity region,  $\sigma_\mu$ , leads to a term in the affine decomposition of the bilinear form. The affine decomposition of the bilinear form and linear form are

$$\begin{aligned} a_\mu(u_0, \varphi) &= \mu \int_{\Omega_{h,i}} \nabla u_0 \cdot \nabla \varphi \, dx + \int_{\Omega} \nabla u_0 \cdot \nabla \varphi \, dx \\ f_\mu(\varphi) &= -\mu \int_{\Omega_{h,i}} \nabla u_s \cdot \nabla \varphi \, dx - \int_{\Omega} \nabla u_s \cdot \nabla \varphi \, dx. \end{aligned} \quad (2.82)$$

The coercivity constant  $\alpha_\mu$  of the corresponding bilinear form with respect to the  $H^1$  norm is bounded from below by  $\alpha_{LB} := \frac{\sigma_{\min}}{c_F^2 + 1}$  where  $\sigma_{\min}$  is the minimal conductivity and  $c_F = \frac{1}{\sqrt{2\pi}}$ . The problem is discretized using  $P^1$  ansatz functions on a structured triangle mesh with maximum triangle size  $h$ . The mesh is carefully constructed to resolve the high conductivity regions, i.e.  $h$  is chosen to be  $1/n$  where  $n$  is a multiple of 200. To mimic “arbitrary local modifications”, the high conductivity region is changed slightly four times, which leads to a sequence of five structures to be simulated in total. The high conductivity regions are defined as:

$$\begin{aligned} \Omega_{h,2} &:= \Omega_{h,1} \setminus [(0.1, 0.11) \times (0.495, 0.505)] \\ \Omega_{h,3} &:= \Omega_{h,2} \setminus [(0.89, 0.9) \times (0.495, 0.505)] \\ \Omega_{h,4} &:= \Omega_{h,3} \cup [(0.1, 0.11) \times (0.515, 0.525)] \\ \Omega_{h,5} &:= \Omega_{h,4} \cup [(0.89, 0.9) \times (0.495, 0.505)] \end{aligned} \quad (2.83)$$

These modifications only affect a very small portion of the domain (actually, only 0.01%), but for high contrast configurations, they lead to global changes in the solution, see Figure 2.5. The *Thermal Channels Example* is used in Section 3.6.1. A slightly modified version of this example, which is driven by a right hand side instead of inhomogeneous Dirichlet boundary conditions is defined and used in Section 6.5.

### 2.7.3. Example for 2D Maxwell Equation

The third example is a two dimensional Maxwell example. We solve the problem in Definition 2.1.1 with the bilinear form and the linear form defined as in Equation (2.58) and the space  $V$  as defined in Equation (2.59). With the two dimensional Maxwell’s equations in the normal magnetic approach as specified in Section 2.6.6. We simulate on the unit square  $\Omega := (0, 1) \times (0, 1)$  with robin boundary conditions at  $\Gamma_R := 0 \times (0, 1) \cup 1 \times (0, 1)$  and Dirichlet zero boundary conditions at  $\Gamma_D := (0, 1) \times 0 \cup (0, 1) \times 1$ . The surface impedance parameter  $\kappa$  is chosen as the impedance of free space,  $\kappa = 1/376.73$  Ohm. We introduce some structure by inserting PEC into the domain and thus shrinking  $\Omega$  and enlarging  $\Gamma_D$ , see Figure 2.6. The PEC is modeled as Dirichlet zero

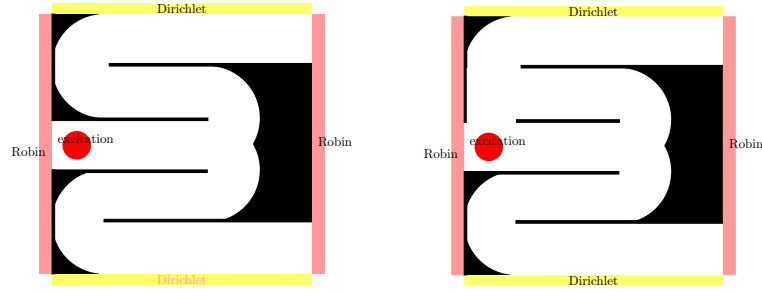


Figure 2.6.: Geometries simulated in *2D Maxwell Example*. Black area is not part of the domain and treated as Dirichlet zero boundary. Note that the change is topology changing.

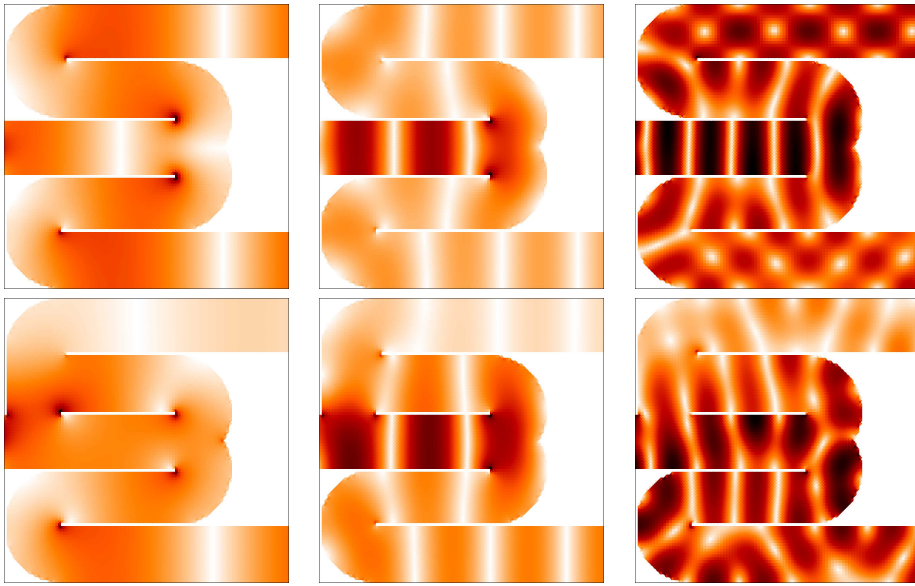
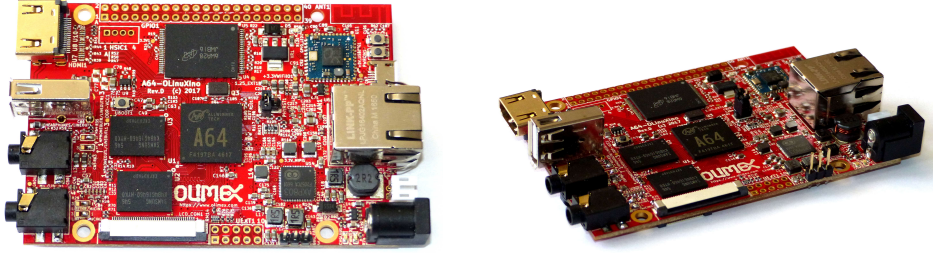


Figure 2.7.: Example solutions for *2D Maxwell Example* for  $\omega = 2\pi \cdot 186$  MHz,  $\omega = 2\pi \cdot 561$  MHz and  $\omega = 2\pi \cdot 1$  GHz for the first and second geometry. Plotted is  $|\Re(\mathbf{E})|$ . (reproduction: Appendix A.4)

boundary condition. Note that the geometry is slightly asymmetric intentionally, to produce more interesting behavior. The mesh does not resolve the geometry. Rather, we use a structured mesh and remove all degrees of freedom which are associated with an edge whose center is inside of the PEC structure. The structured mesh consists of  $100 \times 100$  squares, each of which is divided into four triangles. With each edge, one degree of freedom is associated, which results in 60200 degrees of freedom, some of which are “disabled” because they are in PEC or on a Dirichlet boundary. The parameter domain is the range from 10 MHz to 1 GHz. For the discretization, the software package pyMOR is used. To simulate an “arbitrary local modification”, the part of the PEC within  $(0.01, 0.2) \times (0.58, 0.80)$  is removed and the simulation domain is enlarged. The excitation is a current of

$$\mathbf{J}(x, y) := \exp\left(-\frac{(x - 0.1)^2 + (y - 0.5)^2}{1.25 \cdot 10^{-3}}\right) \cdot \mathbf{e}_y. \quad (2.84)$$

To get an impression of the solutions, some example solutions are plotted in Figure 2.7. The *2D Maxwell Example* is used in Section 3.6.2.

Figure 2.8.: Front and perspective view of *Olimex A64 Example*.

#### 2.7.4. *Olimex A64 Example*

The fourth example is the *Olimex A64 Example*. Here we solve the problem in Definition 2.1.1 with the bilinear form and the linear form defined as in Equation (2.58) and the space  $V$  defined in Equation (2.59). The *Olimex A64 Example* is an example from the targeted application domain: Signal integrity simulation in a high frequency Printed Circuit Board (PCB). It features high geometrical complexity: The geometry is described by six layers of metal, separated by insulating layers (cf. Figure 2.11). In addition, we simulate a layer of air above and below the board. In each metal layer, the shape of the metal is described by polygons. The polygonal description of all metal layers have combined 280.378 vertices. Photos of the board are shown in Figures 2.8 and 2.9. In the experiments, we will be especially concerned with the metal traces connecting CPU and RAM, see right picture in Figure 2.9. Meandering traces are used to get correct signal runtimes. The geometry is provided by the creator and manufacturer Olimex<sup>2</sup>. It is published on Github<sup>3</sup>. We provide a snapshot of the project files used in this thesis at Zenodo [Olimex(2019)] and a snapshot of the software project KiCad, which can read the project file, at [Buhr(2019)]. The calculation domain is

$$\Omega := [(-0.35, 90.35) \times (-0.35, 62.85) \times (-0.35, 1.95)] \text{ mm}^3, \quad (2.85)$$

which is the size of the PCB ( $[(0, 90) \times (0, 62.5) \times (0, 1.6)] \text{ mm}^3$ ) and a surrounding layer of air of  $0.35 \text{ mm}$  thickness. On the outer boundaries, we use Neumann boundary conditions on  $\Gamma_N := \partial\Omega$ . The metal layers are modeled as thin PEC sheets which pose internal Dirichlet boundary conditions. In the air layers, we assume an electric permittivity of  $\varepsilon = \varepsilon_0 = \frac{1}{\mu_0 C^2} \approx 8.854 \cdot 10^{-12} \frac{\text{F}}{\text{m}}$  where  $C = 299792458 \frac{\text{m}}{\text{s}}$  is the speed of light. In the insulating layers, we assume an electric permittivity of  $\varepsilon = \varepsilon_r \cdot \varepsilon_0$  with  $\varepsilon_r = 4.5$  which is a typical relative permittivity in FR4 material which is a typical material for PCBs. For the discretization we use a structured mesh of  $960 \times 673 \times 33 = 21,320,640$  cubes with lowest order Nédélec ansatz functions, which leads to approximately 65 million DoFs, see Figure 2.10 for a part of the mesh. The *Olimex A64 Example* is used in Section 5.4.

<sup>2</sup><https://www.olimex.com>

<sup>3</sup><https://github.com/OLIMEX/OLINUXINO>

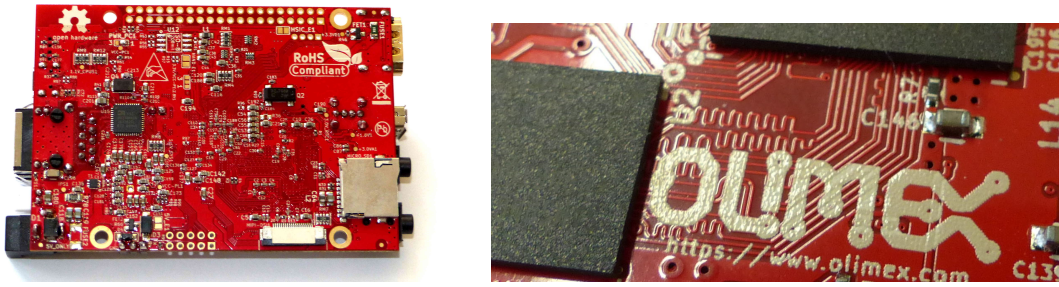


Figure 2.9.: Back and detail view of *Olimex A64 Example*. In the right picture, the meandering traces between the CPU (top) and the RAM (left) are visible.

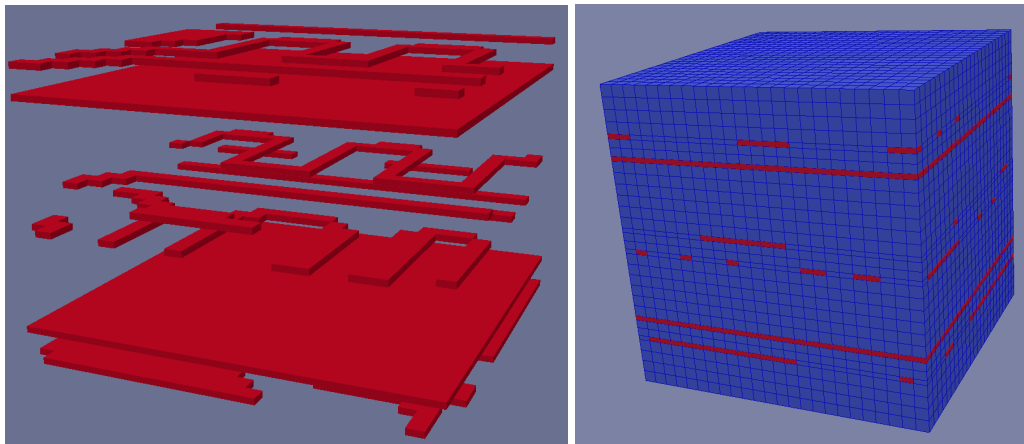


Figure 2.10.: Meshed detail of *Olimex A64 Example*. Metal parts, modeled as Dirichlet boundaries, are shown in red. A staircase approximation of the geometry is used.

	air	350 $\mu\text{m}$	$\epsilon_r = 1$
	copper	35 $\mu\text{m}$	
	prepreg	127 $\mu\text{m}$	$\epsilon_r = 4.5$
	copper	35 $\mu\text{m}$	
	FR4	500 $\mu\text{m}$	$\epsilon_r = 4.5$
	copper	35 $\mu\text{m}$	
	prepreg	127 $\mu\text{m}$	$\epsilon_r = 4.5$
	copper	35 $\mu\text{m}$	
	FR4	500 $\mu\text{m}$	$\epsilon_r = 4.5$
	copper	35 $\mu\text{m}$	
	prepreg	127 $\mu\text{m}$	$\epsilon_r = 4.5$
	copper	35 $\mu\text{m}$	
	air	350 $\mu\text{m}$	$\epsilon_r = 1$

Figure 2.11.: Stackup of *Olimex A64 Example*: Six layers of metal with insulating layers in between. Data provided by Olimex in private communication.



In order to overcome the limitations of existing methods, we devised the simulation methodology ArbiLoMod, named after its main design goal of handling arbitrary local modifications. In this chapter, ArbiLoMod is presented. We discuss the design goals, review the most important design decisions and define the method. ArbiLoMod is a localized model order reduction method as introduced in Section 2.4.2, based on a localizing space decomposition and a Galerkin projection. To define it, first the wirebasket space decomposition is presented. Second, localized basis generation algorithms for interfaces and volume spaces are introduced. Third, a residual based online enrichment is proposed. The fourth major ingredient, a localized a posteriori error estimator, is postponed to Chapter 4 because of its importance, but also because it is coupled only loosely to ArbiLoMod and might be useful in other settings. We conclude this chapter by numerical experiments for the stationary heat equation and time harmonic Maxwell's equation.

### 3.1. Method Design

ArbiLoMod was devised to be a method engineers can rely upon, while at the same time incorporating advanced mathematical algorithms. Besides the ability to handle arbitrary local modifications, the design goals were:

1. Capability of handling interfaces with very complex geometry and complex field patterns on the interfaces.
2. Little communication, possibly at the cost of CPU cycles, to be performant in current cloud environments.
3. Implementable on top of existing, conforming FE codes.
4. Little data dependencies, in order to reuse as many intermediate results as possible after a localized geometry change.
5. Reliable results: The method gives a result of sufficient quality or raise a warning.

To meet these requirements, we designed a new space decomposition which will be described in the following Section 3.2 and structured three core parts (see Figure 3.1) of the algorithm around it:

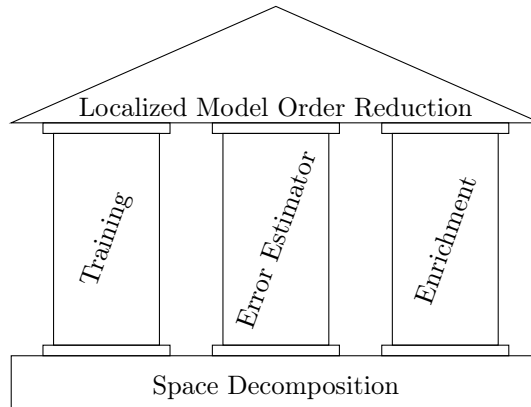


Figure 3.1.: Main components of localized model order reduction

- Localized training
- Localized a posteriori error estimation
- Localized online enrichment

Those parts form a global loop, as visualized in Figure 3.2. Even though there is a global loop, ArbiLoMod is not designed to be an iterative solution method. Rather, it should deliver a solution of sufficient quality in the first iteration. Only if this fails, online enrichment is employed.

### 3.1.1. Design Decision: Handling Channels

Numerical multiscale methods like the MsFEM or the LOD have a fixed number of basis functions per coarse grid element and the basis functions are computed on an oversampling domain. When applying such a method to a problem with channels, some modification has to be made. When a number of channels passes an element and its oversampling region, the basis construction can not know which of these channels is active. So at least one basis function per channel is necessary. If the number of channels is higher than the fixed number of basis functions per coarse grid element, the method probably fails to deliver good results. There are three possible solutions in this situation. The first one is to adapt the coarse mesh, steered by an error indicator. That way, the coarse mesh cells shrink until they contain less channels than they have basis functions. The second option is to increase the oversampling region, to yield more information about the channels in the basis construction. The third option is to allow a variable, adaptive number of basis functions per coarse grid element.

To keep the implementation simple, we would like to keep the coarse mesh fixed and independent of the geometry, therefore we do not want to adapt the coarse mesh. The second option, increasing the oversampling region, would lead to very large oversampling regions in the simulation of PCBs, as the channels are very long. Additionally, it would break the desired localization. The option we have chosen for ArbiLoMod is the third one: Having an adaptive number of basis functions per coarse grid element.

### 3.1.2. Design Decision: Interface Spaces

One major decision in the design of localized model order reduction methods is whether or not to use interface spaces. Many methods do not use interface spaces: For example GFEM, LRBMS,



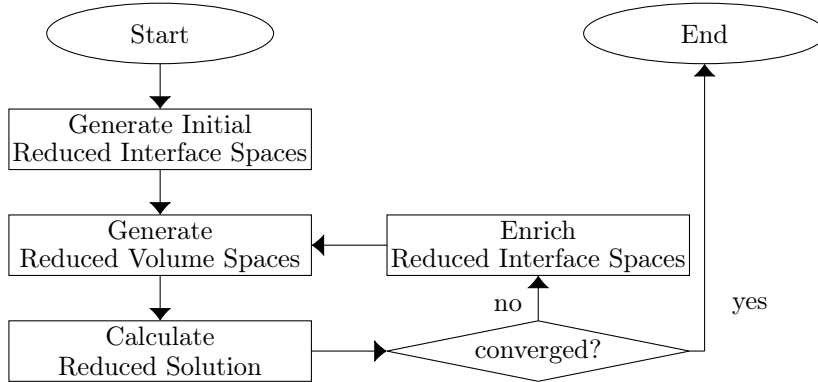


Figure 3.2.: Overview of ArbiLoMod. Generation of initial reduced interface spaces by training and of reduced volume spaces by greedy basis generation is subject of Section 3.3 and Chapter 5. Convergence is assessed with the localized a posteriori error estimator presented in Chapter 4. Enrichment is discussed in Section 3.4 and Chapter 6. On each geometry change, the procedure starts over, where new initial interface spaces are only generated in the region affected by the change.

SRBE, and GMsFEM do not employ interface spaces while CMS, RBE, and PR-SCRBE use them. The methods without interface spaces tend to be easier to implement, as there is usually only one type of local space, while methods with interface spaces have at least spaces associated with volumes and spaces associated with interfaces. The same is reflected in the mathematical description of the methods. Interface spaces lead to more complexity in notation. However, we decided to employ interface spaces, as they lead to a reduction of computational requirements in our setting, due to two reasons: First, interface spaces can usually be approximated by smaller reduced spaces than volume spaces. This is beneficial when coupling is done through the interface spaces, it can reduced communication in a parallel implementation. Second, the generation of a reduced approximation space for an interface space is usually computationally less expensive than the generation of a volume space. This is beneficial in a possible parallel implementation, where the generation of the same space on different compute nodes is desirable to avoid communication of unreduced quantities.

### 3.1.3. Design Decision: Using $a$ -harmonic Extensions

The decision to employ interface spaces is contrary to the design goal of being implementable on top of existing, conforming FE codes. Existing, conforming FE codes usually do not feature interface spaces for mortar-type coupling. Interface spaces can be formed by all ansatz functions having support on that interface. We define these spaces below as “basic spaces” in Section 3.2. However, using these spaces directly would have some disadvantages: First, the mappings into the local subspaces would have a large operator norm in the  $H^1$  norm or energy norm, because very steep gradients would be introduced. Second, it would lead to a bad condition of the reduced system matrices, because of these gradients. Third, the properties of the interface spaces would be very dependent on the fine mesh. These drawbacks can be avoided when using  $a$ -harmonic extensions which spread the support of the interface functions to the adjacent domains by solving a local problem. This will be described in detail below in Section 3.2. Additionally, it has the advantage of smaller reduced volume spaces when the extension is done by solving the underlying equation.

### 3.2. Space Decomposition

In the following, the wirebasket space decomposition, which is used in ArbiLoMod, is defined. Two other common localizing space decompositions were introduced in Section 2.4.3: the partition of unity decomposition on overlapping domains and the restriction decomposition on non overlapping domains. In contrast to the partition of unity decomposition and the restriction decomposition, the wirebasket decomposition which we introduce here is problem dependent, as the bilinear form is used in its construction. The choice of the space decomposition heavily affects the performance of every part of the method.

To define the wirebasket space decomposition, we assume that a variational problem as defined in Definition 2.1.1 is given, which depends on a number of parameters  $\mu \in \mathcal{D}$  as described in Section 2.3. We further assume that the global function space  $V_h$  is a FE approximation space on a fine mesh which resolves a non overlapping domain decomposition  $\{\omega_i^{\text{noI}}\}_{i=1}^{N_{\text{noI}}}$  as defined in Section 2.4.3. The wirebasket space decomposition is defined on non overlapping domains, but has continuous local spaces with overlapping support. The non overlapping domain decomposition forms a coarse mesh. The local spaces  $V_i^{\text{wb}}$  are associated with the vertices, edges, faces and volumes of this coarse mesh. The functions associated with a mesh entity are defined by the function values on that entity. However, they are extended to the neighboring domains to form continuous functions. In the following, we introduce definitions for the different kinds of spaces needed in the wirebasket space decomposition. We first define “basic subspaces” and then, based on these, we define the wirebasket decomposition.

We formulate the method on a discrete level. The definitions here mirror the implementation, wherein the FE ansatz functions are grouped and associated with entities of the coarse mesh, and afterwards basis functions spanning multiple of these groups are constructed.

#### Basic Subspaces

$V_h$  denotes a discrete ansatz space, spanned by ansatz functions  $\{\psi_i\}_{i=1}^N =: \mathcal{B}$ . We assume that the ansatz functions have a localized support, which is true for many classes of ansatz functions like Lagrange- or Nédélec-type functions. To obtain the subspaces we classify the ansatz functions by their support and define each subspace as the span of all ansatz functions of one class. Let  $\omega_i^{\text{noI}}$  be a non overlapping domain decomposition as introduced in Section 2.4.3. For each  $\psi$  in  $\mathcal{B}$ , we call  $I_\psi$  the set of indices of subdomains that have non-empty intersection with the support of  $\psi$ , i.e.

$$I_\psi := \left\{ i \in \{1, \dots, N_{\text{noI}}\} \mid \text{supp}(\psi) \cap \omega_i^{\text{noI}} \neq \emptyset \right\}. \quad (3.1)$$

Let further  $\{\mathcal{E}_i\}_{i=1}^{N_\mathcal{E}}$  be a collection of all inner mesh entities of the coarse mesh formed by the subdomains  $\omega_i^{\text{noI}}$ , i.e. all mesh elements, all inner mesh faces, all inner mesh edges and all inner mesh vertices, where  $N_\mathcal{E}$  is the number of all inner mesh entities of the coarse mesh. We associate one basic subspace with each of them. In order to do so, we call  $I_{\mathcal{E}_i}$  the set of indices of subdomains that contain the coarse mesh element  $\mathcal{E}_i$ , i.e.

$$I_{\mathcal{E}_j} := \left\{ i \in \{1, \dots, N_{\text{noI}}\} \mid \mathcal{E}_j \subseteq \overline{\omega_i^{\text{noI}}} \right\}. \quad (3.2)$$

We define index sets for each codimension:

$$\begin{aligned} \Upsilon_0 &:= \left\{ i \in \{1, \dots, N_\mathcal{E}\} \mid \text{codim}(\mathcal{E}_i) = 0 \right\}, \\ \Upsilon_1 &:= \left\{ i \in \{1, \dots, N_\mathcal{E}\} \mid \text{codim}(\mathcal{E}_i) = 1 \right\}, \\ \Upsilon_2 &:= \left\{ i \in \{1, \dots, N_\mathcal{E}\} \mid \text{codim}(\mathcal{E}_i) = 2 \right\}. \end{aligned} \quad (3.3)$$

The classification is very similar to the classification of mesh nodes in domain decomposition methods, see for example [Klawonn and Widlund(2006), Definition 3.1] or [Toselli and Widlund(2005), Definition 4.2].

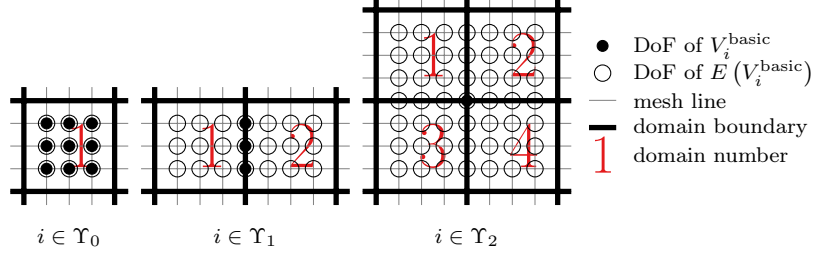


Figure 3.3.: Visualization of basic spaces  $V_i^{\text{basic}}$  and their extension spaces for  $Q^1$  ansatz functions (one DoF per mesh node).

**Definition 3.2.1** (Basic subspaces). *For each element  $i \in \{1, \dots, N_{\mathcal{E}}\}$  we define a basic subspace  $V_i^{\text{basic}}$  of  $V_h$  as:*

$$V_i^{\text{basic}} := \text{span} \left\{ \psi \in \mathcal{B} \mid I_{\psi} = I_{\mathcal{E}_i} \right\}.$$

**Remark 3.2.2** (Basic space decomposition). *The definition of  $V_i^{\text{basic}}$  induces a direct decomposition of  $V_h$ . It holds*

$$V_h = \bigoplus_{i \in \{1, \dots, N_{\mathcal{E}}\}} V_i^{\text{basic}}.$$

#### Wirebasket Space Decomposition

Based on the basic subspaces defined in the previous section, we define the spaces of the wirebasket space decomposition here.

For each of the spaces  $V_i^{\text{basic}}$  defined in Definition 3.2.1, we calculate extensions. The extensions are computed on the “extension space”  $E(V_i^{\text{basic}})$  which is defined as

$$E(V_i^{\text{basic}}) := \bigoplus \left\{ V_j^{\text{basic}} \mid I_{\mathcal{E}_j} \subseteq I_{\mathcal{E}_i} \right\}. \quad (3.4)$$

The functions in one extension space have support in a corresponding extension domain

$$\omega_i^{\text{ext}} := \sum_{j \in I_{\mathcal{E}_i}} \overset{\circ}{\omega_j^{\text{no1}}}. \quad (3.5)$$

Examples for extension spaces are given in Figure 3.3. For each space  $V_i^{\text{basic}}$ , a linear extension operator  $\text{Extend}$  is defined:

$$\text{Extend} : V_i^{\text{basic}} \rightarrow E(V_i^{\text{basic}}). \quad (3.6)$$

For all  $i$  in  $\Upsilon_0$ ,  $\text{Extend}$  is just the identity. For all  $i$  in  $\Upsilon_1$ , we extend by solving the homogeneous version of the equation with Dirichlet zero boundary values for one (arbitrary) chosen  $\bar{\mu} \in \mathcal{D}$ . For all  $i$  in  $\Upsilon_2$ ,  $\text{Extend}$  is defined by first extending linearly to zero on all edges in the extension domain, i.e. in all basic spaces in  $E(V_i^{\text{basic}})$  which belong to  $\Upsilon_1$ . Then, in a second step, the homogeneous version of the equation with Dirichlet boundary values is solved on the basic spaces in  $E(V_i^{\text{basic}})$  which belong to  $\Upsilon_0$ . The procedure is visualized in Figure 3.5. The functions constructed by this two step procedure are the same as the MsFEM basis functions used by Hou and Wu [Hou and Wu(1997)]. Note that the base functions for  $V_i^{\text{wb}}, i \in \Upsilon_2$  form a partition of unity in the interior of the coarse partition of the domain. They can be completed to form a partition of unity on the whole coarse partition of the domain if suitable base functions for the vertices at the boundary of the domain are added. This will be used below for the robust and efficient localization of

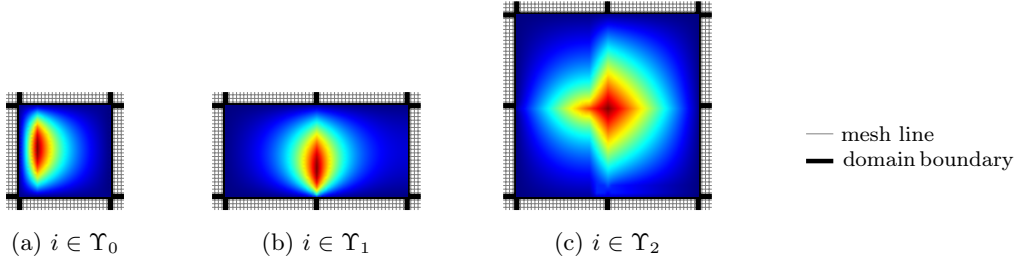


Figure 3.4.: Visualization of some example elements of the local subspaces  $V_i^{\text{wb}}$  for inhomogeneous coefficients. The structure in the solution results from variations in the heat conduction coefficient.

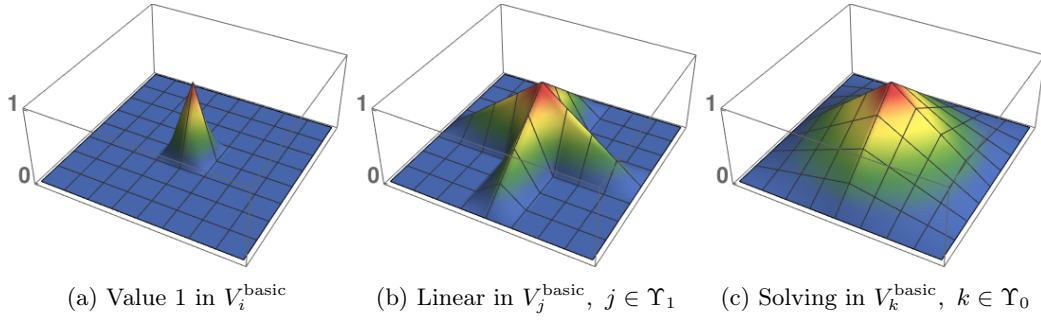


Figure 3.5.: Extend operator is executed in two steps for spaces  $V_i^{\text{wb}}, i \in \Upsilon_2$ . Mesh and spaces as depicted in Figure 3.3. (reproduction: Appendix A.5)

an a posteriori error estimator. Examples of extended functions for all codimensions are given in Figure 3.4. In the case of the Laplace equation these basis functions coincide with the hat functions on the coarse partition (see Figure 3.5). The choice of hat function can be an alternative choice that allows for a better a priori bound of the constants in the localized a posteriori error estimator, as their gradient is controlled by  $1/H$  – where  $H$  denotes the mesh size of the macro partition – independent of the contrast of the data.

For the communication avoiding properties of the ArbiLoMod, it is important to note that extensions can be calculated independently on each domain, i.e.  $\text{Extend}(\varphi)|_{\omega_i^{\text{no1}}}$  can be calculated having only information about  $\varphi$  and  $\omega_i^{\text{no1}}$ , without knowledge about other domains. Using this operator, we define the local subspaces  $V_i^{\text{wb}}$ :

**Definition 3.2.3** (Extended subspaces). *For each element  $i \in \{1, \dots, N_{\mathcal{E}}\}$  we define an extended subspace  $V_i^{\text{wb}}$  of  $V_h$  as:*

$$V_i^{\text{wb}} := \left\{ \text{Extend}(\varphi) \mid \varphi \in V_i^{\text{basic}} \right\}. \quad (3.7)$$

According to the definition in (3.3) we call  $V_i^{\text{wb}}$  a cell, face, or vertex space, if  $i \in \Upsilon_0, i \in \Upsilon_1$ , or  $i \in \Upsilon_2$ , respectively (cf. Figure 3.4).

**Remark 3.2.4** (Extended subspaces). *The definition of  $V_i^{\text{wb}}$  induces a direct decomposition of  $V_h$ :*

$$V_h = \bigoplus_{i \in \{1, \dots, N_{\mathcal{E}}\}} V_i^{\text{wb}}. \quad (3.8)$$

Space decompositions of the same spirit are used in the context of Component Mode Synthesis (CMS), see [Hetmaniuk and Lehoucq(2010), Hetmaniuk and Klawonn(2014)] and recently, it was also applied in the PR-SCRBE context [Lee(2018), Section 5.3.3].

### Projections

**Definition 3.2.5** (Local projection operators). *The projection operators  $\mathcal{P}_{V_i^{\text{basic}}} : V_h \rightarrow V_i^{\text{basic}}$  and  $\mathcal{P}_{V_i^{\text{wb}}} : V_h \rightarrow V_i^{\text{wb}}$  are defined by the relation*

$$\varphi = \sum_{i \in \{1, \dots, N_{\mathcal{E}}\}} \mathcal{P}_{V_i^{\text{basic}}}(\varphi) = \sum_{i \in \{1, \dots, N_{\mathcal{E}}\}} \mathcal{P}_{V_i^{\text{wb}}}(\varphi) \quad \forall \varphi \in V_h. \quad (3.9)$$

As both the subspaces  $V_i^{\text{basic}}$  and the subspaces  $V_i^{\text{wb}}$  form a direct decomposition of the space  $V_h$ , the projection operators are uniquely defined by this relation.

The implementation of the projection operators  $\mathcal{P}_{V_i^{\text{basic}}}$  is very easy: It is just extracting the coefficients of the basis functions forming  $V_i^{\text{basic}}$  out of the global coefficient vector. The implementation of the projection operators  $\mathcal{P}_{V_i^{\text{wb}}}$  is more complicated and involves the solution of local problems, see Algorithm 3.1.

---

**Algorithm 3.1:** Projections of wirebasket decomposition  $\mathcal{P}_{V_i^{\text{wb}}}$ .

---

```

1 Function SpaceDecomposition( $\varphi$ ):
   Input : function  $\varphi \in V_h$ 
   Output: decomposition of  $\varphi$ 
2   /* iterate over all codimensions in decreasing order */
3   for codim  $\in \{d, \dots, 0\}$  do
4     for  $i \in \Upsilon_{\text{codim}}$  do
5        $\varphi_i \leftarrow \text{Extend}(\mathcal{P}_{V_i^{\text{basic}}}(\varphi))$ 
6        $\varphi \leftarrow \varphi - \varphi_i$ 
7   return  $\{\varphi_i\}$ 

```

---

With the projections defined, the definition of the wirebasket space decomposition

$$\left\{ \Omega, V_h, \{\omega_i^{\text{ext}}\}_{i=1}^{N_{\mathcal{E}}}, \{V_i^{\text{wb}}\}_{i=1}^{N_{\mathcal{E}}}, \{\mathcal{P}_{V_i^{\text{wb}}}\}_{i=1}^{N_{\mathcal{E}}} \right\} \quad (3.10)$$

is complete.

### 3.3. Local Basis Generation

For each local subspace  $V_i^{\text{wb}}$ , an initial reduced local subspace  $\tilde{V}_i^{\text{wb}} \subseteq V_i^{\text{wb}}$  is generated, using only local information from an environment around the support of the elements in  $V_i^{\text{basic}}$ . The strategy used to construct these reduced local subspaces depends on the type of the space: whether  $i$  belongs to  $\Upsilon_0$ ,  $\Upsilon_1$  or  $\Upsilon_2$ . The three strategies are given in the following. The local basis generation algorithms on different domains for the same codimension can be run in parallel, completely independent of each other. The basis generation for the spaces  $\tilde{V}_i^{\text{wb}}, i \in \Upsilon_0$  requires the spaces  $\tilde{V}_i^{\text{wb}}, i \in \Upsilon_1 \cup \Upsilon_2$  (for the 2D case). See Section 3.5 for further discussion of the potential parallelization. As the algorithms only use local information, their results do not change when the problem definition is changed outside of the area they took into account. So there is no need to rerun the algorithms in this case. Our numerical results indicate that the spaces obtained by local trainings and greedys have good approximation properties (see Section 3.6.1). The quality of the obtained solution will be guaranteed by the a posteriori error estimator presented in Chapter 4.

#### 3.3.1. Basis Construction for Reduced Vertex Spaces

The spaces  $V_i^{\text{wb}}$  for  $i \in \Upsilon_2$  are spanned by only one function (see Figure 3.4c for an example) and are thus one dimensional. The reduced spaces are therefore chosen to coincide with the original space, i.e.  $\tilde{V}_i^{\text{wb}} := V_i^{\text{wb}}, \forall i \in \Upsilon_2$ .

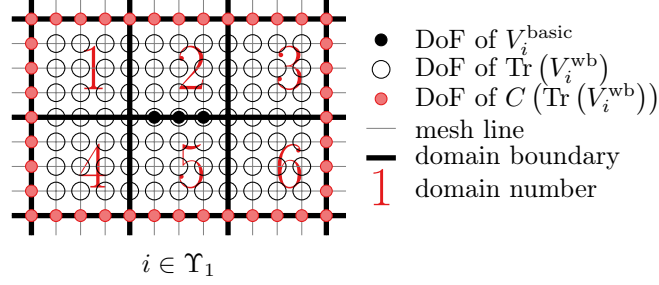


Figure 3.6.: Visualization of spaces for a codim 1 coarse mesh entity. Basic space  $V_i^{\text{basic}}$ , training space, and the coupling space of training space for  $Q^1$  ansatz functions (one DoF per mesh node).

### 3.3.2. Local Training for Basis Construction of Reduced Face Spaces

To generate an initial reduced local subspace  $\tilde{V}_i^{\text{wb}}$ ,  $i \in \Upsilon_1$  we use a local training procedure. We present a simple training procedure here. An improved variant is the topic of Chapter 5. To sample the parameter space  $\mathcal{D}$ , a discrete set  $\Xi \subset \mathcal{D}$  is used. The main four steps of the training are to

1. solve the equation on a small domain around the space in question with zero boundary values for all parameters in the training set  $\Xi$ ,
2. solve the homogeneous equation repeatedly on a small domain around the space in question with random boundary values for all parameters in  $\Xi$ ,
3. apply the space decomposition to all obtained local solutions to obtain the part belonging to the space in question and
4. use a greedy procedure to create a space approximating this set.

The complete algorithm is given in Algorithm 3.3 and explained below.

The training is inspired by the ‘‘Empirical Port Reduction’’ introduced in Eftang et al. [Eftang and Patera(2013)] but differs in some key points. The main differences are: (1) Within [Eftang and Patera(2013)], the trace of solutions at the interface to be trained is used. This leads to the requirement that interfaces between domains do not intersect. In ArbiLoMod, a space decomposition is used instead. This allows ports to intersect, which in turn allows the decomposition of space into domains. (2) The ‘‘Empirical Port Reduction’’ trains with a pair of domains. We use an environment of the interface in question, which contains six domains in the 2D case. In 3D, it contains 18 domains. (3) PR-SCRBE aims at providing a library of domains which can be connected at their interfaces. The reduced interface spaces are used in different domain configurations and have to be valid in all of them. Within the context of ArbiLoMod, no database of domains is created and the interface space is constructed only for the configuration at hand, which simplifies the procedure. (4) The random boundary values used in [Eftang and Patera(2013)] are generalized Legendre polynomials with random coefficients. In ArbiLoMod, the finite element basis functions with random coefficients are used, which simplifies the construction, especially when there is complex structure within the interface.

#### The Training Space

To train a basis for  $\tilde{V}_i^{\text{wb}}$ ,  $i \in \Upsilon_1$ , we define a training space  $\text{Tr}(V_i^{\text{wb}})$  on an environment associated with the face  $\mathcal{E}_i$ . The following definition is geometric and tailored to a domain decomposition in rectangular domains. More complex domain decompositions would need a more complex definition

here. We define the neighborhood

$$\mathcal{N}_j := \left\{ i \in \{1, \dots, N_{\text{noI}}\} \mid \overline{\omega_i^{\text{noI}}} \cap \overline{\mathcal{E}_j} \neq \emptyset \right\} \quad (3.11)$$

and the training spaces

$$\text{Tr}(V_i^{\text{wb}}) := \bigoplus \left\{ V_j^{\text{basic}} \mid I_{\mathcal{E}_j} \subseteq \mathcal{N}_i \right\}. \quad (3.12)$$

The training space is coupled to the rest of the system via its coupling space

$$C(\text{Tr}(V_i^{\text{wb}})) := \bigoplus \left\{ V_j^{\text{basic}} \mid I_{\mathcal{E}_j} \cap \mathcal{N}_i \neq \emptyset, I_{\mathcal{E}_j} \not\subseteq \mathcal{N}_i \right\}. \quad (3.13)$$

A sketch of the degrees of freedom associated with the respective spaces is given in Figure 3.6. These definitions are also suitable in the 3D case. We have fixed the size of the neighborhood to one domain from the interface in question in each direction. This facilitates the setup of local problems and the handling of local changes: After a local change, the affected domains are determined. Afterwards, all trainings have to be redone for those spaces which contain an affected domain in their training domain. While a larger or smaller training domain might be desirable in some cases (see [Henning and Peterseim(2013)]), it is not necessary: As missing global information is added in the enrichment step, ArbiLoMod always converges to the desired accuracy, even if the training domain is not of optimal size. So the advantages of having the size of the training domain fixed to one domain outweighs its drawbacks.

The reduced basis must be rich enough to handle two types of right hand sides up to a given accuracy  $\varepsilon_{\text{train}}$ : (a) source terms and boundary conditions, and (b) arbitrary values on the coupling interface, both in the whole parameter space  $\mathcal{D}$ . We define an extended parameter space  $\mathcal{D} \times C(\text{Tr}(V_i^{\text{wb}}))$ . For this parameter space we construct a training space  $\Xi \times G \subset \mathcal{D} \times C(\text{Tr}(V_i^{\text{wb}}))$ , where  $G$  denotes an appropriate sampling of  $C(\text{Tr}(V_i^{\text{wb}}))$ . We use the finite element basis  $\mathcal{B}_{C(\text{Tr}(V_i^{\text{wb}}))}$  on the coupling space and generates  $M$  random coefficient vectors  $r_i$  of size  $N_{\mathcal{B}_C} := \dim(C(\text{Tr}(V_i^{\text{wb}})))$ . With this an individual coupling space function  $\varphi \in C(\text{Tr}(V_i^{\text{wb}}))$  is constructed as

$$\varphi_i = \sum_{j=1}^{N_{\mathcal{B}_C}} r_{ij} \phi_j; \quad \phi_j \in \mathcal{B}_{C(\text{Tr}(V_i^{\text{wb}}))}. \quad (3.14)$$

For our numerical experiments in Section 3.6.1, we use uniformly distributed random coefficients over the interval  $[-1, 1]$  and Lagrange basis functions. For each  $\mu \in \Xi$  and each pair  $(\mu, g_c) \in \Xi \times G$  we construct snapshots  $u_f$  and  $u_c$  as solutions for right hand sides  $f_\mu(\cdot)$ ,  $a_\mu(g_c, \cdot)$  respectively, i.e. find  $u_f, u_c \in \text{Tr}(V_i^{\text{wb}})$  such that

$$\begin{aligned} a_\mu(u_f, \phi) &= f_\mu(\phi) \quad \forall \phi \in \text{Tr}(V_i^{\text{wb}}), \\ a_\mu(u_c, \phi) &= -a_\mu(g_c, \phi) \quad \forall \phi \in \text{Tr}(V_i^{\text{wb}}). \end{aligned} \quad (3.15)$$

Existence and uniqueness of  $u_f$  and  $u_c$  are guaranteed in the coercive case, as the problem Equation (3.15) is a Galerkin projected variant of the full problem and the coercivity is maintained during projection (cf. Section 2.2). In the inf-sup stable case, existence and uniqueness of  $u_f$  and  $u_c$  are not guaranteed. Based on the set of snapshots which we call  $Z$ , a reduced basis  $\tilde{\mathcal{B}}_{\tilde{V}_i^{\text{wb}}}$  is constructed using the greedy procedure Algorithm 3.2. In the numerical experiments, the  $V$ -norm and  $V$ -inner product are used. The complete generation of the reduced face spaces  $\tilde{V}_i^{\text{wb}}$ ,  $i \in \Upsilon_1$  with basis  $\tilde{\mathcal{B}}_{\tilde{V}_i^{\text{wb}}}$  is summarized in Algorithm 3.3.

### 3.3.3. Basis Construction for Reduced Cell Spaces Using Local Greedy

For each cell space  $V_i^{\text{wb}}$ ,  $i \in \Upsilon_0$  we create a reduced space  $\tilde{V}_i^{\text{wb}}$ . The complete algorithm is given in Algorithm 3.4 and explained here. These spaces should be able to approximate the solution in

**Algorithm 3.2:** SnapshotGreedy

---

```

1 Function SnapshotGreedy( $Z, \varepsilon_{\text{train}}$ ):
   Input : set of elements to approximate  $Z$ ,
           training tolerance  $\varepsilon_{\text{train}}$ 
   Output: basis of approximation space  $\mathfrak{B}$ 
2  $\mathfrak{B} \leftarrow \emptyset$ 
3 while  $\max_{z \in Z} \|z\| > \varepsilon_{\text{train}}$  do
4    $\hat{z} \leftarrow \arg \max_{z \in Z} \|z\|$ 
5    $\hat{z} \leftarrow \frac{\hat{z}}{\|\hat{z}\|}$ 
6    $Z \leftarrow \{z - (z, \hat{z})\hat{z} \mid z \in Z\}$ 
7    $\mathfrak{B} \leftarrow \mathfrak{B} \cup \{\hat{z}\}$ 
8 return  $\mathfrak{B}$ 

```

---

**Algorithm 3.3:** Training to construct reduced face spaces  $\tilde{V}_i^{\text{wb}}$ ,  $i \in \Upsilon_1$ .

---

```

1 Function Training( $i, M, \varepsilon_{\text{train}}$ ):
   Input : space identifier  $i$ ,
           number of random samples  $M$ ,
           training tolerance  $\varepsilon_{\text{train}}$ 
   Output: reduced local subspace  $\tilde{V}_i^{\text{wb}}$ 
2  $G \leftarrow \text{RandomSampling}(i, M)$ 
3  $Z \leftarrow \emptyset$ 
4 foreach  $\mu \in \Xi$  do
5   find  $u_f \in \text{Tr}(V_i^{\text{wb}})$  such that:
6   |  $a_\mu(u_f, \phi) = f_\mu(\phi) \quad \forall \phi \in \text{Tr}(V_i^{\text{wb}})$ 
7   |  $Z \leftarrow Z \cup \mathcal{P}_{V_i^{\text{wb}}}(u_f)$ 
8   foreach  $g_c \in G$  do
9   | find  $u_c \in \text{Tr}(V_i^{\text{wb}})$  such that:
10  | |  $a_\mu(u_c + g_c, \phi) = 0 \quad \forall \phi \in \text{Tr}(V_i^{\text{wb}})$ 
11  | |  $Z \leftarrow Z \cup \mathcal{P}_{V_i^{\text{wb}}}(u_c)$ 
12  $\tilde{\mathfrak{B}}_{\tilde{V}_i^{\text{wb}}} \leftarrow \text{SnapshotGreedy}(Z, \varepsilon_{\text{train}})$ 
13 return  $\text{span}(\tilde{\mathfrak{B}}_{\tilde{V}_i^{\text{wb}}})$ 

```

---



the associated part of the space decomposition for any variation of functions from reduced vertex or face spaces that are coupled with it. We define the reduced coupling space  $\tilde{C}(V_i^{\text{wb}})$  and its basis  $\tilde{\mathcal{B}}_{\tilde{C}(V_i^{\text{wb}})}$ .

$$\Upsilon_i^C := \left\{ j \in 1, \dots, N_{\mathcal{E}} \mid i \in I_{\mathcal{E}_j}, I_{\mathcal{E}_j} \neq \{i\} \right\} \quad (3.16)$$

$$\tilde{C}(\tilde{V}_i^{\text{wb}}) := \bigoplus_{j \in \Upsilon_i^C} \tilde{V}_j^{\text{wb}} \quad \tilde{\mathcal{B}}_{\tilde{C}(V_i^{\text{wb}})} := \bigcup_{j \in \Upsilon_i^C} \tilde{\mathcal{B}}_{\tilde{V}_j^{\text{wb}}} \quad (3.17)$$

We introduce an extended training set:  $\Xi \times \{1, \dots, N_{\tilde{\mathcal{B}}} + 1\}$ ,  $N_{\tilde{\mathcal{B}}} := \dim(\tilde{C}(\tilde{V}_i^{\text{wb}}))$ . Given a pair  $(\mu, j) \in \Xi \times \{1, \dots, N_{\tilde{\mathcal{B}}} + 1\}$ , we define the associated right hand side as

$$g_{\mu,j}(\phi) := \begin{cases} -a_{\mu}(\psi_j, \phi) & \text{if } j \leq N_{\tilde{\mathcal{B}}} \\ f_{\mu}(\phi) & \text{if } j = N_{\tilde{\mathcal{B}}} + 1, \end{cases} \quad (3.18)$$

where  $\psi_j$  denotes the  $j$ -th basis function of  $\tilde{\mathcal{B}}_{\tilde{C}(V_i)}$ . We then construct the reduced cell space  $\tilde{V}_i^{\text{wb}}$  as the classical reduced basis space with respect to the following parameterized local problem: Given a pair  $(\mu, j) \in \Xi \times \{1, \dots, N_{\tilde{\mathcal{B}}} + 1\}$ , find  $u_{\mu,j} \in V_i^{\text{wb}}$  such that

$$a_{\mu}(u_{\mu,j}, \phi) = g_{\mu,j}(\phi) \quad \forall \phi \in V_i^{\text{wb}}. \quad (3.19)$$

The corresponding reduced solutions are hence defined as: Find  $\tilde{u}_{\mu,j} \in \tilde{V}_i^{\text{wb}}$  such that:

$$a_{\mu}(\tilde{u}_{\mu,j}, \phi) = g_{\mu,j}(\phi) \quad \forall \phi \in \tilde{V}_i^{\text{wb}} \quad (3.20)$$

Both problems have unique solutions in the coercive case. For the LocalGreedy we use the standard Reduced Basis residual error estimator, i.e.

$$\|u_{\mu,j} - \tilde{u}_{\mu,j}\|_{V_i} \leq \Delta_{\text{cell}}(\tilde{u}_{\mu,j}) := \frac{1}{\alpha_{LB}} \|\mathcal{R}_{\mu,j}(\tilde{u}_{\mu,j})\|_{V_i^{\text{wb}'}} , \quad (3.21)$$

with the local residual

$$\begin{aligned} \mathcal{R}_{\mu,j} : V_i^{\text{wb}} &\rightarrow V_i^{\text{wb}'} \\ \varphi &\mapsto g_{\mu,j}(\cdot) - a_{\mu}(\varphi, \cdot) \end{aligned} \quad (3.22)$$

and a lower bound for the coercivity constant  $\alpha_{LB}$ . The idea of using a local greedy to generate a local space for all possible boundary values can also be found in [Iapichino(2012), Antonietti et al.(2016)].

### 3.4. Enrichment Procedure

The first ArbiLoMod solution is obtained using the initial reduced local subspaces generated using the local training and greedy procedures described in Section 3.3. The error of this solution is bounded by an a posteriori error estimator  $\Delta_{\text{loc}}^g(\tilde{u}_{\mu})$ . The definition of this a posteriori error estimator is postponed to Chapter 4. If this solution is not good enough according to the a posteriori error estimator, the solution is improved by enriching the reduced local subspaces and then solving the global reduced problem again. The full procedure is given in Algorithm 3.5 and described in the following.

For the enrichment, we use the overlapping local subspaces  $V_i^{\text{pou}}$  introduced in (2.4.3), which are also used for the a posteriori error estimator. Online enrichment on the wirebasket space decomposition itself led to stagnation in numerical experiments. Local problems are solved in the overlapping spaces. The original bilinear form is used, but as a right hand side the residual of the last reduced solution is employed. The local spaces and the parameter values for which the

---

**Algorithm 3.4:** LocalGreedy to construct local cell spaces  $\tilde{V}_i^{\text{wb}}$ ,  $i \in \Upsilon_0$ .

---

```

1 Function LocalGreedy( $i, \varepsilon_{\text{greedy}}$ ):
   Input : space identifier  $i$ ,
           greedy tolerance  $\varepsilon_{\text{greedy}}$ 
   Output: reduced local subspace  $\tilde{V}_i^{\text{wb}}$ 
2  $\tilde{\mathcal{B}}_{\tilde{V}_i^{\text{wb}}} \leftarrow \emptyset$ 
3 while  $\max_{\substack{\mu \in \Xi \\ j \in \{1, \dots, N_{\tilde{\mathcal{B}}}+1\}}} \Delta_{\text{cell}}(\tilde{u}_{\mu,j}) > \varepsilon_{\text{greedy}}$  do
4    $\hat{\mu}, \hat{j} \leftarrow \arg \max_{\substack{\mu \in \Xi \\ j \in \{1, \dots, N_{\tilde{\mathcal{B}}}+1\}}} \Delta_{\text{cell}}(\tilde{u}_{\mu,j})$ 
5   find  $u_{\hat{\mu}, \hat{j}} \in V_i^{\text{wb}}$  such that:
6    $\quad \lfloor \quad a_{\hat{\mu}}(u_{\hat{\mu}, \hat{j}}, \phi) = g_{\hat{\mu}, \hat{j}}(\phi) \quad \forall \phi \in V_i^{\text{wb}}$ 
7    $\quad u_{\hat{\mu}, \hat{j}} \leftarrow u_{\hat{\mu}, \hat{j}} - \sum_{\phi \in \tilde{\mathcal{B}}_{\tilde{V}_i^{\text{wb}}}} (\phi, u_{\hat{\mu}, \hat{j}}) \phi$ 
8    $\quad \tilde{\mathcal{B}}_{\tilde{V}_i^{\text{wb}}} \leftarrow \tilde{\mathcal{B}}_{\tilde{V}_i^{\text{wb}}} \cup \{ \|u_{\hat{\mu}, \hat{j}}\|_V^{-1} u_{\hat{\mu}, \hat{j}} \}$ 
9 return  $\text{span}(\tilde{\mathcal{B}}_{\tilde{V}_i})$ 

```

---

enrichment is performed are selected in a Dörfler-like [Dörfler(1996)] algorithm. The thus obtained local solutions  $u_l$  do not fit into our space decomposition, as they lie in one of the overlapping spaces  $V_i^{\text{pou}}$ , not in one of the local subspaces used for the basis construction  $V_i^{\text{wb}}$ . Therefore, the  $u_l$  are decomposed using the projection operators  $\mathcal{P}_{V_i^{\text{wb}}}$  defined in Definition 3.2.5. In the setting of our numerical example (Section 3.6.1), this decomposition yields at most 9 parts (one codim-2 part, four codim-1 parts and four codim-0 parts). Of these parts, the one worst approximated by the existing reduced local subspace is selected for enrichment. “Worst approximated” is here defined as having the largest part orthogonal to the existing reduced local subspace. We denote the orthogonal projection on  $\tilde{V}_i^{\text{wb}}$  by  $P_{\tilde{V}_i^{\text{wb}}}$ , so  $(1 - P_{\tilde{V}_i^{\text{wb}}})\mathcal{P}_{V_i^{\text{wb}}}(u_l)$  is the part of  $\mathcal{P}_{V_i^{\text{wb}}}(u_l)$  orthogonal to  $\tilde{V}_i^{\text{wb}}$ .

To avoid communication, cell spaces  $\tilde{V}_i^{\text{wb}}, i \in \Upsilon_0$  are not enriched at this point. Such an enrichment would require the communication of the added basis vector, which might be large. Instead, only the other spaces are enriched, and the cell spaces associated with  $\Upsilon_0$  are regenerated using the greedy procedure from Section 3.3.3. For the other spaces, a strong compression of the basis vectors is possible (cf. Section 3.5).

This selection of the local spaces can lead to one reduced local space being enriched several times in one iteration. Numerical experiments have shown that this leads to poorly conditioned systems, as the enrichment might introduce the same feature into a local basis twice. To prevent this, the enrichment algorithm enriches each reduced local subspace at most once per iteration.

### 3.5. Runtime and Communication

A major design goal of ArbiLoMod is communication avoidance and scalability in parallel environments. In the following, we highlight the possibilities offered by ArbiLoMod to reduce communication in a parallel setup.

Similar to overlapping Domain Decomposition methods we require that not only the local domain, but also an overlap region is available locally. For a subdomain  $\omega_i^{\text{sol}}$  the overlap region is the domain itself and all adjacent domains, as depicted in Figure 3.7, i.e. all subdomains in the neighborhood  $\mathcal{N}_i$ . As the overlap region includes the support of all training spaces, one can compute all initial reduced local subspaces with support in  $\omega_i^{\text{sol}}$  without further communication. This

**Algorithm 3.5:** Online Enrichment in ArbiLoMod.

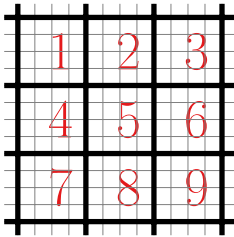
---

```

1 Function OnlineEnrichment( $r, \text{tol}$ ):
   Input : enrichment fraction  $r$ ,
           target error tol
2 while  $\max_{\mu \in \Xi} \Delta(\tilde{u}_\mu) > \text{tol}$  do
3    $E \leftarrow \emptyset$ 
4   while  $\left( \frac{\sum_{(\mu, i) \in E} \|R_\mu(\tilde{u}_\mu)\|_{(V_i^{\text{pou}})'}}{\sum_{(\mu, i) \in (\Xi \times \{1, \dots, N_{\text{ol}}\})} \|R_\mu(\tilde{u}_\mu)\|_{(V_i^{\text{pou}})'}} \right) < r$  do
5      $\hat{\mu}, \hat{i} \leftarrow \arg \max_{(\mu, i) \in (\Xi \times \{1, \dots, N_{\text{ol}}\}) \setminus E} \|R_\mu(\tilde{u}_\mu)\|_{(V_i^{\text{pou}})'}$ 
6      $E \leftarrow E \cup (\hat{\mu}, \hat{i})$ 
7   /*  $S$  is used for double enrichment protection. */
8    $S \leftarrow \emptyset$ 
9   for  $(\mu, i) \in E$  do
10    find  $u_l \in V_i^{\text{pou}}$  such that:
11     $a_\mu(u_l, \varphi) = \mathcal{R}_\mu(\tilde{u}_\mu)(\varphi) \quad \forall \varphi \in V_i^{\text{pou}}$ 
12     $\check{i} \leftarrow \arg \max_{i \in \{1, \dots, N_\mathcal{E}\} \setminus \Upsilon_0} \|(1 - P_{\tilde{V}_i^{\text{wb}}})\mathcal{P}_{V_i^{\text{wb}}}(u_l)\|_{V_i}$ 
13    if  $\check{i} \notin S$  then
14       $\tilde{V}_i^{\text{wb}} \leftarrow \tilde{V}_i^{\text{wb}} \oplus \text{span}((1 - P_{\tilde{V}_i^{\text{wb}}})\mathcal{P}_{V_i^{\text{wb}}}(u_l))$ 
15       $S \leftarrow S \cup \check{i}$ 
16    run LocalGreedy
17    recalculate reduced solutions

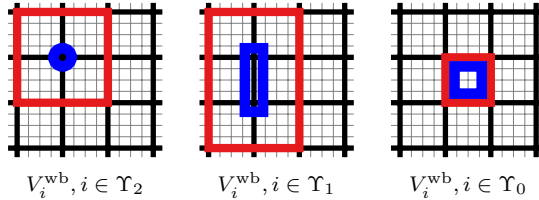
```

---



(a) Example domain numbering.

Create basis functions for vertex, face and cell spaces:



(b) To generate reduced space associated with blue marked entity, only geometry information in red marked area is needed.

Figure 3.7.: Data dependencies in ArbiLoMod: Before online enrichment, it is possible to compute all reduced basis function having support on a domain ( $\omega_5^{\text{ol}}$  here) using only local information about the domain and its surrounding domains.

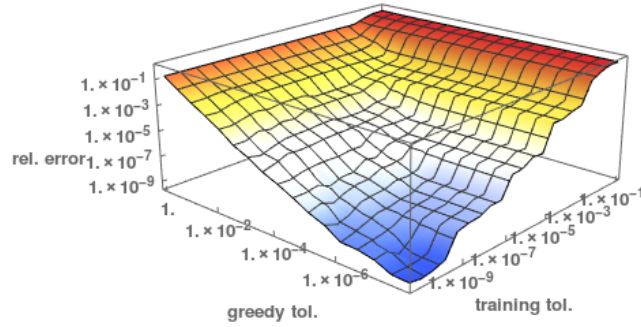


Figure 3.8.: Maximum relative  $H^1$ -error on training set  $\Xi$  in dependence of tolerances in codim 1 training and codim 0 greedy for *Thermal Channels Example*. Online enrichment disabled. (reproduction: Appendix A.6)

work can be distributed on many nodes. Afterwards, only reduced representations of the operator have to be communicated. Using the operator decomposition  $a^b(u, v) = \sum_{i=1}^{N_{\text{noi}}} a_{\omega_i^{\text{poi}}}^b(u, v)$ , a global, reduced operator is collected using an all-to-one communication of reduced matrices. The global reduced problem is then solved on a single node. It is assumed that the global, reduced system is sufficiently small.

If the accuracy is not sufficient, online enrichment is performed. This step requires additional communication; first for the evaluation of the error estimator and second to communicate new basis vectors of reduced face spaces  $\tilde{V}_i^{\text{wb}}$ ,  $i \in \Upsilon_1$ . Note that it is sufficient to communicate the local projection  $\mathcal{P}_{V_i^{\text{basic}}}(\psi)$  and reconstruct the actual basis function as its extension, so that we save communication costs proportional to the volume to surface ratio.

The evaluation of the localized error estimator requires the dual norms of the residual in the localized spaces  $\|\mathcal{R}_\mu(\tilde{u}_\mu)\|_{V_i^{\text{poi}}}$ . Using an offline/online splitting, the evaluation of the error estimator can be evaluated for the full system using only reduced quantities. The computation of the reduced operators is performed in parallel, similar to the basis construction in the first step. The actual evaluation of the error estimator can be performed on a single node and is independent of the number of degrees of freedom of the high fidelity model.

An important parameter for ArbiLoMod's runtime is the domain size  $H$ . The domain size affects the size of the local problems, the amount of parallelism in the algorithm, and the size of the reduced global problem. An  $H$  too large leads to large local problems, while an  $H$  too small leads to a large reduced global problem (see also the numerical example in Section 3.6.1 and especially the results in Table 3.3).  $H$  has to be chosen to balance these two effects.

### 3.6. Numerical Experiments

#### 3.6.1. Numerical Example 1: Thermal Channels

We first demonstrate the ArbiLoMod on *Thermal Channels Example* as defined in Section 2.7.2. The numerical experiments were performed using pyMOR [Milk et al.(2016)]. If not specified otherwise, we use a mesh size of  $1/h = 200$ , a training tolerance of  $\varepsilon_{\text{train}} = 10^{-4}$ , a number of random samplings of  $M = 60$ , a greedy tolerance of  $\varepsilon_{\text{greedy}} = 10^{-3}$ , a convergence criterion of  $\|\mathcal{R}_\mu(\tilde{u}_\mu)\|_{V_h} < 10^{-2}$ , an enrichment fraction of  $r = 0.5$ , a training set of size  $|\Xi| = 6$ , and the parameter for extension calculation is  $\bar{\mu} = 10^5$ . The initial reduced space is created using the local trainings and greedy algorithms. In both the trainings and the greedy algorithms a tolerance parameter steers the quality of the obtained reduced space: In the trainings,  $\varepsilon_{\text{train}}$  is the stopping

geometry	trainings		with training				without training	
	reuse:		greedys		iterations		iterations	
	no	yes	no	yes	no	yes	no	yes
1	112	112 (-0 %)	64	64 (-0 %)	24	24 (-0 %)	46	46 (-0 %)
2	112	5 (-96 %)	64	8 (-88 %)	24	13 (-46 %)	48	28 (-42 %)
3	112	5 (-96 %)	64	8 (-88 %)	20	14 (-30 %)	42	27 (-36 %)
4	112	3 (-97 %)	64	6 (-91 %)	25	10 (-60 %)	54	23 (-57 %)
5	112	5 (-96 %)	64	8 (-88 %)	25	12 (-52 %)	52	27 (-48 %)

Table 3.1.: Number of iterations of online enrichment for *Thermal Channels Example*: (a) With and without codim 1 training. (b) With and without reuse of basis functions of previous simulations. Convergence criterion:  $\|\mathcal{R}_\mu(\tilde{u}_\mu)\|_{V_h'} < 10^{-4}$ , greedy tolerance:  $\varepsilon_{\text{greedy}} = 10^{-5}$ . See also Figures 3.9 and 3.10. (reproduction: Appendix A.7)

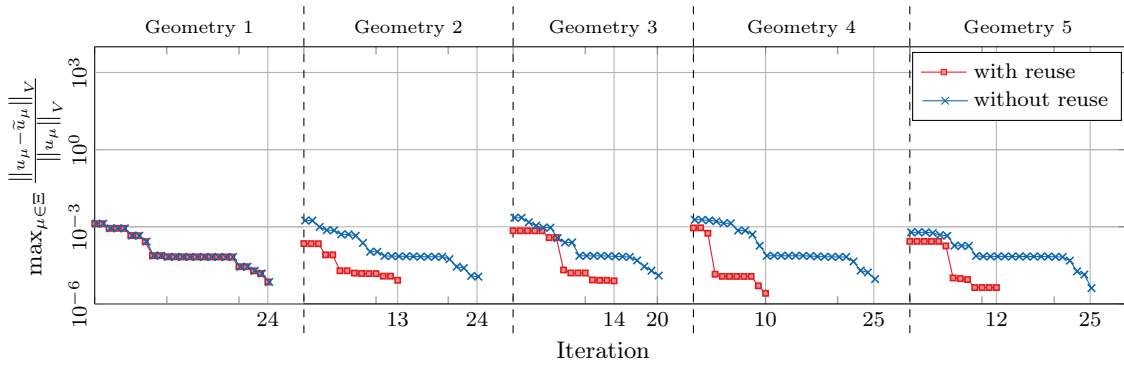


Figure 3.9.: Relative error over iteration with and without basis reuse for after geometry change for *Thermal Channels Example*. With codim 1 training. Convergence criterion:  $\|\mathcal{R}_\mu(\tilde{u}_\mu)\|_{V_h'} < 10^{-4}$ , greedy tolerance:  $\varepsilon_{\text{greedy}} = 10^{-5}$ . See also Table 3.1. (reproduction: Appendix A.7)

criterion for the SnapshotGreedy (Algorithm 3.2) and the local greedys stop when the local error estimator stays below the prescribed tolerance  $\varepsilon_{\text{greedy}}$ . The resulting reduction errors in dependence on the two tolerances are depicted in Figure 3.8.

If the resulting error is too big, it can be further reduced using iterations of online enrichment as depicted in Figure 3.9. Results suggest a very rapid decay of the error with online enrichment. The benefits of ArbiLoMod can be seen in Figure 3.9 and Table 3.1: after the localized geometry changes, most of the work required in the initial basis creation does not need to be repeated and the online enrichments converge faster for subsequent simulations, leading to less iterations. The online enrichment presented here converges even when started on empty bases, as depicted in Figure 3.10. It does not rely on properties of the reduced local subspaces created by trainings and greedys. The performance of the localized a posteriori error estimator (defined below in Section 4.4)  $\Delta_{loc,rel}^g(\tilde{u}_\mu)$  can be seen in Figure 3.11. Comparison of the localized estimator  $\Delta_{loc,rel}^g(\tilde{u}_\mu)$  with the global estimator  $\Delta_{rel}(\tilde{u}_\mu)$  (also defined below in Section 4.4) shows that, for the example considered here, the localization does not add a significant factor beyond the factor  $c_{\text{pu},\tilde{V}}$ , which is neglected in Figure 3.11.

Even though our implementation was not tuned for performance and is not parallel, we present some timing measurements in Table 3.2 and Table 3.3. Table 3.2 shows that, already in our unoptimized implementation, trainings and greedys have a shorter runtime than a single global solve for problems of sufficient size. Taking into account that trainings and greedys create a solution space valid in the whole parameter space, this data is a strong hint that ArbiLoMod can realize its potential for acceleration for large problems, in an optimized implementation and a parallel

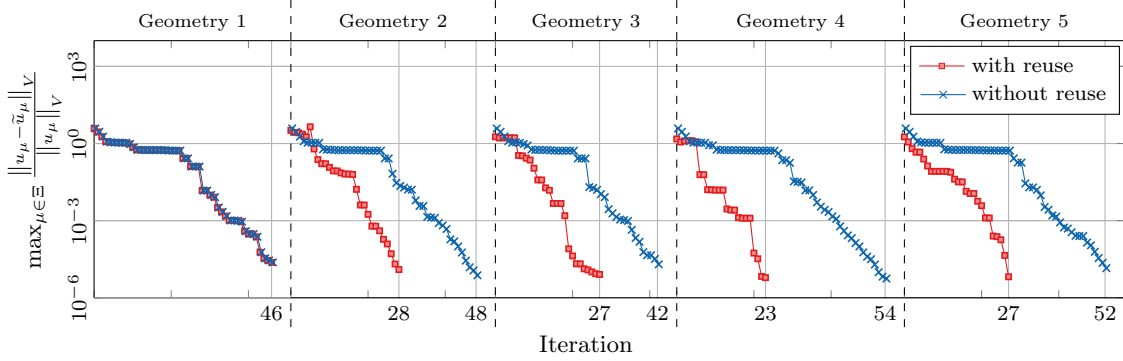


Figure 3.10.: Relative  $H^1$  error over iterations with and without basis reuse for after geometry change for *Thermal Channels Example*. Without codim 1 training. Convergence criterion:  $\|R_\mu(\tilde{u}_\mu)\|_{V'_h} < 10^{-4}$ , greedy tolerance:  $\varepsilon_{\text{greedy}} = 10^{-5}$ . See also Table 3.1. (reproduction: Appendix A.7)

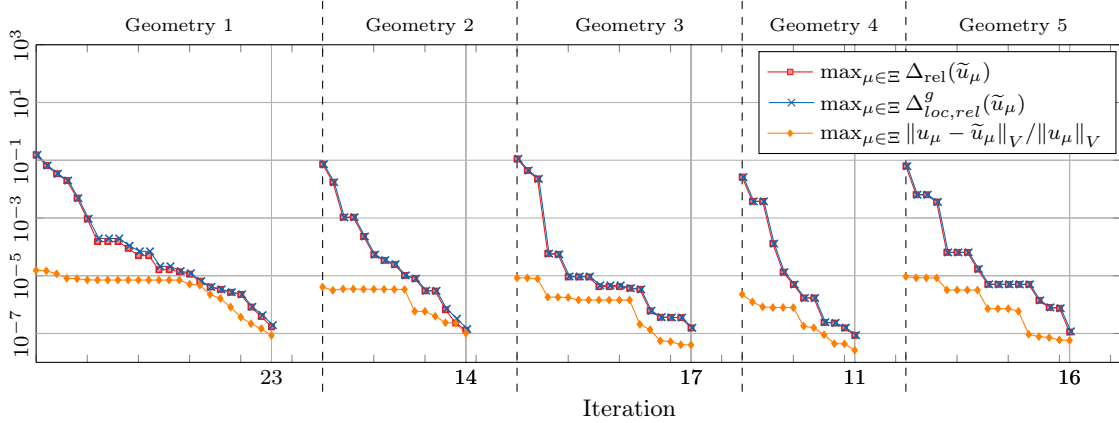


Figure 3.11.: Error estimators  $\Delta_{\text{rel}}(\tilde{u}_\mu)$  and  $\Delta_{\text{loc,rel}}^g(\tilde{u}_\mu)$  over iterations, compared to the relative error for *Thermal Channels Example*. Plotted for  $\alpha_\mu = c_{\text{pu},\tilde{V}} = 1$ . Simulation performed with a convergence criterion of  $\|R_\mu(\tilde{u}_\mu)\|_{V'_h} < 10^{-6}$ , a training tolerance of  $\varepsilon_{\text{train}} = 10^{-5}$ , and a greedy tolerance of  $\varepsilon_{\text{greedy}} = 10^{-7}$ . (reproduction: Appendix A.8)

$1/h$	global DoFs	global solve time [s]	# DoFs, codim 1 training space	avg. time per codim 1 training [s]	# DoFs, codim 0 space	max time per codim 0 greedy [s]	# DoFs, reduced problem	solve time, reduced [ms]	max error [%]
200	80,401	0.656	7,626	1.02	1,201	4.9	1,178	21.8	1.316
400	320,801	4.87	30,251	5.14	4,901	7.04	1,151	22.4	1.433
600	721,201	23.6	67,876	14	11,101	10.7	1,116	19.1	2.035
800	1,281,601	41.8	120,501	29.5	19,801	17.8	1,101	17.1	2.735
1000	2,002,001	86.4	188,126	51.3	31,001	24.2	1,089	18.8	1.351
1200	2,882,401	230	270,751	81.2	44,701	36.6	1,082	18.6	4.462
1400	3,922,801	230	368,376	120	60,901	51.7	1,073	18.2	2.379

Table 3.2.: Runtimes for selected parts of ArbiLoMod without online enrichment for *Thermal Channels Example*. “max error” denotes  $\max_{\mu \in \Xi} \|u_\mu - \tilde{u}_\mu\|_V / \|u_\mu\|_V$ . Runtimes measured using a pure Python implementation, using SciPy solvers (SuperLU sequential). Note that the global solve time is for one parameter value while training and greedy produce spaces valid for all parameter values in the training set  $\Xi$ . (reproduction: Appendix A.9)

$1/H$	# DoFs, codim 1 training space	mean training time [s]	max training time [s]	# DoFs, codim 0 space	mean greedy time [s]	max greedy time [s]	# DoFs, reduced problem	solve time, reduced [ms]	max error [%]
4	30,251	10.9	14.1	4,901	3.07	6.6	403	3.85	0.362
5	19,401	6.88	8.74	3,121	2.32	11.7	517	4.38	0.435
8	7,626	2.63	3.55	1,201	1.35	5.69	1,178	14.9	1.32
10	4,901	1.68	1.94	761	0.655	3.98	1,451	19.8	0.220
20	1,251	0.483	0.661	181	0.305	3.18	5,025	94.4	0.0804

Table 3.3.: Influence of domain size  $H$  in ArbiLoMod for *Thermal Channels Example*. Fine mesh resolution:  $1/h = 200$ . “max error” is  $\max_{\mu \in \Xi} \|u_\mu - \tilde{u}_\mu\|_V / \|u_\mu\|_V$ . Smaller domains lead to more parallelism and smaller local problems, but also to more global DoFs and a worse constant in the a-posteriori error estimator. Measured using a pure Python implementation, using SciPy solvers (SuperLU sequential). (reproduction: Appendix A.10)

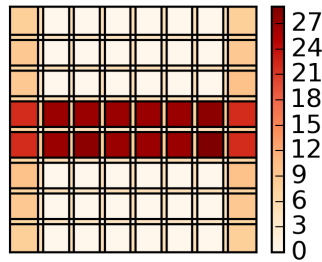


Figure 3.12.: Distribution of local basis sizes after initial training for *Thermal Channels Example*. Relative reduction error at this configuration:  $1.3 \cdot 10^{-3}$ . (reproduction: Appendix A.11)

computing environment. Especially when the solution has to be calculated at multiple parameter values. Table 3.3 shows the effect of choosing the domain size  $H$ : Large domains lead to large local problems, while small domains lead to a large reduced global problem (see also Section 3.5).

### 3.6.2. Numerical Example 2: 2D Maxwell's

The application of ArbiLoMod to inf-sup stable problems has several issues. The local problems in trainings, enrichments and local greedys do not necessarily have a unique solution and also the global reduced problem might be unstable. Nevertheless we apply ArbiLoMod without local greedy algorithms, without online enrichment and without a posteriori error estimator to the inf-sup stable problem *2D Maxwell Example* to numerically investigate its behavior in this case.

#### Global Properties of Example

Before analyzing the behavior of the localized model reduction, we discuss some properties of the full model. For its stability, its continuity constant  $\gamma$  and reduced inf-sup constants  $\tilde{\beta}$  are the primary concern. They guarantee existence and uniqueness of the solution and their quotient enters the best-approximation inequality Theorem 2.2.3. Due to the construction of the norm (see Section 2.6.4), the continuity constant cannot be larger than one, and numerics indicate that it is usually one (Figure 3.13). The inf-sup constant approaches zero when the frequency goes to zero. This is the well known low frequency instability of this formulation. There are remedies to this problem, but they are not considered here. The order of magnitude of the inf-sup constant is around  $10^{-2}$ : Due to the Robin boundaries, the problem is stable. With Dirichlet boundaries only, the inf-sup constant would drop to zero at several frequencies. There are two drops in the inf-sup constant at ca. 770 MHz and 810 MHz. These correspond to resonances in the structure which arise when half a wavelength is the width of a channel ( $\lambda/2 \approx 1/5$ ).

The most important question for the applicability of any reduced basis method is: is the system reducible at all, i.e. can the solution manifold be approximated with a low dimensional solution space? The best possible answer to this question is the Kolmogorov n-width. We measured the approximation error when approximating the solution manifold with a basis generated by a greedy algorithm. The approximation is done by orthogonal projection onto the basis. This error is an upper bound to the Kolmogorov n-width. Already with a basis size of 38, a relative error of  $10^{-4}$  can be achieved, see Figure 3.14. So this problem is well suited for reduced basis methods.

#### Properties of Localized Spaces

The next question is: how much do we lose by localization? Using basis vectors with limited support, one needs a larger total number of basis functions. To quantify this, we compare the



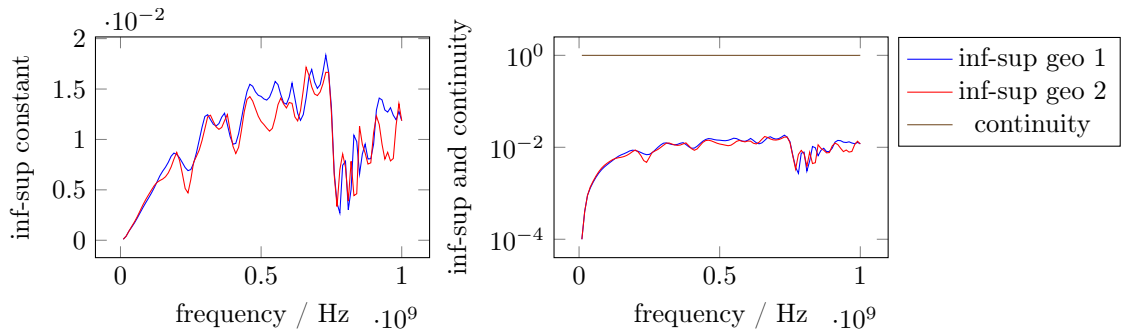


Figure 3.13.: inf-sup and continuity constant of bilinear form for *2D Maxwell Example*. Linear and logarithmic. (reproduction: Appendix A.12)

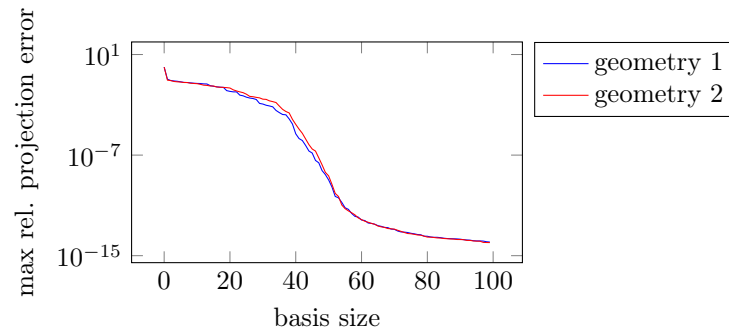


Figure 3.14.: Error when approximating the solution set for all  $\mu \in \Xi$  with an  $n$ -dimensional basis obtained by greedy approximation of this set. This is an upper bound for the Kolmogorov  $n$ -width. (*2D Maxwell Example*) (reproduction: Appendix A.13)

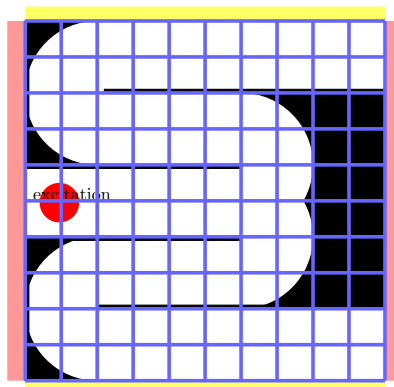


Figure 3.15.: Domain decomposition used for *2D Maxwell Example*.

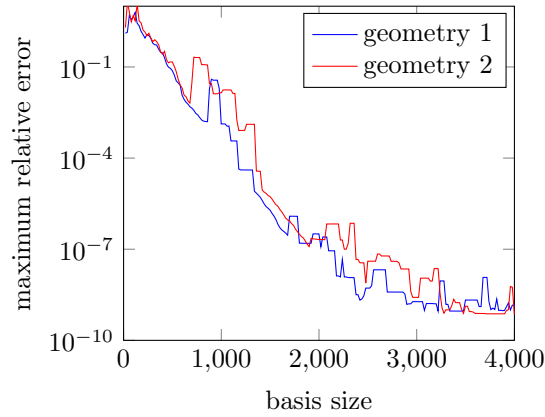


Figure 3.16.: Maximum error when solving *2D Maxwell Example* with a localized basis, generated by global solves. (reproduction: Appendix A.14)

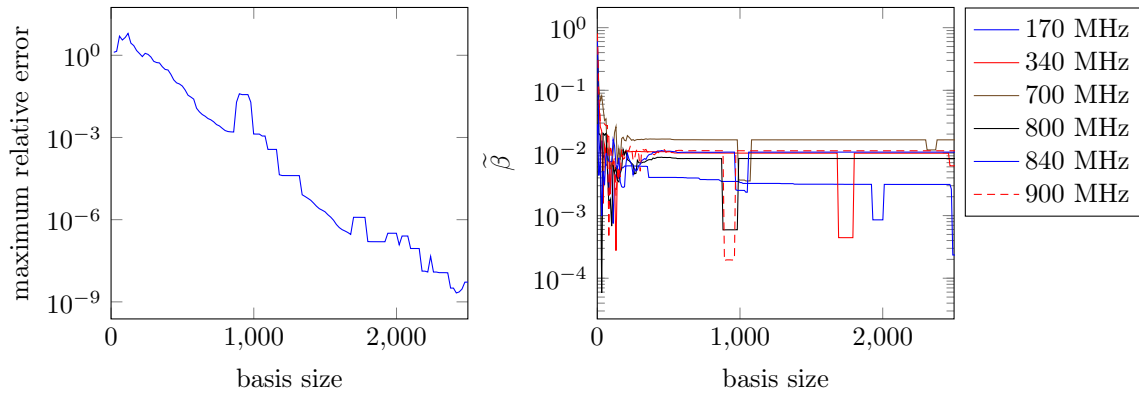


Figure 3.17.: Comparison of maximum error over all frequencies with inf-sup constant of reduced system at selected frequencies for geometry 1. Basis generated by global solves. Increased error and reduced inf-sup constant at basis size of ca. 900 (*2D Maxwell Example*). (reproduction: Appendix A.15)

errors with global approximation from the previous section with the error obtained when solving with a localized basis, using the best localized basis we can generate. We use a  $10 \times 10$  domain decomposition (see Figure 3.15) and the space decomposition introduced in Section 3.2. To construct the best possible basis, we solve the full problem for all parameters in the training set. For each local subspace, we apply the corresponding projection operator  $\mathcal{P}_{V_i^{\text{wb}}}$  to all global solutions and subsequently generate a basis for these local parts of global solutions using a snapshot greedy. The error when solving in the resulting reduced space is depicted in Figure 3.16, right. Much more basis vectors are needed, compared to the global reduced basis approach. However the reduction in comparison to the full model (60200 DoFs) is still significant and in contrast to standard reduced basis methods, the reduced system matrix is not dense but block-sparse. For a relative error of  $10^{-4}$ , 1080 basis vectors are necessary.

In Figure 3.16 the error is observed to jump occasionally. This is due to the instability of a Galerkin projection of an inf-sup stable problem. While the inf-sup constant of the reduced system is observed to be the same as the inf-sup constant of the full system most of the time, sometimes it drops. This is depicted in Figure 3.17. For a stable reduction, a different test space is necessary. However, the application of the known approaches such as [Carlberg et al.(2010),

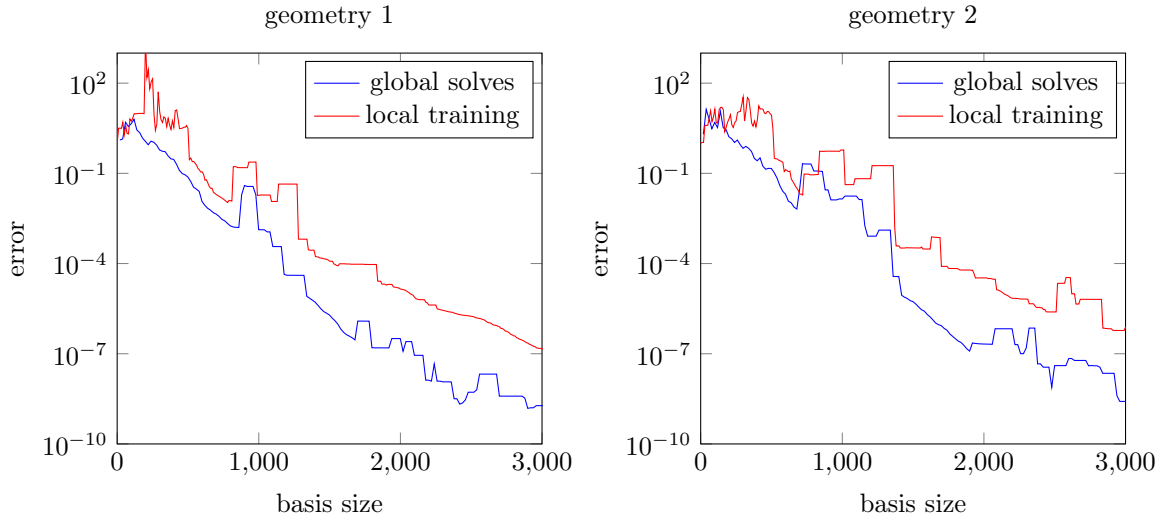


Figure 3.18.: Maximum error over all frequencies for both geometries of *2D Maxwell Example*. Basis generated by global solves vs. basis generated by local training. (reproduction: Appendix A.16)

Dahmen et al.(2014)] to the localized setting is not straightforward.

#### *Properties of Training*

Local basis vectors should be generated using the localized training described in Section 3.3.2. To judge on the quality of these basis vectors, we compare the error obtained using these basis vectors with the error obtained with local basis vectors generated by global solves. The local basis vectors generated by global solves are the reference: These are the best localized basis we can generate. The results for both geometries are depicted in Figure 3.18. While the error decreases more slowly, we still have reasonable basis sizes with training. For a relative error of  $10^{-4}$ , 1280 basis vectors are necessary for geometry 1 and 1380 are necessary for geometry 2.

#### *Application to Local Geometry Change*

If we work with a relative error of 5%, a basis of size 650 is sufficient for the first geometry and size 675 for the second. After the geometry change, the local reduced spaces which have no change in their training domain can be reused. Instead of solving the full system with 60200 degrees of freedom, the following effort is necessary per frequency point (see also Figure 3.19). Because the runtime is dominated by matrix factorizations, we focus on these.

- 14 factorizations of local problems with 5340 DoFs (volume training)
- 20 factorizations of local problems with 3550 DoFs (interface training)
- 1 factorization of global reduced problem with 675 DoFs (global solve)

The error between the reduced solution and the full solution in this case is 4.3%. For reproduction, see Appendix A.17. The spacial distribution of basis sizes is depicted in Figure 3.20.

The application of ArbiLoMod the inf-sup stable problem of the 2D Maxwell's equation in  $H(\text{curl}, \Omega)$  shows that localized training generates bases of good quality. A reduced model with little error for the full problem can be generated using only local solves, which can easily be parallelized. After localized changes to the model, only in the changed region the localized bases

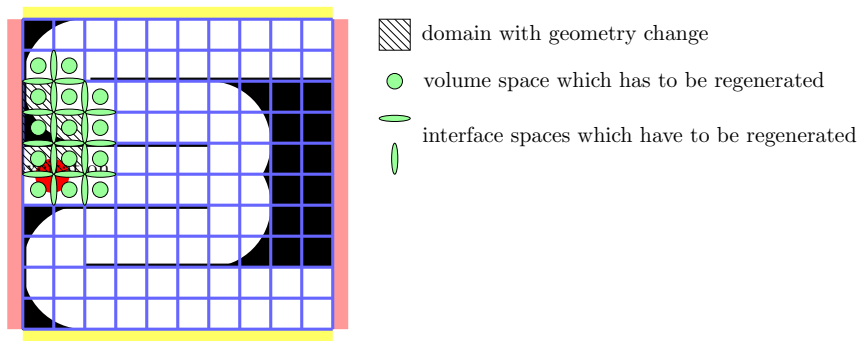


Figure 3.19.: Impact of geometry change of *2D Maxwell Example*: 5 domains contain changes, 14 domain spaces and 20 interface spaces have to be regenerated.

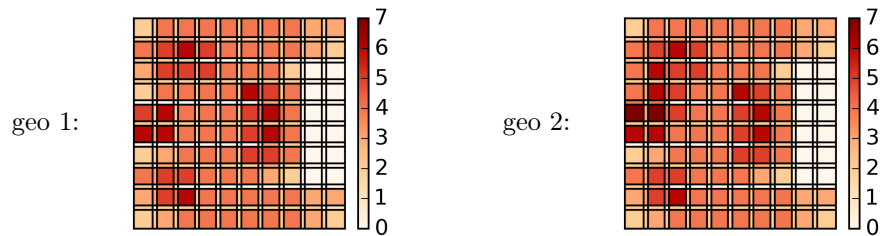


Figure 3.20.: Basis size distribution in *2D Maxwell Example*. (reproduction: Appendix A.11)

have to be regenerated. All other bases can be reused, which results in large computational savings compared to a simulation from scratch. However, the Galerkin projection leads to an unstable global reduced problem, as expected.

### 3.7. Ideas For Future Extension of ArbiLoMod

---

- ***Stable inf-sup reduction***

Using the same spaces for ansatz and test space does not lead to a stable reduction of inf-sup stable problems. The usual approach to enrich the test space with supremizers is not feasible in the localized setting, as the computation of supremizers is a global operation. A construction procedure for test spaces which lead to a stable Petrov-Galerkin projection should be devised.

- ***Better Steering of Local Greedy***

The local greedy to construct the codim-0 spaces in ArbiLoMod treats all interface functions as being equally important. Probably better spaces can be generated when assigning some form of importance factor to each interface function during training and considering this in the greedy. As an alternative, also the codim-0 space could be generated by local training, as it was done in the experiments for *2D Maxwell Example*.

- ***Systematic Comparison of Space Decompositions***

No systematic comparisons of different space decompositions have been done so far, to the author's knowledge. Benchmark examples should be defined and solved with different space decompositions, in order to compare their properties.

- ***Edge Problems in Wirebasket Space Decomposition***

The Extend operator for the construction of  $V_i^{\text{wb}}, i \in \Upsilon_2$  extends linear to zero on the edges first. Probably smaller basis sizes can be obtained by solving a 1D problem, as it was already suggested in [Hou and Wu(1997), Equation 2.7].

- ***Extend Operator at Domain Boundaries***

Close to the domain boundaries, the resulting basis sizes could probably be reduced if the Extend operator incorporated the boundary conditions in the construction of the extensions on edges.



---

Dual Norm Localization – A Posteriori Error Estimation

---

In this chapter, we are concerned with localized a posteriori error estimation. We devise two variants of an a posteriori error estimator which can be calculated using localized quantities only. First we will state two propositions in Section 4.2 in an abstract setting, which bound the norm of any continuous linear functional. We apply these to the residual to obtain localized a posteriori error estimates. Then we derive bounds for the constants involved in Section 4.3. Finally, we state a scheme for an offline/online decomposition of the calculation of the dual norms involved in Section 4.5, which overcomes numerical issues in traditional offline/online splitting schemes.

#### 4.1. Requirements on Localized a Posteriori Error Estimator

The model reduction error in the ArbiLoMod has to be controlled. To this end, an a posteriori error estimator is used which should have the following properties:

1. It is robust and efficient.
2. It is offline/online decomposable.
3. It is parallelizable with little amount of communication.
4. After a localized geometry change, the offline computed data in unaffected regions can be reused.
5. It can be used to steer adaptive enrichment of the reduced local subspaces.

These requirements are fulfilled by the estimator presented in the following. We develop localized bounds for the standard RB error estimator,

$$\Delta(\tilde{u}_\mu) := \frac{1}{\alpha_\mu} \|\mathcal{R}_\mu(\tilde{u}_\mu)\|_{V'}, \quad (4.1)$$

where  $\mathcal{R}_\mu(\tilde{u}_\mu) \in V'$  is the global residual given as  $\mathcal{R}_\mu(\tilde{u}_\mu)(\varphi) = f_\mu(\varphi) - a_\mu(\tilde{u}_\mu, \varphi) \quad \forall \varphi \in V$ . This error estimator is known to be robust and efficient (e.g. [Hesthaven et al.(2016), Proposition 4.4]):

$$\|u_\mu - \tilde{u}_\mu\|_V \leq \Delta(\tilde{u}_\mu) \leq \frac{\gamma_\mu}{\alpha_\mu} \|u_\mu - \tilde{u}_\mu\|_V. \quad (4.2)$$

## 4.2. Abstract Estimates for Dual Norm Localization

In this section, we show two different estimates, holding for any continuous linear functional  $F \in V'$ . In later sections, we will apply these estimates to the residual to obtain localized a posteriori error estimates.

### Setting

Throughout this section, let  $V$  be any ansatz space (continuous or discrete) and let  $\{V_i\}_{i=1}^{N_{V_i}}$ ,  $\{\mathcal{P}_{V_i}\}_{i=1}^{N_{V_i}}$  be local spaces and mappings of a localizing space decomposition as defined in Section 2.4.1. No further assumptions about the space decomposition are required here. Let furthermore

$$\bigcup_{k=1}^{\bar{J}} \Upsilon_{C,k} = \{1, \dots, N_{V_i}\} \quad (4.3)$$

be a partition of  $\{1, \dots, N_{V_i}\}$  such that

$$\forall 1 \leq k \leq \bar{J} : \forall i, j \in \Upsilon_{C,k}, i \neq j : V_i \perp V_j \quad (4.4)$$

i.e. we can partition the local subspaces into  $\bar{J}$  sets so that in each set, all spaces are orthogonal.

In this setting, we show the estimates. To do so, we need following lemma.

**Lemma 4.2.1** (Efficiency of dual element localization). *With the assumptions from above, for any continuous linear functional  $F$  on  $V$  it holds that*

$$\left( \sum_{i=1}^{N_{V_i}} \|F\|_{V_i'}^2 \right)^{\frac{1}{2}} \leq \sqrt{\bar{J}} \|F\|_{V'}. \quad (4.5)$$

*Proof.* Let  $V_i \perp V_j$  be some subspaces of  $V$ , and let  $F$  be a continuous linear functional on  $V_i \oplus V_j$ . If  $v_{F,1} \in V_i$  and  $v_{F,2} \in V_j$  are the Riesz representatives of  $F$  in  $V_i$  and  $V_j$ , then due to the orthogonality of  $V_i$  and  $V_j$ ,  $v_{F,1} + v_{F,2}$  is the Riesz representative of  $F$  on  $V_i \oplus V_j$ . Thus,

$$\begin{aligned} \|F\|_{(V_i \oplus V_j)'}^2 &= \|v_{F,1} + v_{F,2}\|_V^2 \\ &= \|v_{F,1}\|_V^2 + \|v_{F,2}\|_V^2 = \|F\|_{V_i'}^2 + \|F\|_{V_j'}^2, \end{aligned} \quad (4.6)$$

where we have used the orthogonality of the spaces again. The same is true for a larger orthogonal sum of spaces. We therefore obtain:

$$\begin{aligned} \sum_{i=1}^{N_{V_i}} \|F\|_{V_i'}^2 &= \sum_{k=1}^{\bar{J}} \sum_{i \in \Upsilon_{C,k}} \|F\|_{V_i'}^2 \\ &= \sum_{k=1}^{\bar{J}} \|F\|_{(\bigoplus_{i \in \Upsilon_{C,k}} V_i)'}^2 \\ &\leq \bar{J} \|F\|_{V'}^2. \end{aligned} \quad (4.7)$$

□

Using this lemma, we can state the following two localizing estimates for continuous linear functionals. In the following, we assume there is a subspace  $\tilde{V} \subset V_h$  such that  $F(\varphi) = 0$  for all  $\varphi$  in all  $\tilde{V}$ .



**Proposition 4.2.2** (Localization of dual norm with local stability constants). *With the local stability constants defined as*

$$c_{i,\tilde{V}} := \sup_{\varphi \in V \setminus \{0\}} \frac{\left\| \left(1 - P_{\tilde{V} \cap V_i}\right) \mathcal{P}_{V_i}(\varphi) \right\|}{\|\varphi\|}, \quad (4.8)$$

where  $P_{\tilde{V} \cap V_i}$  is the orthogonal projection on  $\tilde{V} \cap V_i$ , the dual norm of any continuous linear functional  $F$  on  $V$  for which it holds

$$F(\varphi) = 0 \quad \forall \varphi \in \tilde{V} \quad (4.9)$$

can be bounded as

$$\|F\|_{V'} \leq \sum_{i=1}^{N_{V_i}} c_{i,\tilde{V}} \|F\|_{V_i'} \leq \left( \sum_{i=1}^{N_{V_i}} c_{i,\tilde{V}}^2 \right)^{\frac{1}{2}} \|F\|_{V'}. \quad (4.10)$$

*Proof.* By definition, it holds that

$$\|F\|_{V'} = \sup_{\varphi \in V \setminus \{0\}} \frac{F(\varphi)}{\|\varphi\|}. \quad (4.11)$$

Applying the space decomposition  $\mathcal{P}_{V_i}$  on  $\varphi$  and using the linearity of the functional, it follows that

$$\|F\|_{V'} = \sup_{\varphi \in V \setminus \{0\}} \sum_{i=1}^{N_{V_i}} \frac{F(\mathcal{P}_{V_i}(\varphi))}{\|\varphi\|}. \quad (4.12)$$

Exchanging the supremum and the sum can only increase the value of the expression. We have

$$\|\varphi\| \geq \frac{1}{c_{i,\tilde{V}}} \left\| \left(1 - P_{\tilde{V} \cap V_i}\right) \mathcal{P}_{V_i}(\varphi) \right\| \quad (4.13)$$

and it follows that

$$\|F\|_{V'} \leq \sum_{i=1}^{N_{V_i}} \sup_{\varphi \in V \setminus \text{Ker}\{(1-P_{\tilde{V} \cap V_i})\mathcal{P}_{V_i}\}} c_{i,\tilde{V}} \frac{F(\mathcal{P}_{V_i}(\varphi))}{\left\| \left(1 - P_{\tilde{V} \cap V_i}\right) \mathcal{P}_{V_i}(\varphi) \right\|}. \quad (4.14)$$

Since the image of  $P_{\tilde{V} \cap V_i}$  is in the kernel of  $F$ , it holds that

$$\begin{aligned} & \sup_{\varphi \in V \setminus \text{Ker}\{(1-P_{\tilde{V} \cap V_i})\mathcal{P}_{V_i}\}} \frac{F(\mathcal{P}_{V_i}(\varphi))}{\left\| \left(1 - P_{\tilde{V} \cap V_i}\right) \mathcal{P}_{V_i}(\varphi) \right\|} \\ &= \sup_{\varphi \in V \setminus \text{Ker}\{(1-P_{\tilde{V} \cap V_i})\mathcal{P}_{V_i}\}} \frac{F\left(\mathcal{P}_{V_i}(\varphi) - P_{\tilde{V} \cap V_i} \mathcal{P}_{V_i}(\varphi)\right)}{\left\| \left(1 - P_{\tilde{V} \cap V_i}\right) \mathcal{P}_{V_i}(\varphi) \right\|} \end{aligned} \quad (4.15)$$

and further

$$\begin{aligned} & \sup_{\varphi \in V \setminus \text{Ker}\{(1-P_{\tilde{V} \cap V_i})\mathcal{P}_{V_i}\}} \frac{F(\mathcal{P}_{V_i}(\varphi))}{\left\| \left(1 - P_{\tilde{V} \cap V_i}\right) \mathcal{P}_{V_i}(\varphi) \right\|} \\ &= \sup_{\varphi \in V \setminus \text{Ker}\{(1-P_{\tilde{V} \cap V_i})\mathcal{P}_{V_i}\}} \frac{F\left(\left(1 - P_{\tilde{V} \cap V_i}\right) \mathcal{P}_{V_i}(\varphi)\right)}{\left\| \left(1 - P_{\tilde{V} \cap V_i}\right) \mathcal{P}_{V_i}(\varphi) \right\|} \\ &= \sup_{\varphi \in \text{Im}\{(1-P_{\tilde{V} \cap V_i})\mathcal{P}_{V_i}\} \setminus \{0\}} \frac{F(\varphi)}{\|\varphi\|} \\ &\leq \sup_{\varphi \in V_i \setminus \{0\}} \frac{F(\varphi)}{\|\varphi\|} = \|F\|_{V_i'} \end{aligned} \quad (4.16)$$

the first inequality follows.

For the second inequality we apply Cauchy-Schwarz

$$\sum_{i=1}^{N_{V_i}} c_{i,\tilde{V}} \|F\|_{V_i'} \leq \left( \sum_{i=1}^{N_{V_i}} c_{i,\tilde{V}} \right)^{\frac{1}{2}} \left( \sum_{i=1}^{N_{V_i}} \|F\|_{V_i'}^2 \right)^{\frac{1}{2}} \quad (4.17)$$

and then use Lemma 4.2.1 to obtain the claim.  $\square$

**Proposition 4.2.3** (Localization of dual norm with global stability constant). *With the global stability constant defined as*

$$c_{\text{pu},\tilde{V}} := \sup_{\varphi \in V \setminus \{0\}} \frac{\left( \sum_{i=1}^{N_{V_i}} \left\| \left( 1 - P_{\tilde{V} \cap V_i} \right) \mathcal{P}_{V_i}(\varphi) \right\|^2 \right)^{\frac{1}{2}}}{\|\varphi\|}, \quad (4.18)$$

the dual norm of any continuous linear functional  $F$  on  $V$  for which it holds

$$F(\varphi) = 0 \quad \forall \varphi \in \tilde{V} \quad (4.19)$$

can be bounded as

$$\|F\|_{V'} \leq c_{\text{pu},\tilde{V}} \left( \sum_{i=1}^{N_{V_i}} \|F\|_{V_i'}^2 \right)^{\frac{1}{2}} \leq c_{\text{pu},\tilde{V}} \sqrt{J} \|F\|_{V'}. \quad (4.20)$$

*Proof.* By definition, it holds that

$$\|F\|_{V'} = \sup_{\varphi \in V \setminus \{0\}} \frac{F(\varphi)}{\|\varphi\|}. \quad (4.21)$$

Applying the space decomposition  $\mathcal{P}_{V_i}$  on  $\varphi$  and using the linearity of the functional, it follows that

$$\|F\|_{V'} = \sup_{\varphi \in V \setminus \{0\}} \frac{\sum_{i=1}^{N_{V_i}} F(\mathcal{P}_{V_i}(\varphi))}{\|\varphi\|}. \quad (4.22)$$

Since the image of  $P_{\tilde{V} \cap V_i}$  is in the kernel of  $F$ , it holds that

$$\|F\|_{V'} = \sup_{\varphi \in V \setminus \{0\}} \frac{\sum_{i=1}^{N_{V_i}} F\left(\left(1 - P_{\tilde{V} \cap V_i}\right) \mathcal{P}_{V_i}(\varphi)\right)}{\|\varphi\|}. \quad (4.23)$$

Using the dual norm of  $F$  in

$$F\left(\left(1 - P_{\tilde{V} \cap V_i}\right) \mathcal{P}_{V_i}(\varphi)\right) \leq \|F\|_{V_i'} \left\| \left(1 - P_{\tilde{V} \cap V_i}\right) \mathcal{P}_{V_i}(\varphi) \right\|, \quad (4.24)$$

applying Cauchy-Schwarz, and rearranging yields

$$\|F\|_{V'} = \sup_{\varphi \in V \setminus \{0\}} \frac{\sum_{i=1}^{N_{V_i}} F\left(\left(1 - P_{\tilde{V} \cap V_i}\right) \mathcal{P}_{V_i}(\varphi)\right)}{\|\varphi\|} \quad (4.25)$$

$$\leq \sup_{\varphi \in V \setminus \{0\}} \frac{\sum_{i=1}^{N_{V_i}} \|F\|_{V_i'} \left\| \left(1 - P_{\tilde{V} \cap V_i}\right) \mathcal{P}_{V_i}(\varphi) \right\|}{\|\varphi\|} \quad (4.26)$$

$$\leq \sup_{\varphi \in V \setminus \{0\}} \frac{\left( \sum_{i=1}^{N_{V_i}} \left\| \left(1 - P_{\tilde{V} \cap V_i}\right) \mathcal{P}_{V_i}(\varphi) \right\|^2 \right)^{\frac{1}{2}} \left( \sum_{i=1}^{N_{V_i}} \|F\|_{V_i'}^2 \right)^{\frac{1}{2}}}{\|\varphi\|} \quad (4.27)$$

$$= c_{\text{pu},\tilde{V}} \left( \sum_{i=1}^{N_{V_i}} \|F\|_{V_i'}^2 \right)^{\frac{1}{2}} \quad (4.28)$$

which is the first inequality.

The second inequality again follows directly from Lemma 4.2.1.  $\square$

There are some obvious relations between these stability constants, namely

$$c_{\text{pu},\tilde{V}} \leq \left( \sum_{i=1}^{N_{V_i}} c_{i,\tilde{V}}^2 \right)^{\frac{1}{2}} \quad (4.29)$$

$$c_{i,\tilde{V}} \leq c_{\text{pu},\tilde{V}} \quad \forall i \in \{1, \dots, N_{V_i}\}. \quad (4.30)$$

A stability constant very similar to  $c_{\text{pu},\tilde{V}}$  appears in the analysis of overlapping domain decomposition methods (e.g. [Toselli and Widlund(2005), Assumption 2.2], [Spillane et al.(2014)]) and in localization of error estimators on stars (e.g. [Cohen et al.(2012)]). Applying these two estimates to the residual, we obtain two efficient, localized error estimators:

**Corollary 4.2.4** (Localization of a posteriori error estimator). *The error estimators  $\Delta_{loc}^l(\tilde{u}_\mu)$  and  $\Delta_{loc}^g(\tilde{u}_\mu)$ , defined by*

$$\Delta_{loc}^l(\tilde{u}_\mu) := \frac{1}{\alpha_\mu} \sum_{i=1}^{N_{V_i}} c_{i,\tilde{V}} \|\mathcal{R}_\mu(\tilde{u}_\mu)\|_{V_i'} \quad (4.31)$$

$$\Delta_{loc}^g(\tilde{u}_\mu) := \frac{1}{\alpha_\mu} c_{\text{pu},\tilde{V}} \left( \sum_{i=1}^{N_{V_i}} \|\mathcal{R}_\mu(\tilde{u}_\mu)\|_{V_i'}^2 \right)^{\frac{1}{2}} \quad (4.32)$$

are robust and efficient. It holds

$$\|u_\mu - \tilde{u}_\mu\|_V \leq \Delta_{loc}^l(\tilde{u}_\mu) \leq \frac{\gamma_\mu}{\alpha_\mu} \left( \sum_{i=1}^{N_{V_i}} c_{i,\tilde{V}}^2 \right)^{\frac{1}{2}} \sqrt{\bar{J}} \|u_\mu - \tilde{u}_\mu\|_V \quad (4.33)$$

$$\|u_\mu - \tilde{u}_\mu\|_V \leq \Delta_{loc}^g(\tilde{u}_\mu) \leq \frac{\gamma_\mu}{\alpha_\mu} c_{\text{pu},\tilde{V}} \sqrt{\bar{J}} \|u_\mu - \tilde{u}_\mu\|_V. \quad (4.34)$$

*Proof.* Applying Proposition 4.2.2 or Proposition 4.2.3 to the error estimator

$$\Delta(\tilde{u}_\mu) = \frac{1}{\alpha_\mu} \|\mathcal{R}_\mu(\tilde{u}_\mu)\|_V, \quad (4.35)$$

yields, together with Equation (4.2), the proposition.  $\square$

#### Discussion of the two variants

Depending on the distribution of the residual in space, the variant with the localized constants  $\Delta_{loc}^l(\tilde{u}_\mu)$  might deliver better or worse results than the variant with globally computed constants  $\Delta_{loc}^g(\tilde{u}_\mu)$ . Whenever both the residual and the constant  $c_{i,\tilde{V}}$  are distributed heterogeneously over the domain, we expect that the localized variant  $\Delta_{loc}^l(\tilde{u}_\mu)$  might be superior. When the residual and the constants are homogeneously distributed over the domain, we expect the variant with globally computed constants  $\Delta_{loc}^g(\tilde{u}_\mu)$  to be superior. As most of the computational effort is in the computation of the localized residuals, it might be the best strategy to always compute both  $\Delta_{loc}^l(\tilde{u}_\mu)$  and  $\Delta_{loc}^g(\tilde{u}_\mu)$  and use the better one. In our experiments in Section 3.6.1 we used  $\Delta_{loc}^g(\tilde{u}_\mu)$ .

Offline/online decomposition of this error estimator can be done by applying the usual strategy for offline/online decomposition used with the standard RB error estimator (see e.g. [Hesthaven et al.(2016), Sec. 4.2.5]) or the numerically more stable approach shown below in Section 4.5 to every dual norm in the localized error estimators.

### 4.3. Choosing Spaces and Bounding Constants

The error estimators defined in Corollary 4.2.4 work for any space decomposition fulfilling the assumptions in Section 2.4.1. It is important to realize that there is no requirement to use the same space decomposition for the decomposition of the ansatz space and for the a posteriori error estimator. In order to obtain good constants, the space decomposition needs to be chosen carefully. For the space decomposition used in the a posteriori error estimator, there are different requirements than for the space decomposition used in constructing the ansatz space. While the main goal in the selection of the localization of the ansatz space for the construction of the reduced space was to achieve a small dimension of the reduced space and especially a small dimension of the reduced spaces coupling the domains, for the space decomposition used for the a posteriori error estimator, the following two requirements are dominant. First, the subspaces should be spanned by FE ansatz functions, allowing the residual to be easily evaluated on these spaces. If we used a wirebasket space decomposition for the a posteriori error estimator, as it was done in [Smetana(2015)], it would be necessary to construct a basis for every local space, in turn needing the construction of extensions of every fine grid DoF on the interfaces. This leads to very high computational cost in the offline phase, which is not a problem in the SCRBE with its complete offline/online decomposition, but is a problem in the ArbiLoMod setting. Second, the inner product matrices on the subspaces should be sparse, as the inner product matrix has to be solved in the computation of the dual norms.

In order to achieve these two goals, we use the partition of unity decomposition given in Section 2.4.3. We define the overlapping domains  $\omega_i^{\text{ol}}$  in terms of the non overlapping domains  $\omega_i^{\text{noI}}$ .

**Definition 4.3.1** (Overlapping space decomposition). *Let  $\mathcal{V}_i$ ,  $i \in \{1, \dots, N_{\mathcal{V}_i}\}$  be the inner vertices of the coarse mesh. We define the overlapping subdomains as*

$$\omega_i^{\text{ol}} := \overline{\bigcup_{j \in I_{\mathcal{V}_i}} \omega_j^{\text{noI}}} \quad i \in \{1, \dots, N_{\mathcal{V}_i}\} \quad (4.36)$$

and we define linear interpolation operator  $\mathcal{I}$  to be the nodal Lagrange interpolation. It holds  $N_{\text{ol}} = N_{\mathcal{V}_i}$ .

Recall the definition of  $I_{\mathcal{V}_i}$  from Equation (3.2):  $I_{\mathcal{V}_i}$  is the set of indices of subdomains that contain the coarse mesh vertex  $\mathcal{V}_i$ , i.e.

$$I_{\mathcal{V}_j} := \left\{ i \in \{1, \dots, N_{\text{noI}}\} \mid \mathcal{V}_j \subseteq \overline{\omega_i^{\text{noI}}} \right\}. \quad (4.37)$$

With these definitions, the local space  $V_i^{\text{pou}}$  is the span of all FE basis functions having support only on the corresponding overlapping domain. With  $I_\psi$  defined as in Equation (3.1), we have

$$V_i^{\text{pou}} = \text{span} \left\{ \psi \in \mathcal{B} \mid I_\psi \subseteq I_{\mathcal{V}_i} \right\}. \quad (4.38)$$

Note that we have  $V_i^{\text{pou}} \subseteq H_0^1(\omega_i^{\text{ol}})$  for the inner domains with  $\partial\omega_i^{\text{ol}} \cap \partial\Omega = \emptyset$ . Contrary to  $V_i^{\text{wb}}$  or  $V_i^{\text{basic}}$ , these spaces do not form a direct sum decomposition of  $V_h$ . We next state a first estimate on the partition of unity constant  $c_{\text{pu}, \tilde{V}}$  of Corollary 4.2.4. The resulting estimate thus depends on  $H^{-1}$ , where  $H$  is the minimum diameter of the subdomains of the macro partition. Typically, the size of the macro partition is moderate such that  $H^{-1}$  is small. However, in the following Proposition 4.3.3 we will show that the constant  $c_{\text{pu}, \tilde{V}}$  can be actually bounded independent of  $H$ , when we choose a partition of unity that is contained in the reduced space  $\tilde{V}$ .

**Proposition 4.3.2** (Estimate of localization constant). *Let  $V$  be a subspace of  $H^1(\Omega)$  equipped with the usual  $H^1$ -norm. Let  $J := \max_{x \in \Omega} \#\{i \in \{1, \dots, N_{\text{ol}}\} \mid x \in \omega_i^{\text{ol}}\}$  be the maximum number of*

overlapping domains  $\omega_i^{\text{ol}}$  overlapping in any point  $x$  of  $\Omega$  and let  $H_i := \text{diam}(\omega_i^{\text{ol}})$ ,  $i \in \{1, \dots, N_{\text{ol}}\}$  and  $H := \min_{\{1, \dots, N_{\text{ol}}\}} H_i$ . Furthermore, assume that there exist partition of unity functions  $\varrho_i \in H^{1, \infty}(\Omega)$ ,  $i \in \{1, \dots, N_{\text{ol}}\}$  and a linear interpolation operator  $\mathcal{I} : V \rightarrow V_h$  such that

$$(i) \sum_{i=1}^{N_{\text{ol}}} \varrho_i(x) = 1 \text{ for all } x \in \Omega,$$

$$(ii) \varrho_i(x) \geq 0 \text{ for all } x \text{ in } \Omega \text{ and all } i \text{ in } \{1, \dots, N_{\text{ol}}\}.$$

$$(iii) \|\nabla \varrho_i\|_{\infty} \leq c'_{\text{pu}} H_i^{-1} \text{ for all } i \in \{1, \dots, N_{\text{ol}}\},$$

$$(iv) \mathcal{I}(\varphi) = \varphi \text{ for all } \varphi \in V_h,$$

$$(v) \|\mathcal{I}(\varrho_i v_h) - \varrho_i v_h\|_V \leq c_I \|v_h\|_{H^1(\omega_i^{\text{ol}})} \text{ for all } i \in \{1, \dots, N_{\text{ol}}\} \text{ and all } v_h \in V_h.$$

Then we have:

$$c_{\text{pu}, \tilde{V}} \leq \sqrt{4 + 2c_I^2 + 4(c'_{\text{pu}} H^{-1})^2} \cdot \sqrt{J}. \quad (4.39)$$

*Proof.* We compute the bound for  $c_{\text{pu}, \tilde{V}}$  using the partition of unity and the interpolation operator. Recall the definition

$$\mathcal{P}_{V_i^{\text{pou}}}(\varphi) := \mathcal{I}(\varrho_i \varphi), \quad i \in \{1, \dots, N_{\text{ol}}\}. \quad (4.40)$$

Using this definition and (v) we have for any  $\varphi \in V_h$

$$\begin{aligned} \sum_{i=1}^{N_{\text{ol}}} \left\| \mathcal{P}_{V_i^{\text{pou}}}(\varphi) \right\|_V^2 &= \sum_{i=1}^{N_{\text{ol}}} \|\mathcal{I}(\varrho_i \varphi)\|_V^2 \\ &= \sum_{i=1}^{N_{\text{ol}}} \|\mathcal{I}(\varrho_i \varphi) - \varrho_i \varphi + \varrho_i \varphi\|_V^2 \\ &\leq 2 \sum_{i=1}^{N_{\text{ol}}} \|\mathcal{I}(\varrho_i \varphi) - \varrho_i \varphi\|_V^2 + \|\varrho_i \varphi\|_V^2 \\ &\leq 2 \sum_{i=1}^{N_{\text{ol}}} c_I^2 \|\varphi\|_{H^1(\omega_i^{\text{ol}})}^2 + \|\varrho_i \varphi\|_V^2. \end{aligned} \quad (4.41)$$

Furthermore, using the properties of the partition of unity, we have

$$\begin{aligned} \|\varrho_i \varphi\|_V^2 &= \int_{\omega_i^{\text{ol}}} |\nabla(\varrho_i \varphi)|^2 + |\varrho_i \varphi|^2 \, dx \\ &= \int_{\omega_i^{\text{ol}}} |\nabla \varrho_i \varphi + \varrho_i \nabla \varphi|^2 + |\varrho_i \varphi|^2 \, dx \\ &\leq \int_{\omega_i^{\text{ol}}} 2|\nabla \varrho_i \varphi|^2 + 2|\varrho_i \nabla \varphi|^2 + |\varrho_i \varphi|^2 \, dx \\ &\leq \int_{\omega_i^{\text{ol}}} 2(c'_{\text{pu}} H_i^{-1})^2 |\varphi|^2 + 2|\nabla \varphi|^2 + |\varphi|^2 \, dx \\ &= \left(1 + 2(c'_{\text{pu}} H_i^{-1})^2\right) \|\varphi\|_{L^2(\omega_i^{\text{ol}})}^2 + 2\|\nabla \varphi\|_{L^2(\omega_i^{\text{ol}})}^2 \\ &\leq \left(2 + 2(c'_{\text{pu}} H_i^{-1})^2\right) \|\varphi\|_{H^1(\omega_i^{\text{ol}})}^2. \end{aligned} \quad (4.42)$$

Inserting Equation (4.42) into Equation (4.41) yields

$$\begin{aligned}
 \sum_{i=1}^{N_{\text{ol}}} \left\| \mathcal{P}_{V_i^{\text{pou}}}(\varphi) \right\|_V^2 &\leq 2 \sum_{i=1}^{N_{\text{ol}}} c_I^2 \|\varphi\|_{H^1(\omega_i^{\text{ol}})}^2 + \left( 2 + 2 (c'_{\text{pu}} H_i^{-1})^2 \right) \|\varphi\|_{H^1(\omega_i^{\text{ol}})}^2 \\
 &\leq \left( 4 + 2c_I^2 + 4 (c'_{\text{pu}} H_i^{-1})^2 \right) \sum_{i=1}^{N_{\text{ol}}} \|\varphi\|_{H^1(\omega_i^{\text{ol}})}^2 \\
 &\leq \left( 4 + 2c_I^2 + 4 (c'_{\text{pu}} H_i^{-1})^2 \right) J \|\varphi\|_V^2.
 \end{aligned} \tag{4.43}$$

This gives us the estimate.  $\square$

A similar estimate for the energy norm is given in Proposition 6.4.1.

For the rectangular domain decomposition used in the numerical example below, the constant  $J$  is  $J = 2^d = 4$ : it is possible to divide the overlapping domains into four classes, so that within each class, no domain overlaps with any other (cf. [Chung et al.(2015), Sec. 5]).

Furthermore, the coercivity constant  $\alpha_\mu$  and the stability constant  $\gamma_\mu$ , or estimates, are required. For the numerical example *Thermal Channels Example* used in Section 3.6.1, those can be calculated analytically. In general this is not possible. The numerical computation of a lower bound for the coercivity constant was subject of extensive research in the RB community (see e.g. [Huynh et al.(2007), Chen et al.(2008)]), but these methods require the calculation of the coercivity constant at some parameter values and thus require the solution of a global, fine scale problem. To the authors' knowledge, there are no publications on localization of these methods so far.

The upper bound on the constant  $c_{\text{pu}, \tilde{V}}$  in Proposition 4.3.2 depends on the domain size  $H$  approximately like  $H^{-1}$ . As the domain size is considered a constant in the context of ArbiLoMod, the error estimator is already considered efficient with this bound. In the next proposition, we however show that the constant  $c_{\text{pu}, \tilde{V}}$  can indeed be bounded independent of  $H$ , if we exploit that the residual vanishes on the reduced space  $\tilde{V}$ .

**Proposition 4.3.3** (*H independent localization constant estimate*). *Let  $\varrho_i$ ,  $i \in \{1, \dots, N_{\text{ol}}\}$  be a partition of unity and  $\mathcal{I}$  an interpolation operator satisfying the prerequisites of Proposition 4.3.2. Furthermore, assume  $V = H_0^1(\Omega)$  and that  $\varrho_i \in \tilde{V} \cap V_i^{\text{pou}}$  for  $i \in D^{\text{int}} := \{i \in \{1, \dots, N_{\text{ol}}\} \mid \omega_i^{\text{ol}} \cap \partial\Omega = \emptyset\}$ , e.g.  $\varrho_i$  is included in the reduced space (see Sections 3.2 and 3.3.1 above). Then the following estimate holds:*

$$c_{\text{pu}, \tilde{V}} \leq \sqrt{4 + 2c_I^2 + 4(c'_{\text{pu}} c_{\text{pc}})^2} \cdot \sqrt{J}, \tag{4.44}$$

with a Poincaré-inequality constant  $c_{\text{pc}}$  (see proof below) that does not depend on the fine or coarse mesh sizes  $(h, H)$ .

*Proof.* For arbitrary  $\varphi \in V_h$  let  $\bar{\varphi}_i := \frac{1}{|\omega_i^{\text{ol}}|} \int_{\omega_i^{\text{ol}}} \varphi$ . We then have with  $D^{\text{ext}} := \{1, \dots, N_{\text{ol}}\} \setminus D^{\text{int}}$

$$\begin{aligned}
 c_{\text{pu}, \tilde{V}} &:= \sup_{\varphi \in V_h \setminus \{0\}} \frac{\left( \sum_{i=1}^{N_{\text{ol}}} \left\| \left( 1 - P_{\tilde{V} \cap V_i^{\text{pou}}} \right) \mathcal{P}_{V_i^{\text{pou}}}(\varphi) \right\|^2 \right)^{\frac{1}{2}}}{\|\varphi\|} \\
 &= \sup_{\varphi \in V_h \setminus \{0\}} \frac{\left( \sum_{i \in D^{\text{int}}} \left\| \left( 1 - P_{\tilde{V} \cap V_i^{\text{pou}}} \right) \mathcal{P}_{V_i^{\text{pou}}}(\varphi) \right\|^2 + \sum_{i \in D^{\text{ext}}} \left\| \left( 1 - P_{\tilde{V} \cap V_i^{\text{pou}}} \right) \mathcal{P}_{V_i^{\text{pou}}}(\varphi) \right\|^2 \right)^{\frac{1}{2}}}{\|\varphi\|} \\
 &\leq \sup_{\varphi \in V_h \setminus \{0\}} \frac{\left( \sum_{i \in D^{\text{int}}} \left\| \mathcal{P}_{V_i^{\text{pou}}}(\varphi) - \bar{\varphi}_i \varrho_i \right\|^2 + \sum_{i \in D^{\text{ext}}} \left\| \mathcal{P}_{V_i^{\text{pou}}}(\varphi) \right\|^2 \right)^{\frac{1}{2}}}{\|\varphi\|},
 \end{aligned} \tag{4.45}$$

where we have used that by construction  $\bar{\varphi}_i \varrho_i \in \tilde{V} \cap V_i^{\text{pou}}$  for all  $i \in D^{\text{int}}$ . For any  $\varphi \in V_h$  and  $i \in D^{\text{int}}$  we then have  $\left\| \mathcal{P}_{V_i^{\text{pou}}}(\varphi) - \bar{\varphi}_i \varrho_i \right\|_V^2 \leq 2c_I^2 \|\nabla \varphi\|_{L^2(\omega_i^{\text{ol}})}^2 + 2\|(\varphi - \bar{\varphi}_i) \varrho_i\|_V^2$ , where

$$\begin{aligned} \|(\varphi - \bar{\varphi}_i) \varrho_i\|_V^2 &\leq \int_{\Omega_\xi} 2|\nabla(\varphi - \bar{\varphi}_i) \varrho_i|^2(x) + 2|(\varphi - \bar{\varphi}_i) \nabla \varrho_i|^2(x) \, dx \\ &\quad + \|(\varphi - \bar{\varphi}_i) \varrho_i\|_{L^2(\omega_i^{\text{ol}})}^2. \end{aligned} \quad (4.46)$$

With a rescaled Poincaré-type inequality

$$\|\varphi - \bar{\varphi}_i\|_{L^2(\omega_i^{\text{ol}})} \leq c_{\text{pc}} H_i \|\nabla \varphi\|_{L^2(\omega_i^{\text{ol}})},$$

and  $\|\varphi - \bar{\varphi}_i\|_{L^2(\omega_i^{\text{ol}})} \leq \|\varphi\|_{L^2(\omega_i^{\text{ol}})}$ , we get

$$\begin{aligned} \int_{\Omega_\xi} 2|\nabla(\varphi - \bar{\varphi}_i) \varrho_i|^2(x) + 2|(\varphi - \bar{\varphi}_i) \nabla \varrho_i|^2(x) \, dx + \|(\varphi - \bar{\varphi}_i) \varrho_i\|_{L^2(\omega_i^{\text{ol}})}^2 \\ \leq (2 + 2(c'_{\text{pu}} c_{\text{pc}})^2) \|\nabla \varphi\|_{L^2(\omega_i^{\text{ol}})}^2 + \|\varphi\|_{L^2(\omega_i^{\text{ol}})}^2. \end{aligned} \quad (4.47)$$

In analogy we obtain for the boundary terms, i.e.  $i \in D^{\text{ext}}$ , the estimates

$$\left\| \mathcal{P}_{V_i^{\text{pou}}}(\varphi) \right\|_V^2 \leq 2c_I^2 \|\nabla \varphi\|_{L^2(\omega_i^{\text{ol}})}^2 + 2\|\varphi \varrho_i\|_V^2, \quad (4.48)$$

and

$$\begin{aligned} \|\varphi \varrho_i\|_V^2 &\leq \int_{\Omega_\xi} 2|\nabla \varphi \varrho_i|^2(x) + 2|\varphi \nabla \varrho_i|^2(x) \, dx + \|\varphi \varrho_i\|_{L^2(\omega_i^{\text{ol}})}^2 \\ &\leq (2 + 2(c'_{\text{pu}} c_{\text{pc}})^2) \|\nabla \varphi\|_{L^2(\omega_i^{\text{ol}})}^2 + \|\varphi\|_{L^2(\omega_i^{\text{ol}})}^2 \end{aligned} \quad (4.49)$$

using a rescaled Poincaré-type inequality which holds for  $i \in D^{\text{ext}}$  as  $\varphi \in V_h$  has zero boundary values, i.e.

$$\|\varphi\|_{L^2(\omega_i^{\text{ol}})} \leq c_{\text{pc}} H_i \|\nabla \varphi\|_{L^2(\omega_i^{\text{ol}})}.$$

Summing up all contributions we then have

$$\begin{aligned} \sum_{i \in D^{\text{int}}} \left\| \mathcal{P}_{V_i^{\text{pou}}}(\varphi) - \bar{\varphi}_i \varrho_i \right\|_V^2 + \sum_{i \in D^{\text{ext}}} \left\| \mathcal{P}_{V_i^{\text{pou}}}(\varphi) \right\|_V^2 \\ \leq \sum_{i \in \{1, \dots, N_{\text{ol}}\}} 2c_I^2 \|\nabla \varphi\|_{L^2(\omega_i^{\text{ol}})}^2 + 2 \left[ (2 + 2(c'_{\text{pu}} c_{\text{pc}})^2) \|\nabla \varphi\|_{L^2(\omega_i^{\text{ol}})}^2 + \|\varphi\|_{L^2(\omega_i^{\text{ol}})}^2 \right] \\ \leq (4 + 2c_I^2 + 4(c'_{\text{pu}} c_{\text{pc}})^2) J \|\varphi\|_V^2. \end{aligned} \quad (4.50)$$

This gives us the estimate.  $\square$

Proposition 4.3.3 gives a bound on  $c_{\text{pu}, \tilde{V}}$  that depends on the contrast of the underlying diffusion coefficient if  $\varrho_i \in \tilde{V}$ ,  $i \in D^{\text{int}}$  is chosen as the MsFEM type hat functions as suggested in Section 3.2 above. However, it is independent on the mesh sizes  $h, H$ . A crucial ingredient to obtain this bound is the fact that we included this macroscopic partition of unity in our reduced approximation space  $\tilde{V}$ . If alternatively we would chose  $\varrho_i \in \tilde{V}$  to be the traditional Lagrange hat functions, the bound on  $c_{\text{pu}, \tilde{V}}$  in Proposition 4.3.3 would be independent of the contrast. In fact, we might expect that  $c_{\text{pu}, \tilde{V}}$  behaves much better than the upper bound due to the approximation properties of the reduced space. It would actually be possible to compute  $c_{\text{pu}, \tilde{V}}$  for given  $V, \tilde{V}$  which would however be computationally expensive and thus not of any use in practical applications. Proposition 4.3.3,

however shows that the localized a posteriori error estimator in Corollary 4.2.4 in the context of ArbiLoMod is indeed robust and efficient, even with respect to  $H \rightarrow 0$ .

Comparing with other localized RB and multiscale methods, one observes a difference in the scaling of the efficiency constants. While in our case,  $c_{pu}$  is independent of both  $h$  and  $H$ , the a posteriori error estimator published for LRBMS has a  $H/h$  dependency [Ohlberger and Schindler(2015), Theorem 4.6] and in the certification framework for SCRBE, a  $h^{-1/2}$  scaling appears [Smetana(2015), Proposition 4.5], which, however, can be removed by using  $H^{1/2}$ -orthogonal port modes [Smetana(2015), Corollary A.1]. The (a priori) error estimators published for GMS-FEM in [Chung et al.(2014)] also have no dependency on  $H$  or  $h$ . However, they also rely on specific properties of the basis generation. The error estimator presented here is independent of the method the basis is generated with, which is advantageous as basis generation algorithms and the error estimator can be developed further independently. Also in the analysis of the DGRBE Pacciarini et.al. have a factor of  $h^{-1/2}$  in the a priori analysis [Antonietti et al.(2016)] and in the a posteriori error estimator [Pacciarini(2016)].

So far we did not use properties of the bilinear form other than coercivity and continuity. Assuming locality of the bilinear form as in (2.36), we get a local efficiency estimate and an improved global efficiency estimate.

**Proposition 4.3.4** (Localized efficiency estimate). *Let the bilinear form  $a_\mu$  be given by (2.36). Then we have the localized efficiency estimate*

$$\|\mathcal{R}_\mu(\tilde{u}_\mu)\|_{V_i^{\text{pou}}} \leq \gamma_\mu \|\nabla(u_\mu - \tilde{u}_\mu)\|_{L^2(\omega_i^{\text{ol}})}. \quad (4.51)$$

*Proof.* Using the error identity

$$a_\mu(u_\mu - \tilde{u}_\mu, \varphi) = \mathcal{R}_\mu(\tilde{u}_\mu)(\varphi),$$

we obtain for any  $\varphi \in V_i^{\text{pou}}$

$$\begin{aligned} \mathcal{R}_\mu(\tilde{u}_\mu)(\varphi) &= \int_{\Omega} \sigma_\mu(x) \nabla(u_\mu - \tilde{u}_\mu)(x) \nabla \varphi(x) \, dx \\ &= \int_{\omega_i^{\text{ol}}} \sigma_\mu(x) \nabla(u_\mu - \tilde{u}_\mu)(x) \nabla \varphi(x) \, dx \\ &\leq \gamma_\mu \|\nabla(u_\mu - \tilde{u}_\mu)\|_{L^2(\omega_i^{\text{ol}})} \|\varphi\|_V, \end{aligned} \quad (4.52)$$

from which the statement follows.  $\square$

**Remark 4.3.5** (Improved efficiency estimates). *Under the assumptions of Proposition 4.3.4, we have the improved efficiency estimate*

$$\Delta_{loc}^g(\tilde{u}_\mu) \leq \frac{\gamma_\mu \sqrt{\bar{J}} c_{\text{pu}, \tilde{V}}}{\alpha_\mu} \|u_\mu - \tilde{u}_\mu\|_V.$$

*In many cases, a better constant can be found. Finite Element ansatz functions are usually not orthogonal if they share support. So if  $J$  spaces have support in one point in space, they have to be placed in different groups when designing a partition for Lemma 4.2.1, so  $J \leq \bar{J}$  (cf. [Toselli and Widlund(2005), p. 67]).*

Reviewing the five desired properties of an a posteriori error estimator at the beginning of this section, we see that the presented error estimator is robust and efficient (1) and is offline/online decomposable (2). Parallelization can be done over the spaces  $V_i^{\text{pou}}$ . Only online data has to be transferred, so there is little communication (3). The offline/online decomposition only has to be repeated for a space  $V_i^{\text{pou}}$ , if a new basis function with support in  $\omega_i^{\text{ol}}$  was added. So reuse in unchanged regions is possible (4). How the adaptive enrichment is steered (5) was already shown in Section 3.4.



#### 4.4. Relative Error Estimators

From the error estimators for the absolute error, we can construct error estimators for the relative error. Estimates for the relative error are given for example in [Hesthaven et al.(2016), Proposition 4.4], but the estimates used here are slightly sharper. The estimates presented in the following were already published in [Hess(2016), Lemma 3.2.2], but efficiency was not shown there.

**Proposition 4.4.1** (Relative error estimators). *Assuming  $\|\tilde{u}_\mu\|_V > \Delta(\tilde{u}_\mu)$  and  $\|\tilde{u}_\mu\|_V > \Delta_{loc}^g(\tilde{u}_\mu)$ , the error estimators defined by*

$$\begin{aligned}\Delta_{\text{rel}}(\tilde{u}_\mu) &:= \frac{\Delta(\tilde{u}_\mu)}{\|\tilde{u}_\mu\|_V - \Delta(\tilde{u}_\mu)} \\ \Delta_{loc,rel}^g(\tilde{u}_\mu) &:= \frac{\Delta_{loc}^g(\tilde{u}_\mu)}{\|\tilde{u}_\mu\|_V - \Delta_{loc}^g(\tilde{u}_\mu)}\end{aligned}\quad (4.53)$$

are robust and efficient:

$$\begin{aligned}\frac{\|u_\mu - \tilde{u}_\mu\|_V}{\|u_\mu\|_V} &\leq \Delta_{\text{rel}}(\tilde{u}_\mu) \leq (1 + 2\Delta_{\text{rel}}(\tilde{u}_\mu)) \frac{\gamma_\mu}{\alpha_\mu} \frac{\|u_\mu - \tilde{u}_\mu\|_V}{\|u_\mu\|_V} \\ \frac{\|u_\mu - \tilde{u}_\mu\|_V}{\|u_\mu\|_V} &\leq \Delta_{loc,rel}^g(\tilde{u}_\mu) \leq (1 + 2\Delta_{loc,rel}^g(\tilde{u}_\mu)) \frac{\gamma_\mu}{\alpha_\mu} c_{\text{pu},\tilde{v}} \sqrt{J} \frac{\|u_\mu - \tilde{u}_\mu\|_V}{\|u_\mu\|_V}\end{aligned}\quad (4.54)$$

See Appendix B for an extensive analysis of these relative error estimators.

#### 4.5. Improved Offline/Online Splitting

One crucial property of an a posteriori error estimator for model order reduction is the possibility of an offline/online splitting of its evaluation. An offline/online splitting is a scheme to evaluate the a posteriori error estimator where all computations in the online phase are independent of the dimension of the unreduced model. For the standard residual based RB error estimator Equation (4.1) a splitting scheme based on the gram matrix of all contributions to the residual is widely used (see e.g. [Hesthaven et al.(2016), Sec. 4.2.5]). We will call this splitting the *traditional offline/online splitting* in the following. An offline/online splitting for the localized a posteriori error estimators defined in Corollary 4.2.4 can be obtained by applying the *traditional offline/online splitting* to all localized dual space norms  $\|\mathcal{R}_\mu(u_\mu)\|_{V_i}$ . However, as observed by several authors [Patera and Rozza(2007), pp. 148–149] [Yano(2014)] [Benner and Hess(2012)], the implementation of this offline/online splitting shows poor numerical accuracy due to round-off errors which can render the estimator unusable when the given problem is badly conditioned and high accuracy is required. Observations suggest that the estimator typically stagnates at a relative error of order  $\sqrt{\varepsilon}$ , where  $\varepsilon$  is the machine accuracy of the floating point hardware used.

In the following, we propose a new algorithm to evaluate the norm of the residual which does not suffer the severe numerical problems of the traditional approach, is free of approximations, has only small computational overhead and is easy to implement. It is based on representing the residual with respect to a dedicated orthonormal basis. The new approach is denoted by *improved offline/online splitting* in the following. It was published in [Buhr et al.(2014)].

To our knowledge, at that time there was only one other contribution in which a numerically stable algorithm for evaluation of the estimator is presented [Casenave(2012), Casenave et al.(2014)]. This approach however comes at the price of a computationally more expensive “online phase” (in [Casenave(2012)]) or increased complexity of offline computations (in [Casenave et al.(2014)]) by application of the empirical interpolation method, which in turn requires additional stabilization. Later, two more approaches were published. In [Sommer et al.(2015)] a splitting is proposed which is equivalent to the *improved offline/online splitting* presented below. Only a Gram-Schmidt algorithm is replaced by a singular value decomposition. Later, in [Chen et al.(2017), Chen et al.(2018)],

a splitting is proposed which is also equivalent, but it was proposed to use a rank revealing QR decomposition instead of the Gram-Schmidt algorithm. In the following, we present both the *traditional offline/online splitting* as well as the *improved offline/online splitting* for the computation of the dual norm of the residual  $\|\mathcal{R}_\mu(u_\mu)\|_{V_h'}$ . We assume that  $u_\mu$  is the solution of a parametric variation problem as defined in Definition 2.1.1 and Section 2.3 and that the bilinear form  $a_\mu$  and the linear form  $f_\mu$  have an affine decomposition. As the splitting scheme is the same for the global a posteriori error estimator and the localized setting, we only consider the simpler global case here.

To calculate the dual norm of the residual  $\mathcal{R}_\mu(\tilde{u}_\mu)$  we make use of the fact that the norm of an element of  $\tilde{V}'$  is equal to the norm of its Riesz representative. Denoting by  $R : V_h' \rightarrow V_h$  the Riesz isomorphism and assuming the existence of a computable lower bound  $\alpha_{\mu, LB} \leq \alpha_\mu$  for the coercivity constant, we obtain a bound for the error containing only computable quantities:

$$\|u_\mu - \tilde{u}_\mu\|_{V_h} \leq \frac{1}{\alpha_{\mu, LB}} \|R(\mathcal{R}_\mu(\tilde{u}_\mu))\|_{V_h} \quad (4.55)$$

#### *Traditional Offline/Online Splitting*

In order to avoid high-dimensional calculations during the online phase, the residual  $\mathcal{R}_\mu(\tilde{u}_\mu)$  can be rewritten using the affine decompositions Equation (2.17) and a basis representation of  $\tilde{u}_\mu$ . Let  $\{\tilde{\psi}_1, \dots, \tilde{\psi}_{\tilde{N}}\}$  be a basis of  $\tilde{V}$  and let  $\tilde{u}_\mu = \sum_{i=1}^{\tilde{N}} \tilde{u}_{\mu_i} \tilde{\psi}_i$ , then the Riesz representative of the residual is given as

$$R(\mathcal{R}_\mu(\tilde{u}_\mu)) = \sum_{q=1}^{Q_f} \theta_f^q(\mu) R(f^q) - \sum_{q=1}^{Q_a} \sum_{i=1}^{\tilde{N}} \theta_a^q(\mu) \tilde{u}_{\mu_i} R(a^q(\tilde{\psi}_i, \cdot)). \quad (4.56)$$

To simplify notation, we rename the  $N_\eta := Q_f + Q_a \tilde{N}$  linear coefficients  $\theta_f^q(\mu)$  and  $\theta_a^q(\mu) \tilde{u}_{\mu_i}$  to  $\alpha_k$  and the vectors  $R(f^q)$  and  $R(a^q(\tilde{\psi}_i, \cdot))$  to  $\eta_k$ , i.e.  $R(\mathcal{R}_\mu(\tilde{u}_\mu)) = \sum_{k=1}^{N_\eta} \alpha_k \eta_k$ . The space  $\text{span}\{\eta_1, \dots, \eta_{N_\eta}\}$  is denoted by  $V_\eta$ . For the norm of the residual we obtain

$$\|R(\mathcal{R}_\mu(\tilde{u}_\mu))\|_{V_h} = \left( \sum_{k=1}^{N_\eta} \sum_{l=1}^{N_\eta} \alpha_k \alpha_l (\eta_k, \eta_l)_{V_h} \right)^{\frac{1}{2}}. \quad (4.57)$$

Using this representation, an offline/online decomposition of the error bound is possible by pre-computing the inner products  $(\eta_k, \eta_l)_{V_h}$  during the offline stage. In the online stage, only the sum in Equation (4.57) has to be evaluated. As the number of summands is independent of the dimension of  $V_h$ , an online run-time independent of the dimension of  $V_h$  is achieved.

While this approach leads to an efficient computation of the residual norm, it shows poor numerical stability: in the sum Equation (4.57), terms with a relative error of order of machine accuracy  $\varepsilon$  are added. Therefore, the sum shows an absolute error of at least  $\varepsilon$  times the largest value of  $|\alpha_k \alpha_l (\eta_k, \eta_l)_{V_h}|$ , and the error in the norm of the residual is thus at least of order  $\sqrt{\varepsilon} \cdot \sqrt{\max_{k,l} |\alpha_k \alpha_l (\eta_k, \eta_l)_{V_h}|}$ . This is in agreement with the observation that this algorithm stops converging at relative errors of order  $\sqrt{\varepsilon}$  (see Section 4.5).

#### *Improved Offline/Online Splitting*

While the floating point evaluation of Equation (4.57) shows poor numerical accuracy, note that the evaluation of

$$\|R(\mathcal{R}_\mu(\tilde{u}_\mu))\|_{V_h} = \left( \sum_{k=1}^{N_\eta} \alpha_k \eta_k, \sum_{k=1}^{N_\eta} \alpha_k \eta_k \right)_{V_h}^{\frac{1}{2}} \quad (4.58)$$

is numerically stable. Based on this observation, we propose a new algorithm to evaluate  $\|R(\mathcal{R}_\mu(\tilde{u}_\mu))\|_{V_h}$  which is offline/online decomposable while maintaining the algorithmic structure of Equation (4.58) to ensure stability.

The algorithm we propose evaluates Equation (4.58) in the subspace  $V_\eta$  using an orthonormal basis for this space. It comprises three steps: 1. The construction of an orthonormal basis  $\Psi^\eta = \{\psi_1^\eta, \dots, \psi_{N_\eta}^\eta\}$  of  $V_\eta$ , 2. the evaluation of the basis coefficients of  $\eta_k$  w.r.t. the basis  $\Psi^\eta$  and 3. the evaluation of Equation (4.58) using this basis representation. Note that this approach is offline/online decomposable: Steps 1 and 2 can be done offline, without knowing the parameter, while step 3 can be performed online. The size of the basis  $\Psi^\eta$  does not depend on the dimension of  $V_h$ .

In principle, any orthonormalization algorithm applied to  $\{\eta_k\}_{k=1}^{N_\eta}$  can be used for the computation of the basis  $\Psi^\eta$ . Note, however, that the algorithm has to compute the basis with very high numerical accuracy. As an example, the standard modified Gram-Schmidt algorithm usually fails to deliver the required accuracy. For the numerical example in Section 4.5, we have chosen an improved variant of the modified Gram-Schmidt algorithm, where vectors are re-orthonormalized until a sufficient accuracy is achieved (Algorithm C.4).

After the basis  $\Psi^\eta$  has been constructed using an appropriate orthonormalization algorithm, we can compute for each  $\eta_k$  ( $1 \leq k \leq N_\eta$ ) basis representations  $\eta_k = \sum_{i=1}^{N_\eta} \bar{\eta}_{k,i} \psi_i^\eta$ , where  $\bar{\eta}_{k,i} = (\psi_i^\eta, \eta_k)_{V_h}$  due to the orthonormality of  $\Psi^\eta$ . The right-hand side of Equation (4.58) can then be evaluated as

$$\|\mathcal{R}_\mu(\tilde{u}_\mu)\|_{V_h} = \left( \sum_{i=1}^{N_\eta} \left( \sum_{k=1}^{N_\eta} \alpha_k \bar{\eta}_{k,i} \right)^2 \right)^{\frac{1}{2}} \quad (4.59)$$

which executes in time independent of the dimension of  $V_h$  and is observed to be numerically stable.

#### Run-Time Complexities

During the offline phase, both the traditional and the new algorithm have to calculate all Riesz representatives appearing in Equation (4.56). This requires the application of the inverse of the inner product matrix for  $V_h$ , which can be computed in complexity  $\mathcal{O}(N \log(N))$  with appropriate preconditioners. As there are  $N_\eta$  Riesz representatives to be calculated, the overall run-time of this step is of order  $\mathcal{O}(N_\eta N \log(N))$ . The traditional algorithm proceeds with calculating all inner products  $(\eta_k, \eta_l)_V$  in Equation (4.57), having a complexity of  $\mathcal{O}(N_\eta^2 N)$ . Thus the overall complexity of the offline phase for the traditional algorithm is  $\mathcal{O}(N_\eta^2 N + N_\eta N \log(N))$ .

After computing the Riesz representatives in Equation (4.56), the improved algorithm generates the orthonormal basis  $\Psi^\eta$ . In practice it was observed that at most four re-iterations per vector are required during orthonormalization with Algorithm C.4. Thus, choosing this algorithm for the generation of  $\Psi^\eta$  leads to a run-time complexity of  $\mathcal{O}(N_\eta^2 N)$  for this step. The calculation of the  $N_\eta^2$  basis coefficients  $\bar{\eta}_{k,i} = (\eta_k, \psi_i^\eta)_{V_h}$  has again complexity  $\mathcal{O}(N_\eta^2 N)$ , resulting in a total complexity of the offline phase for the new algorithm of  $\mathcal{O}(N_\eta^2 N + N_\eta N \log(N))$ , as for the traditional algorithm.

During the online phase, the right-hand sides of Equation (4.57), resp. Equation (4.59), are evaluated using the pre-computed quantities  $(\eta_k, \eta_l)_V$ , resp.  $\bar{\eta}_{k,i}$ . In both cases, a run-time of  $\mathcal{O}(N_\eta^2)$  is required.

All in all, both algorithms for evaluating Equation (4.55) show the same run-time complexity, in the online phase as well as during the offline phase (Table 4.1). Note that  $\mathcal{O}(N_\eta^2) = \mathcal{O}(Q_f^2 + Q_a^2 \tilde{N}^2) = \mathcal{O}(\tilde{N}^2)$  for increasing reduced space dimensions.

#### Numerical Example

To demonstrate the performance of the *improved offline/online splitting*, we apply it to the RB approximation of *Thermal Block Example*. Since the splitting is the same in the standard RB and in the localized setting, we apply it to the simpler case of standard RB. For basis generation, we weak greedy, steered by the a posteriori error estimator under consideration is used: The reduced

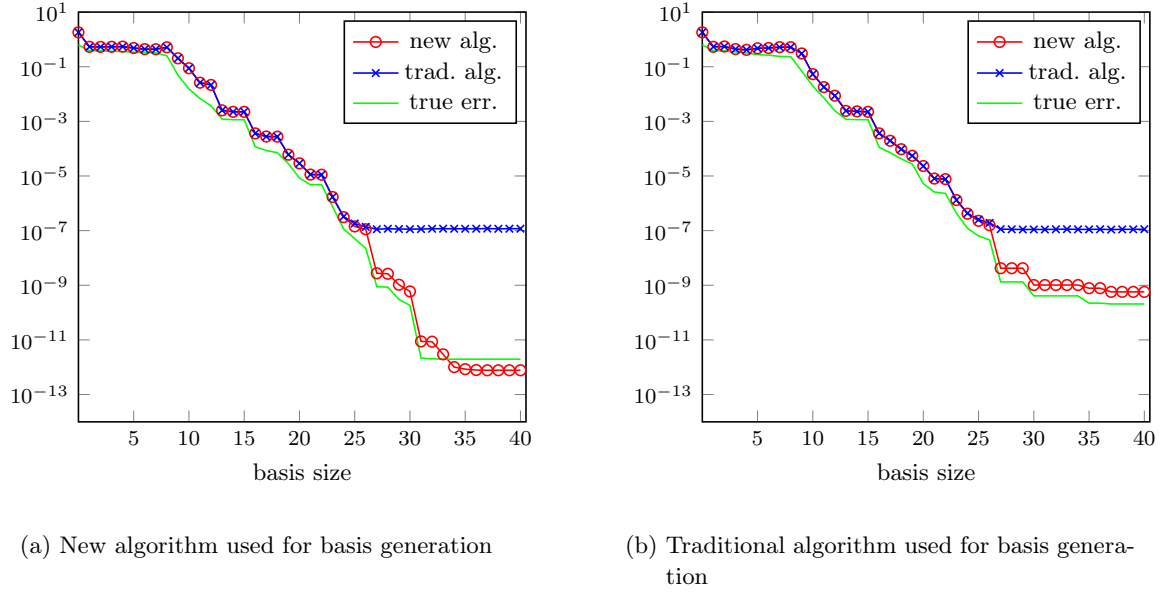


Figure 4.1.: Evaluation of proposed offline/online splitting: maximum relative reduction errors and estimated reduction errors ( $H^1$ -norm) for numerical example *Thermal Block Example*. (reproduction: Appendix A.18)

space  $\tilde{V}$  is constructed from the linear span of solutions to Definition 2.1.1 for parameters selected by the following greedy search procedure: Starting with  $\tilde{V}_0 := \{0\} \subset V_h$ , in each iteration step the reduced problem Definition 2.2.1 is solved and an error estimator is evaluated at all parameters  $\mu$  of a given discrete training set  $\Xi \subset \mathcal{D}$ . If the maximum estimated error is below a prescribed tolerance  $tol$ , the algorithm stops. Otherwise, the high-dimensional problem Definition 2.1.1 is solved for the parameter  $\mu_n^*$  maximizing the estimated error and the reduced space is extended by the obtained solution snapshot:  $\tilde{V}_{n+1} := \tilde{V}_n \oplus \text{span}\{u_{\mu_n^*}\}$ .

A reduced space of dimension 40 was generated with the weak greedy algorithm using our new algorithm for the evaluation of the error estimator. An equidistant training set of  $6^4$  parameters was used. Finally, for each  $n$ -dimensional reduced subspace  $\tilde{V}_n$  ( $0 \leq n \leq 40$ ) produced by the greedy algorithm we computed the maximum reduction error and the maximum estimated reduction errors using both the traditional and our improved algorithm on 30 randomly selected new parameters in  $\mathcal{D}$  (Figure 4.1a). Our results clearly indicate the breakdown of the traditional algorithm for more than 25 basis vectors at a relative error of about  $10^{-7} \approx \sqrt{\varepsilon}$  whereas our new algorithm remains efficient for all tested basis sizes.

To underline the need for accurate error estimation in order to obtain reduced spaces of high approximation quality, we repeated the same experiment using the traditional algorithm for error estimation during basis generation (Figure 4.1b). While the maximum model reduction error still improves from  $10^{-7}$  to  $10^{-8}$  after the breakdown of the error estimator, the final reduced space approximates the solution manifold 3 orders of magnitude worse than the space obtained with our improved algorithm.

Table 4.1.: Run-time complexities of traditional and new algorithm for evaluation of the error estimator.

stage	offline	online
traditional	$\mathcal{O}(N_\eta^2 N) + \mathcal{O}(N_\eta N \log(N))$	$\mathcal{O}(N_\eta^2)$
new	$\mathcal{O}(N_\eta^2 N) + \mathcal{O}(N_\eta^2 N) + \mathcal{O}(N_\eta N \log(N))$	$\mathcal{O}(N_\eta^2)$

#### 4.6. Future Research on Localized a Posteriori Error Estimation

- ***Localization of randomized a posteriori error estimators***

Recently, a residual based, randomized a posteriori error estimator has been proposed in [Smetana et al.(2019)], having favorable properties. Especially, it circumvents the explicit computation of the inf-sup constant and it shows a very good efficiency. It should be investigated if and how this approach could be adapted to the localized setting.

- ***Online computation of estimator constants***

While we present a priori estimates for some of the constants involved in the localized a posteriori error estimators, it should be possible to compute the localized constants  $c_{i,\tilde{V}}$  on the fly using our randomized norm estimator shown in Section 5.2.5. It should also be possible to update the estimates during basis adaption and online enrichment, when the reduced ansatz space grows and thus the constants  $c_{i,\tilde{V}}$  shrink.



---

Improved Local Training

---

The training algorithm introduced in Section 3.3.2, Algorithm 3.3, is a heuristic approach. It has the drawbacks of first having the parameter  $M$ , the number of random samples, which has to be chosen by the user, and second it lacks provable convergence results. In this chapter, we introduce an improved training algorithm which chooses the number of random samples adaptively, based on a prescribed accuracy and for which probabilistic a priori convergence bounds can be shown. The probabilistic a priori bounds hold with high (selectable) probability. First we define an abstract training configuration, corresponding to an abstract localizing space decomposition. Then we show an a priori error estimate in this abstract setting. We proceed introducing the randomized range recovery algorithm, which generates local approximation spaces and controls one of the terms in the abstract estimate. We verify our results on two simple test examples, *Rangefinder Example 1* and *Rangefinder Example 2*, and evaluate the behavior of the range recovery algorithm on the *Olimex A64 Example*.

### 5.1. Abstract Training Configuration

Approximating the image of a suitably defined transfer operator to create approximation spaces in localized model order reduction has been done in [Babuska and Lipton(2011)] for the GFEM and in [Smetana and Patera(2016)] for the PR-SCRBE. This formulation has been combined with a randomized approach by the authors in [Buhr and Smetana(2018)] for the GFEM. All of these approaches were specific to one space decomposition. In the following, we introduce a “localized training configuration” which provides an abstract framework for the generation of localized approximation spaces, based on an abstract localizing space decomposition.

**Definition 5.1.1** (Localized training configuration). *Let  $\{\Omega, V, \{\omega_i\}_{i=1}^{N_{V_i}}, \{V_i\}_{i=1}^{N_{V_i}}, \{\mathcal{P}_{V_i}\}_{i=1}^{N_{V_i}}\}$  be a localizing space decomposition as defined in Definition 2.4.1 and let  $u$  be the solution of a non parametric variational problem as defined in Definition 2.1.1. We define a “localized training configuration” to be a set of*

1.  $N_{V_i}$  training domains  $\omega_i^* \subset \Omega$  with the maximum number overlapping in any point  $x$  of  $\Omega$  denoted by

$$J^* := \max_{x \in \Omega} \#\{i \in \{1, \dots, N_{V_i}\} \mid x \in \omega_i^*\}, \quad (5.1)$$

2.  $N_{V_i}$  Hilbert spaces  $V|_{\omega_i^*}$  equipped with a norm satisfying

$$\sum_{i=1}^{N_{V_i}} \|u|_{\omega_i^*}\|^2 \leq J^* \|u\|^2, \quad (5.2)$$

3.  $N_{V_i}$  Hilbert spaces  $S_i$ ,

4.  $N_{V_i}$  bounded linear operators  $\mathcal{P}_{S_i} : V|_{\omega_i^*} \rightarrow S_i$ ,

5.  $N_{V_i}$  affine linear and compact operators  $T_i : S_i \rightarrow V_i$

for which it holds

$$u = \sum_{i=1}^{N_{V_i}} T_i \mathcal{P}_{S_i} u|_{\omega_i^*}. \quad (5.3)$$

In the case of a parameterized problem as introduced in Section 2.3, the operators  $T_i$  are replaced by parameterized operators  $T_{\mu,i}$  for which it holds

$$u_\mu = \sum_{i=1}^{N_{V_i}} T_{\mu,i} \mathcal{P}_{S_i} u_\mu|_{\omega_i^*} \quad \forall \mu \in \mathcal{D}. \quad (5.4)$$

In the ArbiLoMod setting, the training domains  $\omega_i^*$  are the support of the spaces  $\text{Tr}(V_i^{\text{wb}})$  defined in Equation (3.12). These domains are usually oversampling domains of the domains  $\omega_i$ , but this is not required. The spaces  $V|_{\omega_i^*}$  can usually be defined as  $V|_{\omega_i^*} := \{\varphi|_{\omega_i^*} \mid \varphi \in V\}$  with the norm and inner product of  $V$  where the integrals are restricted to  $\omega_i^*$ . Some norms might however not be a norm when restricted to a subdomain, as for example the  $H^1$  semi-norm on  $H^1(\Omega)$  or the energy norm of a Laplace problem. In these cases, the definition has to be modified. In the ArbiLoMod setting, the simple restriction can be used. In the choice of the spaces  $S_i$ , there is a lot of freedom when designing a localized training configuration. Their inner product can be chosen to obtain good constants in the estimates presented below or to make constants easily computable. The spaces  $S_i$  usually represent some form of boundary values, e.g. Dirichlet or Robin boundary values on  $\partial\omega_i^*$ . In the ArbiLoMod setting,  $S_i$  are the spaces  $C(\text{Tr}(V_i^{\text{wb}}))$  defined in Equation (3.13), which are spanned by all FE functions having support on  $\partial\omega_i^*$ . The operators  $\mathcal{P}_{S_i}$  are usually the corresponding trace operators, or the extraction of the FE-coefficients of  $C(\text{Tr}(V_i^{\text{wb}}))$  in the ArbiLoMod. The operators  $T_i$ , which we denote by the name ‘‘transfer operators’’, are usually defined by solving a local version of the underlying problem with the boundary values in  $S_i$ . In ArbiLoMod, this corresponds to the local solve in Equation (3.15).

In the following, we show an a priori error estimate in this abstract setting. We denote the linear part of  $T_i$  by  $T_i^l$  and the affine part by  $T_i^a \in V_i$ , it holds

$$T_i \varphi = T_i^l \varphi + T_i^a \quad \forall \varphi \in S_i. \quad (5.5)$$

As in Section 4.2 let

$$\bigcup_{k=1}^{\bar{J}} \Upsilon_{C,k} = \{1, \dots, N_{V_i}\} \quad (5.6)$$

be a partition of  $\{1, \dots, N_{V_i}\}$  such that

$$\forall 1 \leq k \leq \bar{J} : \forall i, j \in \Upsilon_{C,k}, i \neq j : V_i \perp V_j \quad (5.7)$$

i.e. we can partition the local subspaces into  $\bar{J}$  sets so that in each set, all spaces are orthogonal. Using these classes, we can formulate the following lemma.



**Lemma 5.1.2** (Norm of sum of localized functions). *For functions  $\{\varphi_i\}_{i=1}^{N_{V_i}}$  with*

$$\varphi_i \in V_i \quad \forall i \in \{1, \dots, N_{V_i}\} \quad (5.8)$$

it holds

$$\left\| \sum_{i=1}^{N_{V_i}} \varphi_i \right\|^2 \leq \bar{J} \sum_{i=1}^{N_{V_i}} \|\varphi_i\|^2. \quad (5.9)$$

*Proof.* Using the classes described in Equation (5.6), we have the identity

$$\left\| \sum_{i=1}^{N_{V_i}} \varphi_i \right\| = \left\| \sum_{k=1}^{\bar{J}} \sum_{i \in \Upsilon_{C,k}} \varphi_i \right\|. \quad (5.10)$$

Using the triangle inequality and Cauchy-Schwarz, it follows

$$\left\| \sum_{i=1}^{N_{V_i}} \varphi_i \right\| \leq \sum_{k=1}^{\bar{J}} \left\| \sum_{i \in \Upsilon_{C,k}} \varphi_i \right\| \quad (5.11)$$

$$\leq \sqrt{\bar{J}} \left( \sum_{k=1}^{\bar{J}} \left\| \sum_{i \in \Upsilon_{C,k}} \varphi_i \right\|^2 \right)^{\frac{1}{2}}. \quad (5.12)$$

Due to the orthogonality of the spaces in each class  $\Upsilon_{C,k}$  it holds

$$\left\| \sum_{i \in \Upsilon_{C,k}} \varphi_i \right\|^2 = \sum_{i \in \Upsilon_{C,k}} \|\varphi_i\|^2 \quad (5.13)$$

and it follows

$$\left\| \sum_{i=1}^{N_{V_i}} \varphi_i \right\| \leq \sqrt{\bar{J}} \left( \sum_{k=1}^{\bar{J}} \sum_{i \in \Upsilon_{C,k}} \|\varphi_i\|^2 \right)^{\frac{1}{2}} \quad (5.14)$$

$$= \sqrt{\bar{J}} \left( \sum_{i=1}^{N_{V_i}} \|\varphi_i\|^2 \right)^{\frac{1}{2}}. \quad (5.15)$$

□

The following proposition is inspired by [Eickhorn(2019), Theorem 4.6] but improves on this, as the error bound derived [Eickhorn(2019), Theorem 4.6] scales in  $\sqrt{N_{V_i}}$  while the error bound presented in the following is independent of the number of local spaces and local domains.

**Proposition 5.1.3** (Training a priori estimate). *Let  $\{\Omega, V, \{\omega_i\}_{i=1}^{N_{V_i}}, \{V_i\}_{i=1}^{N_{V_i}}, \{\mathcal{P}_{V_i}\}_{i=1}^{N_{V_i}}\}$  be a localizing space decomposition as defined in Definition 2.4.1. Let further  $\{\{\omega_i^*\}_{i=1}^{N_{V_i}}, \{V|_{\omega_i^*}\}_{i=1}^{N_{V_i}}, \{S_i\}_{i=1}^{N_{V_i}}, \{\mathcal{P}_{S_i}\}_{i=1}^{N_{V_i}}, \{T_i\}_{i=1}^{N_{V_i}}\}$  be a localized training configuration as defined in Definition 5.1.1. Let  $u$  be the solution of a non parametric, symmetric, coercive variational problem as defined in Definition 2.1.1 and let  $\tilde{u}$  be the reduced solution of a localized Galerkin projection onto  $\tilde{V} = \sum_{i=1}^{N_{V_i}} \tilde{V}_i$  as introduced in Section 2.4.2. Further assume*

$$T_i^a \in \tilde{V}_i \quad \forall i \in \{1, \dots, N_{V_i}\}. \quad (5.16)$$

Then it holds

$$\frac{\|u - \tilde{u}\|}{\|u\|} \leq \sqrt{\frac{\gamma}{\alpha}} \sqrt{\bar{J} J^*} \max_{i \in \{1, \dots, N_{V_i}\}} \left\| (1 - P_{\tilde{V}_i}) T_i^l \right\| \|\mathcal{P}_{S_i}\|. \quad (5.17)$$

*Proof.* Due to the coercivity and symmetry of the problem, the best approximation theorem (Theorem 2.2.2) holds. We have

$$\|u - \tilde{u}\| \leq \sqrt{\frac{\gamma}{\alpha}} \inf_{\tilde{v} \in \tilde{V}} \|u - \tilde{v}\| \quad (5.18)$$

and thereby

$$\|u - \tilde{u}\| \leq \sqrt{\frac{\gamma}{\alpha}} \|u - u_c\| \quad (5.19)$$

with

$$u_c := \sum_{i=1}^{N_{V_i}} P_{\tilde{V}_i} T_i \mathcal{P}_{S_i} u|_{\omega_i^*}. \quad (5.20)$$

Plugging Equation (5.3) and Equation (5.20) into Equation (5.19), we obtain

$$\begin{aligned} \|u - \tilde{u}\| &\leq \sqrt{\frac{\gamma}{\alpha}} \left\| \sum_{i=1}^{N_{V_i}} T_i \mathcal{P}_{S_i} u|_{\omega_i^*} - \sum_{i=1}^{N_{V_i}} P_{\tilde{V}_i} T_i \mathcal{P}_{S_i} u|_{\omega_i^*} \right\| \\ &= \sqrt{\frac{\gamma}{\alpha}} \left\| \sum_{i=1}^{N_{V_i}} (1 - P_{\tilde{V}_i}) T_i \mathcal{P}_{S_i} u|_{\omega_i^*} \right\|. \end{aligned} \quad (5.21)$$

Splitting the operator  $T_i$  into its linear and its affine part, it follows that

$$\begin{aligned} \|u - \tilde{u}\| &\leq \sqrt{\frac{\gamma}{\alpha}} \left\| \sum_{i=1}^{N_{V_i}} (1 - P_{\tilde{V}_i}) T_i^l \mathcal{P}_{S_i} u|_{\omega_i^*} + (1 - P_{\tilde{V}_i}) T_i^a \right\| \\ &= \sqrt{\frac{\gamma}{\alpha}} \left\| \sum_{i=1}^{N_{V_i}} (1 - P_{\tilde{V}_i}) T_i^l \mathcal{P}_{S_i} u|_{\omega_i^*} \right\|. \end{aligned} \quad (5.22)$$

In the last step, we used the assumption that  $T_i^a \in \tilde{V}_i$ . Using Lemma 5.1.2 we see that

$$\|u - \tilde{u}\|^2 \leq \frac{\gamma}{\alpha} \bar{J} \sum_{i=1}^{N_{V_i}} \left\| (1 - P_{\tilde{V}_i}) T_i^l \mathcal{P}_{S_i} u|_{\omega_i^*} \right\|^2. \quad (5.23)$$

Using the operator norms

$$\left\| (1 - P_{\tilde{V}_i}) T_i^l \mathcal{P}_{S_i} u|_{\omega_i^*} \right\| \leq \left\| (1 - P_{\tilde{V}_i}) T_i^l \right\| \|\mathcal{P}_{S_i}\| \|u|_{\omega_i^*}\| \quad (5.24)$$

it follows that

$$\|u - \tilde{u}\|^2 \leq \frac{\gamma}{\alpha} \bar{J} \sum_{i=1}^{N_{V_i}} \left\| (1 - P_{\tilde{V}_i}) T_i^l \right\|^2 \|\mathcal{P}_{S_i}\|^2 \|u|_{\omega_i^*}\|^2 \quad (5.25)$$

$$\leq \frac{\gamma}{\alpha} \bar{J} \max_{i \in \{1, \dots, N_{V_i}\}} \left\| (1 - P_{\tilde{V}_i}) T_i^l \right\|^2 \|\mathcal{P}_{S_i}\|^2 \sum_{i=1}^{N_{V_i}} \|u|_{\omega_i^*}\|^2 \quad (5.26)$$

$$\leq \frac{\gamma}{\alpha} \bar{J} \max_{i \in \{1, \dots, N_{V_i}\}} \left\| (1 - P_{\tilde{V}_i}) T_i^l \right\|^2 \|\mathcal{P}_{S_i}\|^2 J^* \|u\|^2 \quad (5.27)$$

and thereby the claim.  $\square$

Proposition 5.1.3 gives guidance when designing localized training configurations. While the term  $\left\| (1 - P_{\tilde{V}_i}) T_i^l \right\|$  will be controlled by the algorithm given below, the operator norms  $\|\mathcal{P}_{S_i}\|$  have to be controlled otherwise.

## 5.2. Randomized Range Finder Algorithm

In this section we present the randomized range finder algorithm, which, given a compact linear operator between two finite dimensional Hilbert spaces, generates a space to approximate the image of the given operator. It is intended to be used to generate spaces  $\tilde{V}_i$  and control the term  $\left\| \left(1 - P_{\tilde{V}_i}\right) T_i^l \right\|$  in Proposition 5.1.3. While this algorithm is used to create local approximation spaces in this thesis, it is presented in an abstract setting in this section in order to facilitate reuse in other contexts. We drop the index  $i$  and denote the space the transfer operator maps to by  $R$  instead of  $V_i$ . The reduced approximation space we denote by  $\tilde{R}^n$  instead of  $\tilde{V}_i$  where  $n$  is the dimension of  $R^n$ . We only consider the non parametric, real valued case in this chapter. The parametric case and the complex valued case are subject to future research, see also Section 5.5.

We restrict ourselves to affine linear operators between finite dimensional Hilbert spaces. The restriction to finite dimensional spaces originates in the way we draw random vectors. An extension to compact operators between Hilbert spaces of infinite dimension would be possible but would require a new way of drawing random vectors. An extension to nonlinear operators would be a larger project. The restriction to operators between finite dimensional spaces is hardly a restriction in practice, as one usually uses finite dimensional approximations of infinite dimensional spaces anyway in numerical codes.

The algorithm is an adaption of the range finder algorithm from randomized numerical linear algebra (RandNLA) to the setting of linear compact operators between Hilbert spaces. A version of this algorithm for matrices is given in [Halko et al.(2011), Algorithm 4.2]. The results of [Halko et al.(2011)] are recovered if we discretize the linear operator in an orthonormal basis.

### 5.2.1. Randomized Numerical Linear Algebra

Randomized algorithms have gained considerable attention in the field of numerical linear algebra during the last decade. In many cases, randomized algorithms have better performance and better parallelization behavior than classical algorithms while delivering comparable accuracy. The interest of the artificial intelligence (AI) and machine learning (ML) communities in approximate matrix factorizations of large matrices has accelerated this development.

Some of the early publications by Drineas, Kannan, and Mahoney in 2006 used the term “Fast Monte Carlo Algorithms for Matrices” [Drineas et al.(2006a), Drineas et al.(2006b), Drineas et al.(2006c)]. They published algorithms for randomized matrix multiplication, randomized low-rank approximation of matrices and randomized compressed matrix decompositions. Per-Gunnar Martinsson and coworkers published a series of articles [Cheng et al.(2005), Liberty et al.(2007), Martinsson et al.(2011)] and the highly cited SIAM review article [Halko et al.(2011)]. Recently, also open-source software was released [Voronin and Martinsson(2015)].

The content of this section has been developed in collaboration with Kathrin Smetana and has been published in [Buhr and Smetana(2018)]. See references therein for an extensive literature review.

### 5.2.2. Setting

Let  $T$  be an affine linear operator between the finite dimensional Hilbert spaces  $S$  and  $R$

$$T : S \rightarrow R \tag{5.28}$$

where  $S$  is of dimension  $N_S$  and  $R$  is of dimension  $N_R$ . We denote the linear part of  $T$  by  $T^l$  and the affine part by  $T^a \in R$ , it holds

$$T\varphi = T^l\varphi + T^a \quad \forall \varphi \in S. \tag{5.29}$$

Let further  $\psi_1^S, \dots, \psi_{N_S}^S$  be a basis of  $S$  and  $\psi_1^R, \dots, \psi_{N_R}^R$  be a basis of  $R$ .

The target quantity in the approximation of the image of  $T$  is the operator norm

$$\|(1 - P_{\tilde{R}^n}) T^l\| = \sup_{\varphi \in S \setminus \{0\}} \frac{\|(1 - P_{\tilde{R}^n}) T^l \varphi\|_R}{\|\varphi\|_S} \quad (5.30)$$

where  $P_{\tilde{R}^n}$  is the orthogonal projection on the approximation space  $\tilde{R}^n \subset R$ , which is to be generated.

To distinguish clearly between vectors in Hilbert spaces and their coordinate representation, we mark all coordinate vectors and matrices with an underline and introduce Ritz isomorphisms  $D_S : S \rightarrow \mathbb{R}^{N_S}$  and  $D_R : R \rightarrow \mathbb{R}^{N_R}$  which map elements from  $S$  or  $R$  to a vector containing their basis coefficients in  $\mathbb{R}^{N_S}$  or  $\mathbb{R}^{N_R}$ , respectively. For instance,  $D_S$  maps a function  $\xi = \sum_{i=1}^{N_S} \xi_i \psi_i^S \in S$  to  $\underline{\xi} \in \mathbb{R}^{N_S}$ . As a result we have the matrix of the operator  $T$  as  $\underline{T} = D_R T D_S^{-1}$ .

Finally, we denote by  $\underline{M}_S$  the inner product matrix of  $S$  and by  $\underline{M}_R$  the inner product matrix of  $R$ .

### 5.2.3. Optimal Spaces

The best possible space of given dimension  $n$  to minimize  $\|(1 - P_{\tilde{R}^n}) T^l\|$  is the space spanned by the first  $n$  left singular vectors of  $T^l$ . The Singular Value Decomposition (SVD) exists due to the compactness of  $T^l$ . Denoting the SVD of  $T^l$  by

$$T^l \varphi = \sum_{i=1}^{N_T} q_i \sigma_i (v_i, \varphi)_S \quad \forall \varphi \in S, \quad (5.31)$$

where  $N_T$  is the rank of  $T^l$  and it holds  $(q_i, q_j)_R = \delta_{ij}$ ,  $(v_i, v_j)_S = \delta_{ij}$  and  $\sigma_i \in \mathbb{R}^+$ . The optimal spaces defined as

$$\tilde{R}_{\text{opt}}^n := \text{span}\{q_1, \dots, q_n\} \quad (5.32)$$

minimize  $\|(1 - P_{\tilde{R}^n}) T^l\|$  among all spaces of dimension  $n$ . It holds

$$\begin{aligned} \|(1 - P_{\tilde{R}_{\text{opt}}^n}) T^l\| &= \sup_{\varphi \in S \setminus \{0\}} \frac{\|(1 - P_{\tilde{R}_{\text{opt}}^n}) T^l \varphi\|}{\|\varphi\|} \\ &= \sup_{\varphi \in S \setminus \{0\}} \frac{\|(1 - P_{\tilde{R}_{\text{opt}}^n}) \sum_{i=1}^{N_T} q_i \sigma_i (v_i, \varphi)_S\|}{\|\varphi\|} \\ &= \sup_{\varphi \in S \setminus \{0\}} \frac{\|\sum_{i=n+1}^{N_T} q_i \sigma_i (v_i, \varphi)_S\|}{\|\varphi\|} \\ &= \sigma_{n+1}. \end{aligned} \quad (5.33)$$

These optimal spaces were used in [Babuska and Lipton(2011)] and [Smetana and Patera(2016)]. The randomized algorithm presented in the following approximates these spaces. In the numerical experiments below, we use these spaces as a benchmark.

### 5.2.4. Generation of Random Vectors

One of two central parts in the randomized range finder algorithm is the generation of random vectors in the space  $S$ . As we will see later in the analysis, the only important property of the generation of random vectors is the distribution of the inner product with an arbitrary normed vector. For the analysis which follows later, it is necessary that the distribution of the inner product with a normed vector is Gauss distributed with zero mean and a standard deviation  $s$  for which limits  $s_{\min} \leq s \leq s_{\max}$  are known.

The easiest way of drawing random vectors is to use independent Gauss-normal distributed coefficients to the basis vectors  $\psi_i^S$ , i.e. use  $D_S^{-1}\underline{r}$  with a vector of independent, Gauss-normal distributed entries  $\underline{r}$ . This drawing strategy has the required properties, as we show in the following lemma.

**Lemma 5.2.1** (Distribution of inner product). *The inner product of a normed vector  $v$  in  $S$  with a random normal vector  $(v, D_S^{-1}\underline{r})_S$  is a Gaussian distributed random variable with mean zero and variance  $s^2$ , where*

$$\lambda_{\min}^{\underline{M}_S} \leq s^2 \leq \lambda_{\max}^{\underline{M}_S}. \quad (5.34)$$

Where  $\lambda_{\min}^{\underline{M}_S}$  and  $\lambda_{\max}^{\underline{M}_S}$  are the smallest and largest eigenvalue of the matrix of the inner product in  $S$ .

*Proof.* We use the spectral decomposition of the inner product matrix  $\underline{M}_S = \sum_{i=1}^{N_S} \underline{m}_{S,i} \lambda_i^{\underline{M}_S} \underline{m}_{S,i}^T$  with eigenvalues  $\lambda_i^{\underline{M}_S}$  and eigenvectors  $\underline{m}_{S,i}$ . It holds

$$(v, D_S^{-1}\underline{r})_S = \sum_{i=1}^{N_S} (D_S v)^T \underline{m}_{S,i} \lambda_i^{\underline{M}_S} \underline{m}_{S,i}^T \underline{r}. \quad (5.35)$$

As  $\underline{m}_{S,i}$  is normed with respect to the euclidean inner product, the term  $\underline{m}_{S,i}^T \underline{r}$  is a normal distributed random variable. Using the rules for addition and scalar multiplication of Gaussian random variables, one sees that the inner product  $(v, D_S^{-1}\underline{r})_S$  is a Gaussian random variable with variance

$$s^2 = \sum_{i=1}^{N_S} \left( (D_S v)^T \underline{m}_{S,i} \lambda_i^{\underline{M}_S} \right)^2. \quad (5.36)$$

The variance  $s^2$  can easily be bounded as follows:

$$s^2 = \sum_{i=1}^{N_S} \left( (D_S v)^T \underline{m}_{S,i} \lambda_i^{\underline{M}_S} \right)^2 \leq \sum_{i=1}^{N_S} \left( (D_S v)^T \underline{m}_{S,i} \right)^2 \lambda_i^{\underline{M}_S} \max_i(\lambda_i^{\underline{M}_S}) = \lambda_{\max}^{\underline{M}_S} \quad (5.37)$$

$$s^2 = \sum_{i=1}^{N_S} \left( (D_S v)^T \underline{m}_{S,i} \lambda_i^{\underline{M}_S} \right)^2 \geq \sum_{i=1}^{N_S} \left( (D_S v)^T \underline{m}_{S,i} \right)^2 \lambda_i^{\underline{M}_S} \min_i(\lambda_i^{\underline{M}_S}) = \lambda_{\min}^{\underline{M}_S}. \quad (5.38)$$

It holds

$$\sum_{i=1}^{N_S} \left( (D_S v)^T \underline{m}_{S,i} \right)^2 \lambda_i^{\underline{M}_S} = 1 \quad (5.39)$$

because of the spectral decomposition of  $\underline{M}_S$  and the assumption that  $v$  is normed. It holds

$$\begin{aligned} \sum_{i=1}^{N_S} \left( (D_S v)^T \underline{m}_{S,i} \right)^2 \lambda_i^{\underline{M}_S} &= \sum_{i=1}^{N_S} \left( (D_S v)^T \underline{m}_{S,i} \right) \lambda_i^{\underline{M}_S} \left( \underline{m}_{S,i}^T (D_S v) \right) \\ &= (D_S v)^T \left( \sum_{i=1}^{N_S} \underline{m}_{S,i} \lambda_i^{\underline{M}_S} \underline{m}_{S,i}^T \right) (D_S v) \\ &= (D_S v)^T \underline{M}_S (D_S v) \\ &= \|v\|_S^2 = 1. \end{aligned} \quad (5.40)$$

□

## 5.2.5. A Probabilistic a Posteriori Norm Estimator

The second central part to build the adaptive algorithm is a convergence criterion. To this end, we use a probabilistic norm estimator, giving an upper bound for the operator norm of the given operator and apply this norm estimator on  $(1 - P_{\tilde{R}^n}) T^l$ . The norm estimator is simple to compute. Given the number of test vectors  $n_t$ , it applies the operator  $n_t$  times to a random vector and uses the maximum of the  $n_t$  norms of the results. The number  $n_t$  is a user supplied parameter.

**Definition 5.2.2** (Probabilistic a posteriori norm estimator). *To estimate the operator norm of a linear operator  $O : S \rightarrow R$  of rank smaller or equal to  $N_O$ , we define the a posteriori norm estimator  $\Delta(O, n_t, \varepsilon_{\text{testfail}})$  for  $n_t$  test vectors as*

$$\Delta(O, n_t, \varepsilon_{\text{testfail}}) := c_{\text{est}}(n_t, \varepsilon_{\text{testfail}}) \max_{i \in 1, \dots, n_t} \|O D_S^{-1} \underline{r}_i\|_R. \quad (5.41)$$

Here,  $c_{\text{est}}(n_t, \varepsilon_{\text{testfail}})$  is defined as

$$c_{\text{est}}(n_t, \varepsilon_{\text{testfail}}) := \left( \sqrt{2\lambda_{\min}^{\underline{M}_S} \text{erf}^{-1}(\sqrt[n_t]{\varepsilon_{\text{testfail}}})} \right)^{-1}, \quad (5.42)$$

$\underline{r}_i$  are random normal vectors, and  $\lambda_{\min}^{\underline{M}_S}$  is the smallest eigenvalue of the matrix of the inner product in  $S$ .

This norm estimator gives an upper bound to the operator norm with high probability, as we show in the following proposition.

**Proposition 5.2.3** (Norm estimator failure probability). *The norm estimator  $\Delta(O, n_t, \varepsilon_{\text{testfail}})$  is an upper bound of the operator norm  $\|O\|$  with probability greater or equal than  $(1 - \varepsilon_{\text{testfail}})$ :*

$$\Pr\left(\|O\| \leq \Delta(O, n_t, \varepsilon_{\text{testfail}})\right) \geq 1 - \varepsilon_{\text{testfail}}. \quad (5.43)$$

*Proof.* We analyze the probability for the event that the norm estimator  $\Delta(O, n_t, \varepsilon_{\text{testfail}})$  is smaller than the operator norm  $\|O\|$ :

$$\Pr\left(\Delta(O, n_t, \varepsilon_{\text{testfail}}) < \|O\|\right) = \Pr\left(c_{\text{est}}(n_t, \varepsilon_{\text{testfail}}) \max_{i \in 1, \dots, n_t} \|O D_S^{-1} \underline{r}_i\|_R < \|O\|\right). \quad (5.44)$$

The probability that all test vector norms are smaller than a certain value is the the product of the probabilities that each test vector is smaller than that value. So with a new random normal vector  $\underline{r}$  it holds

$$\Pr\left(\Delta(O, n_t, \varepsilon_{\text{testfail}}) < \|O\|\right) = \Pr\left(c_{\text{est}}(n_t, \varepsilon_{\text{testfail}}) \|O D_S^{-1} \underline{r}\|_R < \|O\|\right)^{n_t}. \quad (5.45)$$

Using the singular value decomposition of the operator  $O$ :  $O\varphi = \sum_i u_i \sigma_i(v_i, \varphi) \underline{m}_S$  we obtain

$$\begin{aligned} \Pr\left(\Delta(O, n_t, \varepsilon_{\text{testfail}}) < \|O\|\right) &\leq \Pr\left(c_{\text{est}}(n_t, \varepsilon_{\text{testfail}}) \|u_1 \sigma_1(v_1, D_S^{-1} \underline{r})\|_S < \|O\|\right)^{n_t} \\ &= \Pr\left(c_{\text{est}}(n_t, \varepsilon_{\text{testfail}}) \sigma_1 |v_1, D_S^{-1} \underline{r}|_S < \|O\|\right)^{n_t} \\ &= \Pr\left(c_{\text{est}}(n_t, \varepsilon_{\text{testfail}}) |v_1, D_S^{-1} \underline{r}|_S < 1\right)^{n_t}. \end{aligned} \quad (5.46)$$

The inner product  $|v_1, D_S^{-1} \underline{r}|_S$  is a Gaussian distributed random variable with variance greater  $\lambda_{\min}^{\underline{M}_S}$ , so with a new normal distributed random variable  $r'$  it holds

$$\begin{aligned} \Pr\left(\Delta(O, n_t, \varepsilon_{\text{testfail}}) < \|O\|\right) &\leq \Pr\left(\sqrt{\lambda_{\min}^{\underline{M}_S}} |r'| < \sqrt{2\lambda_{\min}^{\underline{M}_S} \text{erf}^{-1}(\sqrt[n_t]{\varepsilon_{\text{testfail}}})}\right)^{n_t} \\ &= \text{erf}\left(\frac{\sqrt{2}\text{erf}^{-1}(\sqrt[n_t]{\varepsilon_{\text{testfail}}})}{\sqrt{2}}\right)^{n_t} = \varepsilon_{\text{testfail}}. \end{aligned} \quad (5.47)$$

□

In case a good upper bound for the (numerical) rank of the operator  $O$  is known, this estimator is also effective with high probability, as the following proposition shows.

**Proposition 5.2.4** (Norm estimator effectivity). *Let the effectivity  $\eta$  of the norm estimator  $\Delta(O, n_t, \varepsilon_{\text{testfail}})$  be defined as*

$$\eta(O, n_t, \varepsilon_{\text{testfail}}) := \frac{\Delta(O, n_t, \varepsilon_{\text{testfail}})}{\|O\|}. \quad (5.48)$$

Then, it holds

$$\Pr\left(\eta \leq c_{\text{eff}}(n_t, \varepsilon_{\text{testfail}})\right) \geq 1 - \varepsilon_{\text{testfail}}, \quad (5.49)$$

where the constant  $c_{\text{eff}}(n_t, \varepsilon_{\text{testfail}})$  is defined as

$$c_{\text{eff}}(n_t, \varepsilon_{\text{testfail}}) := \left[ Q^{-1} \left( \frac{N_O}{2}, \frac{\varepsilon_{\text{testfail}}}{n_t} \right) \frac{\lambda_{\text{max}}^{M_S}}{\lambda_{\text{min}}^{M_S}} \left( \text{erf}^{-1} \left( \sqrt[n_t]{\varepsilon_{\text{testfail}}} \right) \right)^{-2} \right]^{1/2} \quad (5.50)$$

and  $Q^{-1}$  is the inverse of the upper normalized incomplete gamma function; i.e.

$$Q^{-1}(a, y) = x \quad \text{when} \quad Q(a, x) = y. \quad (5.51)$$

<sup>1</sup>

*Proof.* The constant  $c_{\text{est}}(n_t, \varepsilon_{\text{testfail}})$  is defined as in the proof of Proposition 5.2.3. To shorten notation, we write  $c_{\text{est}}$  for  $c_{\text{est}}(n_t, \varepsilon_{\text{testfail}})$  and  $c_{\text{eff}}$  for  $c_{\text{eff}}(n_t, \varepsilon_{\text{testfail}})$  within this proof. Invoking the definition of  $\Delta(O, n_t, \varepsilon_{\text{testfail}})$  yields

$$\Pr\left(\Delta(O, n_t, \varepsilon_{\text{testfail}}) > c_{\text{eff}}\|O\|\right) = \Pr\left(c_{\text{est}} \max_{i \in \{1, \dots, n_t\}} \|O D_S^{-1} \underline{r}_i\|_R > c_{\text{eff}}\|O\|\right) \quad (5.52)$$

and by employing a new random normal vector  $\underline{r}$  we obtain

$$\Pr\left(\Delta(O, n_t, \varepsilon_{\text{testfail}}) > c_{\text{eff}}\|O\|\right) \leq n_t \Pr\left(c_{\text{est}}\|O D_S^{-1} \underline{r}\|_R > c_{\text{eff}}\|O\|\right). \quad (5.53)$$

Using the singular value decomposition of the operator  $O$ :  $O\varphi = \sum_i u_i \sigma_i (v_i, \varphi)_S$  results in

$$\Pr\left(\Delta(O, n_t, \varepsilon_{\text{testfail}}) > c_{\text{eff}}\|O\|\right) \leq n_t \Pr\left(c_{\text{est}} \left\| \sum_i u_i \sigma_1 (v_i, D_S^{-1} \underline{r})_S \right\|_R > c_{\text{eff}}\|O\|\right). \quad (5.54)$$

For a new random normal variables  $r_i$  we have

$$\begin{aligned} \Pr\left(\Delta(O, n_t, \varepsilon_{\text{testfail}}) > c_{\text{eff}}\|O\|\right) &\leq n_t \Pr\left(c_{\text{est}} \sigma_1 \sqrt{\lambda_{\text{max}}^{M_S}} \sqrt{\sum_i r_i^2} > c_{\text{eff}}\|O\|\right) \\ &= n_t \Pr\left(\sqrt{\sum_i r_i^2} > \frac{c_{\text{eff}}}{c_{\text{est}}} \sigma_1^{-1} \sqrt{\lambda_{\text{max}}^{M_S}}^{-1} \|O\|\right) \\ &= n_t \Pr\left(\sqrt{\sum_i r_i^2} > \frac{c_{\text{eff}}}{c_{\text{est}}} \sqrt{\lambda_{\text{max}}^{M_S}}^{-1}\right) \\ &= n_t \Pr\left(\sum_i r_i^2 > \frac{c_{\text{eff}}^2}{c_{\text{est}}^2} \sqrt{\lambda_{\text{max}}^{M_S}}^{-2}\right). \end{aligned} \quad (5.55)$$

<sup>1</sup> Recall that the definition of the upper normalized incomplete gamma function is

$$Q(a, x) = \frac{\int_x^\infty t^{a-1} e^{-t} dt}{\int_0^\infty t^{a-1} e^{-t} dt}.$$

**Algorithm 5.1:** Adaptive Randomized Range Approximation.

---

```

1 Function AdaptiveRandomizedRangeApproximation( $T, \text{tol}, n_t, \varepsilon_{\text{algofail}}$ ):
   Input : Operator  $T$ ,
           target accuracy  $\text{tol}$ ,
           number of test vectors  $n_t$ ,
           maximum failure probability  $\varepsilon_{\text{algofail}}$ 
   Output: space  $\tilde{R}^n$  with property  $\Pr(\|(1 - P_{\tilde{R}^n})T^l\| \leq \text{tol}) > (1 - \varepsilon_{\text{algofail}})$ 
2 /* initialize basis */
3  $B \leftarrow \{T^a\}$ 
4 /* initialize test vectors */
5  $M \leftarrow \{TD_S^{-1}r_1, \dots, TD_S^{-1}r_{n_t}\}$ 
6 /* orthogonalize test vectors to span( $B$ ) */
7  $M \leftarrow \{(1 - P_{\text{span}(B)})t \mid t \in M\}$ 
8 /* determine error estimator factor */
9  $\varepsilon_{\text{testfail}} \leftarrow \varepsilon_{\text{algofail}}/N_T$ 
10  $c_{\text{est}} \leftarrow \left[ \sqrt{2\lambda_{\min}^{\frac{M_S}{M_S}}} \text{erf}^{-1}(\sqrt{\varepsilon_{\text{testfail}}}) \right]^{-1}$ 
11 /* basis generation loop */
12 while ( $\max_{t \in M} \|t\|_{\tilde{R}} \cdot c_{\text{est}} > \text{tol}$ ) do
13    $B \leftarrow B \cup (TD_S^{-1}r)$ 
14    $B \leftarrow \text{orthonormalize}(B)$ 
15   /* orthogonalize test vectors to span( $B$ ) */
16    $M \leftarrow \{(1 - P_{\text{span}(B)})t \mid t \in M\}$ 
17 return  $\tilde{R}^n = \text{span}(B)$ 

```

---

The sum of squared random normal variables is a random variable with chi-squared distribution. Its cumulative distribution function is the incomplete, normed gamma function. As we have a “greater than” relation, the upper incomplete normed gamma function is used, which we denote by  $Q(\frac{k}{2}, \frac{x}{2})$  here. Therefore, we conclude

$$\begin{aligned}
\Pr(\Delta(O, n_t, \varepsilon_{\text{testfail}}) > c_{\text{eff}}(n_t, \varepsilon_{\text{testfail}}) \|O\|) &\leq n_t Q\left(\frac{N_O}{2}, \frac{c_{\text{eff}}(n_t, \varepsilon_{\text{testfail}})^2}{c_{\text{est}}(n_t, \varepsilon_{\text{testfail}})^2} \frac{1}{2\lambda_{\max}^{\frac{M_S}{M_S}}}\right) \\
&= \varepsilon_{\text{testfail}}.
\end{aligned} \tag{5.56}$$

□

### 5.2.6. Randomized Range Finder Algorithm

Using the random vector generation in Section 5.2.4 and the randomized norm estimator in Section 5.2.5 applied to  $O = (1 - P_{\tilde{R}^n})T^l$ , we can formulate the randomized range finder algorithm. We propose an adaptive randomized range approximation algorithm that constructs an approximation space  $\tilde{R}^n$  by iteratively extending its basis until a convergence criterion is satisfied. In each iteration, the basis is extended by the operator  $T$  applied to a random function.

The full algorithm is given in Algorithm 5.1 and has four input parameters, starting with the operator  $T$ , whose range should be approximated. This could be represented by a matrix, but in the intended context it is usually an implicitly defined operator which is computationally expensive to evaluate. Only the evaluation of the operator on a vector is required. The second input parameter



is the target accuracy  $\text{tol}$  such that  $\|(1 - P_{\tilde{R}^n})T^l\| \leq \text{tol}$ . The third input parameter is the number of test vectors  $n_t$  to be used in the a posteriori error estimator. More test vectors lead to spaces of lower dimension but induce a higher computational cost. A typical  $n_t$  could be 5, 10, or 20. The fourth input parameter is the maximum failure probability  $\varepsilon_{\text{algofail}}$ . The algorithm might fail to deliver a space with the required approximation properties, but only with a probability which is smaller than this parameter. Choosing it as e.g.  $10^{-15}$  leads to an algorithm which virtually never fails. The algorithm returns a space which has the required approximation properties with a probability greater than  $1 - \varepsilon_{\text{algofail}}$  i.e.  $P(\|(1 - P_{\tilde{R}^n})T^l\| \leq \text{tol}) > (1 - \varepsilon_{\text{algofail}})$ .

The basis  $B$  of  $\tilde{R}^n$  is initialized with the affine part  $T^a$  in line 3, test vectors are initialized as the operator applied to random normal vectors in line 5. The test vectors are orthogonalized to the existing basis in line 7. Recall that  $TD_S^{-1}r$  is the operator  $T$  applied to a random normal vector. We use the term ‘‘random normal vector’’ to denote a vector whose entries are independent and identically distributed random variables with normal distribution. The main loop of the algorithm is terminated when the a posteriori norm estimator Definition 5.2.2 applied to  $(1 - P_{\tilde{R}^n})T^l$  is smaller than  $\text{tol}$ . The constant  $c_{\text{est}}(n_t, \varepsilon_{\text{testfail}})$ , which appears in the error estimator, is calculated in line 9 and 10 using  $N_T$  — the rank of operator  $T$ . In practice  $N_T$  is unknown and an upper bound for  $N_T$  such as  $\min(N_S, N_R)$  can be used instead. In line 12 the algorithm assesses if the convergence criterion is already satisfied. Note that the term  $(\max_{t \in M} \|t\|_R) \cdot c_{\text{est}}(n_t, \varepsilon_{\text{testfail}})$  is the norm estimator Equation (5.41) applied to  $(1 - P_{\tilde{R}^n})T^l$ . The test vectors are reused for all iterations. The main loop of the algorithm consists of two parts. First, the basis is extended in line 13 and 14 by applying the operator  $T$  to a random normal vector and adding the result to the basis  $B$ . Then the basis  $B$  is orthonormalized. We emphasize that the orthonormalization is numerically challenging, as the basis functions are nearly linear dependent when  $\tilde{R}^n$  is already a good approximation of the range of  $T$ . In the numerical experiments we use the numerically stable Gram-Schmidt with re-iteration Algorithm C.4 shown in Appendix C. Second, the test vectors are updated in line 16.

In Algorithm 5.1, the smallest eigenvalue of the matrix of the inner product in  $S$ ,  $\lambda_{\min}^M$ , or at least a lower bound for it, is required. The orthonormalization of  $B$  in line 14 and the update of test vectors in line 16 use the inner product in  $R$ .

The presented algorithm has good performance properties for operators  $T$  which are expensive to evaluate. To produce the space  $\tilde{R}^n$  of dimension  $n$ , it evaluates the operator  $n$  times to generate the basis and  $n_t$  times to generate the test vectors, so in total  $n + n_t$  times. Exploiting the low rank structure of  $T$ , one could calculate the eigenvectors of  $T^*T$  using a Lanczos type algorithm as implemented in ARPACK [Lehoucq et al.(1998)], but this would require  $\mathcal{O}(n)$  evaluations of  $T$  and  $T^*$  in every iteration, potentially summing up to much more than  $n + n_t$  evaluations, where the number of iterations is often not foreseeable.

### 5.2.7. A probabilistic a priori error bound

In this subsection we analyze the convergence behavior of Algorithm 5.1. By applying results from randomized numerical linear algebra, it is possible to devise a priori bounds for the projection error  $\|(1 - P_{\tilde{R}^n})T^l\|$  and its expected value. To do so, we first bound  $\|(1 - P_{\tilde{R}^n})T^l\|$  in terms of  $\left\| \left(1 - \underline{P}_{\tilde{R}^n, 2}\right) \underline{T}^l \right\|_2$  where  $\underline{P}_{\tilde{R}^n, 2}$  is the matrix of the orthogonal projection on  $\tilde{R}^n$  in the euclidean inner product in  $\mathbb{R}^{N_R}$  and  $\|\cdot\|_2$  is the spectral matrix norm. This is done in Lemma 5.2.5. In a second step, we use a result from [Halko et al.(2011)] reproduced as Theorem 5.2.6 here to obtain an a priori bound for  $\left\| \left(1 - \underline{P}_{\tilde{R}^n, 2}\right) \underline{T}^l \right\|_2$  in terms of the singular values  $\underline{\sigma}_i$  of the matrix of the transfer operator. In a third step, we devise an upper bound for the singular values of the matrix of the transfer operator  $\underline{\sigma}_i$  in terms of the singular values of the transfer operator  $\sigma_i$  in Lemma 5.2.7. Combining these three results, we obtain our main a priori result, Proposition 5.2.8.

**Lemma 5.2.5** (Projection error of operators and their matrices). *For some given reduced space  $\tilde{R}^n$  it holds*

$$\|(1 - P_{\tilde{R}^n})T^l\| = \sup_{\xi \in S \setminus \{0\}} \inf_{\zeta \in \tilde{R}^n} \frac{\|T^l\xi - \zeta\|_R}{\|\xi\|_S} \leq \sqrt{\frac{\lambda_{max}^{M_R}}{\lambda_{min}^{M_S}}} \|(1 - P_{\tilde{R}^n, 2})T^l\|_2. \quad (5.57)$$

*Proof.*

$$\begin{aligned} \sup_{\xi \in S \setminus \{0\}} \inf_{\zeta \in \tilde{R}^n} \frac{\|T^l\xi - \zeta\|_R}{\|\xi\|_S} &= \sup_{\xi \in S \setminus \{0\}} \frac{\|T^l\xi - P_{\tilde{R}^n}T^l\xi\|_R}{\|\xi\|_S} \\ &= \sup_{\underline{\xi} \in \mathbb{R}^{N_S} \setminus \{0\}} \frac{\left( (T^l\underline{\xi} - P_{\tilde{R}^n}T^l\underline{\xi})^T M_R (T^l\underline{\xi} - P_{\tilde{R}^n}T^l\underline{\xi}) \right)^{1/2}}{\sqrt{\underline{\xi}^T M_S \underline{\xi}}} \\ &\leq \sup_{\underline{\xi} \in \mathbb{R}^{N_S} \setminus \{0\}} \frac{\left( (T^l\underline{\xi} - P_{\tilde{R}^n, 2}T^l\underline{\xi})^T M_R (T^l\underline{\xi} - P_{\tilde{R}^n, 2}T^l\underline{\xi}) \right)^{1/2}}{\sqrt{\underline{\xi}^T M_S \underline{\xi}}} \\ &\leq \sqrt{\frac{\lambda_{max}^{M_R}}{\lambda_{min}^{M_S}}} \sup_{\underline{\xi} \in \mathbb{R}^{N_S} \setminus \{0\}} \frac{\|T^l\underline{\xi} - P_{\tilde{R}^n, 2}T^l\underline{\xi}\|_2}{\|\underline{\xi}\|_2}. \end{aligned} \quad (5.58)$$

□

**Theorem 5.2.6** (A priori convergence of randomized range finder for matrices). *[Halko et al.(2011), Theorem 10.6] Let  $\underline{T} \in \mathbb{R}^{N_R \times N_S}$ . Then for  $n \geq 4$  it holds*

$$\mathbb{E} \left( \left\| \underline{T} - P_{\tilde{R}^n, 2} \underline{T} \right\|_2 \right) \leq \min_{\substack{k+p=n \\ k \geq 2, p \geq 2}} \left[ \left( 1 + \sqrt{\frac{k}{p-1}} \right) \underline{\sigma}_{k+1} + \frac{e\sqrt{n}}{p} \left( \sum_{j>k} \underline{\sigma}_j^2 \right)^{\frac{1}{2}} \right]. \quad (5.59)$$

*Proof.* [Halko et al.(2011), Theorem 10.6]

□

**Lemma 5.2.7** (Singular values of operators and their matrices). *Let the singular values  $\underline{\sigma}_j$  of the matrix  $\underline{T}$  be sorted in non-increasing order, i.e.  $\underline{\sigma}_1 \geq \dots \geq \underline{\sigma}_{N_R}$  and  $\sigma_j$  be the singular values of the operator  $T$ , also sorted non-increasing. Then it holds*

$$\underline{\sigma}_j \leq (\lambda_{max}^{M_S} / \lambda_{min}^{M_R})^{1/2} \sigma_j \quad \forall j \in \{1, \dots, N_T\}. \quad (5.60)$$

*Proof.* For notational convenience we denote within this proof the  $j$ -th eigenvalue of a matrix  $\underline{A}$  by  $\lambda_j(\underline{A})$ . All singular values for  $j \in \{1, \dots, N_T\}$  are different from zero. Therefore, it holds

$$\underline{\sigma}_j^2 = \lambda_j(\underline{T}^t \underline{T}) \quad \text{and} \quad \sigma_j^2 = \lambda_j(M_S^{-1} \underline{T}^t M_R \underline{T}). \quad (5.61)$$

Recall that  $\underline{T}$  is the matrix representation of  $T$  and note that  $M_S^{-1} \underline{T}^t M_R$  is the matrix representation of the adjoint operator  $T^*$ . The non-zero eigenvalues of a product of matrices  $\underline{AB}$  are identical to the non-zero eigenvalues of the product  $\underline{BA}$  (see e.g. [Horn and Johnson(2012), Theorem 1.3.22]), hence

$$\lambda_j(M_S^{-1} \underline{T}^t M_R \underline{T}) = \lambda_j(\underline{T}^t M_R \underline{T} M_S^{-1}). \quad (5.62)$$

We may then apply the Courant minimax principle to infer

$$\lambda_j(\underline{T}^t M_R \underline{T}) (\lambda_{max}^{M_S})^{-1} \leq \lambda_j(M_S^{-1} \underline{T}^t M_R \underline{T}). \quad (5.63)$$

Employing once again cyclic permutation and the Courant minimax principle yields

$$\lambda_j(\underline{T}^t \underline{T}) = \lambda_j(\underline{T} \underline{T}^t) \leq \lambda_j(\underline{T} \underline{T}^t \underline{M}_R) \frac{1}{\lambda_{\min}^{\underline{M}_R}} \leq \lambda_j(\underline{T}^t \underline{M}_R \underline{T}) \frac{1}{\lambda_{\min}^{\underline{M}_R}} \leq \lambda_j(\underline{M}_S^{-1} \underline{T}^t \underline{M}_R \underline{T}) \frac{\lambda_{\max}^{\underline{M}_S}}{\lambda_{\min}^{\underline{M}_R}} \quad (5.64)$$

and thus the claim.  $\square$

**Proposition 5.2.8** (A priori convergence of randomized range finder). *Let  $\lambda_{\max}^{\underline{M}_S}$ ,  $\lambda_{\min}^{\underline{M}_S}$ ,  $\lambda_{\max}^{\underline{M}_R}$ , and  $\lambda_{\min}^{\underline{M}_R}$  denote the largest and smallest eigenvalues of the inner product matrices  $\underline{M}_S$  and  $\underline{M}_R$ , respectively and let  $\tilde{R}^n$  be the outcome of Algorithm 5.1. Then, for  $n \geq 4$  it holds*

$$\mathbb{E} \|(1 - P_{\tilde{R}^n}) T^l\| \leq \sqrt{\frac{\lambda_{\max}^{\underline{M}_R} \lambda_{\max}^{\underline{M}_S}}{\lambda_{\min}^{\underline{M}_R} \lambda_{\min}^{\underline{M}_S}}} \min_{\substack{k+p=n \\ k \geq 2, p \geq 2}} \left[ \left(1 + \sqrt{\frac{k}{p-1}}\right) \sigma_{k+1} + \frac{e\sqrt{n}}{p} \left(\sum_{j>k} \sigma_j^2\right)^{\frac{1}{2}} \right]. \quad (5.65)$$

*Proof.* Combining Lemma 5.2.5, Theorem 5.2.6 and Lemma 5.2.7, the statement follows.  $\square$

The Proposition 5.2.8 extends the results in Theorem 10.6 in [Halko et al.(2011)] to the case of finite dimensional linear operators. The terms consisting of the square root of the conditions of the inner product matrices  $\underline{M}_S$  and  $\underline{M}_R$  in Equation (5.65) are due to our generalization from the spectral matrix norm as considered in [Halko et al.(2011)] to inner products associated with finite dimensional Hilbert spaces.

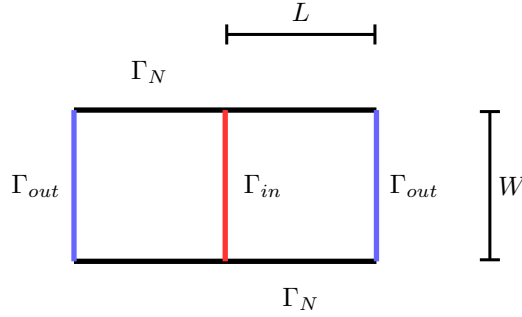
**Remark 5.2.9** (Improved constants for a priori convergence estimate). *The result of Algorithm 5.1, when interpreted as functions and not as coefficient vectors, is independent of the choice of the basis in  $R$ . Disregarding numerical errors, the result would be the same if the algorithm was executed in an orthonormal basis in  $R$ . Thus, we would expect Proposition 5.2.8 to hold also without the factor  $(\lambda_{\max}^{\underline{M}_R}/\lambda_{\min}^{\underline{M}_R})^{1/2}$ .*

### 5.3. Numerical Experiments for Isolated Range Finder

Here we provide numerical examples which only show the performance of the range finder algorithm, without any model reduction. We introduce two artificial examples, designed to test the range finder algorithm, namely *Rangefinder Example 1* and *Rangefinder Example 2*.

In this section we demonstrate first that the reduced local spaces generated by Algorithm 5.1 yield an approximation that converges at a nearly optimal rate. Moreover, we validate the a priori error bound in Equation (5.65) and the a posteriori error estimator Equation (5.41). To this end, we consider two test cases for which the singular values of the transfer operator are known (see [Buhr and Smetana(2018), Supplementary Materials, Section SM2] for details).

The main focus of this subsection is a thorough validation of the theoretical findings in Section 5.2, including a comprehensive testing on how the results depend on various parameters such as the basis size  $n$ , the number of test vectors  $n_t$ , and the mesh size. In addition, CPU time measurements are given. The second numerical example in Section 5.3 examines the behavior of the proposed algorithm in the more challenging case of the Helmholtz equation. For the implementation of the test cases, only NumPy and SciPy, but no FEM software library was used.

Figure 5.1.: Geometry of *Rangefinder Example 1* and *Rangefinder Example 2**Analytic interface problem*

To analyze the behavior of the proposed algorithm, we first apply it to an analytic problem where the singular values of the transfer operator are known. We refer to this numerical example as *Rangefinder Example 1*. We consider the problem  $\mathcal{A} = -\Delta$ ,  $f = 0$ , and assume that  $\Omega = (-L, L) \times (0, W)$ ,  $\Gamma_{out} = \{-L, L\} \times (0, W)$ , and  $\Gamma_{in} = \{0\} \times (0, W)$ . Moreover, we prescribe homogeneous Neumann boundary conditions on  $\partial\Omega \setminus \Gamma_{out}$  and arbitrary Dirichlet boundary conditions on  $\Gamma_{out}$ , see also Figure 5.1 (left). The analytic solution is known to be

$$u(x_1, x_2) = a_0 + b_0 x_1 + \sum_{n=1}^{\infty} \cos(n\pi \frac{x_2}{W}) \left[ a_n \cosh(n\pi \frac{x_1}{W}) + b_n \sinh(n\pi \frac{x_1}{W}) \right]. \quad (5.66)$$

For further discussion see [Buhr and Smetana(2018)]. This example was introduced in [Smetana and Patera(2016), Remark 3.3]. We define  $S$  to be the FE approximation of the space  $L^2(\Gamma_{out})$  and  $R$  to be the FE approximation of the  $L^2(\Gamma_{in})$  with the usual  $L^2$ -inner product on the respective interfaces. The transfer operator maps the Dirichlet data to the inner interface, i.e. with  $H$  as the space of all discrete solutions, we define

$$T(v|_{\Gamma_{out}}) := v|_{\Gamma_{in}} \quad \forall v \in H. \quad (5.67)$$

As this transfer operator is linear, it holds  $T = T^l$ . The singular values of the transfer operator are  $\sigma_i = 1 / (\sqrt{2} \cosh((i-1)\pi L/W))$ .

For the experiments, we use  $L = W = 1$ , unless stated otherwise. We discretize the problem by meshing it with a regular mesh of squares of size  $h \cdot h$ , where  $1/h$  ranges from 20 to 320 in the experiments. On each square, we use bilinear Q1 ansatz functions, which results in e.g. 51,681 DoFs,  $N_S = 322$  and  $N_R = 161$  for  $1/h = 160$ .

In Figure 5.2b the first five basis vectors as generated by Algorithm 5.1 in one particular run are shown side by side with the first five basis vectors of the optimal space, i.e. the optimal modes in Figure 5.2a. While not identical, the basis functions generated using the randomized approach are smooth and have strong similarity with the optimal ones. Unless stated otherwise, we present statistics over 100,000 evaluations, use a maximum failure probability of  $\varepsilon_{\text{algofail}} = 10^{-15}$ , and use  $\min(N_S, N_R)$  as an upper bound for the rank of  $T^l$ ,  $N_T$ .

We first quantify the approximation quality of the spaces  $\tilde{R}^n$  in dependence of the basis size  $n$ , disregarding the adaptive nature of Algorithm 5.1. In Figure 5.3a, statistics over the achieved projection error  $\|(1 - P_{\tilde{R}^n}) T^l\|$  are shown along with the singular values  $\sigma_{n+1}$  of the transfer operator  $T$ .  $\sigma_{n+1}$  is a lower bound for the projection error and it is the projection error that is achieved using an optimal basis. It shows that while the algorithm most of the time produces a basis nearly as good as the optimal basis, sometimes it needs two or three basis vectors more. This is in line with the predictions by theory, see the discussion after Proposition 5.2.8. The mean

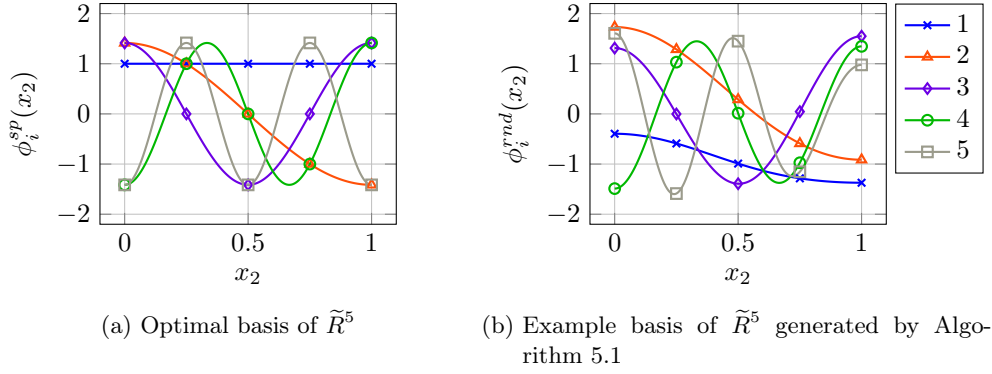


Figure 5.2.: Comparison of optimal basis functions with the basis functions generated by Algorithm 5.1 for *RangeFinder Example 1*. Basis functions are normalized to an  $L^2(\Gamma_{in})$  norm of one. (reproduction: Appendix A.19)

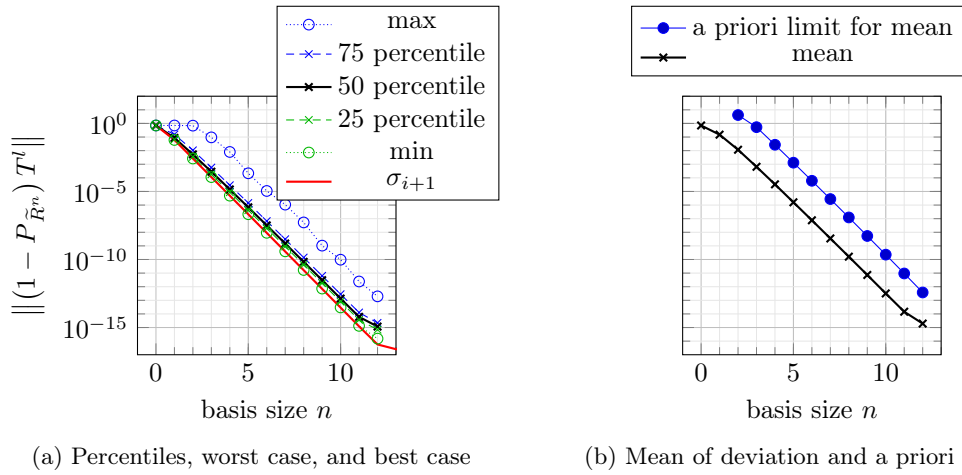


Figure 5.3.: Projection error  $\sup_{\xi \in \mathcal{S} \setminus \{0\}} \inf_{\zeta \in \tilde{R}^n} \frac{\|T\xi - \zeta\|_R}{\|\xi\|_S} = \|(1 - P_{\tilde{R}^n}) T^l\|$  over basis size  $n$  for *RangeFinder Example 1* with mesh size  $h = 1/160$ . (reproduction: Appendix A.20)

value of the projection error converges with the same rate as the a priori error bound given in Proposition 5.2.8 with increasing basis size. The a priori error bound is consistently around three orders of magnitude larger than the actual error, until the actual error hits the numerical noise between  $10^{-14}$  and  $10^{-15}$ , see Figure 5.3b. This is mainly due to the fact that the singular values decay very fast for the present example and an index shift in the singular values by  $p \geq 2$  as required by the a priori error bound Equation (5.65) therefore results in a much smaller error than predicted by the a priori error bound. Note that we have  $(\lambda_{\max}^{M_R}/\lambda_{\min}^{M_R})^{1/2} \approx (\lambda_{\max}^{M_S}/\lambda_{\min}^{M_S})^{1/2} \approx 2$ .

The adaptive behavior of Algorithm 5.1 is analyzed in Figure 5.4. Figure 5.4a shows that for  $n_t = 10$  the algorithm succeeded to generate a space with the requested approximation quality every single time in the 100,000 test runs and most of the time, the approximation quality is about one or two orders of magnitude better than required. Figure 5.4b shows the influence of the number of test vectors  $n_t$ : With a low number of test vectors like 3 or 5, the algorithm produces spaces with an approximation quality much better than requested, which is unfavorable as the basis sizes are larger than necessary. 10 or 20 test vectors seem to be a good compromise, as enlarging  $n_t$  to 40 or 80 results in only little improvements while increasing computational cost. This different behavior of Algorithm 5.1 for various numbers of test vectors  $n_t$  is due to the scaling of the effectivity of the a posteriori error estimator  $\eta((1 - P_{\tilde{R}^n})T^l, n_t, \varepsilon_{\text{testfail}})$  as defined in Equation (5.48) in the number of test vectors  $n_t$ : The median effectivity  $\eta((1 - P_{\tilde{R}^n})T^l, n_t, \varepsilon_{\text{testfail}})$  is 29.2 for  $n_t = 10$ , 10.4 for  $n_t = 20$ , and 6.1 for  $n_t = 40$ . We may thus also conclude that the a posteriori error estimator Equation (5.41) is a sharp bound for the present test case.

The quality of the produced spaces  $\tilde{R}^n$  should be independent of the mesh size  $h$ . Figure 5.5a confirms this. After a preasymptotic regime, the deviation  $\|(1 - P_{\tilde{R}^n})T^l\|$  is independent of the mesh size. In the preasymptotic regime, the finite element space is not capable of approximating the corresponding modes. But while the deviation  $\|(1 - P_{\tilde{R}^n})T^l\|$  is independent of the mesh size, the norm of the test vectors used in the a posteriori error estimator in Algorithm 5.1 is not (see Figure 5.5b). The maximum norm of test vectors scales with the deviation and with  $\sqrt{h}$ . In the adaptive algorithm, the scaling with  $\sqrt{h}$  is compensated by the factor  $(\lambda_{\min}^{M_S})^{-1/2}$  in  $c_{\text{est}}(n_t, \varepsilon_{\text{testfail}})$ . To analyze the behavior in  $h$ , the geometry parameters were chosen as  $L = 0.5$  and  $W = 1$  to have a slower decay of the singular values of the transfer operator.

To examine CPU times we use *Rangefinder Example 1* in a larger configuration with  $L = 1$ ,  $W = 8$  and  $1/h = 200$ . This results in 638.799 unknowns,  $N_S = 3202$ , and  $N_R = 1601$ . The measured CPU times for a simple, single threaded implementation are given in Table 5.1. The transfer operator is implemented implicitly. Its matrix is not assembled. Instead, the corresponding problem is solved using the sparse direct solver SuperLU [Li et al.(1999),Demmel et al.(1999)] each time the operator is applied. For Algorithm 5.1, a target accuracy  $\text{tol}$  of  $10^{-4}$ , the number of testvectors  $n_t = 20$ , and a maximum failure probability  $\varepsilon_{\text{algofail}} = 10^{-15}$  is used. In one test run, it resulted in an approximation space  $\tilde{R}^n$  of dimension 39. It only evaluated the operator  $n + n_t = 59$  times. Each operator evaluation was measured to take 0.301 seconds, so a runtime of approximately  $(n + n_t) * 0.301\text{s} \approx 17.8\text{s}$  is expected. The measured runtime of 20.4 seconds is slightly higher, due to the orthonormalization of the basis vectors and the projection of the test vectors.

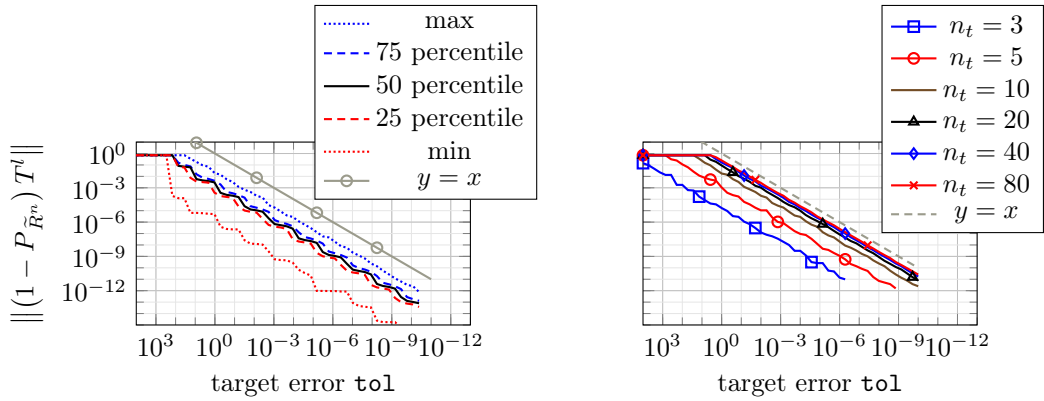
CPU times for the calculation of the optimal space of same size are given for comparison. The “eigs” function in “scipy.sparse.linalg”, which is based on ARPACK, is used to find the eigensystem of  $TT^*$ . However, the calculation using ARPACK is not adaptive. To employ ARPACK, the required number of vectors has to be known in advance, which is why we expect that in general, the comparison would be even more in favor of the adaptive randomized algorithm.

### Helmholtz Equation

In this subsection we analyze the behavior of the proposed algorithm in a numerical test case approximating the solution of the Helmholtz equation. The domain  $\Omega$ , the boundaries  $\Gamma_{in}$  and

<i>Properties of transfer operator</i>		
unknowns of corresponding problem	638,799	
LU factorization time	14.1 s	
operator evaluation time	0.301 s	
adjoint operator evaluation time	0.301 s	
<i>Properties of basis generation</i>		
	Algorithm 5.1	Scipy/ARPACK
(resulting) basis size $n$	39	39
operator evaluations	59	79
adjoint operator evaluations	0	79
execution time (w/o factorization)	20.4 s	47.9 s

Table 5.1.: CPU times for *Rangefinder Example 1* with  $L = 1$ ,  $W = 8$  and  $1/h = 200$  in single threaded implementation. (reproduction: Appendix A.21)



(a) Quartiles for 10 test vectors.

(b) Maximum error for given number of test vectors.

Figure 5.4.: Projection error  $\sup_{\xi \in S \setminus \{0\}} \inf_{\zeta \in \tilde{R}^n} \frac{\|T\xi - \zeta\|_R}{\|\xi\|_S} = \|(1 - P_{\tilde{R}^n})T^l\|$  over target projection error for *Rangefinder Example 1* with mesh size  $h = 1/160$ . (reproduction: Appendix A.22)

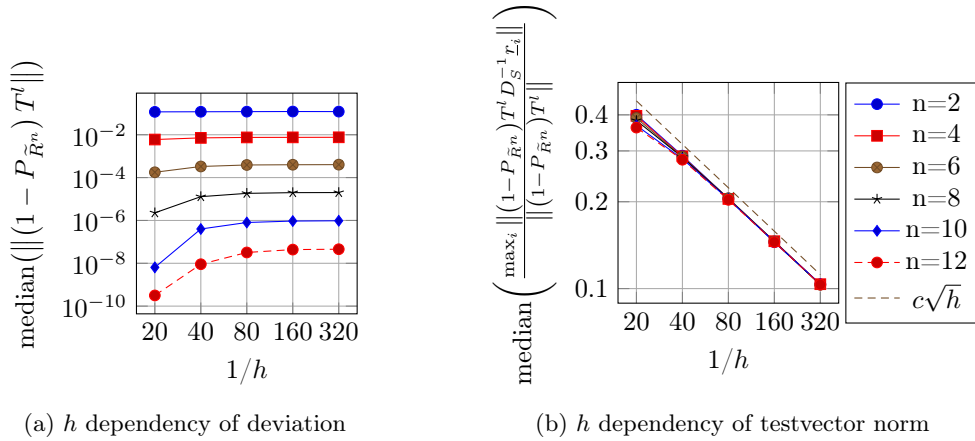


Figure 5.5.:  $h$  dependency in *Rangefinder Example 1*; Statistics over 10,000 samples. (reproduction: Appendix A.23)

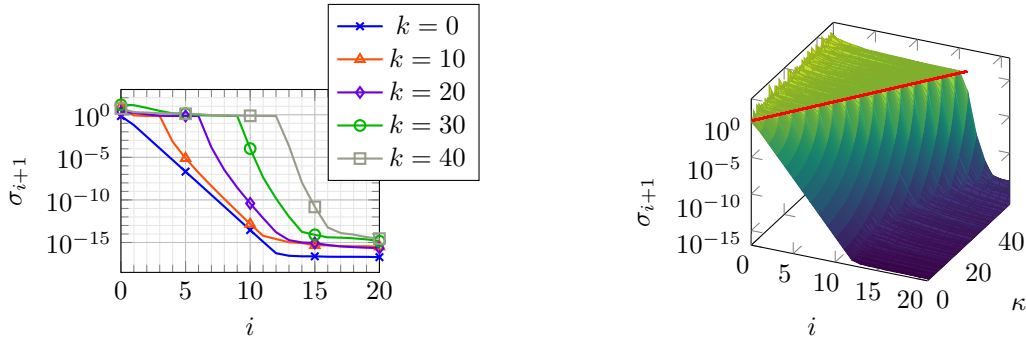


Figure 5.6.: Singular value decay for *Rangefinder Example 2*. The red line at  $i = k/\pi$  in the right plot marks the observed length of the plateau. (reproduction: Appendix A.24)

$\Gamma_{out}$  and the boundary conditions are the same as in Section 5.3, only the operator  $\mathcal{A}$  differs and is defined as  $\mathcal{A} := -\Delta - k^2$  in this subsection where  $k$  is the wave number. As for *Rangefinder Example 1*, it has 51,681 DoFs,  $N_S = 322$  and  $N_R = 161$  for  $1/h = 160$ . We refer to this numerical example as *Rangefinder Example 2*. We assume the problem to be inf-sup stable and thus uniquely solvable, which is the case as long as it is not in a resonant configuration.

For  $k = 0$  we obtain *Rangefinder Example 1*. We observe that the singular values of the transfer operator first have a plateau and then decay exponentially, see Figure 5.6. The longer the plateau, the faster is the exponential decay. The length of the plateau is observed to be very close to the length of the inner interface divided by a half wavelength, i.e.  $1/(\lambda/2) = k/\pi$ . Comparing this with the analysis of Finite Element methods for the Helmholtz equation (cf. [Ihlenburg(2006)]), one finds this similar to the “minimal resolution condition”  $1/h \geq \sqrt{12}/k$ . However, we do not observe an equivalent of the “pollution effect”: When doubling the frequency, doubling the number of degrees of freedom is more than sufficient to maintain the same approximation quality. For example, at  $k = 10$  the optimal space of size 5 reaches an approximation quality of about  $10^{-6.7}$ . For  $k = 20$ , the optimal space of size 10 reaches an approximation quality of about  $10^{-10.5}$  (Figure 5.6). Of course, both the discretization used to compute the transfer operator as well as the approximation scheme used to solve the global problem using the locally computed approximation spaces might still suffer from the pollution effect.

Algorithm 5.1 succeeds to generate reduced spaces  $\tilde{R}^n$  which achieve a projection error



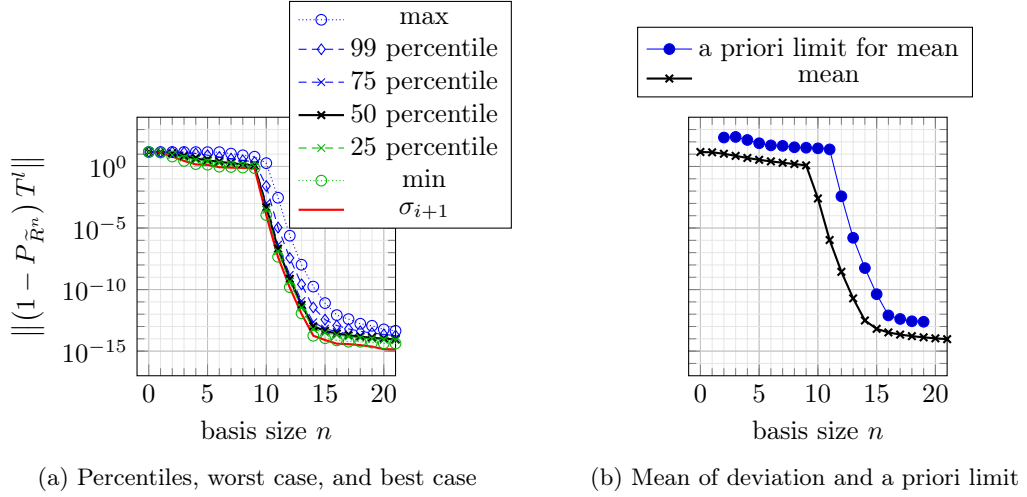


Figure 5.7.: Projection error  $\sup_{\xi \in S \setminus \{0\}} \inf_{\zeta \in \tilde{R}^n} \frac{\|T\xi - \zeta\|_R}{\|\xi\|_S} = \|(1 - P_{\tilde{R}^n})T^l\|$  over basis size  $n$  for *Rangefinder Example 2* with  $k = 30$ . Meshsize  $h = 1/160$ . (reproduction: Appendix A.25)

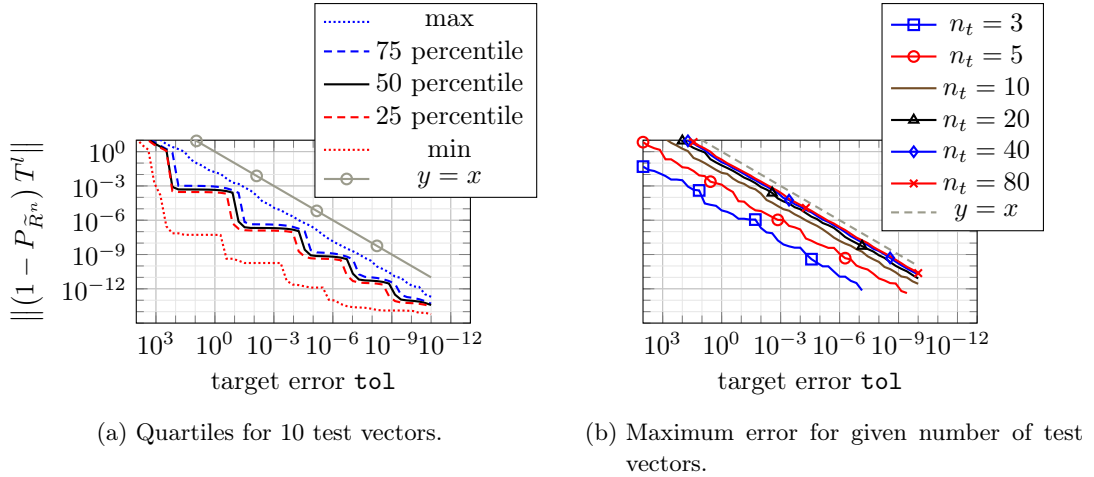


Figure 5.8.: Projection error  $\sup_{\xi \in S \setminus \{0\}} \inf_{\zeta \in \tilde{R}^n} \frac{\|T\xi - \zeta\|_R}{\|\xi\|_S} = \|(1 - P_{\tilde{R}^n})T^l\|$  over target projection error for *Rangefinder Example 2* with  $k = 30$ . Meshsize  $h = 1/160$ . (reproduction: Appendix A.26)

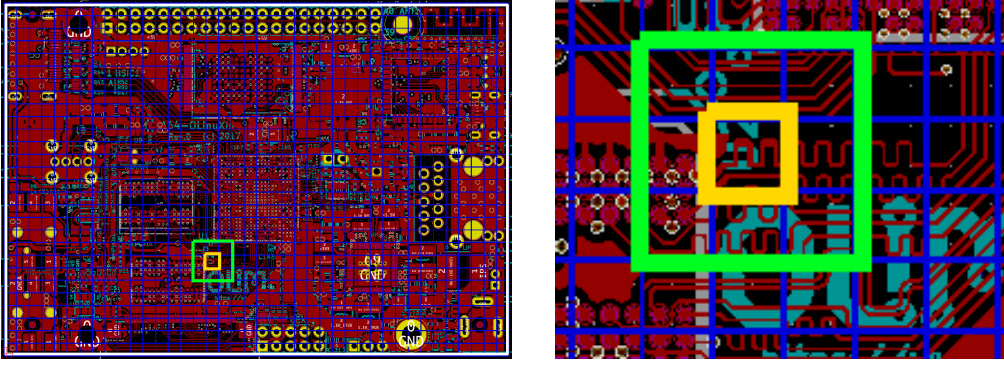


Figure 5.9.: Domain decomposition used for *Olimex A64 Example* with  $40 \times 28$  domains. For each domain  $\omega_i$  (e.g.  $\omega_{816}$ , yellow) we introduce an oversampling domain  $\omega_i^*$  (e.g.  $\omega_{816}^*$ , green).

$\|(1 - P_{\tilde{R}^n}) T^l\|$  which is close to the optimal projection error given by the singular values of the transfer operator. We show results for  $k = 30$  in Figure 5.7. Also in the adaptive case, we observe the expected behavior, see Figure 5.8a and Figure 5.8b. The plateaus which can be observed in Figure 5.8a are due to the very fast decay of the singular values. For example the first plateau is at an error of about  $10^{-3}$ , which is the error usually achieved at a basis size of 10 (cf. Figure 5.7a). The next plateau at an error of about  $10^{-7}$  corresponds to a basis size of 11.

#### 5.4. Olimex A64 Example

Proposition 5.1.3, our results in Chapter 3 as well as the results in [Buhr and Smetana(2018)] suggest that good reduction errors can be achieved if the local approximation spaces capture the most important parts of the image of the transfer operators and thus  $\|(1 - P_{\tilde{V}_i}) T_i^l\|$  is small. Both the theoretical results about the randomized range finder in Section 5.2.7 as well as the numerical results in Section 5.3 show that good approximation spaces can be generated in reasonable time if the singular value decay of the transfer operators is strong enough. In this section, we compute the singular value decay of transfer operators defined in *Olimex A64 Example* to judge on the applicability of our methodology to this example.

We analyze *Olimex A64 Example* described in Section 2.7.4 for a fixed frequency of  $\omega = 2\pi \cdot 10^5 \text{ Hz}$ . We use a two dimensional non overlapping domain decomposition  $\{\omega_i^{\text{no1}}\}_{i=1}^{N_{\text{no1}}}$  with  $N_{\text{no1}} = 1120$  depicted in Figure 5.9. The size of each domain is approximately  $(2\text{mm})^3$ . Due to its simplicity, we use the basic space decomposition defined in Definition 3.2.1, where FE ansatz functions are grouped by the domains they have support in. We assume that one could obtain better results using the wirebasket space decomposition. We focus on domain  $\omega_{816}$ , which is shown along with its oversampling domain  $\omega_{816}^*$  in Figures 5.9 and 5.10. It contains a part of the traces connecting the CPU to the RAM and has exceptional high geometric complexity.

We define the transfer operator as in Section 3.3.2, except that we project to  $V_i^{\text{basic}}$  instead of  $V_i^{\text{wb}}$  at the end. So let  $\mathcal{E}_{816}$  be  $\omega_{816}$ , then we define

$$\begin{aligned} T_{816}^l : \quad & C(\text{Tr}(V_{816}^{\text{basic}})) \rightarrow V_{816}^{\text{basic}} \\ & \varphi \mapsto \mathcal{P}_{V_{816}^{\text{basic}}}(u_l) \end{aligned} \quad (5.68)$$

where  $u_l \in \text{Tr}(V_{816}^{\text{basic}})$  solves

$$a(u_l + \varphi, \psi) = 0 \quad \forall \psi \in \text{Tr}(V_{816}^{\text{basic}}). \quad (5.69)$$

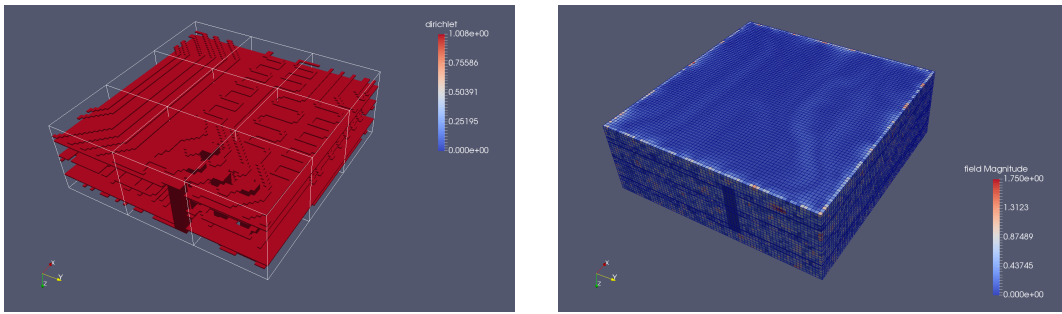


Figure 5.10.: Example randomized solution in oversampling domain of  $\omega_{816}$  of *Olimex A64 Example* (approx. 350.000 unknowns).

For simplicity, we use the euclidean norm of the coefficient vectors in  $V_{816}^{\text{basic}}$  and compare with the singular values of the matrix of  $T_{816}^l$ . In Figure 5.11, the singular values of the matrix of  $T_{816}^l$  are shown. Already at a basis size of 50, a relative reduction of almost three orders of magnitude can be seen. At a basis size of 100, a relative reduction of about 4.5 orders of magnitude can be seen. For comparison, the value of the a posteriori norm estimator used in the randomized range finder is plotted. The randomized norm estimator behaves approximately like  $\|(1 - P_{\tilde{R}^n}) T^l\|$  but is much faster to compute. As expected, it behaves like  $\underline{\sigma}_{n+1} \sqrt{n}$ . Runtimes for the randomized range finder applied to 40 different domains can be seen in Figure 5.12. For most domains, the runtime was between 5 and 10 minutes, in an unoptimized, sequential implementation.

While these preliminary results are not conclusive, they are encouraging. The singular value decay suggests that good approximation spaces of dimension less than 100 per domain exist and can be generated in reasonable time. In a domain decomposition with about 1000 domains, this would result in a global reduced model of around 100 000 unknowns, which could probably be solved quickly, given that the matrices of a localized reduction scheme are block-sparse. The generation of the reduced spaces can easily be parallelized and executed in a cloud environment.

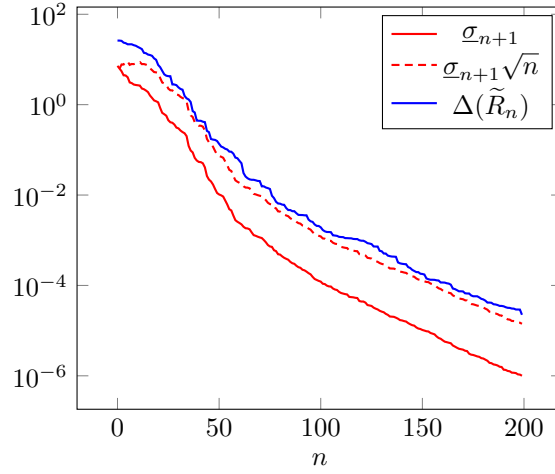


Figure 5.11.: Singular value decay of  $T_{816}$  and decay of randomized norm estimator for *OlimeX A64 Example*. (reproduction: Appendix A.27)

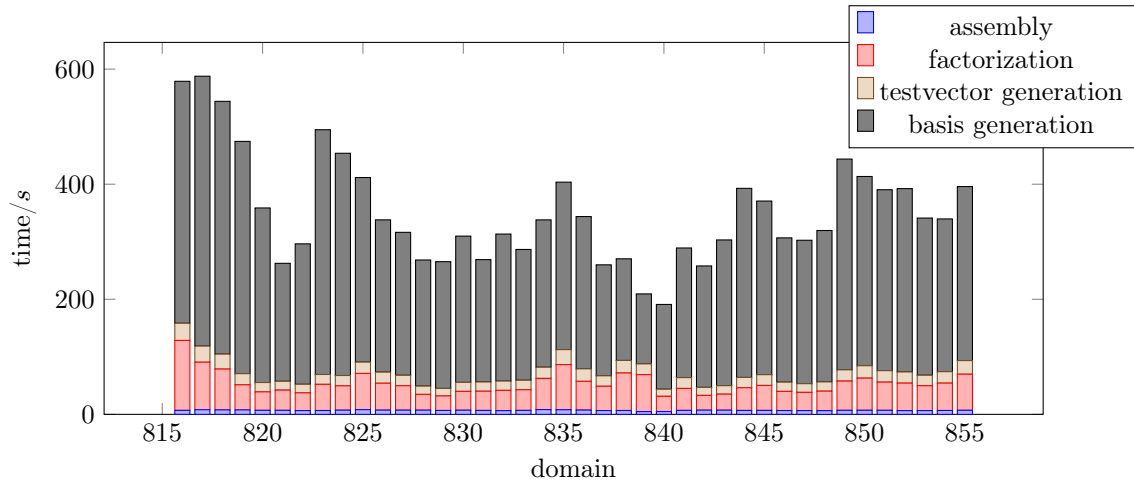


Figure 5.12.: Runtimes for randomized range finder on *OlimeX A64 Example*. (reproduction: Appendix A.27)

## 5.5. Future Research on Randomized Range Finder

While a fast and efficient algorithm was devised for approximating the image of a linear operator, there is lots of room for improvement and future research. In the following, we state what we consider the most interesting or important improvements which could be tackled in future research projects.

- ***Parameterized problems***

The presented algorithm approximates the image of a linear operator. In the context of model reduction, one often deals with parameterized problems, which results in parameterized transfer operators  $T_{\mu,i}$ . The only published ways the authors are aware of to approximate the image of a parameterized operator are the “spectral greedy” in [Smetana and Patera(2016), Algorithm 4.1] and the Proper Orthogonal Decomposition (POD) strategy in [Taddei and Patera(2018)]. Both approaches require the execution of the randomized range finder at every training parameter and are thus very expensive for large training sets  $\Xi$ . It would be desirable to have an algorithm to approximate the image of a parameterized operator without evaluating it at each training parameter.

- ***Complex numbers***

The results presented here are only valid for the real case. An extension to complex numbers should be done. This, however, would require reevaluation of lot of results from RandNLA. Michael Mahoney and his coworkers only deal with the real case in their publications. Per-Gunnar Martinsson and his coworkers mention the complex case in their publications. The relevant proofs are, however, only done for the real case. Most results in RandNLA use estimates for eigenvalues of random matrices like the condition number estimates in [Chen and Dongarra(2005)], which are published also for complex matrices. Recreating the results from RandNLA for complex matrices, starting at the results from [Chen and Dongarra(2005)] to finally devise a complex randomized range finder algorithm would be an interesting project.

- ***Better random vectors***

The drawing of random vectors presented here is simple and the quality of the generated spaces deteriorates when the condition of the matrix of the inner product in  $S$  becomes high. A better way of drawing random vectors should be developed, taking into account the inner product in  $S$ , removing the dependency on the condition of the matrix of the inner product in  $S$ .

- ***Better a posteriori error estimator***

The presented a posteriori error estimator only uses the maximum of all norms of all test vectors and thus loses information. Probably, a better a posteriori error estimator can be devised using information from all test vector norms.

- ***Better bases through postprocessing***

In the presented version of the randomized range finder, all basis vectors produced are used. It would probably lead to better basis vectors if one generated some more vectors than necessary and reduce the number using an SVD afterwards.

- ***Infinite dimensional case***

It would be interesting to formulate a randomized range finder which works on compact operators in Hilbert spaces. This would require a new way of drawing random vectors.

### 5.6. Future Research for Transferoperator Based Training

While the previous items were concerned with improving the randomized range finder algorithm itself, the training procedure can also be further improved.

---

- ***Better Transfer Operators***

While we can approximate the image of the presented transfer operators in an optimal way, there might be better transfer operators with faster decay of singular values. Recently, slightly better results have been demonstrated by using Robin- instead of Dirichlet boundary values to formulate the transfer operator [Eickhorn(2019)].

- ***Application to ArbiLoMod***

While the application of Algorithm 5.1 in the ArbiLoMod context is straightforward, application of Proposition 5.1.3 needs estimates for  $\|\mathcal{P}_{S_i}\|$ , which are not available so far.

In this chapter, we introduce two algorithms for localized online enrichment in an abstract localized model order reduction setting. We show a priori convergence rates and verify the results in a numerical example.

### 6.1. Introduction

By the term “online enrichment”, we denote the extension of our localized approximation spaces  $\tilde{V}_i$ , based on a previous solution of the global, reduced problem. In contrast to the trainings, where only local information is used, online enrichment uses global information, by using the previous global, reduced solution. Online enrichment serves two purposes. First, it can be used in a situation where local approximation spaces have been generated using a training procedure, but the reduced solution is not good enough according to the a posteriori error estimator. Second, it provides a means to generate local approximation spaces in settings where a training procedure fails to generate good approximation spaces. This could be for instance in problems with many channels, of which only very few are used. Enrichment is done by solving the original problem in a local space, using the residual of the last solution as right hand side.

Online enrichment is a widely used technique in localized model order reduction methods. ArbiLoMod, introduced in [Buhr et al.(2017a)], employs online enrichment. For the LRBMS which was introduced in [Albrecht et al.(2012)], online enrichment was presented in [Albrecht and Ohlberger(2013)] and in [Ohlberger and Schindler(2015)]. For the GMsFEM which was introduced in [Efendiev et al.(2013)], online enrichment was discussed in [Chung et al.(2015)]. For the Constraint Energy Minimization - Generalized Multiscale Finite Element Method (CEM-GMsFEM) which was introduced in [Chung et al.(2018b)], online enrichment was discussed in [Chung et al.(2018c)]. However, no a priori convergence analysis is available for the ArbiLoMod and the LRBMS. For the GMsFEM and CEM-GMsFEM, exponential convergence was shown in [Chung et al.(2015)] and [Chung et al.(2018c)].

### 6.2. Enrichment Algorithms

In Section 3.4, an enrichment procedure was introduced. This is, however, only a heuristic approach for which no a priori convergence bounds can be shown. In this section, we introduce two

**Algorithm 6.1:** Residual Based Online Enrichment.

---

```

1  $n \leftarrow 0$ 
2  $\tilde{V}_n \leftarrow \text{span}\{0\}$ 
3 while not converged do
4   /* solve reduced system */
5   find  $\tilde{u}_n \in \tilde{V}_n$  such that:
6   |  $a(\tilde{u}_n, \varphi) = f(\varphi) \quad \forall \varphi \in \tilde{V}_n$ 
7   /* find maximum local residual */
8    $k \leftarrow \arg \max_{i=1, \dots, N_{V_i}} \|\mathcal{R}(\tilde{u}_n)\|_{V_i}$ 
9   /* solve local enrichment problem */
10  find  $\hat{u}_n \in V_k$  such that:
11  |  $a(\hat{u}_n, \varphi) = \mathcal{R}(\tilde{u}_n)(\varphi) \quad \forall \varphi \in V_k$ 
12  /* form enriched space */
13   $\tilde{V}_{n+1} \leftarrow \tilde{V}_n \oplus \text{span}\{\hat{u}_n\}$ 
14   $n \leftarrow n + 1$ 

```

---

**Algorithm 6.2:** Globally Coupled Online Enrichment.

---

```

1  $n \leftarrow 0$ 
2  $\tilde{V}_n \leftarrow \text{span}\{0\}$ 
3 while not converged do
4   /* solve reduced system */
5   find  $\tilde{u}_n \in \tilde{V}_n$  such that:
6   |  $a(\tilde{u}_n, \varphi) = f(\varphi) \quad \forall \varphi \in \tilde{V}_n$ 
7   /* solve local enriched problems */
8   for  $i = 1, \dots, N_{V_i}$  do
9   | find  $\hat{u}_{n,i} \in \tilde{V}_n \oplus V_i$  such that:
10  | |  $a(\hat{u}_{n,i}, \varphi) = f(\varphi) \quad \forall \varphi \in \tilde{V}_n \oplus V_i$ 
11  /* find maximum solution shift */
12   $k \leftarrow \arg \max_{i=1, \dots, N_{OS}} \|\tilde{u}_n - \hat{u}_{n,i}\|_a$ 
13  /* form enriched space */
14   $\tilde{V}_{n+1} \leftarrow \tilde{V}_n \oplus \text{span}\{\hat{u}_{n,k}\}$ 
15   $n \leftarrow n + 1$ 

```

---



enrichment procedures in an abstract setting as introduced in Section 2.4, for which we can show a priori convergence rates in the following section.

### Setting

Let  $\{\Omega, V, \{\omega_i\}_{i=1}^{N_{V_i}}, \{V_i\}_{i=1}^{N_{V_i}}, \{\mathcal{P}_{V_i}\}_{i=1}^{N_{V_i}}\}$  be a localizing space decomposition as defined in Definition 2.4.1 and let  $u$  be the solution of a non parametric variational problem as defined in Definition 2.1.1. Let  $a$  be symmetric and coercive and let the full space  $V$  be equipped with the energy norm induced by  $a$ . Starting with the nullspace  $\tilde{V}_0$ , we construct a sequence of subspaces of  $V$  which we denote by  $\tilde{V}_n$ . The full problem is reduced by Galerkin projection on these reduced spaces. We denote the solutions of the reduced problems by  $\tilde{u}_n$ . Each reduced space  $\tilde{V}_n$  is constructed by enriching the previous reduced space with an additional basis function  $\hat{u}_n$ , which lies in one of the localized spaces  $V_i$ .

### Residual Based Enrichment

The residual based enrichment algorithm (given as Algorithm 6.1) first selects the local enrichment space from which the enrichment function  $\hat{u}_n$  is taken. The local space  $V_k$  which maximizes the dual norm of the residual  $\|\mathcal{R}(\tilde{u}_n)\|_{V_i'} = \sup_{\varphi \in V_i \setminus \{0\}} \frac{\mathcal{R}(\tilde{u}_n)(\varphi)}{\|\varphi\|_a}$  is chosen, i.e.

$$k := \arg \max_{i \in \{1, \dots, N_{V_i}\}} \|\mathcal{R}(\tilde{u}_n)\|_{V_i'}. \quad (6.1)$$

The residual  $\mathcal{R}(\tilde{u}_n) \in V'$  is defined as  $\mathcal{R}(\tilde{u}_n)(\cdot) := f(\cdot) - a(\tilde{u}_n, \cdot)$ . Then a localized problem is formed by a Galerkin projection of the original problem onto this local space  $V_k$ , and replacing the right hand side  $f$  by the last residual  $\mathcal{R}(\tilde{u}_n)$ . The solution of the localized problem is the enrichment function  $\hat{u}_n$ .

### Globally Coupled Local Enrichment

The globally coupled local enrichment algorithm (given as Algorithm 6.2) couples the global reduced space with the full local space. First it iterates over all local spaces  $V_i$  and solves the coupled problem: It solves the original problem projected on the space  $\tilde{V}_n \oplus V_i$ , the solution of this coupled problem is called  $\hat{u}_{n,i}$ . Then the local space  $V_k$  is selected which maximizes the change in the solution  $\|\tilde{u}_n - \hat{u}_{n,k}\|_a$ , i.e.

$$k := \arg \max_{i \in \{1, \dots, N_{V_i}\}} \|\tilde{u}_n - \hat{u}_{n,i}\|_a. \quad (6.2)$$

The function  $\hat{u}_{n,k}$  is used to enrich the space  $\tilde{V}_n$ . Note that this is an enrichment in  $V_k$ , even though  $\hat{u}_{n,k}$  has global support.

## 6.3. A Priori Convergence Estimates

First we prove exponential convergence for the residual based enrichment.

**Theorem 6.3.1** (Exponential convergence of residual based online enrichment). *With the assumptions from above, for the reduced solutions  $\tilde{u}_{n+1}$  in Algorithm 6.1 it holds*

$$\|u - \tilde{u}_{n+1}\|_a \leq c_{\text{rbe}} \cdot \|u - \tilde{u}_n\|_a \quad (6.3)$$

with

$$c_{\text{rbe}} := \sqrt{1 - \frac{1}{N_{V_i}} \frac{1}{c_{\text{pu}, \tilde{V}}^2}} \quad (6.4)$$

with the constant  $c_{\text{pu}, \tilde{V}}$  as defined in Proposition 4.2.3.

*Proof.* As we use the energy norm, the solution is the best approximation

$$\|\tilde{u}_{n+1} - u\|_a \leq \|\varphi - u\|_a \quad \forall \varphi \in \tilde{V}_{n+1}. \quad (6.5)$$

This holds for  $\varphi = \tilde{u}_n + \alpha \hat{u}_n$  for all  $\alpha$  in  $\mathbb{R}$ . Because of the symmetry of  $a$  it holds

$$\|\tilde{u}_n + \alpha \hat{u}_n - u\|_a^2 = \|\tilde{u}_n - u\|_a^2 - 2\alpha \mathcal{R}(\tilde{u}_n)(\hat{u}_n) + \alpha^2 \|\hat{u}_n\|_a^2.$$

This term is minimized by choosing  $\alpha = \mathcal{R}(\tilde{u}_n)(\hat{u}_n) / \|\hat{u}_n\|_a^2$ . We use this  $\alpha$  and realize that  $\mathcal{R}(\tilde{u}_n)(\hat{u}_n) = \|\hat{u}_n\|_a^2 = \|\mathcal{R}(\tilde{u}_n)\|_{V'_k}^2$ , because  $\hat{u}_n$  is the Riesz representative of  $\mathcal{R}(\tilde{u}_n)$  in  $V_k$  in the energy norm. It follows that

$$\|\tilde{u}_{n+1} - u\|_a^2 \leq \|\tilde{u}_n - u\|_a^2 - \|\mathcal{R}(\tilde{u}_n)\|_{V'_k}^2. \quad (6.6)$$

Till this point, the proof followed the structure given in [Chung et al.(2015), Section 4]. We defined  $k$  to select the largest local residual, so it holds

$$\|\mathcal{R}(\tilde{u}_n)\|_{V'_k}^2 \geq \frac{1}{N_{V_i}} \sum_{i=1}^{N_{V_i}} \|\mathcal{R}(\tilde{u}_n)\|_{V'_i}^2. \quad (6.7)$$

Furthermore, from Proposition 4.2.3 we know

$$\|\mathcal{R}(\tilde{u}_n)\|_{V'} \leq c_{\text{pu}, \tilde{V}} \left( \sum_{i=1}^{N_{V_i}} \|\mathcal{R}(\tilde{u}_n)\|_{V'_i}^2 \right)^{\frac{1}{2}} \quad (6.8)$$

As we use the energy norm, we have

$$\|\mathcal{R}(\tilde{u}_n)\|_{V'}^2 = \|\tilde{u}_n - u\|_a^2. \quad (6.9)$$

Combining (6.7), (6.8), and (6.9) we obtain

$$\|\mathcal{R}(\tilde{u}_n)\|_{V'_k}^2 \geq \frac{1}{N_{V_i}} \frac{1}{c_{\text{pu}, \tilde{V}}^2} \|\tilde{u}_n - u\|_a^2. \quad (6.10)$$

Combining (6.10) with (6.6) yields

$$\|\tilde{u}_{n+1} - u\|_a^2 \leq \left( 1 - \frac{1}{N_{V_i}} \frac{1}{c_{\text{pu}, \tilde{V}}^2} \right) \|\tilde{u}_n - u\|_a^2 \quad (6.11)$$

and thus the claim.  $\square$

**Corollary 6.3.2** (Exponential convergence from iteration 0). *For the reduced solutions  $\tilde{u}_n$  in Algorithm 6.1 it holds*

$$\|\tilde{u}_n - u\|_a \leq c_{\text{rbe}}^n \cdot \|u\|_a \quad (6.12)$$

with  $c_{\text{rbe}}$  as defined in (6.4).

*Proof.* This follows from Theorem 6.3.1, because  $\tilde{u}_0 = 0$ .  $\square$

### Globally coupled enrichment

The globally coupled enrichment given in Algorithm 6.2 is the optimal enrichment: Among all enrichment functions from all local spaces, it selects the one which minimizes the resulting error in the energy norm.

**Theorem 6.3.3** (Optimality of globally coupled online enrichment (Algorithm 6.2)). *For the reduced solutions  $\tilde{u}_{n+1}$  in Algorithm 6.2 it holds*

$$\|u - \tilde{u}_{n+1}\|_a = \min_{i=1, \dots, N_{V_i}} \min_{\psi_e \in V_i} \left\{ \|u - \tilde{u}_e\|_a \mid \begin{array}{l} \tilde{u}_e \in \tilde{V}_n \oplus \text{span}\{\psi_e\} \text{ solves} \\ a(\tilde{u}_e, \varphi) = f(\varphi) \quad \forall \varphi \in \tilde{V}_n \oplus \text{span}\{\psi_e\} \end{array} \right\}. \quad (6.13)$$

*Proof.* First we realize that the solution  $\tilde{u}_{n+1}$  is identical to  $\hat{u}_{n,k}$ , because  $\hat{u}_{n,k}$  solves  $a(\hat{u}_{n,k}, \varphi) = f(\varphi)$  in  $\tilde{V}_{n+1}$ , which is a subspace of  $\tilde{V}_n \oplus V_k$  and the solution is unique:

$$\tilde{u}_{n+1} = \hat{u}_{n,k}. \quad (6.14)$$

Second, since  $u - \hat{u}_{n,i}$  is  $a$ -orthogonal to  $\hat{u}_{n,i} - \tilde{u}_n$ , it holds

$$\|u - \tilde{u}_n\|_a^2 = \|u - \hat{u}_{n,i}\|_a^2 + \|\hat{u}_{n,i} - \tilde{u}_n\|_a^2 \quad (6.15)$$

and thus

$$k = \arg \max_{i \in \{1, \dots, N_{V_i}\}} \|\tilde{u}_n - \hat{u}_{n,i}\|_a \quad (6.16)$$

implies

$$k = \operatorname{argmin}_{i \in \{1, \dots, N_{V_i}\}} \|u - \hat{u}_{n,i}\|_a. \quad (6.17)$$

So  $\hat{u}_{n,k}$  is closest to  $u$  among all  $\hat{u}_{n,i}$ .

Third,  $\hat{u}_{n,i}$  is the best approximation in  $\tilde{V}_n \oplus V_i$ . It is not possible to get closer to  $u$  with any other enrichment in  $V_i$ .  $\square$

**Corollary 6.3.4** (Exponential convergence of globally coupled online enrichment). *The results in Theorem 6.3.1 and Corollary 6.3.2 also hold for Algorithm 6.2.*

*Proof.* The enrichment in Algorithm 6.2 is optimal in every step, so it is not worse than the enrichment of Algorithm 6.1. Any bound for Algorithm 6.1 holds also for Algorithm 6.2.  $\square$

## 6.4. Application to Partition of Unity Decomposition

While the two enrichment algorithms given above can be formulated in an abstract setting, there are some constraints in implementing them. The residual based enrichment requires the evaluation of dual norms of the residuals in  $V_i$ , which usually require a basis of these spaces. This would be prohibitively expensive for e.g. the wirebasket space decomposition, as the construction of a basis for e.g. an edge space would require one local solve operation for every DoF on the edge. In addition, the storage requirements of these vectors would be high. Furthermore, even if the basis was available, the computation of the Riesz representative for the evaluation of the dual norm could be computationally expensive, as the matrix for the inner product could become dense. A similar argument holds for the globally coupled local enrichment. Here the solution in  $\tilde{V}_n \oplus V_i$  would require a basis of  $V_i$ . From the different space decompositions introduced in this thesis, only the partition of unity decomposition introduced in Section 2.4.3 allows for a straightforward implementation, as

its local spaces are spanned by FE ansatz functions. So a basis is already available and also the computation of Riesz representatives for the evaluation of the dual norm is quickly possible, as the inner product matrices are sparse. We use the partition of unity decomposition in the following numerical example.

In Section 4.3, we derived an upper bound for  $c_{\text{pu},\tilde{V}}$  for the partition of unity decomposition and the  $H^1$ -norm. As the a priori estimates derived here require the energy norm, we give an upper bound for  $c_{\text{pu},\tilde{V}}$  in the energy norm in the following.

**Proposition 6.4.1** (Upper bound of  $c_{\text{pu},\tilde{V}}$ ). *With the assumptions about the energy norm from above, for the partition of unity decomposition as defined in Section 2.4.3 based on the partition of unity functions  $\{\varrho_i\}_{i=1}^{N_{\text{ol}}}$ . Let  $J$  be the maximum number of functions  $\varrho_i$  having support in any given point  $x$  in  $\Omega$ , let  $\frac{\sigma_{\text{max}}}{\sigma_{\text{min}}}$  being the contrast of the problem, let  $c_F$  the constant of the Friedrich's inequality on  $\Omega$  and  $\|\cdot\|_\infty$  the infinity norm. Neglecting the interpolation operator mapping back to the FE space, it holds that*

$$c_{\text{pu},\tilde{V}}^2 \leq 2J \left( c_F \frac{\sigma_{\text{max}}}{\sigma_{\text{min}}} \max_{i \in \{1, \dots, N_{V_i}\}} \|\nabla \varrho_i\|_\infty^2 + \max_{i \in \{1, \dots, N_{V_i}\}} \|\varrho_i\|_\infty^2 \right). \quad (6.18)$$

*Proof.* Starting from

$$c_{\text{pu},\tilde{V}} \leq \sup_{\varphi \in V \setminus \{0\}} \frac{\sum_{i=1}^{N_{\text{ol}}} \|\varrho_i \varphi\|_a^2}{\|\varphi\|_a^2} \quad (6.19)$$

we estimate  $\sum_{i=1}^{N_{V_i}} \|\varrho_i \varphi\|_a^2$ . It holds that

$$\sum_{i=1}^{N_{V_i}} \|\varrho_i \varphi\|_a^2 = \sum_{i=1}^{N_{V_i}} \int_{\omega_i^{\text{ol}}} \sigma |\nabla(\varrho_i \varphi)|^2 dx \quad (6.20)$$

$$\leq \sum_{i=1}^{N_{V_i}} \int_{\omega_i^{\text{ol}}} \sigma (2|(\nabla \varrho_i) \varphi|^2 + 2|\varrho_i (\nabla \varphi)|^2) dx. \quad (6.21)$$

For the second term in (6.21) it holds that

$$\sum_{i=1}^{N_{V_i}} \int_{\omega_i^{\text{ol}}} 2\sigma |\varrho_i (\nabla \varphi)|^2 dx \leq 2J \max_{i \in \{1, \dots, N_{V_i}\}} \|\varrho_i\|_\infty^2 \|\varphi\|_a^2 \quad (6.22)$$

and for the first term we have

$$\begin{aligned} \sum_{i=1}^{N_{V_i}} \int_{\omega_i^{\text{ol}}} 2\sigma |(\nabla \varrho_i) \varphi|^2 dx &\leq 2J \sigma_{\text{max}} \max_{i \in \{1, \dots, N_{V_i}\}} \|\nabla \varrho_i\|_\infty^2 \int_{\Omega} |\varphi|^2 dx \\ &\leq 2J c_F \frac{\sigma_{\text{max}}}{\sigma_{\text{min}}} \max_{i \in \{1, \dots, N_{V_i}\}} \|\nabla \varrho_i\|_\infty^2 \|\varphi\|_a^2. \end{aligned} \quad (6.23)$$

Combining these yields the claim.  $\square$

## 6.5. Numerical Example

While the method and the proofs work both in two and three dimensions, experiments were conducted for the two dimensional case only. The example used here is the *Thermal Channels Variant*,



Figure 6.1.: Geometry of *Thermal Channels Variant*. Left: Coefficient field  $\sigma$ . White is 1, black is  $10^5$ . Middle: right hand side  $q$ . Black is  $-10^5$ , gray is 0, white is  $10^5$ . Right: reference solution  $u$ . (reproduction: Appendix A.28)

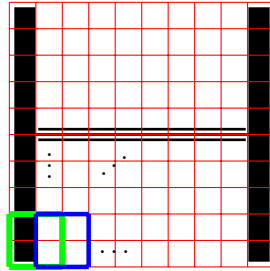


Figure 6.2.: Overlapping domain decomposition  $\omega_i$  (green and blue) constructed from  $2 \times 2$  patches of non-overlapping domain decomposition (red) for *Thermal Channels Variant*.

a variant of the *Thermal Channels Example* but driven by a right hand side instead of inhomogeneous boundary conditions. We define  $\Omega$  to be the unit square  $(0, 1)^2$ . We discretize the problem using P1 finite elements on a regular grid of  $200 \times 200$  squares, each divided into four triangles, resulting in 80,401 degrees of freedom. We use a coefficient field  $\sigma$  with high contrast ( $\sigma_{max}/\sigma_{min} = 10^5$ ) and high conductivity channels to get interesting behavior (see Figure 6.1). As domain decomposition  $\omega_i^{ol}$  we use domains of size  $0.2 \times 0.2$  with overlap 0.1, resulting in 81 subdomains (Figure 6.2). We use a partition of unity space decomposition as defined in Section 2.4.3 with a conforming partition of unity  $\varrho_i$  with  $\max_{i \in \{1, \dots, N_{V_i}\}} \|\nabla \varrho_i\|_{\infty}^2 = 2H^{-2} = 200$  and  $\max_{i \in \{1, \dots, N_{V_i}\}} \|\varrho_i\|_{\infty}^2 = 1$ . The resulting error decay is shown in Figures 6.3 to 6.5. To compare with the theory, we calculate an upper bound for  $c_{pu, \tilde{V}}$  using  $J = 4$ ,  $c_F = 1/(\sqrt{2}\pi)$ ,  $\sigma_{max}/\sigma_{min} = 10^5$ , and obtain  $c_{pu, \tilde{V}}^2 \leq 3.6013 \cdot 10^7$ . This results in an estimate of  $1 - c \geq 1.714 \cdot 10^{-10}$ . The rate of convergence observed in the experiment is several orders of magnitude better than the rate guaranteed by the a priori theory and is close to the optimal convergence rate (Figure 6.5).

To investigate the reason for this, we plot the quotient of the larger part and the smaller part of the estimates Equations (6.6) to (6.8) in Figure 6.6. It can be observed that the estimate Equation (6.6) is rather sharp, except when the error drops after a plateau. In estimate Equation (6.7), around one order of magnitude is lost. This could be improved by not enriching only one space but using a marking strategy instead. However, the main reason for the a priori theory to be so pessimistic seems to be the estimate in Equation (6.8).

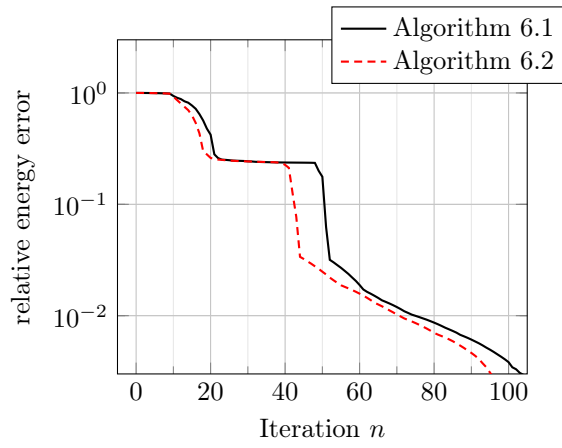


Figure 6.3.: Decay of relative energy error during iteration for *Thermal Channels Variant* (zoom). (reproduction: Appendix A.29)

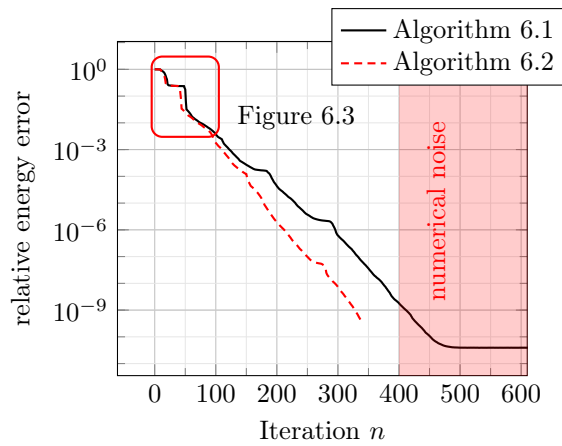


Figure 6.4.: Decay of relative energy error during iteration. (reproduction: Appendix A.29)

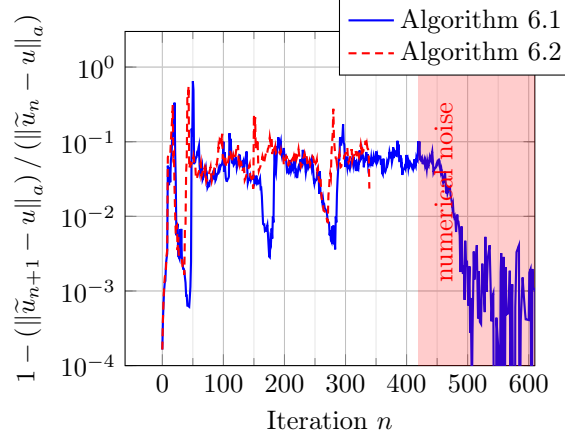


Figure 6.5.: Convergence of online enrichment in *Thermal Channels Variant*. 1 would be convergence within one iteration, 0 would be stagnation. (reproduction: Appendix A.29)

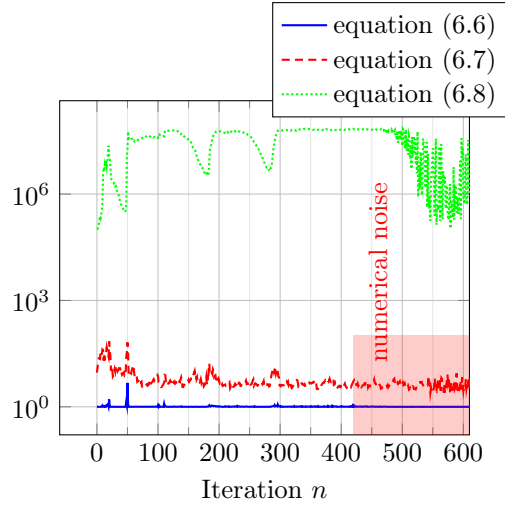


Figure 6.6.: Sharpness of inequalities in Algorithm 6.1: For equation (6.6),  $\left(\|\tilde{u}_n - u\|_a^2 - \|\mathcal{R}(\tilde{u}_n)\|_{\mathcal{O}'_k}^2\right) / \left(\|\tilde{u}_{n+1} - u\|_a^2\right)$  is plotted. For equation (6.7),  $\left(\|\mathcal{R}(\tilde{u}_n)\|_{V'_k}^2\right) / \left(\frac{1}{N_{V_i}} \sum_{i=1}^{N_{V_i}} \|\mathcal{R}(\tilde{u}_n)\|_{V'_i}^2\right)$  is plotted. For equation (6.8),  $\left(c_{\text{pu}, \tilde{V}}^2 \sum_{i=1}^{N_{V_i}} \|\mathcal{R}(\tilde{u}_n)\|_{V'_i}^2\right) / \left(\|\mathcal{R}(\tilde{u}_n)\|_{\tilde{V}'}^2\right)$  is plotted. (reproduction: Appendix A.29)

## 6.6. Discussion

In this chapter, exponential convergence of two enrichment algorithms has been shown. The second enrichment algorithm, the “globally coupled local enrichment” for which a form of optimality can be shown, is a new idea which was not published before, to the author’s knowledge. The results shown here are a first step. To be integrated with the ArbiLoMod, several improvements are necessary. First, the algorithms presented here only use one space decomposition. In the context of the ArbiLoMod, in the enrichment introduced in Section 3.4, we used two different space decompositions for their favorable properties in approximation and error estimation, respectively. Furthermore, an extension to parameterized problems is required, ideally combining the convergence rate with the Kolomogorov  $n$ -width of the localized solution manifolds.



---

### 6.7. Future Research in the Context of Localized Online Enrichment

---

- ***Numerical Experiment Exposing Training Breakdown***

We suspect that online enrichment is crucial for examples with many channels of which only few are used. It would be interesting to see this confirmed in a numerical experiment. A numerical example should be devised where training as described in Chapter 5 produces very large local bases and enrichment produces only few basis vectors.

- ***Introduce Basis Cleanup Step***

Online enrichment increases the basis size, possibly after a local geometry change. It could also happen that local basis vectors become superfluous. We think that localized reduced basis methods should comprise a “cleanup step”, where unnecessary basis functions are removed. Implementing and analyzing this would be an interesting project.

- ***Different Boundary Conditions***

The local problems in online enrichment are always formulated with Dirichlet boundary conditions in this thesis. Probably better results can be obtained using Robin-type boundary conditions or DtN operators.

- ***Parameterized Case***

The results in this chapter are only for the non parametric case. The online enrichment presented before in Section 3.4 was designed for the parametric case. It would be desirable if convergence results in the parametric case could be derived.



Localized model order reduction is a reliable simulation tool for problems with fine scale features but without scale separation. The favorable parallelization opportunities match current trends to cloud based computing. Possibilities for data reuse after localized geometry changes promise fast interactive simulations.

We have shown that local bases of reasonable size can be generated only local information at acceptable computational cost for the stationary heat conduction. For the wave equation, the same holds true as long as the wavelength is large in comparison to the local domain size. Results from randomized numerical linear algebra helped us building a solid theoretical foundation for randomized training algorithms. Both localized a posteriori error estimators as well as localized online enrichment algorithms have been derived and analyzed. However, for localized a posteriori error estimation for inf-sup stable problems, the question of how to quickly derive a lower bound for the inf-sup constant is still open.

Localized model order reduction is a field of active research, which seems to start maturing now. The main questions (as outlined in Section 1.3) and their answers are similar, regardless of whether it is GFEM, PR-SCRBE, GMsFEM, LRBMS, or ArbiLoMod. We hope that the community will find a common formulation and join forces to proceed faster in the future. Maybe the abstract localizing space decomposition and the abstract localized training configuration in this thesis serve as an inspiration.

The relation between domain decomposition methods and localized model order reduction still seems to be not completely understood. The training step in localized model order reduction seems to be related to the generation of a coarse space in domain decomposition methods and the online enrichment seems related to the iteration step in domain decomposition. Knowledge transfer could probably benefit both communities.

The largest future challenge on the way to a quick and reliable solver for electromagnetic fields inside of printed circuit boards, which was our initial motivating example, seems to be a stable localized reduction scheme for inf-sup stable problems, which is not available to date.

**Contributions**

New contributions of the thesis are the following.

- Application: The use of localized model order reduction for handling of arbitrary changes is proposed.
- Application: The singular value decay of a transfer operator defined in a PCB board was computed, suggesting good applicability of training based localized model order reduction.
- Formulation: An abstract definition of a localizing space decomposition is proposed, providing a common formulation for different localization strategies.
- Formulation: An abstract definition of a localized training configuration is proposed, providing a common framework for different training strategies. An a priori error bound is provided, formulated completely in the abstract setting.
- Space Decomposition: A definition of the wirebasket space decomposition is given which is valid in 2 and 3 dimensions for both Lagrange and Nédélec ansatz functions.
- Training: A randomized training algorithm with provable convergence rates is proposed.
- A posteriori error estimator: A localized, offline/online decomposable a posteriori error estimator with computable constants was proposed.
- A posteriori error estimator: A new strategy for offline/online decomposition of residual based error estimators in RB contexts was proposed, drastically reducing numerical noise.
- Online Enrichment: For the simplest case of online enrichment, exponential convergence was proven.
- Online Enrichment: The globally coupled online enrichment was proposed, which leads to optimal convergence of online enrichment for coercive problems.

---

## Reproduction of Results

---

For all results presented in this thesis, source code for reproduction is provided, which is published in [Buhr(2019)]. This chapter contains instructions to reproduce each figure in this thesis. The provided source code generates data files, which are used to generate the plots in this document. The plots are generated using pgfplots [Feuersänger(2011)]. The sources to generate the plots from the data files can be found in the L<sup>A</sup>T<sub>E</sub>X source of this thesis, which is provided with this thesis. The format of the data files is unspecified, the meaning of the columns can be inferred from the generating scripts.

Most examples require Python 2.7 and pyMOR 0.4. Some visualizations are generated using Mathematica<sup>®</sup> by Wolfram (Mathematica<sup>®</sup>). The code requires some libraries to be installed. It is advised to disable parallelization by setting the environment variable `OMP_NUM_THREADS` to “1”, as the automatic parallelization inside numpy and scipy often leads to increased execution time in the small localized problems.

The following sequence of commands leads to a working installation on Ubuntu 18.04 LTS:

```
$> sudo apt-get install python-pip python-virtualenv python-numpy \
python-scipy python-pyside cython python-matplotlib python-dev \
python git python-pil
$> export PATH_TO_VIRTUALENV=~/.virtualenv
$> virtualenv --system-site-packages $PATH_TO_VIRTUALENV
$> source $PATH_TO_VIRTUALENV/bin/activate
$> pip install --upgrade numpy scipy progress pyopengl ipython
$> pip install --upgrade git+https://github.com/pymor/pymor.git@0.4.x
$> pip install --upgrade \
git+https://github.com/sdrave/simdb.git@143d6b9f9f5b7bf55ab2bf\
56d3cb19166cc1abcb
$> export SIMDB_PATH=~/.simdb
```

### A.1. Reproduction of Figure 2.1

In the directory `code/nedelec_ansatz_function` execute the Mathematica<sup>®</sup> notebook `simplex_2d.nb`. The visualizations appear in the notebook.

### A.2. Reproduction of Figure 2.3

In the directory `code/thermalblock` run the file `full_solution.py`. A window will open showing the solution.

### A.3. Reproduction of Figure 2.5

In the directory `code/arbilomod` run the file `create_full_solutions.py`. The solution plots are created in “`sol1.png`” to “`sol5.png`”.

### A.4. Reproduction of Figure 2.7

In the directory `code/arbilomod_maxwell` run the file `maxwell_create_solutions.py`. The solution plots are created in `msol_0_1.png` to `msol_0_3.png` and `msol_1_1.png` to `msol_1_3.png`.

### A.5. Reproduction of Figure 3.5

In the directory `code/vertex_extension_plot` run the Mathematica<sup>®</sup> notebook `generate_vertex_extension_plots.nb`. The images will be exported as “png”-images in the directory of the notebook.

### A.6. Reproduction of Figure 3.8

In the directory `code/arbilomod` run the file `experiment_tolerances.py` and afterwards `postprocessing_tolerances.py`. The results are written to `errors_tolerances.txt`. The Mathematica<sup>®</sup> file `create_tolerances_plot.nb` generates the image from the txt file.

### A.7. Reproduction of Table 3.1, Figure 3.9, and Figure 3.10

In the directory `code/arbilomod` run the file `experiment_basisreuse.py` and the file `experiment_basisreuse_with_training.py`. Then run `postprocessing_basisreuse.py` and `postprocessing_basisreuse_with_training.py`. The data for Table 3.1 is printed to stdout. The data for Figure 3.9 is written to `basisreuse_training_with_reuse_0.dat` to `basisreuse_training_with_reuse_4.dat` and `basisreuse_training_without_reuse_0.dat` to `basisreuse_training_without_reuse_4.dat`. The data for Figure 3.10 is written to `basisreuse_with_reuse_0.dat` to `basisreuse_with_reuse_4.dat` and `basisreuse_without_reuse_0.dat` to `basisreuse_without_reuse_4.dat`.

### A.8. Reproduction of Figure 3.11

In the directory `code/arbilomod` run the file `experiment_estimatorperformance.py`. Then run `postprocessing_estimatorperformance.py`. The data is written to `estimatorperformance_0.dat` to `estimatorperformance_4.dat`.

### A.9. Reproduction of Table 3.2

Set the environment variable `OMP_NUM_THREADS` to 1 by executing `export OMP_NUM_THREADS=1` for single-thread performance measurement. It is not used by the provided scripts directly, but inside of `numpy` and/or `scipy`. Then, in the directory `code/arbilomod` run the file `experiment_create_timings.py`. Then run `postprocessing_create_timings.py`. The timings are written to stdout.

**A.10. Reproduction of Table 3.3**

In directory `code/arbilomod` run the file `experiment_H_study.py` and afterwards `postprocessing_H_study.py`. Results are written to `stdout`.

**A.11. Reproduction of Figure 3.12**

In directory `code/arbilomod` run the file `experiment_draw_basis_sizes.py` and afterwards `postprocessing_draw_basis_sizes.py`. The picture will be written to `basis_sizes.png`.

**A.12. Reproduction of Figure 3.13**

In directory `code/arbilomod_maxwell` run the file `maxwell_calculate_infsup.py`. The inf-sup constants are written to `infsups0.txt` for the first geometry and to `infsups1.txt` for the second geometry. The continuity constants are written to `continuities0.txt` for the first geometry and to `continuities1.txt` for the second geometry.

**A.13. Reproduction of Figure 3.14**

In directory `code/arbilomod_maxwell` run the file `maxwell_global_n_width.py`. The data for geometry 1 will be in `n_width0.txt` and the data for geometry 2 will be in `n_width1.txt`.

**A.14. Reproduction of Figure 3.16**

In directory `code/arbilomod_maxwell` run the file `maxwell_local_n_width.py`. The data for geometry 1 will be in `localized0.txt` and the data for geometry 2 will be in `localized1.txt`.

**A.15. Reproduction of Figure 3.17**

In directory `code/arbilomod_maxwell` run the file `maxwell_infsup_during_reduction.py`. The inf-sup constants are written to `infsup_constant_0.txt` and `infsup_constant_1.txt`. The convergence graph on the left is in `localized0.txt`, generated by `maxwell_local_n_width.py`, see above.

**A.16. Reproduction of Figure 3.18**

In directory `code/arbilomod_maxwell` run the file `maxwell_training_benchmark.py`. The errors will be in `maxwell_training_benchmark0.txt` and `maxwell_training_benchmark1.txt`. The data for global solves is in `localized0.txt` and `localized1.txt`, generated by `maxwell_local_n_width.py`, see above.

**A.17. Reproduction of Figure 3.20**

In directory `code/arbilomod_maxwell` run the file `experiment_maxwell_geochange.py` and afterwards `postprocessing_draw_basis_sizes_maxwell_geochange.py`. The images are written to `basis_sizes_maxwell_0.png` and `basis_sizes_maxwell_1.png`.

**A.18. Reproduction of Figure 4.1**

In directory `code/thermalblock` run the file `run_thermalblock.sh`. The results will be in `traditional.txt` for bases generated with the *traditional offline/online splitting* and in `residual_basis.txt` for bases generated with the *improved offline/online splitting*.

**A.19. Reproduction of Figure 5.2**

In directory `code/rangefindertest/example1` run `experiment_twosquares_images.py`. Results will be in `modes.dat` and `omodes.dat`. If you encounter errors related to `umfpack`, uninstall `scikit-umfpack` (`pip uninstall scikit-umfpack`) as its python bindings are buggy at the time of writing.

**A.20. Reproduction of Figure 5.3**

In directory `code/rangefindertest/example1`, run the four files `experiment_twosquares_svddecay.py`, `experiment_twosquares_algo_convergence.py`, `postprocessing_twosquares_operator_norm_decay.py`, and `postprocessing_twosquares_a_priori_comparison.py` (in that order).

Results for Figure (a) will be in `twosquares_percentiles.dat`. Results for Figure (b) will be in `twosquares_means.dat` and `twosquares_expectation.dat`.

**A.21. Reproduction of Table 5.1**

Set the environment variable `OMP_NUM_THREADS` to 1 by executing `export OMP_NUM_THREADS=1` for single-thread performance measurement. In directory `code/rangefindertest/cpu_times` run file `measure_cpu_times.py`. Results will be on `stdout`.

**A.22. Reproduction of Figure 5.4**

In directory `code/rangefindertest/example1`, run files `experiment_twosquares_svddecay.py` and `experiment_twosquares_algo_convergence.py`.

To reproduce (a), run `postprocessing_twosquares_adaptive_convergence.py`, results will be in `twosquares_adaptive_convergence.dat`.

To reproduce (b), run `postprocessing_twosquares_adaptive_num_testvecs.py`, results will be in `twosquares_adaptive_num_testvecs.dat`.

**A.23. Reproduction of Figure 5.5**

In directory `code/rangefindertest/example1`, run files `experiment_h_svddecay.py`, `experiment_h_algo_convergence.py`, and `postprocessing_h.py`. Results will be in `experiment_h_deviation.dat` and `experiment_h_testvecs.dat`.

**A.24. Reproduction of Figure 5.6**

In directory `code/rangefindertest/example2`, run `helmholtz.py`. Results will be in `helmholtz_selected.dat` (for left figure) and `helmholtz_3d.dat` (for right figure).

**A.25. Reproduction of Figure 5.7**

In directory `code/rangefindertest/example2`, run `helmholtz.py`. Then run `postprocessing_helmholtz_operator_norm_decay.py`. Result for left figure will be in `helmholtz_percentiles.dat`. Then run `postprocessing_helmholtz_a_priori_comparison.py` and



`postprocessing_helmholtz_operatornorm_decay.py`. Results for right figure will be in `helmholtz_expectation.dat` and `helmholtz_means.dat`.

### A.26. Reproduction of Figure 5.8

In directory `code/rangefindertest/example2`, run `helmholtz.py`. Then run `postprocessing_helmholtz_adaptive_convergence.py`. Result for left figure will be in `helmholtz_adaptive_convergence.dat`. Then run `postprocessing_helmholtz_adaptive_num_testvecs.py`. Result for right figure will be in `helmholtz_adaptive_num_testvecs.dat`.

### A.27. Reproduction of Figures 5.11 and 5.12

The Olimex A64 board design is a KiCad project file. We provide the project file used here at [Olimex(2019)]. The code to generate the transfer operators is developed in a fork of KiCad. KiCad's unit test mechanism was used to set this up. The complete KiCad source code with the changes to compute the transfer operators can be found in `code/kicad`.

To build it, you need a C++ development environment. On a Ubuntu 18.04 LTS the following command leads to a working environment:

```
$> sudo apt-get install build-essential cmake libwxgtk3.0-gtk3-dev \
    libglew-dev libglm-dev libcairo2-dev libboost1.65-all-dev swig \
    python-wxgtk3.0 libssl-dev libsuitesparse-dev libcurl4-openssl-dev
```

To build it, create a build directory. Inside of the build directory, execute `cmake -DCMAKE_BUILD_TYPE=Release -DKICAD_SPICE=OFF -DBUILD_GITHUB_PLUGIN=OFF \ -DKICAD_USE_OCE=OFF path/to/code/kicad`.

Enter the subdirectory `qa/polygon_generator` and run `make`. After successful build, save the file `A64-OlinuXino_Rev_D.kicad_pcb` from [Olimex(2019)] and the file `kicad.ini` from the `code/kicad/qa/polygon_generator` in the current directory and execute `test_polygon_generator`.

The script will compute the transfer operators for 40 domains and run the adaptive range finder algorithm on all of these. The timings for Figure 5.12 are written to `timings.dat`.

Additionally, the script will output matrices in `sysmat_816.mtx` and `rsmat_816.mtx` from which the transfer operator can be computed. Install `umfpack` for python in a setup as specified above by using the command `pipinstall--upgradescikit-umfpack`. Copy the file `apply_arpack.py` from `code/kicad/qa/polygon_generator` to the local directory and execute it. The singular values for the transfer operator visible in Figure 5.11 will be written to `svals_816.dat` and the maximum testvector values will be written to `maxnorms_2norm_816.dat`.

### A.28. Reproduction of Figure 6.1

In directory `code/enrichment`, run `create_full_solution.py`. The result is written to `solution.png`.

### A.29. Reproduction of Figures 6.3 to 6.6

In directory `code/enrichment`, run the following four files: `experiment_residual_based.py`, `experiment_globally_coupled.py`,

`postprocessing_residual_based.py`, `postprocessing_globally_coupled.py`. The data is written to data files: `errors.dat` will contain relative energy-, h1- and l2-errors for residual based enrichment, `convergence.dat` will contain data for Figure 6.5 for residual based enrichment, `ineq.dat` will contain data for Figure 6.6, `errors_g_c.dat` will contain relative energy errors for globally coupled enrichment, `convergence_g_c.dat` will contain data for Figure 6.5 for globally coupled enrichment.

**A.30. Reproduction of Figure C.1, Figure C.2, and Figure C.3**

In the directory `code/gram_schmidt` run the file `experiment.py`. For each algorithm, a file is created: `Schmidt-GS.dat`, `Gram-GS.dat`, `ReIt-GS_2.dat`, `ReIt-GS_3.dat`, `AReIt-GS.dat`. Each contains the orthogonality error in the first column and the reproduction error in the second column. In addition, the file `iterations.dat` is created, containing the median number of iterations for each vector.

**A.31. Reproduction of Table D.1**

To regenerate the timings for the proposed code, run the tests in `code/high_performance_assembly` using Valgrind/Callgrind. One output file is written for each evaluation of the functions.

To regenerate the timings for the dune code, add the files in `code/high_performance_assembly/dune` in a dune module, compile them and run them with Valgrind/Callgrind. One output file is written for each evaluation. Note that the first two evaluations show higher instruction counts because of initializations. The tests were performed with dune 2.6 and dune-pdelab 2.0.

---

A Posteriori Error Estimation for Relative Errors

---

**B.1. Introduction**

In the context of model order reduction, it is often the case that an a posteriori error estimator for the absolute error is available, but an estimator for the relative error is required. It is possible to derive an upper bound for the relative error based on the error estimator for the absolute error and the norm of the reduced solution. Most introductory texts to reduced basis methods state one, which we will call the classic relative error estimator in the following. This approach is widely used in the model order reduction community. In our manuscript introducing ArbiLoMod, we used a different approach [Buhr et al.(2017a), Proposition 5.10]. This approach can also be found in [Hess(2016), Lemma 3.2.2]. In this section, we compare these two approaches and conclude that the new approach is better than the classic approach in almost every aspect. This is not a new result, it is known to experts in the field. However, to our knowledge, this is the first comprehensive comparison of the two approaches.

**B.2. Two relative error estimators***B.2.1. Setting*

We assume a full model with solution  $u$  and a reduced model with solution  $\tilde{u}$  are given and furthermore, an efficient a posteriori error estimator  $\Delta(\tilde{u})$  satisfying

$$\|u - \tilde{u}\| \leq \Delta(\tilde{u}) \leq \eta \|u - \tilde{u}\| \quad (\text{B.1})$$

with efficiency constant  $\eta$  is available. Based on that, an efficient relative a posteriori error estimator  $\Delta_{\text{rel}}(\tilde{u})$  should be derived satisfying

$$\frac{\|u - \tilde{u}\|}{\|u\|} \leq \Delta_{\text{rel}}(\tilde{u}) \leq \eta_{\text{rel}} \frac{\|u - \tilde{u}\|}{\|u\|} \quad (\text{B.2})$$

with efficiency constant  $\eta_{\text{rel}}$ . It should not require the norm of the solution  $\|u\|$ , as this is usually not available in the context of a posteriori error estimation.

**B.3. Definition of Relative a Posteriori Error Estimators**

In this subsection, two relative a posteriori error estimators are defined. The first one is the classic one, which can be found in many introductory texts on reduced basis methods, for example

in [Patera and Rozza(2007), Proposition 4D], in [Haasdonk(2017), Proposition 2.27] or [Hesthaven et al.(2016), Proposition 4.4].

**Definition B.3.1** (Classic relative a posteriori error estimator). *Given a solution  $u$  and a reduced solution  $\tilde{u}$  and an a posteriori error estimator  $\Delta(\tilde{u})$ , the classic relative a posteriori error estimator is defined by*

$$\Delta_{\text{rel}}^c(\tilde{u}) := 2 \frac{\Delta(\tilde{u})}{\|\tilde{u}\|}. \quad (\text{B.3})$$

The second approach is the “new” relative a posteriori error estimator, which was used by the authors in [Buhr et al.(2017a), Proposition 5.10] but can also be found in other publications, for example [Hess(2016), Lemma 3.2.2].

**Definition B.3.2** (New relative a posteriori error estimator). *Given a solution  $u$  and a reduced solution  $\tilde{u}$  and an a posteriori error estimator  $\Delta(\tilde{u})$ , the new relative a posteriori error estimator is defined by*

$$\Delta_{\text{rel}}^{\text{new}}(\tilde{u}) := \frac{\Delta(\tilde{u})}{\|\tilde{u}\| - \Delta(\tilde{u})}. \quad (\text{B.4})$$

These two approaches will be analyzed in the following sections.

**Remark B.3.3** (Dividing by reduced error norm). *Sometimes, the quantity  $\frac{\Delta(\tilde{u})}{\|\tilde{u}\|}$  is used to analyze the relative error, for example in [Quarteroni et al.(2016), Section 9.1]. While this is a very good approximation of the relative error when  $\Delta(\tilde{u}) \ll \|\tilde{u}\|$ , it is not an upper bound to the relative error  $\|u - \tilde{u}\|/\|u\|$ .*

#### B.4. Rigorosity and Effectivity of Relative a Posteriori Error Estimators

Assuming that the underlying absolute a posteriori error estimator is rigorous and efficient with efficiency constant  $\eta$ , i.e. assuming that

$$\|u - \tilde{u}\| \leq \Delta(\tilde{u}) \leq \eta \|u - \tilde{u}\|, \quad (\text{B.5})$$

we show that the two relative a posteriori error estimators are in turn rigorous and efficient for the relative error. These results can also be found in the references cited above. The following proposition is for the classic approach.

**Proposition B.4.1** (Classic relative a posteriori error estimator). *If  $\Delta(\tilde{u}) \leq \frac{1}{2}\|\tilde{u}\|$ , it holds that*

$$\frac{\|u - \tilde{u}\|}{\|u\|} \leq \Delta_{\text{rel}}^c(\tilde{u}) \leq \eta_{\text{rel}}^c \frac{\|u - \tilde{u}\|}{\|u\|} \quad (\text{B.6})$$

with  $\eta_{\text{rel}}^c := 3\eta$ .

*Proof.* First, we realize that  $\|\tilde{u}\| \leq 2\|u\|$  because

$$\|u\| = \|u - \tilde{u} + \tilde{u}\| \geq \|\tilde{u}\| - \|u - \tilde{u}\| \geq \|\tilde{u}\| - \Delta(\tilde{u}) \geq \|\tilde{u}\| - \frac{1}{2}\|\tilde{u}\| = \frac{1}{2}\|\tilde{u}\|. \quad (\text{B.7})$$

Using this, the first inequality of the proposition follows by

$$\frac{\|u - \tilde{u}\|}{\|u\|} \leq \frac{\Delta(\tilde{u})}{\|u\|} = \frac{\Delta(\tilde{u})}{\|\tilde{u}\|} \frac{\|\tilde{u}\|}{\|u\|} \leq 2 \frac{\Delta(\tilde{u})}{\|\tilde{u}\|} = \Delta_{\text{rel}}^c(\tilde{u}). \quad (\text{B.8})$$

For the second inequality, we first realize that  $\|u\| \leq \frac{3}{2}\|\tilde{u}\|$ , because

$$\|u\| = \|u - \tilde{u} + \tilde{u}\| \leq \|u - \tilde{u}\| + \|\tilde{u}\| \leq \Delta(\tilde{u}) + \|\tilde{u}\| \leq \frac{1}{2}\|\tilde{u}\| + \|\tilde{u}\| = \frac{3}{2}\|\tilde{u}\| \quad (\text{B.9})$$

and use this to show

$$\Delta_{\text{rel}}^c(\tilde{u}) = \frac{2\Delta(\tilde{u})}{\|\tilde{u}\|} \leq \frac{2\eta\|u - \tilde{u}\|}{\|\tilde{u}\|} \leq \frac{2\eta\|u - \tilde{u}\|}{\frac{2}{3}\|u\|} = 3\eta \frac{\|u - \tilde{u}\|}{\|u\|}. \quad (\text{B.10})$$

□

For the new relative a posteriori error estimator, a very similar result can be obtained, which is given in the following proposition.

**Proposition B.4.2** (New relative a posteriori error estimator). *If  $\Delta(\tilde{u}) < \|\tilde{u}\|$ , it holds that*

$$\frac{\|u - \tilde{u}\|}{\|u\|} \leq \Delta_{\text{rel}}^{\text{new}}(\tilde{u}) \leq \eta_{\text{rel}}^{\text{new}} \frac{\|u - \tilde{u}\|}{\|u\|} \quad (\text{B.11})$$

with  $\eta_{\text{rel}}^{\text{new}} := (1 + 2\Delta_{\text{rel}}^{\text{new}}(\tilde{u}))\eta$ .

*Proof.* Realizing that  $(\|\tilde{u}\| - \Delta(\tilde{u})) \leq \|u\|$ , it is easy to see that

$$\frac{\|u - \tilde{u}\|}{\|u\|} \leq \frac{\Delta(\tilde{u})}{\|u\|} \leq \frac{\Delta(\tilde{u})}{\|\tilde{u}\| - \Delta(\tilde{u})}, \quad (\text{B.12})$$

which is the first inequality. Using

$$\frac{\|\tilde{u}\| + \Delta(\tilde{u})}{\|\tilde{u}\| - \Delta(\tilde{u})} = 1 + 2\Delta_{\text{rel}}^{\text{new}}(\tilde{u}) \quad (\text{B.13})$$

the second inequality can be shown:

$$\Delta_{\text{rel}}^{\text{new}}(\tilde{u}) = \frac{\Delta(\tilde{u})}{\|\tilde{u}\| - \Delta(\tilde{u})} \leq \eta \frac{\|u - \tilde{u}\|}{\|\tilde{u}\| - \Delta(\tilde{u})} \quad (\text{B.14})$$

$$= \eta \frac{\|u - \tilde{u}\|}{\|\tilde{u}\| + \Delta(\tilde{u})} (1 + 2\Delta_{\text{rel}}^{\text{new}}(\tilde{u})) \quad (\text{B.15})$$

$$\leq \eta \frac{\|u - \tilde{u}\|}{\|u\|} (1 + 2\Delta_{\text{rel}}^{\text{new}}(\tilde{u})). \quad (\text{B.16})$$

□

## B.5. Comparison of Relative A Posteriori Error Estimators

In the following, we argue that the new relative a posteriori error estimator is better than the classic one in almost every regard.

### B.5.1. Comparison of Range of Validity

The classic relative a posteriori error estimator is valid if  $\Delta(\tilde{u}) \leq \frac{1}{2}\|\tilde{u}\|$ . The new approach is valid if  $\Delta(\tilde{u}) < \|\tilde{u}\|$ . So the range of validity for the new estimator is larger than and completely contains the range of validity of the classic relative a posteriori error estimator.

## B.5.2. Comparison of Sharpness

**Proposition B.5.1** (Sharpness of relative a posteriori error estimators). *Whenever both relative a posteriori error estimators are defined, i.e. when  $\Delta(\tilde{u}) \leq \frac{1}{2}\|\tilde{u}\|$ , the new relative a posteriori error estimator is not worse than the classic one, in mathematical terms:*

$$\Delta(\tilde{u}) \leq \frac{1}{2}\|\tilde{u}\| \quad \Rightarrow \quad \Delta_{\text{rel}}^{\text{new}}(\tilde{u}) \leq \Delta_{\text{rel}}^{\text{c}}(\tilde{u}). \quad (\text{B.17})$$

*Proof.* This can be shown by the following simple computation.

$$\Delta(\tilde{u}) \leq \frac{1}{2}\|\tilde{u}\| \quad (\text{B.18})$$

$$\Rightarrow \quad \frac{1}{2}\|\tilde{u}\| \leq \|\tilde{u}\| - \Delta(\tilde{u}) \quad (\text{B.19})$$

$$\Rightarrow \quad \frac{2}{\|\tilde{u}\|} \geq \frac{1}{\|\tilde{u}\| - \Delta(\tilde{u})} \quad (\text{B.20})$$

$$\Rightarrow \quad \frac{2\Delta(\tilde{u})}{\|\tilde{u}\|} \geq \frac{\Delta(\tilde{u})}{\|\tilde{u}\| - \Delta(\tilde{u})} \quad (\text{B.21})$$

$$\Rightarrow \quad \Delta_{\text{rel}}^{\text{c}}(\tilde{u}) \geq \Delta_{\text{rel}}^{\text{new}}(\tilde{u}) \quad (\text{B.22})$$

We can always invert in Equation (B.19) as  $\|\tilde{u}\| - \Delta(\tilde{u})$  is positive.  $\square$

## B.5.3. Comparison of Efficiency

**Proposition B.5.2** (Efficiency constant of relative a posteriori error estimators). *Whenever both relative a posteriori error estimators are defined, i.e. when  $\Delta(\tilde{u}) \leq \frac{1}{2}\|\tilde{u}\|$ , the new relative a posteriori error estimator has a better efficiency constant than the classic one, in mathematical terms:*

$$\Delta(\tilde{u}) \leq \frac{1}{2}\|\tilde{u}\| \quad \Rightarrow \quad \eta_{\text{rel}}^{\text{new}} \leq \eta_{\text{rel}}^{\text{c}}. \quad (\text{B.23})$$

*Proof.* This can be shown by the following simple computation.

$$\Delta(\tilde{u}) \leq \frac{1}{2}\|\tilde{u}\| \quad (\text{B.24})$$

$$\Rightarrow \quad \Delta(\tilde{u}) \leq \|\tilde{u}\| - \Delta(\tilde{u}) \quad (\text{B.25})$$

$$\Rightarrow \quad \frac{\Delta(\tilde{u})}{\|\tilde{u}\| - \Delta(\tilde{u})} \leq 1 \quad (\text{B.26})$$

$$\Rightarrow \quad \Delta_{\text{rel}}^{\text{new}} \leq 1 \quad (\text{B.27})$$

$$\Rightarrow \quad (1 + 2\Delta_{\text{rel}}^{\text{new}})\eta \leq 3\eta \quad (\text{B.28})$$

$$\Rightarrow \quad \eta_{\text{rel}}^{\text{new}} \leq \eta_{\text{rel}}^{\text{c}} \quad (\text{B.29})$$

We can always divide by  $\|\tilde{u}\| - \Delta(\tilde{u})$  in Equation (B.25) as this term is positive.  $\square$

## B.6. Conclusion on Relative A Posteriori Error Estimators

The approach to construct an a posteriori error estimator for the relative error presented above and named the “new” approach is in almost every regard better than the “classic” approach. It has a wider range of validity, gives tighter error bounds and has a better efficiency constant. However, it might be more convenient to use the classic approach in some cases, for example when analyzing rates of convergence.

---

## Numerically Stable Gram-Schmidt Algorithm

---

### C.1. Introduction

The Gram-Schmidt algorithm is a widely used orthonormalization procedure. It exists in different variants, four of which we present in the following. Some of them, which are widely used in numerical codes today, suffer from numerical instabilities when the input vectors are almost linear dependent. In our publication on numerically stable a posteriori estimation, we also published a numerically more stable variant of the Gram-Schmidt algorithm [Buhr et al.(2014), Algorithm 1]. In this chapter, we compare the different variants of the Gram-Schmidt algorithm and compare their performance in numerical experiments.

### C.2. Algorithms

In this section, we present four variants of the Gram-Schmidt algorithm. All of them are mathematically equivalent and would yield the same results if executed in exact arithmetic. Erhard Schmidt published his algorithm in 1907 [Schmidt(1907), p.442]. It is a one pass algorithm. For each vector, first, all inner products with the already orthonormal vectors are computed. Then, the projections on the already orthonormal vectors is subtracted. We present Schmidt's variant in Algorithm C.1 on page 120. Jørgen Pedersen Gram published his algorithm already 1883 [Gram(1883)]. Gram's algorithm is usually called "Modified Gram-Schmidt" (MGS) in today's literature. It is also a one pass algorithm. In contrast to Schmidt's variant, the calculation of the inner products with the already orthonormal vectors and the subtraction of the projections are interleaved. This can lead to smaller numerical errors. However, there is still the problem that later orthogonalization steps can break the orthogonality achieved in earlier steps. We present Gram's variant in Algorithm C.2 on page 120. These numerical instabilities are often addressed by executing the Gram-variant multiple times, usually two times. We give the (Modified) Gram-Schmidt algorithm with re-iteration in Algorithm C.3 on page 122. However, we observed in numerical experiments that two iterations are usually sufficient, but not always. Always executing three or more iterations would be a waste of computational resources. We further observed that numerical accuracy is lost when the norm of the vector under consideration shrinks. This led us to devise the Gram-Schmidt algorithm with adaptive re-iteration, which iterates until the norm of the vector under consideration does not shrink any more. This new algorithm is given in Algorithm C.4 on page 122. We reiterate, if the norm of the vector under consideration has decreased by more than a factor of 0.1. This factor can

---

**Algorithm C.1:** Erhard Schmidt's variant of Gram-Schmidt algorithm.

---

**Input:** vectors  $\varphi_i$ ,  $i \in 1, \dots, N$   
**Output:** orthonormal vectors  $\psi_i$

```

1 for  $i \leftarrow 1, \dots, N$  do
2    $\psi_i \leftarrow \varphi_i - \sum_{j=1}^{i-1} (\psi_i, \varphi_j) \psi_j$ ;
3    $\psi_i \leftarrow \psi_i / \|\psi_i\|$ ;
4 end
```

---



---

**Algorithm C.2:** Jørgen Pedersen Gram's variant of Gram-Schmidt algorithm.

---

**Input:** vectors  $v_i$ ,  $i \in 1, \dots, N$   
**Output:** orthonormal vectors  $v_i$

```

1 for  $i \leftarrow 1, \dots, N$  do
2   for  $j \leftarrow 1, \dots, (i-1)$  do
3      $v_i \leftarrow v_i - (v_j, v_i) v_j$ ;
4   end
5    $v_i \leftarrow v_i / \|v_i\|$ ;
6 end
```

---

be tuned: Setting it close to one (e.g. 0.99) leads to high numerical accuracy with more iterations. A smaller factor (e.g. 0.01) leads to less numerical accuracy and less iterations.

### C.3. Numerical Comparison

We perform a numerical comparison of the four algorithms in  $\mathbb{C}^{10000}$  with the inner product defined by  $(u, v) := u^H v$ . To numerically test the four algorithms, we follow a four step procedure. In a first step, we randomly generate an orthonormal set of  $N$  vectors which we denote by  $\varphi_i$ ,  $i \in 1, \dots, N$  with  $(\varphi_i, \varphi_j) = \delta_{ij}$ . In a second step, we form almost linear dependent test vectors using the definition

$$t_i := \sum_{j=1}^i \left(\frac{1}{2}\right)^j \varphi_j. \quad (\text{C.1})$$

These vectors are linear independent in exact arithmetic, but numerical effects render them linear dependent. In a third step, we hand these vectors to one of the Gram-Schmidt algorithms and denote its result by  $\psi_i$ . In exact arithmetic, the vectors  $\psi_i$  are identical to  $\varphi_i$ . In a fourth step, we quantify the errors. To do so, we calculate two quantities. The first is the orthonormality error, judging whether the resulting vectors are orthonormal. We define it as

$$e_{1,i} := \max_{j \in 1, \dots, (i-1)} |(\psi_i, \psi_j)|. \quad (\text{C.2})$$

The second is the reproduction error. It quantifies whether the original vectors are recovered by the algorithm. We define it as

$$e_{2,i} := \|\varphi_i - \psi_i\|. \quad (\text{C.3})$$

Because we are interested in worst-case behavior, we run each test 200 times and report the worst result.

We can see in the results that re-iteration is crucial for good numerical performance. The orthogonality error, plotted in Figure C.1 stays at very low levels for all re-iterated versions, while it grows exponentially for the two traditional variants. Gram's version of the algorithm (the "MGS") performs slightly better than Schmidt's version. The reproduction error grows exponentially for all variants. That is due to the construction of the testvectors. The way they are constructed loses



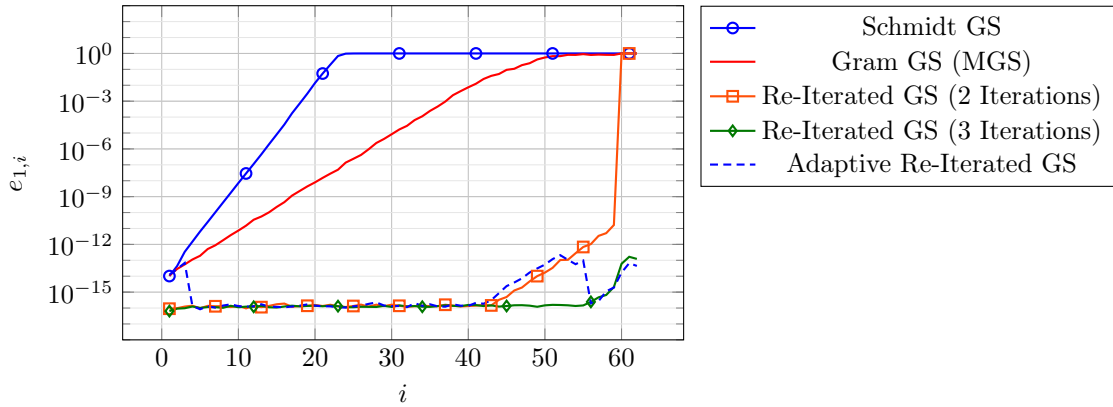


Figure C.1.: Orthogonality Error of Gram-Schmidt algorithms. (reproduction: Appendix A.30)

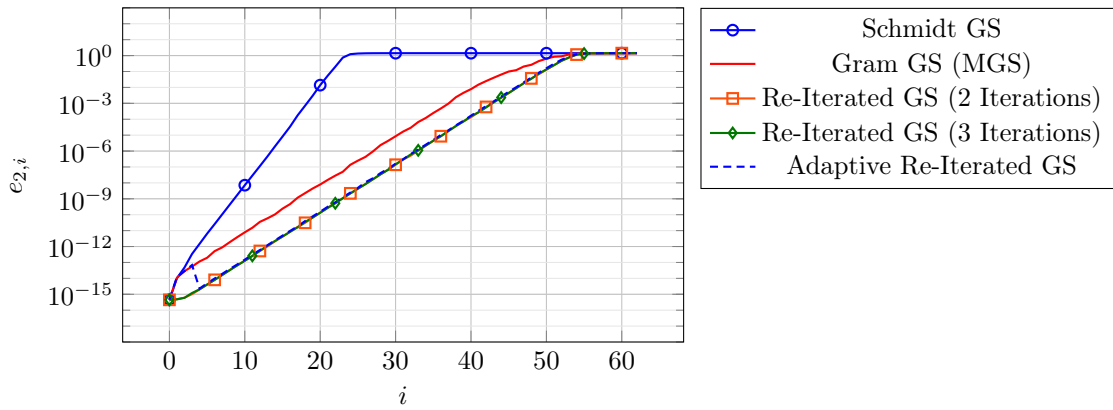


Figure C.2.: Reproduction Error of Gram-Schmidt algorithms. (reproduction: Appendix A.30)

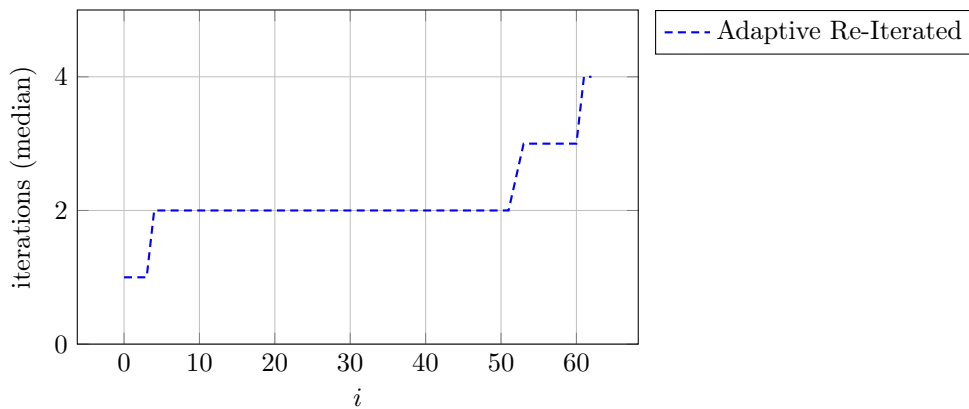


Figure C.3.: Median of Iterations in Adaptive Re-Iterated Gram-Schmidt (reproduction: Appendix A.30)

**Algorithm C.3:** Gram-Schmidt with re-iteration.

---

**Input:** vectors  $v_i, i \in 1, \dots, N$   
 $n_r$ : number of iterations  
**Output:** orthonormal vectors  $v_i$

```

1 for  $i \leftarrow 1, \dots, N$  do
2   for  $r \leftarrow 1, \dots, n_r$  do
3     for  $j \leftarrow 1, \dots, (i-1)$  do
4        $v_i \leftarrow v_i - (v_j, v_i) v_j$ ;
5     end
6   end
7    $v_i \leftarrow v_i / \|v_i\|$ ;
8 end
```

---

**Algorithm C.4:** Gram-Schmidt with adaptive re-iteration.

---

**Input:** vectors  $v_i, i \in 1, \dots, N$   
**Output:** orthonormal vectors  $v_i$

```

1 for  $i \leftarrow 1, \dots, N$  do
2    $v_i \leftarrow v_i / \|v_i\|$ ;
3   repeat
4     for  $j \leftarrow 1, \dots, (i-1)$  do
5        $v_i \leftarrow v_i - (v_j, v_i) v_j$ ;
6     end
7     newnorm  $\leftarrow \|v_i\|$ ;
8      $v_i \leftarrow v_i / \text{newnorm}$ ;
9   until newnorm  $> 0.1$ ;
10 end
```

---

information about the later vectors. This lost information can not be recovered by the Gram-Schmidt algorithm. All re-iterated variants have a reproduction error which is indistinguishable from the optimal error, see Figure C.2. The two traditional variants perform worse and again, Gram's version performs better than Schmidt's version. The adaptive variant yields results as good as the re-iterated algorithm with fixed number of iterations. The median of the number of iterations performed by the adaptive variant is shown in Figure C.3.

**C.4. Summary**

The Gram-Schmidt algorithm in the form it was published by Gram and Schmidt suffers from numerical instability when applied to nearly linear dependent vectors. This problem can be mitigated by re-iteration, effectively executing the algorithm several times. In most cases, two iterations are sufficient. Adaptive re-iteration has two advantages. In comparison to a fixed number of two iterations, it saves computational resources when re-iteration is not necessary. This might happen for example when the input vectors are already nearly orthogonal. Second, it assures a low numerical error on nearly linear dependent input vectors by re-iterating as necessary.

---

High Performance Nédélec Assembly

---

At the core of each FE software is an assembly routine computing local integrals on mesh elements. Usually these integrals are computed by a quadrature summation procedure. We followed a different path and implemented functions to compute the local integrals based on automatic symbolic computations and code generation for lowest order Nédélec ansatz functions. The results are presented in the following. We list these results here for completeness. There have been multiple publications considering fast FE assembly recently, see e.g. [Melenk et al.(2001), Ølgaard and Wells(2010), Bastian et al.(2016)].

**D.1. Problem Setting**

In FE assembly, the core routine has to compute the terms occurring in the bilinear form on each mesh element  $K$ , for all combinations of ansatz functions  $\psi$  which have support on that element. For lowest order Nédélec ansatz functions (Section 2.6.5) and the bilinear form defined in Equation (2.58), it is the two integrals

$$I_{1,ij} := \int_K \psi_i \psi_j \, dx \quad (\text{D.1})$$

$$I_{2,ij} := \int_K (\nabla \times \psi_i) \cdot (\nabla \times \psi_j) \, dx. \quad (\text{D.2})$$

In order to implement a fast evaluation of these integrals, we interpret the evaluation of these integrals as functions. In two dimensions, a triangle is defined by the coordinates of its corners, which can be interpreted as an element of  $\mathbb{R}^6$ . The resulting matrices are  $3 \times 3$  matrices, as three basis functions have support on each triangle. We define the two assembly functions

$$\text{ASSEMBLY2DIDID} : \quad \mathbb{R}^6 \rightarrow \mathbb{R}^{3 \times 3} \quad (\text{D.3})$$

$$\text{ASSEMBLY2DCURLCURL} : \quad \mathbb{R}^6 \rightarrow \mathbb{R}^{3 \times 3} \quad (\text{D.4})$$

mapping from the coordinates of the corners of the triangle to the matrices containing the evaluated integrals, where ASSEMBLY2DIDID corresponds to Equation (D.1) and ASSEMBLY2DCURLCURL corresponds to Equation (D.2). In three dimensions, a tetrahedron is defined by the three coordinates of its four corners, and there are six ansatz functions having

Operator	dune-pdelab	proposed	factor
IDID 3D	11 003	770	14.3
CURLCURL 3D	11 260	454	24.8
IDID 2D	4 336	139	31.2
CURLCURL 2D	1 704	41	41.6

Table D.1.: Number of instructions for one local matrix evaluation (Valgrind measurement). (reproduction: Appendix A.31)

support on each tetrahedron. We define accordingly

$$\text{ASSEMBLY3DIDID} : \quad \mathbb{R}^{12} \rightarrow \mathbb{R}^{6 \times 6} \quad (\text{D.5})$$

$$\text{ASSEMBLY3DCURLCURL} : \quad \mathbb{R}^{12} \rightarrow \mathbb{R}^{6 \times 6}. \quad (\text{D.6})$$

The usual procedure to evaluate these functions is to use a mapping to a reference element and a quadrature formula on the reference element. The integrand is then evaluated at each quadrature point, the evaluated values are added using quadrature weights. We accelerated this procedure using automatic symbolic computation and code generation. The software package Mathematica<sup>®</sup> can evaluate the integrals with the corner coordinates as symbolic parameters. The resulting formulas can easily be transformed to C++ code. Also a completely automatic code generation would be possible, but yielded slightly inferior results.

## D.2. Source Code

The Mathematica<sup>®</sup> code to generate the assembly routines can be found in the directory `code/high_performance_assembly/`. In the file `simplex_2d.nb`, the analytic expressions for triangles for both integrals in question are computed. In the file `simplex_3d.nb`, the analytic expressions for tetrahedra for both integrals are computed. Note that only one entry of the element matrix is computed. The entry can be chosen in the Mathematica<sup>®</sup> file. From Mathematica<sup>®</sup>'s output, the assembly routines in the files `simplex_2d_curlcurl.hh`, `simplex_2d_idid.hh`, `simplex_3d_curlcurl.hh`, and `simplex_3d_idid.hh` are created, containing the local assembly. The code is templated, making it suitable for both assembly using the `double` data type or a high precision data type. As an example, the two dimensional curlcurl assembly is shown in Listing D.1.

## D.3. Quality Control

To check the correctness of the assembly functions, a Mathematica<sup>®</sup> file was written which computes the local integrals on a set of random elements and generates C++ code with the reference results. All numbers are written as strings in predefined accuracy. The four files `simplex_(2|3)d_(idid|curlcurl)_testcases.nb` generate the four header files `simplex_(2|3)d_(idid|curlcurl)_testcases.hh`, containing the test cases. The Mathematica<sup>®</sup> notebooks require the notebooks `simplex_2d.nb` or `simplex_3d.nb` to be executed before. Based on these files, the results are compared with reference results generated by Mathematica<sup>®</sup>.

## D.4. Performance Measurement

We evaluated the performance of the generated routines by executing them in Valgrind [Nethercote and Seward(2007)] / Callgrind. Valgrind simulates a CPU and outputs the number of instructions used in this simulated CPU. In comparison to timing based performance measurements, Valgrind measurements are exactly reproducible. The measured numbers are given in Table D.1. The proposed code is between 14.3 and 41.6 times faster than the dune-pdelab implementation.

---

```

1  #ifndef SIMPLEX_2D_CURLCURL_H_INCLUDED_
2  #define SIMPLEX_2D_CURLCURL_H_INCLUDED_
3
4  #include <math.h> // for "fabs"
5
6  #include "simplex_2d_points.hh"
7
8  template <typename ctype>
9  inline ctype len(const ctype& p1x, const ctype& p1y, const ctype& p2x,
10     const ctype& p2y) {
11     ctype abslength(p1x - p2x);
12     abslength *= abslength;
13     ctype temp(p1y - p2y);
14     temp *= temp;
15     abslength += temp;
16     return sqrt(abslength);
17 }
18
19 template <typename ctype>
20 void simplex_2d_curlcurl_localoperator(
21     ctype* result, const simplex_2d_points<ctype>& p) {
22
23     // copying input values to local variables resulted in speedup
24     ctype p1x(p.p1x);
25     ctype p1y(p.p1y);
26
27     ctype p2x(p.p2x);
28     ctype p2y(p.p2y);
29
30     ctype p3x(p.p3x);
31     ctype p3y(p.p3y);
32
33     ctype lene1 = len(p1x, p1y, p2x, p2y);
34     ctype lene2 = len(p1x, p1y, p3x, p3y);
35     ctype lene3 = len(p2x, p2y, p3x, p3y);
36
37     ctype volume(fabs(ctype(1) / ctype(2) * ((p2x - p1x) * (p3y - p1y) -
38         (p2y - p1y) * (p3x - p1x))));
39
40     // precompute inverse, as multiplication is faster than division
41     ctype volinvers(ctype(1.) / volume);
42
43     result[0 * 3 + 0] = lene1 * lene1 * volinvers;
44     result[1 * 3 + 1] = lene2 * lene2 * volinvers;
45     result[2 * 3 + 2] = lene3 * lene3 * volinvers;
46
47     result[0 * 3 + 1] = result[1 * 3 + 0] = -volinvers * lene1 * lene2;
48
49     result[0 * 3 + 2] = result[2 * 3 + 0] = +volinvers * lene1 * lene3;
50     result[1 * 3 + 2] = result[2 * 3 + 1] = -volinvers * lene2 * lene3;
51 }
52
53 #endif // SIMPLEX_2D_CURLCURL_H_INCLUDED_

```

---

Listing D.1: C++ curlcurl assembly for a triangle.



---

## Handling of Complex Numbers in pyMOR

---

As part of this research project, the software package pyMOR [Milk et al.(2016)] was adapted to handle complex numbers. A question is to decide whether the inner product should be antilinear in its **first** or in its **second** argument. Both are possible choices, but it is beneficial to be as consistent as possible with the rest of the world. Because this question arises very often in discussions, we document our findings here. A short survey yields the following:

- Software packages:
  - Numpy [Travis E(2006)] does no complex conjugation in its “numpy.inner” function. It does, however, conjugate the **first** argument in its “numpy.vdot” function.
  - DUNE [Bastian et al.(2008b)] does complex conjugation on the **first** argument in the “dot” function, see the file “dune/common/dotproduct.hh”, line 16 in git hash 3091dfd1d65f9c50b9cb5e56c0cde4c9614ba816.
  - Fenics [Alnæs et al.(2015)] does complex conjugation on the **first** argument, see for example the file “dolfin/la/EigenVector.cpp”, line 252, in git hash b99d156dfcbf97d958f539172bbf74addeef1b4e, where the arguments are forwarded in the same order to the “dot” function of Eigen, which does complex conjugation on the **first** argument.
  - Eigen [Guennebaud et al.(2010)] does complex conjugation on the **first** argument, see the file “Eigen/src/Core/Dot.h”, line 61 in Mercurial hash 1b5aaf8108e8594083d45d43c08c2c113748cbda.
  - Deal.II [Alzetta et al.(2018)] is not consistent. In git hash 884c11cbce4595fea7337aa72e6745f928879247, one finds the following.
    - \* It does complex conjugation in the **second** argument, see file “dealii/include/deal.II/lac/vector.h”, line 438.
    - \* It does complex conjugation in the **first** argument, see file “dealii/include/deal.II/lac/petsc\_vector\_base.h”, line 518.
    - \* It does complex conjugation in the **second** argument, see file “dealii/include/deal.II/lac/vector\_operations\_internal.h”, line 744.
  - Matlab does complex conjugation in the **first** argument, tested with version R2017a.

- PetSc [Balay et al.(2018)]: The function “VecDot” does complex conjugation of the **second** argument. see the file “petsc/src/vec/vec/interface/rvector.c” line 93 in git commit 57f8f5fd4131aa625156f794bdbd51339abe2d6c.
- In BLAS there are the functions “zdotu” doing no complex conjugation and “zdotc” doing complex conjugation of the **first** argument.

- Publications

- Barbara Verfürth defines the sesquilinear form to conjugate the test function, see for example [Ohlberger and Verfürth(2018), equation (2.2)].
- Jan Heasthaven defines the inner product to be antilinear in the second argument and the sesquilinear form to be antilinear in the test function in [Chen et al.(2010), page 973].
- Peter Monk defines the sesquilinear form to be antilinear in the test function in his book “Finite Element Methods for Maxwell’s Equations” [Monk(2003), equation (4.1)].
- Dolean et.al. define the sesquilinear form to conjugate the test function in [Dolean et al.(2008)].
- C ea, Jean defines the sesquilinear form to conjugate the test function in [C ea(1964)].

We observe that there is no consensus whether the inner product should be antilinear in the first or second argument. Since most software have implemented it antilinear in the first argument, pyMOR follows this route and has the inner product antilinear in the first argument.

In the formulation of the sesquilinear form it is common to do a complex conjugation of the test function. pyMOR follows this pattern.

This implies that the functionals used as right hand side are antilinear.



---

## List of Symbols

---

- $\text{tol}$  target error of Algorithm 5.1. 80, 81, 86
- $\omega$  angular frequency. 18–22, 27, 90
- $a$  bilinear form. 11–13, 17, 20, 23, 33, 64, 66, 90, 96–98
- $\Gamma$  boundary of  $\Omega$ . 16, 17, 19, 20, 23, 24, 26, 28, 84–86, 88
- $c_{\text{eff}}$  effectivity constant of probabilistic a posteriori norm estimator. 79, 80
- $c_{\text{est}}$  constant in probabilistic a posteriori norm estimator. 78–81, 86
- $\varrho$  charge density. 17, 18, 21, 22
- $N_{\mathcal{E}}$  number of inner coarse mesh entities. 34–37, 41, 43
- $\mathcal{E}$  coarse mesh entity. 34, 35, 38, 39, 90
- $\alpha$  coercivity constant of  $a$ . 11–13, 17, 26, 41, 46, 55, 59, 62, 64–66, 73, 74
- $\mathbb{C}$  set of complex numbers. 11, 12, 120, 130
- $c_{\text{pc}}$  constant in rescaled Poincaré inequality  $\|\varphi - \bar{\varphi}_i\|_{L^2(\omega_i^{\text{pl}})} \leq c_{\text{pc}} H_i \|\nabla \varphi\|_{L^2(\omega_i^{\text{pl}})}$ . 62, 63
- $c'_{\text{pu}}$  constant to delimit derivative of partition of unity in  $\|\nabla \varrho_i\|_{\infty} \leq c'_{\text{pu}} H_i^{-1}$ . 61–63, 129
- $\gamma$  continuity constant of  $a$ . 11–13, 17, 48, 55, 59, 62, 64, 65, 73, 74
- $C$  coupling space. 39, 72, 90
- $\mathbf{J}$  current density. 17–19, 21, 22, 27
- $d$  dimension of the problem, 2 or 3. 14, 20, 37, 62
- $N_R$  dimension of  $R$ . 75, 76, 81, 82, 84, 86, 88
- $N_S$  dimension of  $S$ . 75–77, 81, 82, 84, 86, 88, 132
- $I$  domains associated:  $I_X$  is the set of domain numbers containing all domains which intersect with  $X$ . 34, 35, 39, 41, 60

- $\kappa$  specific electric conductivity. 19, 20, 26
- E** electric field. 17, 18, 21, 22, 27
- D** electric flux. 17, 18, 21, 22
- $\varepsilon$  electric permittivity. 17–22, 28
- $r$  enrichment fraction. 43, 44
- $\varepsilon_{\text{algofail}}$  maximum probability of randomized algorithm to fail. 80, 81, 84, 86
- $\varepsilon_{\text{testfail}}$  maximum probability of one randomized test to fail. 78–81, 86
- $\Delta(\tilde{u}_\mu)$  error estimator, standard RB variant. 55, 59, 65
- $\Delta_{\text{rel}}(\tilde{u}_\mu)$  relative error estimator, standard RB variant. xiii, 45, 46, 65
- $\Delta_{\text{loc,rel}}^g(\tilde{u}_\mu)$  relative error estimator, localized, improved variant with global constant. xiii, 45, 46, 65
- $\mathbb{E}$  expectation value. 82, 83
- Extend Extend operator. xiii, 35–37, 53
- $E$  extension space. 35
- $\mathbb{K}$  field, either  $\mathbb{R}$  or  $\mathbb{C}$ . 11, 13
- $\mathcal{B}$  finite element basis. 34, 35, 39, 60
- $c_F$  constant in Friedrich’s inequality. 17, 26, 100, 101
- $V$  function space. 11–15, 20, 23, 24, 26, 42, 47, 55–67, 71–73, 97, 100, 131
- $V^{\text{DG}}$  DG function space. 14, 15
- $V_h$  discrete function space. 15, 34–37, 44, 45, 56, 60–63, 66–68, 131
- $V_i$  local function space. 14, 37–44, 56–59, 65, 66, 71–75, 90, 95–99, 103, 131, 133
- $V_i^{\text{basic}}$  local function space of basic decomposition. xiii, 35–38, 60, 90, 131
- $V_i^{\text{pou}}$  local function space of partition of unity decomposition. 15, 41–44, 60, 62–64, 131
- $V_i^{\text{res}}$  local function space of restriction decomposition. 14, 15, 131
- $V_i^{\text{wb}}$  local function space of wirebasket decomposition. xiii, 34–43, 53, 60, 72, 90, 131
- $V|_{\omega_i^*}$  function space, restricted to training domain. 72, 73
- $H^1(\Omega)$  space of all square integrable functions with square integrable derivative. 60, 72
- $H(\text{curl}, \Omega)$  space of all square integrable functions with square integrable curl. vii, 19, 20, 51
- $\sigma$  heat conductivity. xiv, 15–17, 23–26, 64, 100, 101
- $q$  heat source. 15, 16, 101
- $k$  Helmholtz wavenumber. 88–90

- Im image of. 57
- $\beta$  inf-sup constant of  $a$ . 11–13
- $\underline{M}_R$  inner product matrix in  $R$ . 76, 82, 83, 86
- $\underline{M}_S$  inner product matrix in  $S$ . 76–83, 86
- $\underline{m}_{S,i}$  eigenvector of inner product matrix in  $S$ . 77
- $S_i$  intermediate space of localized training configuration. 72, 73, 131, 133
- $\mathcal{I}$  interpolation operator  $V \rightarrow V_h$ . 15, 60–62, 133
- Ker kernel of. 57
- $q$  left singular vector. 76
- $L$  length of *Rangefinder Example 1*. 84, 86, 87
- $f$  linear form. 11–13, 16, 26, 66, 96, 97
- $\Delta_{loc}^g(\tilde{u}_\mu)$  error estimator, localized, improved variant with global constant. 41, 59, 64, 65
- $\Delta_{loc}^l(\tilde{u}_\mu)$  error estimator, localized, improved variant with local constants. 59
- $\mathbf{H}$  magnetic field. 17, 18, 21, 22
- $\mathbf{B}$  magnetic flux. 17, 18, 21, 22
- $\mu_0$  magnetic permeability. 17–22, 28
- $\mathcal{P}_{V_i}$  mapping from full space  $V$  to local space  $V_i$ . 14, 56–58, 71, 73, 97, 131
- $\mathcal{P}_{V_i^{\text{basic}}}$  mapping from full space  $V_h$  to local space  $V_i^{\text{basic}}$ . 37, 44
- $\mathcal{P}_{V_i^{\text{pou}}}$  mapping from full space  $V_h$  to local space  $V_i^{\text{pou}}$ . 15, 61–63
- $\mathcal{P}_{V_i^{\text{res}}}$  mapping from full space  $V_h$  to local space  $V_i^{\text{res}}$ . 15
- $\mathcal{P}_{V_i^{\text{wb}}}$  mapping from full space  $V_h$  to local space  $V_i^{\text{wb}}$ . xvii, 37, 40, 42, 43, 50
- $\mathcal{P}_{S_i}$  mapping from full space  $V$  to local space  $S_i$ . 72–74, 94
- $h$  mesh size of fine mesh. xiv, 26, 44, 47, 62–64, 84–89
- $H$  mesh size of coarse mesh / domain decomposition. xi, xv, 36, 44, 47, 48, 60–64, 101
- $\mathcal{N}$  neighborhood. 39, 42
- $c_{i,\tilde{v}}$  norm of local mapping  $\mathcal{P}_{V_i}$ . 57–59, 69
- $N_{OS}$  number of overlapping spaces. 96
- $P$  number of parameters. 13
- $N_{V_i}$  number of local spaces. 14, 56–59, 71–74, 96–101, 103
- $N_{\text{noI}}$  number of subdomain of non overlapping domain decomposition. 14, 15, 34, 39, 44, 60, 90
- $N_{\text{oI}}$  number of subdomain of overlapping domain decomposition. 15, 43, 60–63, 100

- $n_t$  number of test vectors in randomized range finder. 78–81, 86
- $\Omega$  calculation domain, assumed to be Lipschitz. 14–20, 23, 24, 26, 28, 37, 60–62, 64, 71, 73, 84, 86, 97, 100, 101, 132
- $\omega_i^{\text{ext}}$  subdomain of wirebasket space decomposition, extension domain. 35, 37
- $\omega_i^{\text{noI}}$  subdomain of non overlapping space decomposition. 14, 15, 34, 36, 39, 42, 44, 60, 90
- $\omega_i^{\text{ol}}$  subdomain of overlapping space decomposition. 15, 60–64, 100, 101, 129
- $\omega_i$  subdomain of localizing space decomposition. xiv, 14, 71–73, 90, 97, 101, 132
- $\omega_i^*$  subdomain of localized training configuration. 71–74, 132
- $P$  orthogonal projection,  $P_X$  maps into  $X$ . 42, 43, 57, 58, 62, 73–76, 78, 80–87, 89–91
- $\bar{J}$  number of subspace sets required so all spaces in each set are orthogonal. 56, 58, 59, 64, 65, 72–74
- $J$  maximum number of domains  $\omega_i$  at any point in  $\Omega$ . 60–64, 100, 101
- $J^*$  maximum number of domains  $\omega_i^*$  at any point in  $\Omega$ . 71–74
- $\mu$  parameter. xiii, 13, 14, 16, 23–26, 34, 35, 39–47, 49, 55, 59, 62, 64–68, 72, 130, 131
- $\mathcal{D}$  parameter space. 13, 23, 26, 34, 35, 38, 39, 68, 72
- $\varrho_i$  partition of unity function,  $\sum_i \varrho_i \equiv 1$ . 15, 61–63, 100, 101, 129
- Pr operator giving the probability of a statement. E.g.:  $\Pr(1 > 0) = 1$ . 78–80
- $\Delta$  randomized a posteriori norm estimator. 78–80
- $R$  range space of the transfer operator  $T$ . 75, 76, 78, 81, 83–85, 87, 89, 129, 131, 133
- $\tilde{R}^n$  reduced range space of the transfer operator  $T$  of size  $n$ . 75, 76, 78, 80–91
- $\Re$  real part. 18, 27
- $\mathbb{R}$  set of real numbers. 11, 13, 14, 76, 81, 82, 98, 123, 124, 130, 132
- $\tilde{\alpha}$  reduced coercivity constant of  $a$ . 12, 13
- $\tilde{\gamma}$  reduced continuity constant of  $a$ . 12, 13
- $\tilde{V}$  reduced function space. 12–14, 56–58, 60, 62, 63, 66, 68, 73, 74, 96–99
- $\tilde{\beta}$  reduced inf-sup constant of  $a$ . 12, 13, 48
- $\tilde{u}$  reduced solution. xiii, 12, 13, 41, 43–47, 55, 59, 64–67, 73, 74, 96–99, 103, 115–118, 130, 131
- $\mathcal{R}$  residual. 41, 43–45, 55, 59, 64–67, 96–98, 103
- R Riesz isomorphism. 66, 67
- $v$  right singular vector. 76
- $D_S$  Ritz isomorphism  $D_S : S \rightarrow \mathbb{R}^{N_S}$ . 76, 77, 132
- $D_S^{-1}$  Ritz isomorphism  $D_S^{-1} : \mathbb{R}^{N_S} \rightarrow S$ . 77–81, 132

- $\sigma$  singular value. 76, 78, 79, 82–84, 91
- $u$  solution. 11–17, 19, 20, 23, 24, 59, 65, 66, 71–74, 97–99, 101, 103, 115–117
- $\mathbf{X}$  some field. 18, 19
- $O$  some bounded linear operator. 78–80
- $S$  source space of the transfer operator  $T$ . 75–78, 81, 82, 84, 85, 87, 89, 93, 129, 131–133
- $\Upsilon$  set of spaces in wirebasket space decomposition. xiii, 34–44, 53
- $C$  speed of light. 28
- $c_I$  stability constant of FE interpolation  $\mathcal{I}$ . 61–63
- $c_{\text{pu},\tilde{V}}$  improved stability constant of localizing space decomposition. xii, 45, 46, 58–65, 97, 98, 100, 101, 103
- $\Xi$  training set,  $\Xi \subset \mathcal{P}$ . xiii, 38–44, 47, 49, 68, 93
- $\text{Tr}$  training space. 38–40, 72, 90
- $T$  affine linear compact transfer operator, mapping from some outer space  $S$  to some inner space  $R$ . xiv, 75, 76, 80–87, 89, 92, 132, 133
- $T^a$  affine part of  $T$ . 75, 80, 81
- $T_i$  affine linear compact operator, mapping from  $S_i$  to  $V_i$ . 72–74, 133
- $T_i^a$  affine part of  $T_i$ . 72–74
- $T_i^l$  linear part of  $T_i$ . 72–75, 90
- $T^l$  linear part of  $T$ . 75, 76, 78, 80–87, 89–91
- $T_{\mu,i}$  parameterized affine linear compact operator, mapping from  $S_i$  to  $V_i$ . 72, 93
- $W$  width of *Rangefinder Example 1*. 84, 86, 87



- ACMS** Approximate Component Mode Synthesis. 7
- ArbiLoMod** method designed for Arbitrary Local Modifications. 2, 6, 8, 9, 31–34, 36, 38, 39, 41–45, 47, 48, 51, 53, 55, 60, 62, 64, 72, 94, 95, 104, 107, 115
- CEM-GMsFEM** Constraint Energy Minimization - Generalized Multiscale Finite Element Method. 95
- CMS** Component Mode Synthesis. 7, 33
- DD** Domain Decomposition. 7
- DFG** Deutsche Forschungsgemeinschaft. 2
- DG** Discontinuous Galerkin. 4, 5, 14, 15
- DGRBE** Discontinuous Galerkin Reduced Basis Element. 4, 64
- DoF** Degree of Freedom. 7, 22, 28, 35, 38, 47, 50, 51, 60, 84, 88, 99
- DtN** Dirichlet-to-Neumann. 6, 7, 105
- DUNE** Distributed and Unified Numerics Environment. 5
- ESMsFEM** Edge Spectral Multiscale Finite Element Method. 6
- FE** Finite Element. 4–6, 16–18, 31, 33, 34, 60, 72, 84, 90, 100, 123
- FEA** Finite Element Analysis. 2
- FEM** Finite Element Method. 3, 15
- FETI-DP** finite element tearing and interconnecting - dual primal. 7
- GFEM** Generalized Finite Element Method. 15, 32, 71, 107
- GMsFEM** Generalized Multiscale Finite Element Method. 6, 33, 64, 95, 107
- HMM** Heterogeneous Multiscale Method. 6

- LOD** Local Orthogonal Decomposition Method. 6, 32
- LRBMS** Localized Reduced Basis Multiscale Method. 5, 6, 15, 32, 64, 95, 107
- Mathematica<sup>®</sup>** Mathematica<sup>®</sup> by Wolfram. 109, 110, 124
- MsFEM** Multiscale Finite Element Method. 6, 7, 32, 35, 63
- PCB** Printed Circuit Board. 28, 32, 108
- PDE** Partial Differential Equation. 15
- PEC** Perfect Electric Conductor. 21, 26–28
- POD** Proper Orthogonal Decomposition. 93
- PR-SCRBE** Port Reduced Static Condensation Reduced Basis Element Method. 5, 33, 36, 38, 71, 107
- pyMOR** pyMOR – Model Order Reduction with Python. 23, 27, 44, 109, 127, 128
- RB** Reduced Basis. 4, 5, 55, 59, 62, 64, 65, 67, 108, 130
- RBE** Reduced Basis Element. 4, 33
- RBHDD** Reduced Basis for Heterogeneous Domain Decomposition. 5
- RBHM** Reduced Basis Hybrid Method. 4
- RDF** Reduced Basis - Domain Decomposition - Finite Element Method. 4
- RFB** Residual Free Bubbles Method. 6
- SCM** Successive Constraint Method. 20
- SCRBE** Static Condensation Reduced Basis Element Method. 5, 60, 64
- SRBE** Seamless Reduced Basis Element Method. 4, 33
- SVD** Singular Value Decomposition. 76, 93
- VMM** Variational Multiscale Method. 6



---

## Bibliography

---

- [Aarnes and Hou(2002)] J. AARNES, T. Y. HOU. *Multiscale domain decomposition methods for elliptic problems with high aspect ratios*. Acta Mathematicae Applicatae Sinica, English Series, 18 (2002) (1), pp. 63–76. doi: 10.1007/s102550200004.
- [Abdulle(2005)] A. ABDULLE. *On a priori error analysis of fully discrete heterogeneous multiscale FEM*. Multiscale Modeling and Simulation, 4 (2005) (2), pp. 447–459. doi: 10.1137/040607137.
- [Albrecht and Ohlberger(2013)] F. ALBRECHT, M. OHLBERGER. *The localized reduced basis multiscale method with online enrichment*. Oberwolfach Reports, 7 (2013), pp. 406–409. doi: 10.4171/OWR/2013/07.
- [Albrecht et al.(2012)] F. ALBRECHT, B. HAASDONK, M. OHLBERGER, S. KAULMANN. *The Localized Reduced Basis Multiscale Method*. Proceedings of Algorithm 2012, Conference on Scientific Computing, Vysoke Tatry, Podbanske, September 9-14, 2012, (2012), pp. 393–403. doi: n/a.
- [Alnæs et al.(2015)] M. S. ALNÆS, J. BLECHTA, J. HAKE, A. JOHANSSON, B. KEHLET, A. LOGG, C. RICHARDSON, J. RING, M. E. ROGNES, G. N. WELLS. *The FEniCS Project Version 1.5*. Archive of Numerical Software, 3 (2015) (100). doi: 10.11588/ans.2015.100.20553.
- [Alzetta et al.(2018)] G. ALZETTA, D. ARNDT, W. BANGERTH, V. BODDU, B. BRANDS, D. DAVYDOV, R. GASSMOELLER, T. HEISTER, L. HELTAI, K. KORMANN, M. KRONBICHLER, M. MAIER, J.-P. PELTERET, B. TURCK SIN, D. WELLS. *The deal.II Library, Version 9.0*. Journal of Numerical Mathematics, 26 (2018) (4), pp. 173–183. doi: 10.1515/jnma-2018-0054.
- [Antonietti et al.(2016)] P. F. ANTONIETTI, P. PACCARINI, A. QUARTERONI. *A discontinuous Galerkin Reduced Basis Element method for elliptic problems*. ESAIM: Mathematical Modelling and Numerical Analysis, 50 (2016) (2), pp. 337–360. doi: 10.1051/m2an/2015045.
- [Babuska and Lipton(2011)] I. BABUSKA, R. LIPTON. *Optimal Local Approximation Spaces for Generalized Finite Element Methods with Application to Multiscale Problems*. Multiscale Modeling & Simulation, 9 (2011) (1), pp. 373–406. doi: 10.1137/100791051.
- [Balay et al.(2018)] S. BALAY, S. ABHYANKAR, M. F. ADAMS, J. BROWN, P. BRUNE, K. BUSCHELMAN, L. DALCIN, V. EIJKHOUT, W. D. GROPP, D. KAUSHIK, M. G. KNEPLEY, D. A. MAY, L. C. MCINNES, R. T. MILLS, T. MUNSON, K. RUPP, P. SANAN, B. F. SMITH, S. ZAMPINI, H. ZHANG, H. ZHANG. *PETSc Web page*. <http://www.mcs.anl.gov/petsc>, 2018.

- [Bampton and Craig(1968)] M. C. C. BAMPTON, R. R. CRAIG, JR. *Coupling of substructures for dynamic analyses*. AIAA Journal, 6 (1968) (7), pp. 1313–1319. doi: 10.2514/3.4741.
- [Bastian et al.(2008a)] P. BASTIAN, M. BLATT, A. DEDNER, C. ENGWER, R. KLÖFKORN, M. OHLBERGER, O. SANDER. *A generic grid interface for parallel and adaptive scientific computing. Part I: abstract framework*. Computing, 82 (2008a) (2-3), pp. 103–119. doi: 10.1007/s00607-008-0003-x.
- [Bastian et al.(2008b)] P. BASTIAN, M. BLATT, A. DEDNER, C. ENGWER, R. KLÖFKORN, R. KORNUBER, M. OHLBERGER, O. SANDER. *A generic grid interface for parallel and adaptive scientific computing. Part II: implementation and tests in DUNE*. Computing, 82 (2008b) (2), pp. 121–138. doi: 10.1007/s00607-008-0004-9.
- [Bastian et al.(2014)] P. BASTIAN, C. ENGWER, D. GÖDDEKE, O. ILIEV, O. IPPISCH, M. OHLBERGER, S. TUREK, J. FAHLKE, S. KAULMANN, S. MÜTHING, D. RIBBROCK. *EXA-DUNE: Flexible PDE Solvers, Numerical Methods and Applications*. In L. LOPES, J. ŽILINSKAS, A. COSTAN, R. G. CASCELLA, G. KECSKEMETI, E. JEANNOT, M. CANNATARO, L. RICCI, S. BENKNER, S. PETIT, V. SCARANO, J. GRACIA, S. HUNOLD, S. L. SCOTT, S. LANKES, C. LENGAUER, J. CARRETERO, J. BREITBART, M. ALEXANDER, eds., *Euro-Par 2014: Parallel Processing Workshops*. Springer International Publishing, Cham. ISBN 978-3-319-14313-2, 2014 pp. 530–541.
- [Bastian et al.(2016)] P. BASTIAN, C. ENGWER, J. FAHLKE, M. GEVELER, D. GÖDDEKE, O. ILIEV, O. IPPISCH, R. MILK, J. MOHRING, S. MÜTHING, M. OHLBERGER, D. RIBBROCK, S. TUREK. *Hardware-Based Efficiency Advances in the EXA-DUNE Project*. In *Lecture Notes in Computational Science and Engineering*, pp. 3–23. Springer International Publishing, 2016. doi: 10.1007/978-3-319-40528-5\_1.
- [Benner and Hess(2012)] P. BENNER, M. HESS. *The Reduced Basis Method for Time-Harmonic Maxwell's Equations*. Proceedings in Applied Mathematics and Mechanics, 12 (2012) (1), pp. 661–662. doi: 10.1002/pamm.201210319.
- [Benner et al.(2017)] P. BENNER, M. OHLBERGER, A. COHEN, K. E. WILCOX. *Model Reduction and Approximation: Theory and Algorithms*. SIAM-Society for Industrial & Applied Mathematics, 2017. ISBN 9781611974829.
- [Bourquin(1992)] F. BOURQUIN. *Component mode synthesis and eigenvalues of second order operators: discretization and algorithm*. ESAIM: Mathematical Modelling and Numerical Analysis, 26 (1992) (3), pp. 385–423. doi: 10.1051/m2an/1992260303851.
- [Buhr(2009)] A. BUHR. *Finite Elements in PCB Structures*. Master's thesis, TU Darmstadt, Darmstadt, Germany, 2009.
- [Buhr(2017)] A. BUHR. *Exponential Convergence of Online Enrichment in Localized Reduced Basis Methods*. IFAC-PapersOnLine, 51 (2017) (2), pp. 302–306. doi: n/a. MATHMOD 2018.
- [Buhr(2019)] A. BUHR. *Source Code for PhD Thesis by Andreas Buhr*, 2019. doi: 10.5281/zenodo.2555623.
- [Buhr and Smetana(2018)] A. BUHR, K. SMETANA. *Randomized Local Model Order Reduction*. SIAM Journal on Scientific Computing, 40 (2018) (4), pp. A2120–A2151. doi: 10.1137/17M1138480.
- [Buhr et al.(2014)] A. BUHR, C. ENGWER, M. OHLBERGER, S. RAVE. *A Numerically Stable a Posteriori Error Estimator for Reduced Basis Approximations of Elliptic Equations*. In X. O. E. ONATE, A. HUERTA, eds., *Proceedings of the 11th World Congress on Computational Mechanics*. CIMNE, Barcelona, 2014 pp. 4094–4102. doi: n/a.

- [Buhr et al.(2017a)] A. BUHR, C. ENGWER, M. OHLBERGER, S. RAVE. *ArbiLoMod, a Simulation Technique Designed for Arbitrary Local Modifications*. SIAM Journal on Scientific Computing, 39 (2017a) (4), pp. A1435–A1465. doi: 10.1137/15M1054213.
- [Buhr et al.(2017b)] A. BUHR, C. ENGWER, M. OHLBERGER, S. RAVE. *ArbiLoMod: Local Solution Spaces by Random Training in Electrodynamics*, pp. 137–148. Springer International Publishing, Cham. ISBN 978-3-319-58786-8, 2017b. doi: 10.1007/978-3-319-58786-8\_9.
- [Buhr et al.(2019)] A. BUHR, L. IAPICHINO, M. OHLBERGER, S. RAVE, F. SCHINDLER, K. SMETANA. *Handbook on Model Order Reduction*, chap. Localized model reduction for parameterized problems. Walter De Gruyter GmbH, 2019+. Submitted for publication.
- [Carlberg et al.(2010)] K. CARLBERG, C. BOU-MOSLEH, C. FARHAT. *Efficient non-linear model reduction via a least-squares Petrov-Galerkin projection and compressive tensor approximations*. International Journal for Numerical Methods in Engineering, 86 (2010) (2), pp. 155–181. doi: 10.1002/nme.3050.
- [Casenave(2012)] F. CASENAVE. *Accurate a posteriori error evaluation in the reduced basis method*. Comptes Rendus Mathematique, 350 (2012) (9-10), pp. 539–542. doi: 10.1016/j.crma.2012.05.012.
- [Casenave et al.(2014)] F. CASENAVE, A. ERN, T. LELIÈVRE. *Accurate and online-efficient evaluation of the a posteriori error bound in the reduced basis method*. ESAIM: Mathematical Modelling and Numerical Analysis, 48 (2014) (1), pp. 207–229. doi: 10.1051/m2an/2013097.
- [Céa(1964)] J. CÉA. *Approximation variationnelle des problèmes aux limites*. Université de Grenoble, 14 (1964) (fasc. 2), pp. 345–444.
- [Chen et al.(2008)] Y. CHEN, J. S. HESTHAVEN, Y. MADAY, J. RODRÍGUEZ. *A monotonic evaluation of lower bounds for inf-sup stability constants in the frame of reduced basis approximations*. Comptes Rendus Mathematique, 346 (2008) (23), pp. 1295–1300. doi: 10.1016/j.crma.2008.10.012.
- [Chen et al.(2009)] Y. CHEN, J. S. HESTHAVEN, Y. MADAY, J. RODRÍGUEZ. *Improved successive constraint method based a posteriori error estimate for reduced basis approximation of 2D Maxwell’s problem*. ESAIM: Mathematical Modelling and Numerical Analysis, 43 (2009) (6), pp. 1099–1116. doi: 10.1051/m2an/2009037.
- [Chen et al.(2010)] Y. CHEN, J. S. HESTHAVEN, Y. MADAY, J. RODRÍGUEZ. *Certified Reduced Basis Methods and Output Bounds for the Harmonic Maxwell’s Equations*. SIAM Journal on Scientific Computing, 32 (2010) (2), pp. 970–996. doi: 10.1137/09075250X.
- [Chen et al.(2011)] Y. CHEN, J. S. HESTHAVEN, Y. MADAY. *A seamless reduced basis element method for 2D Maxwell’s problem: an introduction*. In *Spectral and high order methods for partial differential equations*, vol. 76 of *Lect. Notes Comput. Sci. Eng.*, pp. 141–152. Springer, Heidelberg, 2011. doi: 10.1007/978-3-642-15337-2\_11.
- [Chen et al.(2017)] Y. CHEN, J. JIANG, A. NARAYAN. *Robust residual-based and residual-free greedy algorithms for reduced basis methods*. arXiv e-prints, (2017). <http://arxiv.org/abs/1710.08999v1>.
- [Chen et al.(2018)] Y. CHEN, J. JIANG, A. NARAYAN. *A robust error estimator and a residual-free error indicator for reduced basis methods*. Computers & Mathematics with Applications, (2018). doi: 10.1016/j.camwa.2018.11.032.

- [Chen and Dongarra(2005)] Z. CHEN, J. J. DONGARRA. *Condition numbers of Gaussian random matrices*. SIAM Journal on Matrix Analysis and Applications, 27 (2005) (3), pp. 603–620. doi: 10.1137/040616413.
- [Cheng et al.(2005)] H. CHENG, Z. GIMBUTAS, P. G. MARTINSSON, V. ROKHLIN. *On the compression of low rank matrices*. SIAM Journal on Scientific Computing, 26 (2005) (4), pp. 1389–1404. doi: 10.1137/030602678.
- [Chung et al.(2014)] E. T. CHUNG, Y. EFENDIEV, W. T. LEUNG. *Generalized multiscale finite element methods for wave propagation in heterogeneous media*. Multiscale Modeling and Simulation, 12 (2014) (4), pp. 1691–1721. doi: 10.1137/130926675.
- [Chung et al.(2015)] E. T. CHUNG, Y. EFENDIEV, C. S. LEE. *Mixed generalized multiscale finite element methods and applications*. Multiscale Modeling and Simulation, 13 (2015) (1), pp. 338–366. doi: 10.1137/140970574.
- [Chung et al.(2018a)] E. T. CHUNG, Y. EFENDIEV, W. T. LEUNG. *An adaptive generalized multiscale discontinuous Galerkin method for high-contrast flow problems*. Multiscale Modeling and Simulation, 16 (2018a) (3), pp. 1227–1257. doi: 10.1137/140986189. 1409.3474.
- [Chung et al.(2018b)] E. T. CHUNG, Y. EFENDIEV, W. T. LEUNG. *Constraint Energy Minimizing Generalized Multiscale Finite Element Method*. Computer Methods in Applied Mechanics and Engineering, 339 (2018b), pp. 298–319. doi: 10.1016/j.cma.2018.04.010.
- [Chung et al.(2018c)] E. T. CHUNG, Y. EFENDIEV, W. T. LEUNG. *Fast Online Generalized Multiscale Finite Element Method using Constraint Energy Minimization*. Journal of Computational Physics, 355 (2018c), pp. 450–463. doi: 10.1016/j.jcp.2017.11.022.
- [Cohen et al.(2012)] A. COHEN, R. DEVORE, R. H. NOCHETTO. *Convergence rates of AFEM with  $H^{-1}$  data*. Foundations of Computational Mathematics, 12 (2012) (5), pp. 671–718. doi: 10.1007/s10208-012-9120-1.
- [Dahmen et al.(2014)] W. DAHMEN, C. PLESKEN, G. WELPER. *Double greedy algorithms: Reduced basis methods for transport dominated problems*. ESAIM: Mathematical Modelling and Numerical Analysis, 48 (2014) (3), pp. 623–663. doi: 10.1051/m2an/2013103.
- [Demmel et al.(1999)] J. W. DEMMEL, S. C. EISENSTAT, J. R. GILBERT, X. S. LI, J. W. H. LIU. *A supernodal approach to sparse partial pivoting*. SIAM J. Matrix Analysis and Applications, 20 (1999) (3), pp. 720–755. doi: 10.1137/S0895479895291765.
- [Dolean et al.(2008)] V. DOLEAN, H. FOL, S. LANTERI, R. PERRUSSEL. *Solution of the time-harmonic Maxwell equations using discontinuous Galerkin methods*. Journal of Computational and Applied Mathematics, 218 (2008) (2), pp. 435–445. doi: 10.1016/j.cam.2007.05.026. The Proceedings of the Twelfth International Congress on Computational and Applied Mathematics.
- [Dolean et al.(2012)] V. DOLEAN, F. NATAF, R. SCHEICHL, N. SPILLANE. *Analysis of a Two-level Schwarz Method with Coarse Spaces Based on Local Dirichlet-to-Neumann Maps*. Computational Methods in Applied Mathematics, 12 (2012) (4). doi: 10.2478/cmam-2012-0027.
- [Dörfler(1996)] W. DÖRFLER. *A convergent adaptive algorithm for Poisson’s equation*. SIAM Journal on Numerical Analysis, 33 (1996) (3), pp. 1106–1124. doi: 10.1137/0733054.
- [Drineas et al.(2006a)] P. DRINEAS, R. KANNAN, M. MAHONEY. *Fast Monte Carlo Algorithms for Matrices I: Approximating Matrix Multiplication*. SIAM Journal on Computing, 36 (2006a) (1), pp. 132–157. doi: 10.1137/S0097539704442684.

- 
- [Drineas et al.(2006b)] P. DRINEAS, R. KANNAN, M. MAHONEY. *Fast Monte Carlo Algorithms for Matrices II: Computing a Low-Rank Approximation to a Matrix*. SIAM Journal on Computing, 36 (2006b) (1), pp. 158–183. doi: 10.1137/S0097539704442696.
- [Drineas et al.(2006c)] P. DRINEAS, R. KANNAN, M. W. MAHONEY. *Fast Monte Carlo Algorithms for Matrices. III. Computing a compressed approximate matrix decomposition*. SIAM Journal on Computing, 36 (2006c) (1), pp. 184–206. doi: 10.1137/S0097539704442702.
- [E and Engquist(2003)] W. E, B. ENGQUIST. *The Heterogeneous Multiscale Methods*. Communications in Mathematical Sciences, 1 (2003) (1), pp. 87–132. doi: 10.4310/cms.2003.v1.n1.a8.
- [E and Engquist(2005)] W. E, B. ENGQUIST. *The Heterogeneous Multi-Scale Method for Homogenization Problems*. In *Lecture Notes in Computational Science and Engineering*, vol. 44 of *Lect. Notes Comput. Sci. Eng.*, pp. 89–110. Springer-Verlag, Berlin, 2005. doi: 10.1007/3-540-26444-2\_4.
- [Efendiev and Hou(2009)] Y. EFENDIEV, T. Y. HOU. *Multiscale Finite Element Methods: Theory and Applications (Surveys and Tutorials in the Applied Mathematical Sciences, Vol. 4)*, vol. 4 of *Surveys and Tutorials in the Applied Mathematical Sciences*. Springer, New York, 2009. ISBN 0387094954. Theory and applications.
- [Efendiev et al.(2011)] Y. EFENDIEV, J. GALVIS, X.-H. WU. *Multiscale finite element methods for high-contrast problems using local spectral basis functions*. Journal of Computational Physics, 230 (2011) (4), pp. 937–955. doi: 10.1016/j.jcp.2010.09.026.
- [Efendiev et al.(2013)] Y. EFENDIEV, J. GALVIS, T. Y. HOU. *Generalized Multiscale Finite Element Methods (GMsFEM)*. Journal of Computational Physics, 251 (2013), pp. 116–135. doi: 10.1016/j.jcp.2013.04.045.
- [Eftang and Patera(2013)] J. L. EFTANG, A. T. PATERA. *Port reduction in parametrized component static condensation: approximation and a posteriori error estimation*. International Journal for Numerical Methods in Engineering, 96 (2013) (5), pp. 269–302. doi: 10.1002/nme.4543.
- [Eftang and Patera(2014)] J. L. EFTANG, A. T. PATERA. *A port-reduced static condensation reduced basis element method for large component-synthesized structures: approximation and a posteriori error estimation*. Advanced Modeling and Simulation in Engineering Sciences, 1 (2014) (3), p. 3. doi: 10.1186/2213-7467-1-3.
- [Eickhorn(2019)] D. EICKHORN. *Randomisierte lokalisierte Modellreduktion mit Robin-Transferoperator*. Master’s thesis, Westfälische Wilhelms Universität Münster, 2019. [https://www.uni-muenster.de/AMM/includes/ohlberger/team/eickhorn/MA\\_Eickhorn.pdf](https://www.uni-muenster.de/AMM/includes/ohlberger/team/eickhorn/MA_Eickhorn.pdf).
- [Engwer et al.(2019)] C. ENGWER, P. HENNING, A. MÅLQVIST, D. PETERSEIM. *Efficient implementation of the localized orthogonal decomposition method*. Computer Methods in Applied Mechanics and Engineering, 350 (2019), pp. 123–153. doi: 10.1016/j.cma.2019.02.040.
- [Feuersänger(2011)] C. FEUERSÄNGER. *Manual for Package pgfplots*. online, 17 (2011).
- [Fink and Rheinboldt(1983)] J. P. FINK, W. C. RHEINBOLDT. *On the Error Behavior of the Reduced Basis Technique for Nonlinear Finite Element Approximations*. ZAMM-Journal of Applied Mathematics and Mechanics/Zeitschrift für Angewandte Mathematik und Mechanik, 63 (1983) (1), pp. 21–28. doi: 10.1002/zamm.19830630105.
- [Fu et al.(2018)] S. FU, E. CHUNG, G. LI. *Edge Multiscale Methods for elliptic problems with heterogeneous coefficients*. arXiv, (2018). <http://arxiv.org/abs/1810.10398v1>.

- [Galvis and Efendiev(2010)] J. GALVIS, Y. EFENDIEV. *Domain decomposition preconditioners for multiscale flows in high-contrast media*. Multiscale Modeling & Simulation, 8 (2010) (4), pp. 1461–1483. doi: 10.1137/090751190.
- [Gander and Loneland(2017)] M. J. GANDER, A. LONELAND. *SHEM: an optimal coarse space for RAS and its multiscale approximation*. In *Domain decomposition methods in science and engineering XXIII*, vol. 116 of *Lecture Notes in Computational Science and Engineering*, pp. 313–321. Springer, Cham, 2017. doi: 10.1007/978-3-319-52389-7\_32.
- [Graham and Scheichl(2007)] I. GRAHAM, R. SCHEICHL. *Robust domain decomposition algorithms for multiscale PDEs*. Numerical Methods for Partial Differential Equations, 23 (2007) (4), pp. 859–878. doi: 10.1002/num.20254.
- [Graham et al.(2007)] I. G. GRAHAM, P. O. LECHNER, R. SCHEICHL. *Domain decomposition for multiscale PDEs*. Numerische Mathematik, 106 (2007) (4), pp. 589–626. doi: 10.1007/s00211-007-0074-1.
- [Gram(1883)] J. P. GRAM. *Ueber die Entwicklung reeller Functionen in Reihen mittelst der Methode der kleinsten Quadrate*. Journal für die reine und angewandte Mathematik, 94 (1883), pp. 41–73.
- [Guennebaud et al.(2010)] G. GUENNEBAUD, B. JACOB, ET AL. *Eigen v3*. <http://eigen.tuxfamily.org>, 2010.
- [Haasdonk(2017)] B. HAASDONK. *Chapter 2: Reduced Basis Methods for Parametrized PDEs—A Tutorial Introduction for Stationary and Instationary Problems*. In *Model Reduction and Approximation*, pp. 65–136. Society for Industrial and Applied Mathematics, 2017. doi: 10.1137/1.9781611974829.ch2.
- [Halko et al.(2011)] N. HALKO, P.-G. MARTINSSON, J. A. TROPP. *Finding structure with randomness: Probabilistic algorithms for constructing approximate matrix decompositions*. SIAM Review, 53 (2011) (2), pp. 217–288. doi: 10.1137/090771806.
- [Heaviside(1892)] O. HEAVISIDE. *Electrical Papers*. Macmilland And Company, 1892.
- [Heinlein et al.(2018)] A. HEINLEIN, A. KLAWONN, J. KNEPPER, O. RHEINBACH. *Multiscale coarse spaces for overlapping Schwarz methods based on the ACMS space in 2D*. Electronic Transactions on Numerical Analysis, 48 (2018), pp. 156–182. doi: 10.1553/etna\_vol48s156.
- [Henning and Peterseim(2013)] P. HENNING, D. PETERSEIM. *Oversampling for the Multiscale Finite Element Method*. Multiscale Modeling & Simulation, 11 (2013) (4), pp. 1149–1175. doi: 10.1137/120900332.
- [Henning et al.(2014a)] P. HENNING, A. MÅLQVIST, D. PETERSEIM. *A localized orthogonal decomposition method for semi-linear elliptic problems*. ESAIM: Mathematical Modelling and Numerical Analysis, 48 (2014a) (5), pp. 1331–1349. doi: 10.1051/m2an/2013141.
- [Henning et al.(2014b)] P. HENNING, M. OHLBERGER, B. SCHWEIZER. *An Adaptive Multiscale Finite Element Method*. Multiscale Modeling & Simulation, 12 (2014b) (3), pp. 1078–1107. doi: 10.1137/120886856.
- [Hess(2016)] M. W. HESS. *Reduced Basis Approximations for Electromagnetic Applications*. Ph.D. thesis, Otto-von-Guericke Universität Magdeburg, 2016.
- [Hesthaven et al.(2016)] J. S. HESTHAVEN, G. ROZZA, B. STAMM. *Certified Reduced Basis Methods for Parametrized Partial Differential Equations*. SpringerBriefs in Mathematics, Springer International Publishing, New York, 2016. ISBN 978-3-319-22469-5; 978-3-319-22470-1. doi: 10.1007/978-3-319-22470-1. BCAM SpringerBriefs.

- [Hetmaniuk and Klawonn(2014)] U. HETMANIUK, A. KLAWONN. *Error estimates for a two-dimensional special finite element method based on component mode synthesis*. *Electronic Transactions on Numerical Analysis*, 41 (2014), pp. 109–132. doi: n/a.
- [Hetmaniuk and Lehoucq(2010)] U. L. HETMANIUK, R. B. LEHOUCQ. *A special finite element method based on component mode synthesis*. *ESAIM: Mathematical Modelling and Numerical Analysis*, 44 (2010) (3), pp. 401–420. doi: 10.1051/m2an/2010007.
- [Horn and Johnson(2012)] R. A. HORN, C. R. JOHNSON. *Matrix Analysis*. Cambridge University Press, 2012. ISBN 978-0521548236.
- [Hou and Wu(1997)] T. Y. HOU, X.-H. WU. *A Multiscale Finite Element Method For Elliptic Problems In Composite Materials And Porous Media*. *Journal of Computational Physics*, 134 (1997) (1), pp. 169–189. doi: 10.1006/jcph.1997.5682.
- [Hughes(1995)] T. J. HUGHES. *Multiscale phenomena: Green’s functions, the Dirichlet-to-Neumann formulation, subgrid scale models, bubbles and the origins of stabilized methods*. *Computer Methods in Applied Mechanics and Engineering*, 127 (1995) (1–4), pp. 387–401. doi: 10.1016/0045-7825(95)00844-9.
- [Hughes et al.(1998)] T. J. HUGHES, G. R. FEIJÓO, L. MAZZEI, J.-B. QUINCY. *The variational multiscale method — a paradigm for computational mechanics*. *Computer Methods in Applied Mechanics and Engineering*, 166 (1998) (1), pp. 3–24. doi: 10.1016/S0045-7825(98)00079-6.
- [Hurty(1965)] W. C. HURTY. *Dynamic analysis of structural systems using component modes*. *AIAA journal*, 3 (1965) (4), pp. 678–685. doi: 10.2514/3.2947.
- [Huynh et al.(2007)] D. HUYNH, G. ROZZA, S. SEN, A. PATERA. *A successive constraint linear optimization method for lower bounds of parametric coercivity and inf-sup stability constants*. *Comptes Rendus Mathematique*, 345 (2007) (8), pp. 473–478. doi: 10.1016/j.crma.2007.09.019.
- [Iapichino(2012)] L. IAPICHINO. *Reduced basis methods for the solution of parametrized PDEs in repetitive and complex networks with application to CFD*. Ph.D. thesis, École polytechnique fédérale de Lausanne, 2012. doi: 10.5075/epfl-thesis-5529.
- [Iapichino et al.(2012)] L. IAPICHINO, A. QUARTERONI, G. ROZZA. *A reduced basis hybrid method for the coupling of parametrized domains represented by fluidic networks*. *Computer Methods in Applied Mechanics and Engineering*, 221–222 (2012), pp. 63–82. doi: 10.1016/j.cma.2012.02.005.
- [Iapichino et al.(2016)] L. IAPICHINO, A. QUARTERONI, G. ROZZA. *Reduced basis method and domain decomposition for elliptic problems in networks and complex parametrized geometries*. *Computers & Mathematics with Applications*, 71 (2016) (1), pp. 408–430. doi: 10.1016/j.camwa.2015.12.001.
- [Ihlenburg(2006)] F. IHLENBURG. *Finite element analysis of acoustic scattering*, vol. 132. Springer Science & Business Media, 2006. doi: 10.1007/b98828.
- [Jakobsson et al.(2011)] H. JAKOBSSON, F. BENZON, M. G. LARSON. *Adaptive component mode synthesis in linear elasticity*. *International Journal for Numerical Methods in Engineering*, 86 (2011) (7), pp. 829–844.
- [Kaulmann et al.(2011)] S. KAULMANN, M. OHLBERGER, B. HAASDONK. *A new local reduced basis discontinuous Galerkin approach for heterogeneous multiscale problems*. *Comptes Rendus Mathematique*, 349 (2011) (23), pp. 1233–1238. doi: 10.1016/j.crma.2011.10.024.

- [Kerfriden et al.(2013)] P. KERFRIDEN, O. GOURY, T. RABCZUK, S. BORDAS. *A partitioned model order reduction approach to rationalise computational expenses in nonlinear fracture mechanics*. *Computer Methods in Applied Mechanics and Engineering*, 256 (2013), pp. 169–188. doi: 10.1016/j.cma.2012.12.004.
- [Klawonn and Widlund(2006)] A. KLAWONN, O. B. WIDLUND. *Dual-primal FETI methods for linear elasticity*. *Communications on Pure and Applied Mathematics*, 59 (2006) (11), pp. 1523–1572. doi: 10.1002/cpa.20156.
- [Klawonn et al.(2016)] A. KLAWONN, P. RADTKE, O. RHEINBACH. *A comparison of adaptive coarse spaces for iterative substructuring in two dimensions*. *Electronic Transactions on Numerical Analysis*, 45 (2016), pp. 75–106.
- [Kornhuber and Yserentant(2016)] R. KORNHUBER, H. YSERENTANT. *Numerical homogenization of elliptic multiscale problems by subspace decomposition*. *Multiscale Modeling and Simulation*, 14 (2016) (3), pp. 1017–1036. doi: 10.1137/15M1028510.
- [Kornhuber et al.(2017)] R. KORNHUBER, J. PODLESNY, H. YSERENTANT. *Direct and iterative methods for numerical homogenization*. In *Domain decomposition methods in science and engineering XXIII*, vol. 116 of *Lecture Notes in Computational Science and Engineering*, pp. 217–225. Springer International Publishing, 2017. doi: 10.1007/978-3-319-52389-7\_21.
- [Kornhuber et al.(2018)] R. KORNHUBER, D. PETERSEIM, H. YSERENTANT. *An analysis of a class of variational multiscale methods based on subspace decomposition*. *Mathematics of Computation*, 87 (2018) (314), pp. 2765–2774. doi: 10.1090/mcom/3302.
- [Larson and Målqvist(2005)] M. G. LARSON, A. MÅLQVIST. *Adaptive Variational Multiscale Methods Based on A Posteriori Error Estimation: Duality Techniques for Elliptic Problems*. In *Lecture Notes in Computational Science and Engineering*, vol. 44 of *Lect. Notes Comput. Sci. Eng.*, pp. 181–193. Springer, Berlin, 2005. doi: 10.1007/3-540-26444-2\_9.
- [Larson and Målqvist(2007)] M. G. LARSON, A. MÅLQVIST. *Adaptive variational multiscale methods based on a posteriori error estimation: energy norm estimates for elliptic problems*. *Computer Methods in Applied Mechanics and Engineering*, 196 (2007) (21-24), pp. 2313–2324. doi: 10.1016/j.cma.2006.08.019.
- [Larson and Målqvist(2009a)] M. G. LARSON, A. MÅLQVIST. *An adaptive variational multiscale method for convection-diffusion problems*. *Communications in Numerical Methods in Engineering*, 25 (2009a) (1), pp. 65–79. doi: 10.1002/cnm.1106.
- [Larson and Målqvist(2009b)] M. G. LARSON, A. MÅLQVIST. *A mixed adaptive variational multiscale method with applications in oil reservoir simulation*. *Mathematical Models and Methods in Applied Sciences*, 19 (2009b) (07), pp. 1017–1042. doi: 10.1142/s021820250900370x.
- [Lax and Milgram(1954)] P. LAX, A. MILGRAM. *Contributions to the Theory of Partial Differential Equations*, vol. 33, chap. IX. parabolic equations, pp. 167–190. Princeton University Press, 1954.
- [Lee(2018)] M. A. LEE. *An approach for efficient, conceptual-level aerospace structural design using the static condensation reduced basis element method*. Ph.D. thesis, Georgia Institute of Technology, 2018.
- [Lehoucq et al.(1998)] R. B. LEHOUCQ, D. C. SORENSEN, C. YANG. *ARPACK Users' Guide*. online, 6 (1998), pp. xvi+142. doi: 10.1137/1.9780898719628.



- [Li et al.(1999)] X. LI, J. DEMMEL, J. GILBERT, I.L. GRIGORI, M. SHAO, I. YAMAZAKI. *SuperLU Users' Guide*. Tech. Rep. LBNL-44289, Lawrence Berkeley National Laboratory, 1999. <http://crd.lbl.gov/~xiaoye/SuperLU/>. Last update: August 2011.
- [Liberty et al.(2007)] E. LIBERTY, F. WOOLFE, P.-G. MARTINSSON, V. ROKHLIN, M. TYGERT. *Randomized algorithms for the low-rank approximation of matrices*. Proceedings of the National Academy of Sciences, 104 (2007) (51), pp. 20167–20172. doi: 10.1073/pnas.0709640104.
- [Løvgren et al.(2006)] A. E. LØVGREN, Y. MADAY, E. M. RØNQUIST. *A reduced basis element method for the steady Stokes problem*. ESAIM: Mathematical Modelling and Numerical Analysis, 40 (2006) (3), pp. 529–552. doi: 10.1051/m2an:2006021.
- [Maday and Rønquist(2002)] Y. MADAY, E. M. RØNQUIST. *A reduced-basis element method*. Journal of scientific computing, 17 (2002) (1-4), pp. 447–459. doi: 10.1023/a:1015197908587.
- [Maday and Rønquist(2004)] Y. MADAY, E. M. RØNQUIST. *The Reduced Basis Element Method: Application to a Thermal Fin Problem*. SIAM Journal on Scientific Computing, 26 (2004) (1), pp. 240–258 (electronic). doi: 10.1137/s1064827502419932.
- [Maier and Haasdonk(2014)] I. MAIER, B. HAASDONK. *A Dirichlet-Neumann reduced basis method for homogeneous domain decomposition problems*. Applied Numerical Mathematics, 78 (2014), pp. 31–48. doi: 10.1016/j.apnum.2013.12.001.
- [Målqvist and Peterseim(2014)] A. MÅLQVIST, D. PETERSEIM. *Localization of elliptic multiscale problems*. Mathematics of Computation, 83 (2014) (290), pp. 2583–2603. doi: 10.1090/s0025-5718-2014-02868-8.
- [Mandel and Sousedík(2007)] J. MANDEL, B. SOUSEDÍK. *Adaptive selection of face coarse degrees of freedom in the BDDC and the FETI-DP iterative substructuring methods*. Computer Methods in Applied Mechanics and Engineering, 196 (2007) (8), pp. 1389–1399. doi: 10.1016/j.cma.2006.03.010.
- [Martini et al.(2014)] I. MARTINI, G. ROZZA, B. HAASDONK. *Reduced basis approximation and a-posteriori error estimation for the coupled Stokes-Darcy system*. Advances in Computational Mathematics, 41 (2014) (5), pp. 1131–1157. doi: 10.1007/s10444-014-9396-6.
- [Martini et al.(2017)] I. MARTINI, G. ROZZA, B. HAASDONK. *Certified Reduced Basis Approximation for the Coupling of Viscous and Inviscid Parametrized Flow Models*. Journal of Scientific Computing, (2017). doi: 10.1007/s10915-017-0430-y.
- [Martinsson et al.(2011)] P.-G. MARTINSSON, V. ROKHLIN, M. TYGERT. *A randomized algorithm for the decomposition of matrices*. Applied and Computational Harmonic Analysis, 30 (2011) (1), pp. 47–68. doi: 10.1016/j.acha.2010.02.003.
- [Maxwell(1861)] J. C. MAXWELL. *On physical lines of force*. The London, Edinburgh, and Dublin Philosophical Magazine and Journal of Science, 21 (1861) (139), pp. 161–175. doi: 10.1080/14786431003659180.
- [Maxwell(1865)] J. C. MAXWELL. *A dynamical theory of the electromagnetic field*. Proceedings of the Royal Society of London, 13 (1865), pp. 531–536. doi: 10.1098/rspl.1863.0098.
- [Melenk and Babuška(1996)] J. M. MELENK, I. BABUŠKA. *The partition of unity finite element method: basic theory and applications*. Computer Methods in Applied Mechanics and Engineering, 139 (1996) (1), pp. 289–314. doi: 10.1016/s0045-7825(96)01087-0.

- [Melenk et al.(2001)] J. M. MELENK, K. GERDES, C. SCHWAB. *Fully discrete hp-finite elements: fast quadrature*. Computer Methods in Applied Mechanics and Engineering, 190 (2001) (32–33), pp. 4339–4364. doi: 10.1016/S0045-7825(00)00322-4.
- [Milk et al.(2016)] R. MILK, S. RAVE, F. SCHINDLER. *pyMOR – Generic Algorithms and Interfaces for Model Order Reduction*. SIAM Journal on Scientific Computing, 38 (2016) (5), pp. S194–S216. doi: 10.1137/15M1026614.
- [Milk et al.(2017)] R. MILK, F. T. SCHINDLER, T. LEIBNER. *Extending DUNE: The dune-xt modules*. Archive of Numerical Software, Vol 5, No 1 (2017), (2017). doi: 10.11588/ans.2017.1.27720.
- [Monk(2003)] P. MONK. *Finite element methods for Maxwell’s equations*. Oxford University Press, 2003. ISBN 9780191545221.
- [Nataf et al.(2010)] F. NATAF, H. XIANG, V. DOLEAN. *A two level domain decomposition preconditioner based on local Dirichlet-to-Neumann maps*. Comptes Rendus Mathematique, 348 (2010) (21-22), pp. 1163–1167. doi: 10.1016/j.crma.2010.10.007.
- [Nedelec(1980)] J. C. NEDELEC. *Mixed finite elements in  $R^3$* . Numerische Mathematik, 35 (1980) (3), pp. 315–341. doi: 10.1007/bf01396415.
- [Nedelec(1986)] J. C. NEDELEC. *A new family of mixed finite elements in  $R^3$* . Numerische Mathematik, 50 (1986) (1), pp. 57–81. doi: 10.1007/bf01389668.
- [Nethercote and Seward(2007)] N. NETHERCOTE, J. SEWARD. *Valgrind*. ACM SIGPLAN Notices, 42 (2007) (6), p. 89. doi: 10.1145/1273442.1250746.
- [Nečas(1962)] J. NEČAS. *Sur une méthode pour résoudre les équations aux dérivées partielles du type elliptique, voisine de la variationnelle*. Annali della Scuola Normale Superiore di Pisa - Classe di Scienze, 16 (1962) (4), pp. 305–326.
- [Noor and Peters(1980)] A. K. NOOR, J. M. PETERS. *Reduced basis technique for nonlinear analysis of structures*. AIAA Journal, 18 (1980) (4), pp. 455–462.
- [Ohlberger(2005)] M. OHLBERGER. *A Posteriori Error Estimates for the Heterogeneous Multi-scale Finite Element Method for Elliptic Homogenization Problems*. Multiscale Modeling & Simulation, 4 (2005) (1), pp. 88–114. doi: 10.1137/040605229.
- [Ohlberger and Rave(2017)] M. OHLBERGER, S. RAVE. *Localized Reduced Basis Approximation of a Nonlinear Finite Volume Battery Model with Resolved Electrode Geometry*. In *Model Reduction of Parametrized Systems*, vol. 17 of *MS&A. Modeling, Simulation and Applications*, pp. 201–212. Springer International Publishing, 2017. doi: 10.1007/978-3-319-58786-8\_13.
- [Ohlberger and Schindler(2014)] M. OHLBERGER, F. SCHINDLER. *A-Posteriori Error Estimates for the Localized Reduced Basis Multi-Scale Method*, vol. 77 of *Springer Proc. Math. Stat.*, pp. 421–429. Springer International Publishing, Cham. ISBN 978-3-319-05684-5, 2014. doi: 10.1007/978-3-319-05684-5\_41.
- [Ohlberger and Schindler(2015)] M. OHLBERGER, F. SCHINDLER. *Error control for the localized reduced basis multi-scale method with adaptive on-line enrichment*. SIAM Journal on Scientific Computing, 37 (2015) (6), pp. A2865–A2895. doi: 10.1137/151003660.
- [Ohlberger and Schindler(2017)] M. OHLBERGER, F. SCHINDLER. *Non-conforming Localized Model Reduction with Online Enrichment: Towards Optimal Complexity in PDE Constrained Optimization*. In *Springer Proceedings in Mathematics & Statistics*, vol. 200 of *Springer Proc. Math. Stat.*, pp. 357–365. Springer International Publishing, 2017. doi: 10.1007/978-3-319-57394-6\_38.

- [Ohlberger and Verfürth(2018)] M. OHLBERGER, B. VERFÜRTH. *A New Heterogeneous Multiscale Method for the Helmholtz Equation with High Contrast*. Multiscale Modeling and Simulation, 16 (2018) (1), pp. 385–411. doi: 10.1137/16m1108820.
- [Ohlberger et al.(2018)] M. OHLBERGER, M. SCHAEFER, F. SCHINDLER. *Localized Model Reduction in PDE Constrained Optimization*. In V. SCHULZ, D. SECK, eds., *Shape Optimization, Homogenization and Optimal Control*, pp. 143–163. Springer International Publishing, Cham. ISBN 978-3-319-90469-6, 2018. doi: 10.1007/978-3-319-90469-6\_8.
- [Ølgaard and Wells(2010)] K. B. ØLGAARD, G. N. WELLS. *Optimisations for Quadrature Representations of Finite Element Tensors Through Automated Code Generation*. ACM Transactions on Mathematical Software, 37 (2010). doi: 10.1145/1644001.1644009.
- [Olimex(2019)] OLIMEX. *Project files for Olimex A64 PCB*, 2019. doi: 10.5281/zenodo.2547973.
- [Pacciarini(2016)] P. PACCIARINI. *Discontinuous Galerkin Reduced Basis Element Methods for Parametrized Partial Differential Equations in Partitioned Domains*. Ph.D. thesis, Politecnico Di Milano, Milan, Italy, 2016.
- [Pacciarini et al.(2016)] P. PACCIARINI, P. GERVASIO, A. QUARTERONI. *Spectral based discontinuous Galerkin reduced basis element method for parametrized Stokes problems*. Computers & Mathematics with Applications, 72 (2016) (8), pp. 1977–1987. doi: 10.1016/j.camwa.2016.01.030.
- [Patera and Rozza(2007)] A. PATERA, G. ROZZA. *Reduced Basis Approximation and A Posteriori Error Estimation for Parametrized Partial Differential Equations*. Version 1.0, Copyright MIT (2006-2007), to appear in (tentative rubric) MIT Pappalardo Graduate Monographs in Mechanical Engineering., 2007.
- [Pechstein and Scheichl(2008)] C. PECHSTEIN, R. SCHEICHL. *Analysis of FETI methods for multiscale PDEs*. Numerische Mathematik, 111 (2008) (2), pp. 293–333. doi: 10.1007/s00211-008-0186-2.
- [Phuong Huynh et al.(2013)] D. B. PHUONG HUYNH, D. J. KNEZEVIC, A. T. PATERA. *A Static condensation Reduced Basis Element method: approximation and a posteriori error estimation*. ESAIM: Mathematical Modelling and Numerical Analysis, 47 (2013) (1), pp. 213–251. doi: 10.1051/m2an/2012022.
- [Quarteroni et al.(2016)] A. QUARTERONI, A. MANZONI, F. NEGRI. *Reduced Basis Methods for Partial Differential Equations*, vol. 92 of *La Matematica per il 3+2*. Springer, 2016. ISBN 978-3-319-15430-5; 978-3-319-15431-2. doi: 10.1007/978-3-319-15431-2. An introduction, *La Matematica per il 3+2*.
- [Sangalli(2003)] G. SANGALLI. *Capturing Small Scales in Elliptic Problems Using a Residual-Free Bubbles Finite Element Method*. Multiscale Modeling & Simulation, 1 (2003) (3), pp. 485–503. doi: 10.1137/s1540345902411402.
- [Schmidt(1907)] E. SCHMIDT. *Zur Theorie der linearen und nichtlinearen Integralgleichungen*. Mathematische Annalen, 63 (1907), pp. 433–476.
- [Smetana(2015)] K. SMETANA. *A new certification framework for the port reduced static condensation reduced basis element method*. Computer Methods in Applied Mechanics and Engineering, 283 (2015), pp. 352–383. doi: 10.1016/j.cma.2014.09.020.
- [Smetana and Patera(2016)] K. SMETANA, A. T. PATERA. *Optimal Local Approximation Spaces for Component-Based Static Condensation Procedures*. SIAM Journal on Scientific Computing, 38 (2016) (5), pp. A3318–A3356. doi: 10.1137/15M1009603.

- [Smetana et al.(2019)] K. SMETANA, O. ZAHM, A. T. PATERA. *Randomized Residual-Based Error Estimators for Parametrized Equations*. SIAM Journal on Scientific Computing, 41 (2019) (2), pp. A900–A926. doi: 10.1137/18m120364x.
- [Sommer et al.(2015)] A. SOMMER, O. FARLE, R. DYCZIJ-EDLINGER. *A New Method for Accurate and Efficient Residual Computation in Adaptive Model-Order Reduction*. IEEE Transactions on Magnetics, 51 (2015) (3), pp. 1–4. doi: 10.1109/tmag.2014.2352812.
- [Spillane et al.(2014)] N. SPILLANE, V. DOLEAN, P. HAURET, F. NATAF, C. PECHSTEIN, R. SCHEICHL. *Abstract robust coarse spaces for systems of PDEs via generalized eigenproblems in the overlaps*. Numerische Mathematik, 126 (2014) (4), pp. 741–770. doi: 10.1007/s00211-013-0576-y.
- [Strouboulis et al.(2001)] T. STROUBOULIS, K. COPPS, I. BABUŠKA. *The generalized finite element method*. Computer Methods in Applied Mechanics and Engineering, 190 (2001) (32), pp. 4081–4193. doi: 10.1016/S0045-7825(01)00188-8.
- [Taddei and Patera(2018)] T. TADDEI, A. T. PATERA. *A Localization Strategy for Data Assimilation; Application to State Estimation and Parameter Estimation*. SIAM Journal on Scientific Computing, 40 (2018) (2), pp. B611–B636. doi: 10.1137/17m1116830.
- [Toselli and Widlund(2005)] A. TOSELLI, O. WIDLUND. *Domain decomposition methods—algorithms and theory*, vol. 34 of *Springer Series in Computational Mathematics*. Springer-Verlag, Berlin, 2005. ISBN 3-540-20696-5. doi: 10.1007/b137868.
- [Travis E(2006)] O. TRAVIS E. *A guide to NumPy*. Trelgol Publishing, 2006.
- [Voronin and Martinsson(2015)] S. VORONIN, P.-G. MARTINSSON. *RSVDPACK: An implementation of randomized algorithms for computing the singular value, interpolative, and CUR decompositions of matrices on multi-core and GPU architectures*. Tech. rep., arXiv:1502.05366, 2015. doi: n/a.
- [Weinan and Engquist(2003)] E. WEINAN, B. ENGQUIST. *Multiscale modeling and computation*. Notices of the AMS, 50 (2003) (9), pp. 1062–1070. doi: n/a.
- [Whitney(1957)] H. WHITNEY. *Geometric integration theory*. Princeton Univ. Press, 1957.
- [Xu and Zikatanov(2003)] J. XU, L. ZIKATANOV. *Some observations on Babuška and Brezzi theories*. Numerische Mathematik, 94 (2003) (1), pp. 195–202. doi: 10.1007/s002110100308.
- [Yano(2014)] M. YANO. *A Space-Time Petrov–Galerkin Certified Reduced Basis Method: Application to the Boussinesq Equations*. SIAM Journal on Scientific Computing, 36 (2014) (1), pp. A232–A266. doi: 10.1137/120903300.
- [Zaglmayr(2006)] S. ZAGLMAYR. *High Order Finite Elements for Electromagnetic Field Computation*. Ph.D. thesis, Universität Linz, 2006.



